UNIVERSITÀ DEGLI STUDI DI TRIESTE

XXIX CICLO DEL DOTTORATO DI RICERCA IN

NANOTECNOLOGIA

Inkjet printing of solutions as precursors of: i) organic semiconducting single crystals on self-assembled monolayers modified substrates and ii) nanoscale-thin dielectric layers

Settore scientifico-disciplinare: **ING/IND-22**

DOTTORANDO
GIULIO PIPAN

COORDINATORE
LUCIA PASQUATO

SUPERVISORE DI TESI
ALESSANDRO FRALEONI MORGERA

ANNO ACCADEMICO 2015/2016

“Imagination is more important than knowledge. For knowledge is limited to all we now know and understand, while imagination embraces the entire world and all there ever will be to know and understand”

- Albert Einstein

INDEX

Abstract

In the last years inkjet Printing (IJP) has become a very important technology for creating flexible devices for electronics, due to its simplicity, low cost and high precision. In this frame, the European Project i-FLEXIS sought for realizing novel ionizing radiation detectors based on Organic Semiconducting Single Crystals (OSSCs) on flexible substrates, capable of low power operation, flexibility, optical transparency, all at low fabrication costs and high throughput. This Thesis covers my PhD work in the frame of i-FLEXIS.

In Chapter 1 – Introduction – the main characteristics of the organic semi-conductors (§ 1.2), on which the organic electronics (§ 1.1) is based, will be indicated and described. In addition, the production methodologies will be illustrated (§ 1.5), focusing on the wet technologies that promote the single crystals growth via solution evaporation. Among these technologies, all the PhD work has been based on Inkjet printing, which will be described in detail, starting from the types of printers until the description of the inks (§ 1.6). The surface on which the crystals grow has an important role since its chemical and physical characteristics influence two fundamental aspects: first, the crystal type, and second, the electrical conduction inside an electronic device (§ 1.3). The characteristics of the surface can be modified using different procedures, from mechanical to chemical. This work has been focused on Self Assembled Monolayers (SAMs), used to cover the surface and optimize its characteristics; these organic molecules have been studied and their properties, functions and applications will be described in § 1.4. At the end of Chapter 1, the growth via low temperature combustion reaction of a nanolayer of AlOx, used as a dielectric inside of a TFT, will be illustrated. The solution containing the precursors is deposited using ink jet printing.

Chapter 2 – Results, Discussions, Materials and Methods – will concern one of the currently main prospected applications of IJP, which is the fabrication of organic electronics devices based on organic semiconductors crystals (§ 2.2). The organic molecule involved in this PhD research is the TIPS-pentacene (§ 2.1), due to its excellent semiconducting behavior and its capability to detect X-rays. The defects and the heterogeneity of the substrates, in addition to the high evaporation rate caused by the spreading of the printed drop, promote the formation of small crystals and poly-crystalline domains. This problem can be solved using the printing of a

solvo-phobic corral based on fluorinated SAMs (§ 2.3), which keeps the printed drop compact reducing the evaporation rate and creating TIPS single crystals in the range of 1 to 2,5 mm length. The increase of the electrical conduction between the electrodes and the TIPS crystals is made possible by their orientation. The method used to achieve directional growth of the crystals involves printing a corral with a high length versus width ratio; this promotes crystals growth along the major axe of the corral (§ 2.4). Thanks to this method, the crystals have been oriented along the desired direction. The verification of the electrical conduction (§ 2.5) between the electrodes and the TIPS crystals has been carried out by preliminary tests at the University of Trieste and, subsequently, by tests on the X-ray detection at the University of Bologna, a collaborating group in the frame of the i-FLEXIS project. The printed TIPS single crystals are able to collect charge carriers created by the absorption of ionizing radiation, joining together, in printable devices, the two concepts of organic direct X-ray detectors based on solution-grown single crystals and high sensitivity of low-voltage TIPS thin film detectors.

Chapter 3 – Ink jet printed nano-thin dielectric layers – will be about the development of a printed dielectric layer made by AlOx (§ 3.5) at the New University of Lisbon, in order to obtain a completely printed device (§ 3.2). The dielectric layer has been grown through the chemical reaction of combustion at low temperature (§ 3.1), after its printing on a silicon substrate (§ 3.3). The ink formulation has been limited by the precursors type and concentration, in addition to the limitations provided by the printer itself (§ 3.4). All the inks have been printed and tested via UV, FTIR, elipsometry, viscosity test, SEM and capacitance measurements. The best ink obtained from the tests has been adopted as a dielectric layer inside the TFTs (§ 3.6), which have been then electrically tested.

Chapter 4 – Conclusions and future works – will report a summary of the main results achieved and the possible future works.

Keywords: inkjet printing, Organic Semiconductor Single Crystals, TIPS-pentacene, Self-Assembled Monolayers, printed solvo-phobic corral, geometrical crystals orientation, AlOx, combustion reaction, printed nano-thin dielectric layer.

MOTIVATIONS

The European project i-FLEXIS, in which this PhD work is involved, aims at prototyping a printable type of sensor for direct detection ionizing radiation suitable for medical applications. This sensor is based on Organic Semiconductor Single Crystals (OSSCs) grown via slow solvent evaporation process on flexible substrates. The main characteristics of the detector must be flexibility, optical transparency, portability, low cost and environmental sustainability.

The main groups involved in the European project, and with which the PhD work has collaborated, are: University of Bologna, department of Physics and Astrophysics; University of Cagliari, department of electronic engineering; New University of Lisbon, UNIVOCA-CENIMAT, department of materials and nano-materials engineering.

The PhD work has been focused mainly on the modification of the chemical and physical properties of the printing surfaces. The modification of the surfaces has been carried out via inkjet printing process with the deposition of Self-Assembled Monolayers (SAMs) at room temperature, giving special attention to the possible negative effects on the transport of the carriers. The generation of new inks based on organic molecules and the development of a proper production and deposition protocol have been important aims strongly connected with the OSSCs growth.

Until now organic crystals grown on heterogenous surface are mainly poly-crystals or low quality small crystals, due to substrate induced heterogeneous nucleation. The growth of high quality OSSCs on heterogenous surfaces was an important aim of the PhD work, because good quality crystals have high electrical and X-ray detection properties. As for the SAMs, they also must be deposited via inkjet printing process, and for this reason an ink development and optimization protocol was required.

In the part of the work developed at the New University of Lisbon, was aimed the design of inks suitable for inkjet printing and able to generate AlOx dielectric layer through low-temperature combustion, as part of fully inkjet printed electronics devices.

CHAPTER – 1

INTRODUCTION

1.1 ORGANIC ELECTRONICS

During the second part of the 20th century the possibility to use organic materials in electronics started to be explored. While first studies about the electronic transport properties of organic materials were made in the '60s [1, 2, 3], the theme became popular only in the '80s, after the fundamental work of Alan J. Heeger, Alan G. MacDiarmid and Hideki Shirakawa on charge transport inside conjugated polymers [4, 5, 6]. The first organic light-emitting device (OLED) in 1987 by Tang and Van Slyke [7] attracted a lot of attention on organic materials applications in electronics, also from industries. Further interest was raised by the discover of the organic field effect transistor (OFET) [8, 9] and by the quasi-simultaneous finding of the photoelectric effect inside of these materials, that opened the door to the possibility of producing organic photovoltaic cells.

The very high application potential of these materials is empowered by their extraordinary characteristics, as flexibility, stretch-ability and softness ("soft electronics"), not available when using conventional silicon or other inorganic semiconductors. Moreover, it is possible to tailor the molecular structure of organic compounds, thus changing their chemical and physical properties. Mixing different organic molecules, either small ones or long polymer chains, also with other completely different materials, allows to further afford changes in electronic structures and the emerging of unique properties, as conductive textile where we find a combination between the strength of fibers and the electrical properties of small molecules or polymers [10]. This is a very exciting possibility for the future: the complete engineering of a functional material, creating untold potential for novel applications. Moreover, the intrinsic features of OE materials (lightness, low power operations, very small amounts of material needed per device) make them naturally eco-friendly, favoring a green approach to the next generation of our electronic world [11]. In particular, OE materials are based on carbon, hence they make reduced use of mined ores, and they are easily recyclable, or in case disposed of via incineration.

The huge application potential of OE in industry, besides the exceptional chemical and physical properties that are not achieved by other means, stems from an extremely low production cost ("cheap" electronics), and a considerable production speed, available thanks to the translation of established printing technologies to the new materials (*figure* 1.1-1).

Figure 1.1-1: electronic paper based on organic flexible film on the left, and chips for credit cards made of polymeric film on the right.

The vision of being able to print electronic circuits on a substrate, using existing print technology, is very attractive. However, there are some limitations, starting from the production temperature, which must be below 200°C to avoid the degradation of the materials.

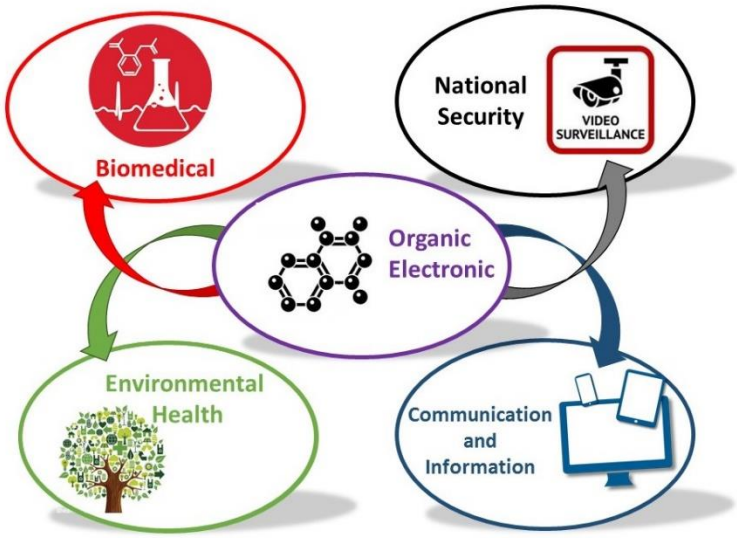

Figure 1.1-2: schematic illustration about all the potential OE applications.

The potential of OE applications extends in a large number of fields, including medicine and biomedical research, information and communications, and national security (*figure* 1.1-2). Nowadays several devices that include OE-based technologies are on the market: organic display base on OLEDs [12], RFID, solar cell [13, 14], transistor, as in *figure* 1.1-3.

In general, the success of OE will depend on three different key achievements: i) Organic electronic devices will do things that silicon-based electronics cannot do, expanding the functionality and accessibility of electronics; ii) Organic electronic devices will be more energy-

efficient and otherwise “eco-friendly” than today’s electronics, contributing to a more sustainable electronic world; iii) Organic electronic devices will be manufactured using more resource-friendly and energy-efficient processes than today’s methods, further contributing to a more sustainable electronic world.

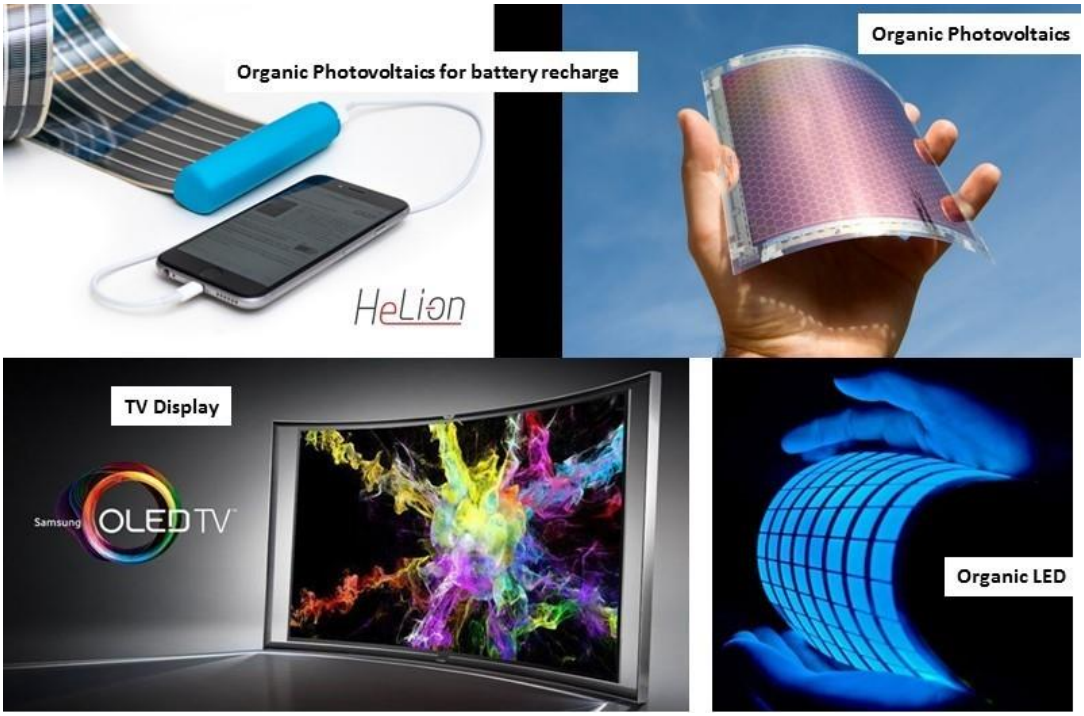

Figure 1.1-3: examples of actual devices based on organic electronics available on the market.

These fundamental steps will be enabled by an effective upscale from the laboratory to the industrial level. For achieving this goal, it is indispensable to both optimize all the production technologies and characterization techniques used until now, and to develop new ones. One very promising OE fabrication technologies is the Inkjet Printing Process (IJPP) [15], which will be discussed in the subsequent chapter.

Only with these fundamental implementations the OE will be able to perform its tasks and to become a relevant technology in the next years.

1.2 ORGANIC SEMICONDUCTORS (OS)

There are many motivations to use organic materials in electronic devices, due to the extraordinary chemical and physical properties of these compounds. The main advantage is the possibility to easy functionalize the molecule or to change their active group, but the opportunities don't end here: light weight, low cost, possibility of easily realizing thin-films, large-area device fabrication, flexibility, etc. are all very interesting characteristics of these materials. Soluble OS "inks" can also be deposited and patterned by a variety of traditional printing techniques, such as ink-jet printing or screen printing, [16] further driving the development of OS. Polymers [17] and small molecules [18, 19, 20, 21] can be used as semiconductors in devices, if they are correctly designed and prepared. An example of this potential is the organic field effect transistor (OFET), which holds promises for displays, sensors [22, 23, 24], smart card and memories [25]. These devices can be completely organics-based, from the dielectric to the active layers and the electrodes. Therefore, an intensive research is ongoing in this field, towards better performances enabled by molecular design/synthesis, device fabrication, material morphology control and charge transport properties improvement. In particular, in the last ten years a huge improvement in performance, stability and solution process production of OS has been realized. Development of high performance OS allowed to reach charge carriers mobility nearing or even surpassing that of amorphous silicon (0.1 cm^2 /V•s), letting envisage a high application potential for these materials.

1.2.1 ORGANIC SEMICONDUCTORS (OSs): AN OVERVIEW

Organic semiconducting materials (OSs) are constituted by organic molecules mainly composed by carbon (C) and hydrogen (H) atoms. In addition, it is possible to have, and in the clear majority of cases it is so, other types of elements, as oxygen (O), nitrogen (N) and sulfur (S). OSs show properties typically associated with a semiconductor material. They are formed by pi-bonded C atoms reorganized in building blocks to form molecules and/or polymers.

Depending on their long-range order in the bulk, OSs can be divided in two main categories:

1. Amorphous: usually deposed as films, amorphous OSs are constituted by molecules or polymers lacking any meaningful long range order. These films are usually obtained by spin-coating or evaporation under high vacuum.
2. Crystalline: in OSs molecules are held together by van-der-Waals interactions, and not by covalent bonds. Nonetheless, organic molecules can form ordered crystalline lattices, hence it is possible to obtain OSs-based crystals, that may be also single crystals (Organic Semiconducting Single Crystals, OSSCs). OSSCs usually have higher charge carrier motilities compared to amorphous OSs, and due to the intrinsic geometrical asymmetry of organic molecules, their general electronic properties are anisotropic [117]. Polycrystals, constituted by several crystalline domains of different sizes and orientations within the same bulk of material, are generally obtained from fast deposition processes, either via solution or vacuum.

1.2.1.1: Types Of OSSs

The Organic Semiconductors compounds con be divided in two groups: polymers and short molecules. The polymers can be deposited via solution or via chemical vapor deposition (CVD) of precursor that polymerize directly on the surface [118]. The polymer structure is amorphous or semi-crystalline. The short molecules are usually engineered to become completely soluble in the majority of the organic solvents, and can be deposited trough solution and vacuum (CVD or PVD) methods. They can be prepared as amorphous, crystalline or semi-crystalline layer depending on the environmental and surface conditions, characteristics and properties.

1.2.1.1.1: Semiconducting Polymers (Spoly)

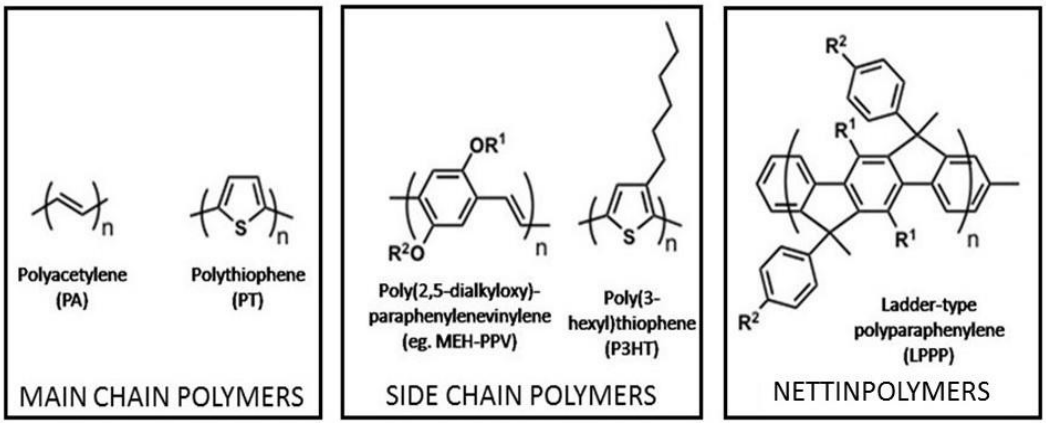

Figure 1.2-1: example of different semiconducting polymers divided by their chain ramifications.

The name "polymer" is composed by the Greek words "poli" and "meros", which mean “Many” and “Parts”, respectively. Polymers are made by fundamental units (monomers) covalently bound between them, regularly repeating along one (linear) or more (branched) chains, that can also be three-dimensionally bound (crosslinked, or netting polymers). The monomers can be equal (originating a homopolymer) or different between them (originating a copolymer) (*figure* 1.2-1 and 1.2-2)

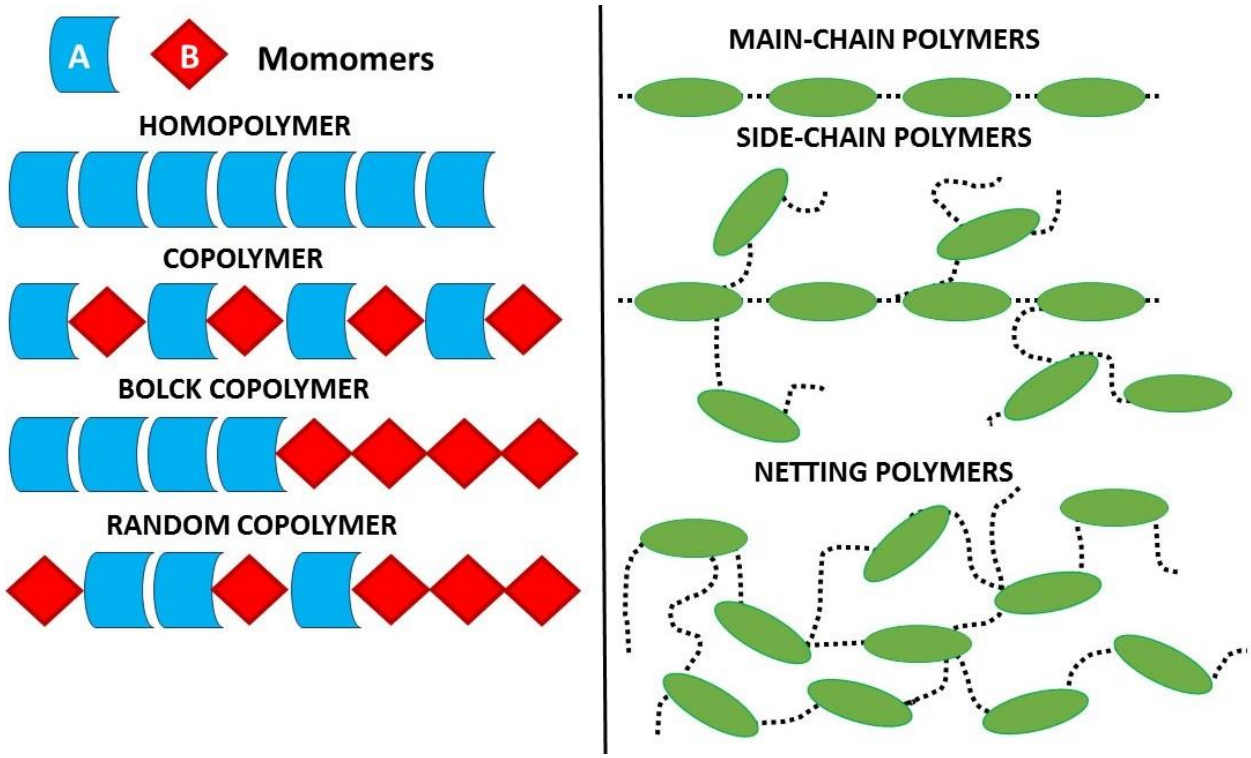

Figure 1.2-2: on the left, scheme of the main possible monomers arrangement inside the polymer chains. On the right, scheme of the possible chain ramifications.

The chain of a semiconducting polymer (SPoly) is constituted by carbon atoms with alternating single and double bonds. The chain can include heteroatoms, as sulfur (S), oxygen (O), fluorine (F), etc., and even molecules like for example aromatic cycles. The presence of these atoms influences the chemical and physical properties of the SPoly bulk material. Polymers can be engineered to achieve desired functional properties. For example, the presence of phenyl rings in the main chain increases both the conductivity and the rigidity of the polymer. Lateral branching chains are fundamental for the charge transport inside of the material, because they act as physical spacers between the main chains and considerably influence the photo-physical properties of the bulk. This property is exploited for example separating the main chains by means of lateral bulky substituents, thus hindering the chains from exchanging localized excited states and improving in this way OLEDs efficiencies, or by promoting a better main chain packing via linear allylic side chain substituents, as a mean to increase the chain-to-chain charge transport to increase the efficiency of photovoltaic devices [34, 35, 36, 37]. Lateral chains engineering is also used to increase the solubility of the polymers in specific organic solvents, so they can be dissolved in al liquid solvent and wet processed, for example realizing a film.

The solution process is very simple, and it allows also to realize multiple layers of material, exploiting the concept of "orthogonal solvents", i.e. solvents that do not dissolve the underlying layers. For example, it is possible to realize a film of a given SPoly1 from a first solution. After careful evaporation of the used solvent, the resulting film can be used as a substrate for a further deposition of SPoly2, if the solvent used for SPoly2 cannot dissolve the underlying. SPolys can also be chemically doped, so to achieve truly conducting plastic materials [38, 39].

1.2.1.1.2: Semiconducting Molecules (Scs)

OS molecules can be organized in perfect order in 3D space, originating crystalline lattices, that can be translated at the macroscopic level as poly or single crystalline (OSSCs) materials. Most OSSCs are composed by molecules including aromatic cycles, that allow a higher lattice rigidity and facilitate charge carriers mobility. Same example of these type of molecules are: naphthalene, anthracene, tetracene, pentacene, pyrene *figure* 1.2-3.

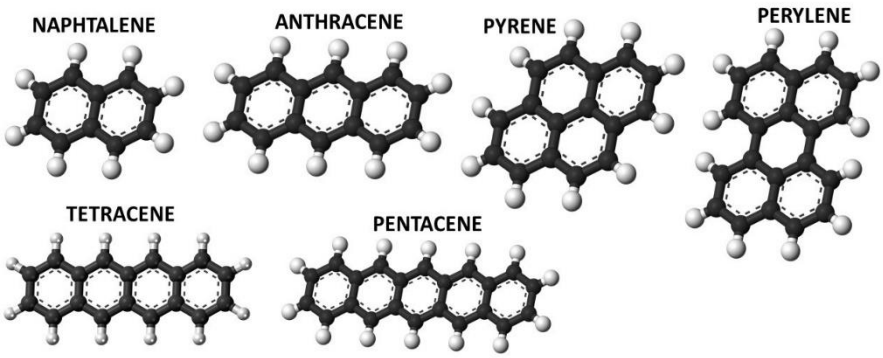

Figure 1.2-3: structure of the main aromatic semiconducting molecules.

The forces that keep the cohesion between molecules in OSSCs are typically weak, as Van-der-Waals or Induced Dipole forces [40, 41, 42]. In general, these forces depend from different parameters, the most important of which are the distance $\boldsymbol{r}$ among the molecules and their polarizability $\boldsymbol{\alpha}$, with the proportionality $V_{VdW} \propto \frac{\alpha^2}{r^6}$ [43, 44]. Therefore, to achieve a meaningful charge transport between neighboring molecules, the latter must be well packed and their external π-orbitals must be large and well delocalized, in order to allow efficient orbitals overlapping. An example of molecules that allow such an arrangement are flat molecules like polyarenes. For example, in *figure* 1.2-4 it is shown the crystal lattice of pentacene.

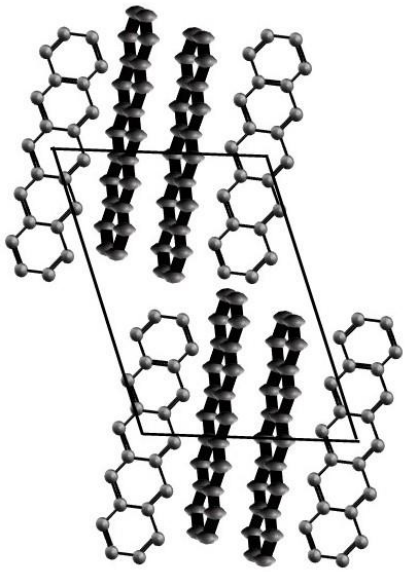

Figure 1.2-4: representation of pentacene crystal lattice.

In the last few years the mobility of holes in OSSCs has reached the range between 1 to 50 $cm^2\ V^{-1}s^{-1}$ [45, 46, 47, 48, 49, 50]. These values have been obtained thanks to deep investigations over the OSSCs growth methods, as well as over the purity of the crystals themselves [46, 67]. In fact, to achieve high charge transport performances, the organic molecule constituting the crystal must be as pure as possible, because impurities tend to act as charge carriers traps in the crystal or as energetic walls hindering the charge transfer and promote charges recombination, markedly decreasing the overall transport capabilities of the OSSC. The organic solvent molecules can become one of these impurities if they remain included within the grown crystal, hence particular attention must be paid to solvent purification when OSSCs are grown from solution.

1.2.1.1.3: Other Organic Semiconductor Compounds

Fullerenes and carbon nanotubes (CNTs) are the probably most famous carbon-based compounds (figure 1.2-5). Fullerenes (C_{60}) was discovered by Kroto et al. [51] in 1985, it is formed by 60 carbon atoms arranged into 12 pentagons and 20 hexagons creating a sphere with a diameter of 7,1 Å [52]. Its applications cover multiple field applications as photovoltaics, medicine, chemical catalysis, biology ect. [53, 54, 55, 56, 57]. Carbon NanoTubes (CNTs) were discovered in 1991 by Iijima et al.[58], they are 1D materials with cylindrical morphology, with diameter in the range of a few to hundreds nanometers, and a length up to centimeters [59]. They can be divided

in three different families: i) Single Wall CNTs (SWCNTs); ii) Double Wall CNTs (DWCNTs); iii) Multi Wall CNTs (MWCNTs). CNTs have extraordinary mechanical properties combined with superior electrical conductivity, as metals or semiconductors depending of the graphitic hexagonal lattice chirality [60, 61, 62, 63].

The last type of organic materials used in electronic applications are LCs. They have an intermediate phase where there are both solid and liquid properties. For instance, a liquid crystal may flow like a liquid, but its molecules may be oriented in a crystal-like way. Their main application is in displays (Liquid Crystals Display (LCD) present in all house, office etc. [64]). To better Understand the chemical and physical characteristics of these extraordinary type of material it is possible to read the review of Freek J. M. et al. "About Supramolecular Assemblies of π-Conjugated Systems" [65].

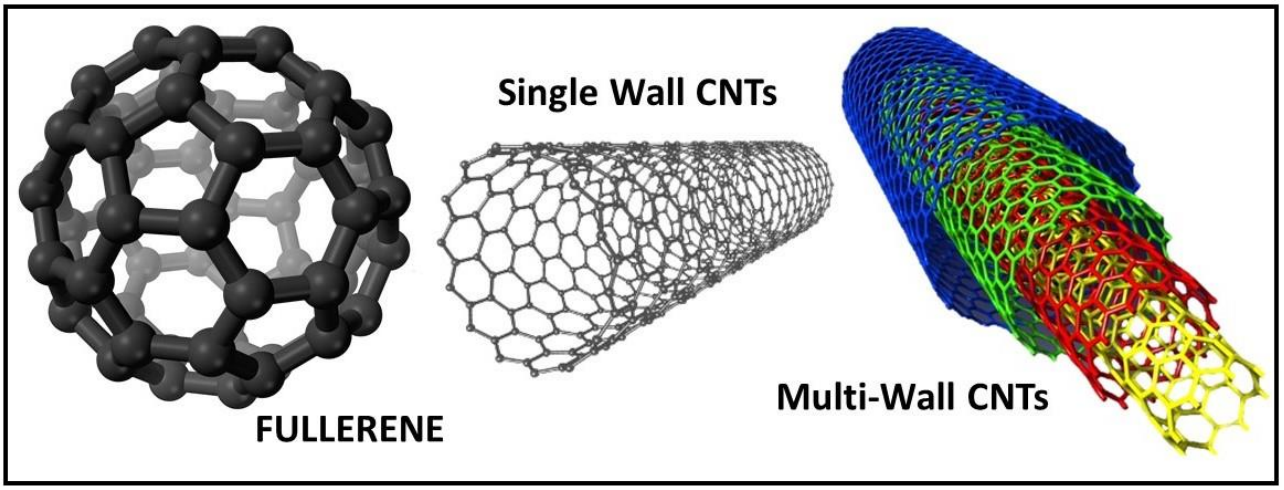

Figure 1.2-5: scheme of the structure of: Fullerene, Single-Wall CNTs and multi-Wall CNTs.

1.2.2 ELECTRICAL PROPERTIES OF ORGANIC SEMICONDUCTORS

Organic Semiconductors aren't currently believed able to replace silicon-based materials, since their electronic performances are by far still lower than those of their inorganic counterparts. In fact, in the best cases the range of charge mobility inside of a OSSCs is from 1 to 50 $cm^2V^{-1}s^{-1}$, at room temperature [66, 67], while in amorphous materials these values are at maximum ranging around 0.1 $cm^2V^{-1}s^{-1}$ [68, 69]. For comparison, crystalline silicon has a hole mobility of about 500 $cm^2V^{-1}s^{-1}$[264].

This lower charge transport capabilities with respect to inorganic semiconductors comes from the basic electronic structure of OS. OSs are carbon-based materials, where carbon atoms can be hybridized with three different possibilities: sp, sp2, sp3. In sp3 hybridization four hybrid orbitals promote a covalent bond of C with the other atoms of the molecules, generating a strong and directional σ bond. When hybridized sp2 are involved in the C-C bond in addition to a σ bond free p_z orbital generates molecular orbital π, that is arranged over and below the interatomic plane and is characterized by a high polarizability. A simple example of this arrangement is the ethylene molecule, where HOMO (highest occupied molecular orbital) and LUMO (lowest unoccupied molecular orbital) energetic levels corresponding to the bonding and antibonding π orbitals (*figure* 1.2-6) are established. If more ethylene molecules are connected, more carbon atoms are covalently bound via sp2 bonds, and the related π bonds become delocalized (*figure* 6-1.2) (conjugate chain). Allowing the electrons to travel along the chain. In the OSs molecules, the energy gap between the HOMO and LUMO depends on the chain length: increasing the chain length results in a decrease of the band gap because of increasing electron delocalization. If the band gap doesn't exceed few eV (no more than 2 eV), the organic compound has the electric characteristic of a semiconductor [70].

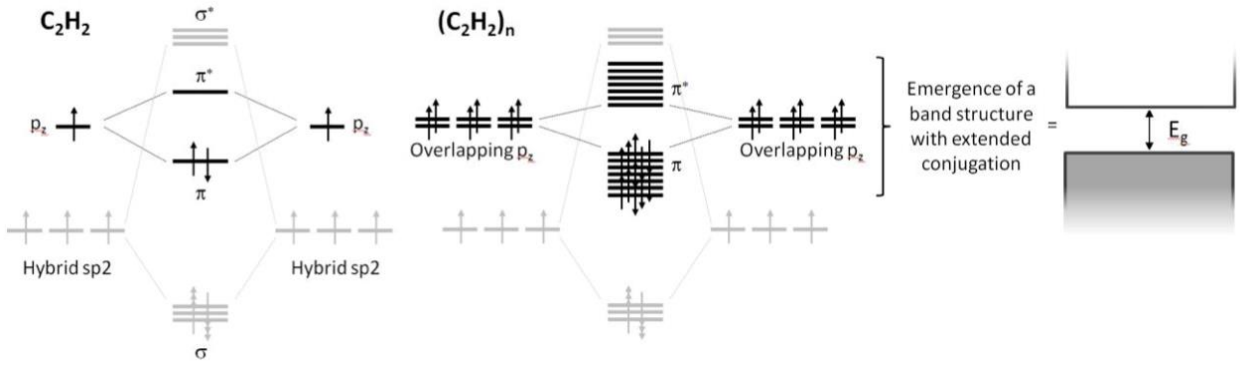

Figure 1.2-6: bonding and anti-bonding level in an ethylene molecule (left), in a Polyethylene short polymer (center) chain and in a long one (right). From the simple molecule (monomer) to the long polymer chain a band structure emerges and the π bonds become delocalized.

In organic materials, the overlap of the molecules inside the bulk generate orbitals overlap, that determinate the carriers transport at the macroscale [70]. The molecular disorder affects the charge transfer: an increase in disorder decrease the charge mobility and increases the recombination. In organic materials, the main charge transport mechanism between the molecules is the "hopping", that is the charge hop from a conjugate unit to its next one. The

hopping process depends mainly from the compound purity and its order, but also from the temperature. As visible in *figure* 1.2-7, the electrons can jump between adjacent molecules, adjacent polymer chains or parts of a same polymer chain. Ordered materials favor the hopping of the charge, but in general OSs are rather disordered materials with a broad distribution of energy states. All the energy states that are far (in energy) from the band gap become trap states, and hinder the passage of the electrons or holes [71].

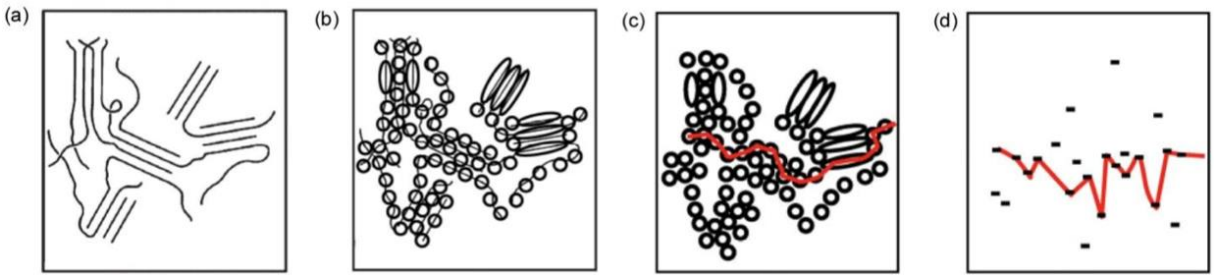

Figure 1.2-7: hopping of electrons through the polymer chain or part of them.

Some of the most investigated organic semiconducting molecules are listed in Table 1.2-1

Table 1.2-1

Oligoacenes: [72 , 73]	The most promising molecules in this big family are tetracene and pentacene, due to their good crystallinity and acceptable semiconductors properties.	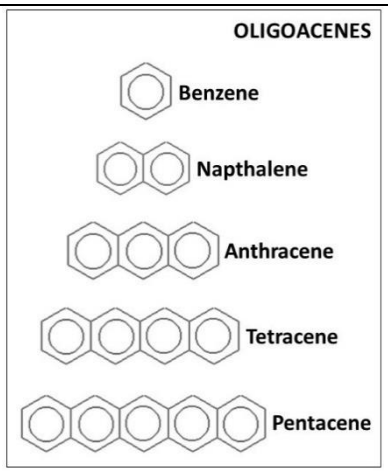
Oligothiophenes: [74, 75, 76]	They are used as N-Type materials, or as P-Type with the introduction of fluorine (F) atoms in the structure [77, 78]. They	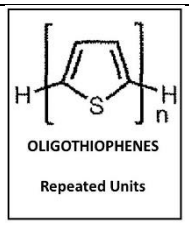

	are usually composed by 2 to 8 oligomers.	
Fullerene: [79, 80]	It is mainly use as electron acceptor in organics blends for photovoltaics applications.	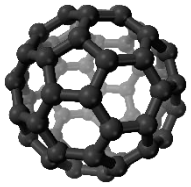
Perylenes: [81]	They have good N-Type properties, and they are used as blue-emitting dopant in OLEDs. The dimers are arranged in a herringbone packed structure.	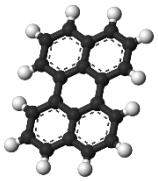
Discotic liquid crystals: [82]	They are made of 2D disc-molecules with complete saturated chain on the border and a conjugated core. The N or P characteristics depend on the nature of the substituent. They are organized in 1D columns that force the electrons along of their main axis. Their typical mobility is around 0,5 $cm^2V^{-1}s^{-1}$ [83].	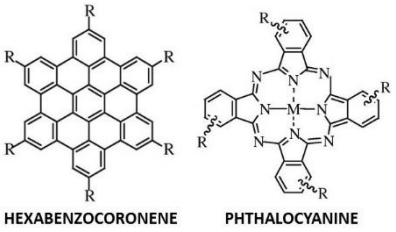 HEXABENZOCORONENE PHTHALOCYANINE
Triphenylamines: [84]	Vacuum-deposited as amorphous films, they are used as hole transporting materials in LED.	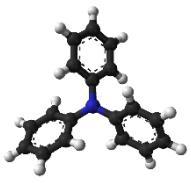

In polymeric materials, the mobility of charges is in the range of 10^{-6} to 10^{-3} $cm^2V^{-1}s^{-1}$, due to the inherently disordered arrangement of the chains in the bulk. In general, π-conjugated

polymers are p-type materials, but polymers with a high electron affinity can behave as n-type materials.

1.2.3 PARAMETERS AFFECTING CHARGE TRANSPORT IN OSS

The charge transport efficiency of OSs depends from a multitude of parameters, including: molecular packing/arrangement, degree of disorder, presence of impurities, temperature, electric field, charge-carrier density, size/molecular weight of the considered molecules, pressure. Hereafter a brief overview of the influence of these parameters over the charge transport capabilities of OSs is given.

1.2.3.1: Molecular Packing/arrangement

The electronic properties of OSs are very sensitive to the geometrical arrangement of molecules in the 3D space, for the reasons explained in par. 1.2.2. While this is less important for amorphous materials, like polymers, and moderately important for poly-crystals, an optimal mutual orientation of the OS's molecules is crucial for single crystalline materials. OSSCs have anisotropic electrical characteristics, and in the majority of these features are orthotropic: i.e. they change along three space directions. In OSSCs the herringbone is an often-observed packing structure. This structure promotes a 2D charge transfer around every single lattice layer [85], while between the layers the transport is less efficient. The best packing for obtaining a high 3D carrier mobility is the cofacial one, where the molecules are perfectly superimposed [86, 87]. This was theoretically demonstrated, but it is structure not achievable in real materials due to the electrostatic repulsions among the molecules, that causes a shift between the molecules along the main axis. The crystal packing effectiveness can also change the color of the crystal, as for example in perylene derivatives [88, 89], due to better/worst π-π interaction between the packed molecules.

1.2.3.2: Geometrical disorder

There are two different type of geometrical disorder:

1. Diagonal: it represents and reflects the fluctuations of the energy inside the material bulk. The main contribution of this parameter to the overall geometrical disorder of the considered bulk comes from the molecular torsion of the non-rigid part of the molecules/chains. In the case of polymers, for example, the presence of impurities and the distribution of torsion angles generate a modification in the HOMO and LUMO levels of the chains, due to the different lengths of the twisted, conjugated segments. The diagonal disorder is influenced also by the local dipole moment, which amplifies, and in some case, is induced by, the electrostatic and/or polarization effects coming from neighboring molecules [90, 91].
2. Off-Diagonal: it represents the different bonding strength in nearby molecules, which depends on mutual orientation and on the possible presence of impurities.

The behavior of a medium in which carrier transport occurs through a solid where highly conducting areas and disordered ones coexist can be described by the multiple trapping and release (MTR) model [92]. This model was subsequently considered, by Shmidin [97] and Noolandin [98], as specific case of the most general continuous time random walk (CTRW) model developed by Scher and Lax [93]. When the traps are homogeneously distributed in the medium, the charge carrier mobility is described by equation (1) :

$$\mu = \mu_0 \alpha e^{\left(-\frac{Et}{k_b T}\right)} \qquad (1)$$

where ***Et*** is the trapping energy and ***α*** represents the ratio between the density of delocalized levels available for transport and the density of traps. The other parameters are: k_b is the Boltzmann constant, μ_0 is the mobility without disorder and ***T*** the temperature in Kelvin. As it is possible to see from this equation, the mobility has a strong dependence from the temperature of the sample. The mobility becomes temperature-independent if the traps are not homogeneously distributed, and this happens only if they are localized in a disordered region, like for example a

grain boundary [94]. To calculate the mobility in both (ordered and disordered) regions it is possible to use the following equation (2):

$$\frac{1}{\mu} = \frac{1}{\mu_{low}} + \frac{1}{\mu_{high}} \quad (2)$$

which resembles the equation describing the electrical behavior of a series of two capacitors. Obviously, since $\mu_{low} << \mu_{high}$, this expression highlights the fact that the mobility is limited by the poorly conducting regions of the material [94].

1.2.3.3: Temperature

As discussed in the previous point, the temperature affects crystalline (ordered) and amorphous (disordered) regions in a completely different way. In ordered zones, the mobility follow the law: $\mu \approx T^{-n}$, because the mobility decreases with the increase of the temperature. In the case of the disordered regions, the occurring charge transport occurs via hopping, which is thermally activated. In particular, high temperatures reflect increment in kinetic energy that help the charge carrier to hop from one molecule to the other, overcoming the energetic barriers generated from the disordered molecular/chains arrangement [95].

1.2.3.4: Electric Field

The mobility under electrical field has different behavior depending if the bulk material is a single crystal or a disorder solid. In the high purity, single crystal there is a mobility dependence only along the highest charge mobility direction, in which an increase of the electrical field reduces the mobility [96]. Generally, the Poole-Frenkel law is used to describe the mobility of a charge carrier in disorder OS under a high electrical field [97, 98]. Low electrical field allows the charges some freedom of movement in following the most convenient path around the defects present in the bulk. Vice versa, a strong field forces the charges along a specific path, also traveling through the defects, within which they are slowed. For this reason, it is possible to observe the electric field effect only in very disordered materials (for which a larger field delivers a larger mobility), and in ultra-pure crystals [99].

1.2.3.5: Impurities

Not all the impurities have a strong impact on the electrical, chemical and physical properties of OSs. In particular, impurities change the transport ability of the material only if the energy levels resulting from this unintentional doping fall inside of the HOMO-LUMO gap of the bulk OS. In all the other cases, they can introduce local variation of the energetical walls or real physical walls (i.e., geometrical distortions) that make the carriers pathway difficult, and promote the recombination of the charges. When impurities are materials radically different from the considered OS-constituting molecules, the purification is usually easy. Vice versa, if they are chemically similar the purification process can be very difficult, and even impossible.

1.234.6: Pressure

Application of an external pressure can result in a better charge transport through the material, as what happens in pentacene. This can be attributed to a reduction in intermolecular distance between adjacent molecules [100].

1.2.3.7: Size and molecular weight

Several studies tried to find a connection between the molecular weight of a OS molecule and its electrical transport properties, but with not univocal results. Polymers are the only materials in which molecular weight have been demonstrated to have a crucial role, showing that an increase in the length of the chain (equivalent to an increase in molecular weight) corresponds to a growth in charge carriers' mobility. This occurs probably because long polymer chains can act as "electronic connectors" between separated, yet locally organized. An example of this behavior is P3HT, whose holes' mobility increases by almost 4 orders of magnitude when the chain grows from 20 to 220 units [101, 102].

1.2.4 MAIN CHARGE-TRANSPORT MECHANISMS

The study of electrons-holes mobility in OSs has a long history that starts in 1960s [103, 104, 105]. During the 1970s industries like Xerox, IBM and Kodak Investigated the temperature dependence of the mobility inside highly pure crystals [106, 107, 108]. In the middle of 1970 Scher and Lax [109] described theoretically the hopping transport mechanism. After all these studies the main models to descried this electron-hole mobility inside a pure crystal are two, the Polaron Models and the Disorder one.

1.2.4.1: Polaron Models

The OS bulk properties are deeply linked with its packing, intermolecular distances, and the mutual orientations (geometry) of the lattice molecules. Any movement or vibration from the equilibrium position of the molecular atoms represents change in π-orbitals overlapping, which is reflected in the charge transport. To define the total mobility, a good approximation is given by (3):

$$\mu = \mu_{tun} + \mu_{hopp} \quad (3)$$

where $\boldsymbol{\mu_{tun}}$ is the tunneling mobility and $\boldsymbol{\mu_{hopp}}$ is the hopping mobility. The phonons are the temperature-activated vibration inside the bulk material, occurring between the atoms inside the molecule, and between the molecules inside the crystal lattice. Low temperature promotes a tunneling mobility while high temperature the electrons have sufficient kinetic energy to jump between the molecules, allowing hopping dominate the mobility.

If the electrons-phonons coupling is large or week the temperature dependent mobility has different behavior (*figure* 1.2-8) [110, 111].

- Weak local electrons-coupling interaction the mobility is dominated by tunneling, $\mu \sim T^n$ with n>0, and show a bandlike dependent;
- For intermediate couplings at low temperature these is a bandlike mobility, but the increasing in hopping contribute decrease the high temperature dependence;

- Strong electron-photon interaction behavior is divided in three different zone: i) low temperature (T<<T1) the mechanism is based on tunneling and the mobility is bandlike; ii) intermediate zone (T1<T<T2) where the temperature starts to increase, the tunneling mechanism is substitute by the hopping one; iii) high temperature (T>>T2) the mobility starts to decrease because thermal phonon scatters the electrons.

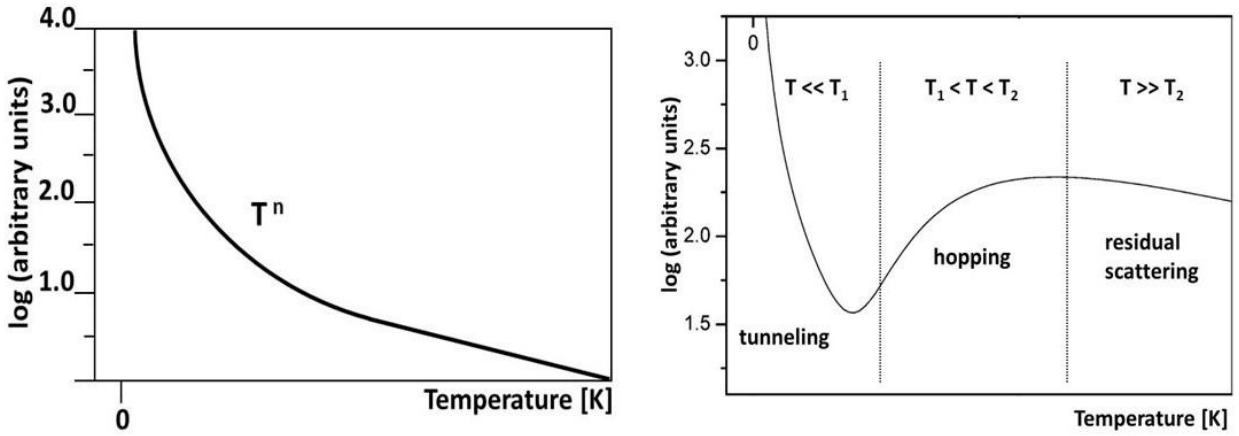

Figure 1.2-8: different temperature-dependent behaviors of electrons-phonons cupping. On the left, diagram of weak interaction, where the mobility is dominated by the tunneling. On the right, diagram of strong interaction, divided in the three different mobility zones.

1.2.4.2: Disorder Model

In a perfect material without any chemical and physical defects, the charge transport depends only by the electrons-phonon interaction. Static anomalies and impurities are present in real materials, and that perturb the charge movement and its transport mechanism. These types of disorder are very common in organic materials, where there is a strong presence of amorphous structures. Disorder promotes the localization of the band state, that in an ideal thoroughly ordered material are completely delocalized. Only the edge band states are localized in a weakly disordered material. The addition of disorder state promotes the electron hopping transport mechanism between the molecules (*figure* 1.2-9).

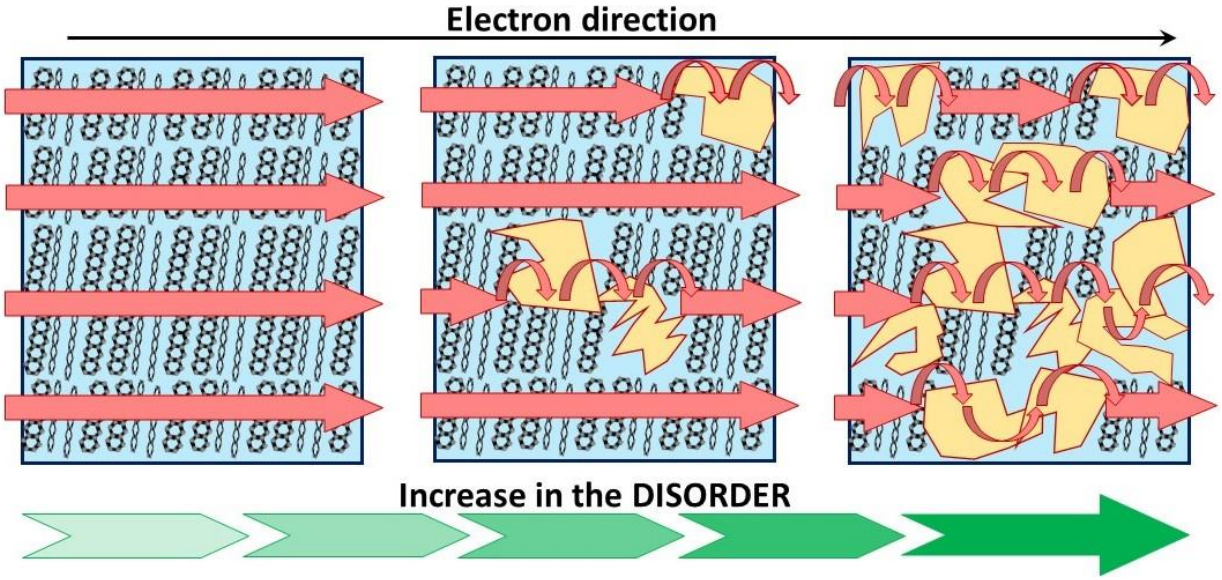

Figure 1.2-9: the figure shows the increasing in hopping mechanism from a perfect homogeneous structure to a complete disorder structure.

1.2.5 OPTICAL PROPERTIES OF ORGANIC SEMICONDUCTORS

The optical properties of an ordered OS are based on the presence of a quasi-particle named "Exciton". A clear definition of this physical element is found in the Knox [112] book: an exciton is a quantum of electronic excitation travelling in a periodic structure, whose motion is characterized by a wave vector. This quasi-particle is generated from an adsorbed photon in an OS, that excites an electron from the valence band to the conductive one, creating an electron-hole couple relatively strongly bound to the molecule onto which it has been generated [113]. It is a neutral quasi-particle, and it can transport energy without any electrical charge. The promoted electrons can be in a singlet or in a triplet configuration, resulting in a singlet or a triplet exciton. These quasi particles can be interchain or intrachain, and they are distributed only on few conjugated units. The small life time of exciton limits its diffusion inside the organic bulk materials, with an average distance at room temperature of ten to twenty nanometers. The main and important phenomenon that excitons undergo are:

- Energy Transfer: the exciton moves from the generator place to another;
- Dissociation or Splitting: It is possible to divide the exciton in the electron and a hole depending on the system conditions.
- Quenching: in contact with the border-line of a defect, there is a non-radioative recombination of the defect;

- Annihilation: at high exciton densities collisions between the excited states are possible, with a consequent dissociation or quenching of the bound states.

The typical exciton found in OSs, that are based on weak intermolecular interactions, is the Frenkel-exciton one [114)]. This type of exciton has a very small electron-hole radius (< 5 Å) because of its relatively high binding energy, near 0,3 eV (contrary to what happens in inorganic materials, where the binding forces are weak and the electron-hole radius has an average radius in the range of 50 to 85 Å). It is localized essentially on a single molecule or on a single site.

The excitons are classified upon their different physical properties, that depend from the molecular structure and from its packing inside the solid, as follows:

1. Charge transfer (CT) excitons [115]: in this type of exciton the electron and hole are delocalized along different adjacent molecules. CT excitons are considered the primary species involved in the photoconduction process. The CT transition energy can be interpreted as the intermolecular distance inside the crystal lattice, whereas they are delocalized states. The lifetime of CT exciton is estimated around 10^{-7} seconds [116]
2. Exciton Dimers (Excimers): they are formed by two different photo-excited, adjacent molecules. These molecules can create excimers only if they are both in an excited state, and if there are the suitable geometric conditions (molecules very close to each other in the solid state): when they relax, the excimers are dissociated and the molecules repel each other. The excimer emitted from this dissociation is less energetic than that formed on a single molecule. Excimers have a very short life-time, in the order of nanoseconds. An example of this type of exciton is that formed by the perylene and pyrene molecules, where the packing conformation is favorable for excimer formation.
3. Surface Excitons: these types of excitons are rare, and they exist only in crystals at very low temperature. They originate from molecules present on the surface of the organic crystals, that undergo sudden environment change in comparison with the bulk ones. This occurrence influences heavily the photoluminescence features of the material. Surface excitons have narrow transition bands, and absence of vibrionic progression and null Stokes shift.

In general, the optical properties of an OS are influenced by its molecular arrangement. The presence of impurities or the disorder introduce perturbations in molecular orbitals, and modify the exciton-photon transition. The same phenomena occur with the modification induced by the substrate, the roughness, and the presence of active group, that can change the crystal morphology. The incident light has a different behavior, depending on of its energy. The crystal/layer of the OS can be completely transparent, can absorb the energy of the photon, or even can be degraded and damaged from the high energy of the radiation.

1.3 SURFACE

In OE the surface at the interface between the organic semiconductor (OS) and the electrodes is a very important component for proper device operation. Therefore, it is extremely important to investigate the chemical and physical properties of these interfaces to optimize surface treatments and materials matching. In fact, most of the peculiar features of OE devices (low cost, flexibility, softness and stretch-ability) are enabled by accurate tuning of the OS/electrode interface, in both mechanical and electronic terms. For example, it is impossible to flex organic semiconducting crystals with a thickness of more than a few tens of microns; to achieve this result, it is necessary to reduce the crystal thickness down to less than 30-40 microns, and, at the same time, to improve the interface between the crystal and the substrate, to reduce the possibility of reciprocal slipping.

The charge transfer through different layers is another very important point, worth an accurate investigation of the surface characteristics in OE. Several different parameters influence charge transfer between OE and the underlying electrodes: physical adherence, electronic characteristics of the OS, metal work function, and so on. Therefore, in the following an overview of the main parameters affecting the quality of interface surfaces in OE is given.

1.3.1: SURFACE ROUGHNESS

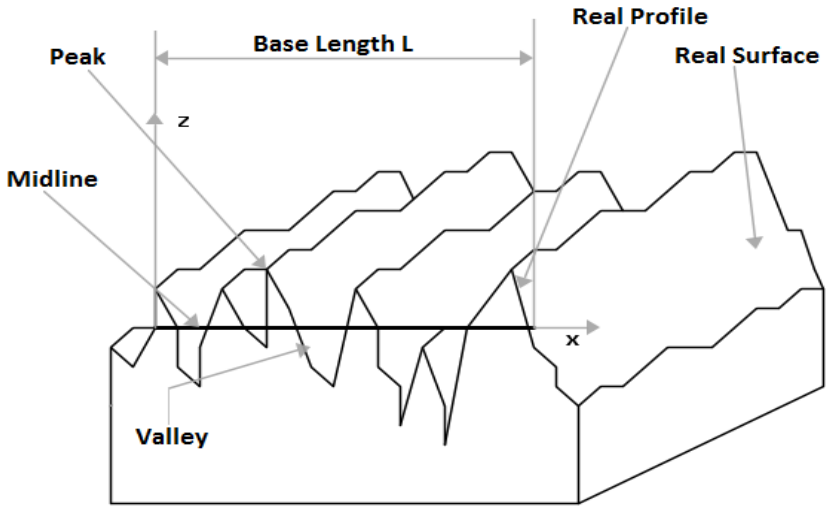

Figure 1.3-1: scheme of the roughness characteristics.

Surface roughness can be defined as a measure of the irregularities in a surface texture, and it usually derives from mechanical, chemical of physical treatments (like general manufacturing techniques). Roughness is characterized by sequences of peaks and valleys, which are found with frequencies and amplitudes (*figure* 1.3-1). The range of sizes of peaks and valleys can go from atomic scale to millimeters, characterizing a smooth surface from a rough one, and it is possible to change the interaction between surfaces and their surrounding environment (liquid, solid or gaseous) by altering the surface properties.

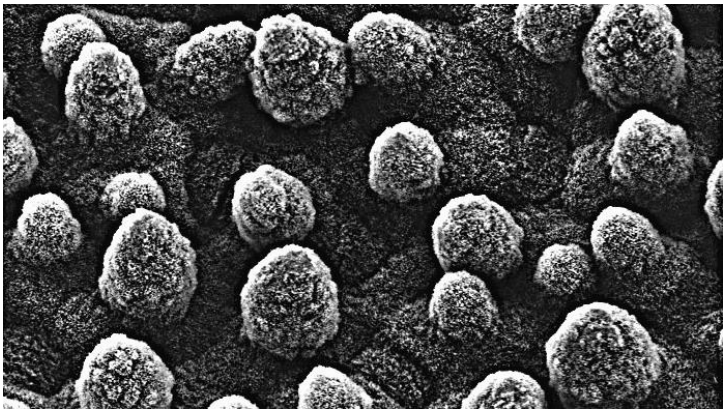

Figura 1.3-2: Magnification of a leaf of Nembulo nucifera, the roughness made by surface papilla cells that give rise to the lotus effect is clear.

The roughness has a very important role in determining the surface characteristics of the substrate/sample. For example, roughness has a direct connection with the wettability and friction of the surface, as in the case of the "lotus effects" [119]. In particular, the lotus leaf presents two different levels of roughness: the first one is recognizable at the microns scale, with bumps emerging from the leaf surface, while the second one is nanometric, with extremely tiny spikes all over the leaf's surface, including the micrometric bumps (*figure* 1.3-2). This surface arrangement, aided by the presence of hydrophobic wax nanoparticles, makes it extremely hydrophobic, promoting the formation of quasi-perfect sphere drops, that flow along the surface at any minimal inclination, washing it effectively and maintaining the characteristic lotus leaf shine.

There are several methods to change a surface's roughness. The selection of a given method depends on the desired result and on the considered material. For example, to smooth very rough metal and ceramic samples the normal approach is to lap them with different grainy sandpaper, moving gradually from μm to nm size. To obtain a close to atomically smooth surface,

electrochemical corrosion or plasma treatments are the most effective options. Polymeric materials are usually too soft for this approach; hence they are smoothed via the deposition of a coating layer of an appropriate thickness, that fills up the valleys. In this case, however, in addition to the surface topology also the surface chemistry and its properties are modified.

The descritpion of the surface roughness can be achieved in two main ways: by profile (line roughness) or by surface (area roughness), even though the most common one is the first one.

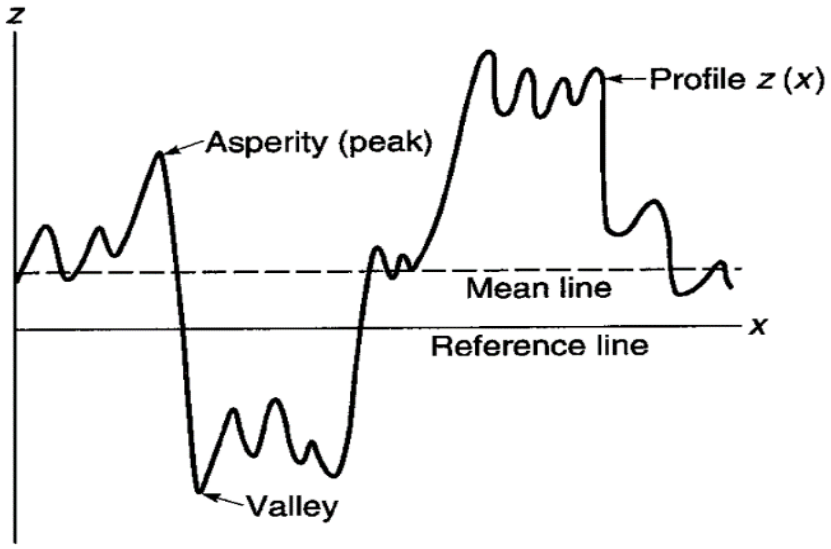

Figura 1.3-3: scheme of a surface profile z(x)

i) <u>Profile roughness parameters:</u>

In a profile line z(x), as shown in *figure* 1.3-3, the peak heights and the valley depths are calculated from the reference line, while the mean line divides the total area under the profile line into two areas characterized by the same value. The main statistical parameters used to evaluate the profile roughness are: $\mathbf{R_a}$, that represent the center-line average (CLA) or the arithmetic average (AA) [120, 121] of the profile roughness,; $\mathbf{R_q}$, that represent the root mean square (RMS) of the profile roughness [122]. The $\mathbf{R_a}$ and $\mathbf{R_b}$ have an important limitation, they can't distinguish between two complete morphologically different surfaces that have the same average roughness. Ra is calculated through the equation (4):

$$R_a = \frac{1}{L}\int_0^L |z - m|\, dx \quad (4)$$

In which the parameters ***m*** is calculated using the equation (5)

$$m = \frac{1}{L}\int_0^L z\, dx \quad (5)$$

L is defined as the base length or sampling length of the profile.

The variance is calculated with the equation (6), in which $\boldsymbol{\sigma}$ represents the standard deviation, while $\mathbf{R_q}$ is calculated with the equation (7) and it is the square root of the arithmetic mean of the square of the vertical deviation from a reference line.

$$\sigma^2 = \frac{1}{L}\int_0^L (z-m)^z \, dx = R_q^2 - m^2 \quad (6)$$

$$R_q^2 = \frac{1}{L}\int_0^2 (z^2)\, dx \quad (7)$$

In the specific case of m = 0 the standard deviation $\boldsymbol{\sigma}$ is equal to the root mean square $\mathbf{R_q}$.

Othes profile parameters used are listed in the table 1.3-1.

Table 1.3-1: roughness main parameters.

PARAMETER	DESCRIPTION	FORMULA
S_k	Skewness – statistical parameter	$Sk = \frac{1}{\sigma^3 L}\int_0^L (z-m)^3 \, dx$
K	Kurtosis – statistical parameter	$k = \frac{1}{\sigma^4 L}\int_o^L (z-m)^4 \, dx$
R_t	Maximum peak-to-valley height	$R_t = R_p + R_v$
R_p	Maximum peak height	$R_P = \lvert\max_i[z(x)]\rvert; 0 < x < L$
R_v	Maximum valley depth	$R_v = \lvert m_{in}[z(x)]\rvert; 0 < x < L$
R_z	Average peak-to-valley height	$R_z = R_{tm} = \frac{1}{M}\sum_{i=1}^{M} R_{ti}$
R_{pm}	Average peak-to-mean height	$R_{pm} = \frac{1}{M}\sum_{i=1}^{M} R_{pi}$

ii) *<u>Spatial Roughness Parameters</u>*

The definition of spatial roughness parameters allows to determine the density of peaks (N_p), which measures the number of peaks per analyzed length, and the zero-crossing density (N_0), which represents the number of peaks that cross the mean line.

Depending on the application, there are several methods of surface analysis. Usually, industrial applications employ optical microscopy or electromechanical profilomtery for surface analysis, while in research environment, more sophisticated techniques are used, such as Atomic Force Microscopy (AFM), Low Energy Electron Diffraction (LEED) or Scanning Tunneling Microscopy (STM). Surface investigation methods can be further be divided into contact methods and non-contact ones, depending on the type of interaction between the probe and the sample.

The table 1.3-2 (B. Bhushan, 2001, "Introduction to Tribology") summarizes the most commonly used surface analysis techniques.

Table 1.3-2: surface analysis technique.

Method	Quantitative Information	Three-Dimensional Data	Resolution (nm)		On-line Measurement Capability	Limitations
			Spatial	Vertical		
Stylus instrument	Yes	Yes	15–100	0.1–1	No	Contact type can damage the sample, slow measurement speed in 3D mapping
Optical methods						
Taper sectioning	Yes	No	500	25	No	Destructive, tedious specimen preparation
Light sectioning	Limited	Yes	500	0.1–1	No	Qualitative
Specular reflection	No	No	10^5–10^6	0.1–1	Yes	Semiquantitative
Diffuse reflection (scattering)	Limited	Yes	10^5–10^6	0.1–1	Yes	Smooth surfaces (<100 nm)
Speckle pattern	Limited	Yes			Yes	Smooth surfaces (<100 nm)
Optical interference	Yes	Yes	500–1000	0.1–1	No	
Scanning tunneling microscopy	Yes	Yes	0.2	0.02	No	Requires a conducting surface; scans small areas
Atomic force microscopy	Yes	Yes	0.2–1	0.02	No	Scans small areas
Fluid/electrical	No	No			Yes	Semiquantitative
Electron microscopy						Expensive
Reflection/replication	No	Yes	5	10–20	No	instrumentation,
Integration of backscattered signal	Yes	Yes	5	10–20	No	tedious, limited data, requires a conducting
Stereomicroscopy	Yes	Yes	5	50	No	surface, scans small areas

1.3.2: PRESENCE OF CHEMICAL COMPOUNDS ON THE SURFACE AND CLEANING PROCEDURES

Surfaces are never totally clean: chemical contamination is due both to the production methods and to the interaction with the external environment. For electronic devices, this latter phenomenon is critical, because the direct interaction with atmosphere can compromise the behavior of devices. The most common impurities that can be found on a surface are:

i) *Oxides:*

Oxides usually grow on metals as a passivation (protection) layers (i.e. in aluminum, titanium or molybdenum), but they can also be formed as a result of production methods. The main problem concerning oxides, from an electronic application point of view, is that they form an insulating layer covering the surface of the metallic material, which is usually hard to be removed.

It is possible to find oxides also in other materials as for example on plastic samples. In this case their presence is caused by the falling of metal-oxide powder from the tools used for the same samples processing. A sonication bath is required to eliminate all these external impurities.

ii) *Presence of dirt*:

Dirt can be due to dust present in the atmosphere or to the greasy which can be employed inside the production cycle; anyway, a simple washing can be used to eliminate dirt. For applications, which require a high level of cleanliness, such as micro-electronics, silicon-wafer or pharmaceutical industries, a cleanroom should be equipped to decrease the risk of contamination of the surface.

iii) *Adsorbed molecules*:

Atmosphere is composed by different chemical species; some of them can interact with the considered surface and get adsorbed on it. One of the most omnipresent molecules, that can drastically alter the electrical proprieties of the surfaces, is water. Water increases the capacitance of dielectric layers, and it often allows the dissolution

of other atmospheric chemical compounds. In order to prevent water adsorption, cleaning or manufacturing must take place in controlled atmosphere.

Once a surface is well clean and/or known in terms of roughness, adsorbed species and electronic and chemical properties, it is possible to functionalize it (i.e., add on it further compounds to change its chemical/electronic nature). In general, it is possible to cover the surface with organic molecules or with oxides.

1.3.2.1: Surface cleaning procedures

Proper washing of a surface requires a previous knowledge of the surface's properties, to avoid unwanted damage or modifications. In general, cleaning a surface involves the use of both chemical (solvents) and physical (typically ultrasounds) treatments. Chemicals used for surface cleaning include sequential washing with acetone and alcohols, that can remove dust and grease. If contaminants or undesired chemicals/compounds are still left after this type of treatment, then acids are used. The most common acids for this purpose are nitric, hydrochloric or hydrofluoric acid, which are effective on different types of oxides and metallic contaminants. If the high concentrated pure acids do not have the desired effects, it is possible to use mixtures, like Aqua Regia (3 parts of concentrated hydrochloric acid and 1 part of concentrated nitric acid), or the so-called Piranha Solution (3 parts of concentrated sulfuric acid and 1 part of 30% hydrogen peroxide solution), due to their increment in oxidation power they can dissolve all the organic residue and noble metals also (Aqua Regia).

Mechanical-physical methods can be used to clean surfaces, but with some care. For example, scraping with particles of different sizes can eliminate a lot of impurities, but it can also damage the surface and increase its roughness. Dynamic fluxes of different fluids can eliminate dust or the water monolayer. It is also possible to use plasma gases or ion-beam techniques to remove all the impurities present on the surface, but also in this case the surface roughness will be affected (these techniques tend to smooth the surface).

1.3.3: SURFACE ENERGY

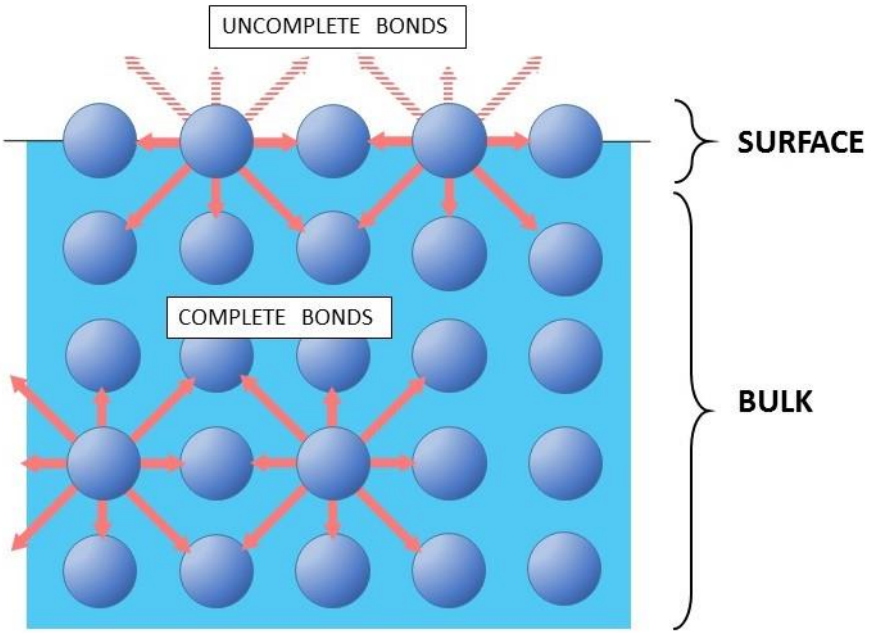

Figure 1.3-4: binding difference between surface and bulk atoms.

Surface energy is a property of the surfaces of materials. The atoms in the material bulk have a complete bonding shell. In this case the external electron cloud of these atoms is complete, and the atoms are neutral in charge and not reactive. In the case of the surface atoms, the situation is different: the most external ones lack some bonds, and they are less tightly interacting with the material bulk than the inner atoms (*figure* 1.3-4).

Therefore, on surface, there is an excess of energy with respect to the bulk: the sum of this excess energy is defined as surface energy, and it is considered positive. A second possible definition is based on the energy needed to create a new surface and to break the atomics bond [123]. In this case, the considered energy is the double of the total surface energy, because two different surfaces are generated.

It is possible to quantify the surface energy using the Gibbs free energy equation (8):

$$dG \equiv -S\,dT + V\,dP + \gamma\,dA \;\Rightarrow\; \gamma \equiv \left(\frac{\partial G}{\partial A}\right)_{T,P} \qquad (8)$$

where ***S*** is the system entropy, ***T*** is the temperature in Kelvin, ***P*** is the pressure, ***V*** is the volume and ***γdA*** is the internal energy, that comes from the multiplication of the area ***A*** with the surface energy ***γ.*** The surface energy of a solid (that for a pure liquid coincide with the surface tension) can

be measured with different wet techniques, as contact angle with goniometer measurement [124], Zisman diagram [125], OWRK/Fowlkes [126]. The most used techniques, specifically in the industrial field, are the contact angle measurements, based on the Young's equation and the Zisman diagram. In the first case, there are different possibility to determinate the contact angle of solids, from the direct tests, as used of sessile drop or the capillary rise, or indirect tests, as chromatography methods or calorimetry analysis [127].

1.3.3.1: Young equation

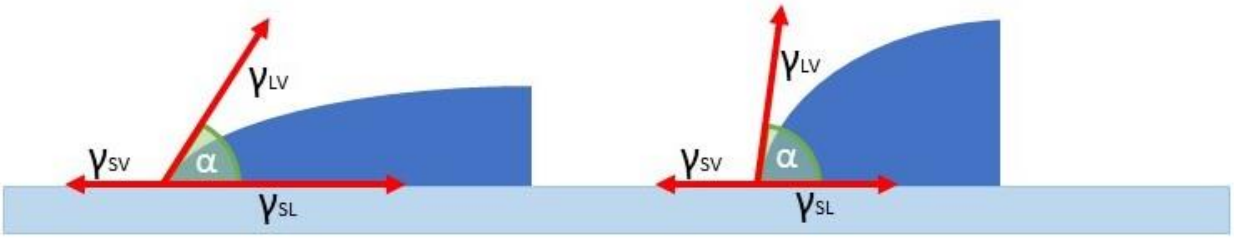

Figure 1.3-5: representation of different contact angles (α).

The Young equation (9) [128] analyzes the contact angle $\boldsymbol{\alpha}$ of a drop of a liquid on the surface of a solid (*figure* 1.3-5):

$$\gamma_{LV}\cos\alpha = \gamma_{SV} - \gamma_{SL} \quad (9)$$

γ_{LG} , γ_{SG} and γ_{SL} represent respectively the energies of the interaction between liquid-vapor, solid-vapor and solid-liquid. This equation is valid with the approximation of a solid surface that is complete, smooth, homogeneous, solid and completely inert, which is often not completely the case. Moreover, it is practically impossibile to experimentally measure all the variables, hence the Young equation *per se* does not generally allow to calculate the surface energy.

1.3.3.2: Zisman diagram

A simple, quick and low-cost way for the determination of the surface energy of solids [129] and, at the same time, its wettability [130] has been developed by Zisman and co-workers [131]. The original idea of Zisman is considered the difference $\boldsymbol{\gamma_{SV}-\gamma_{SL}}$ (Young equation 9) as independent from the used liquids and a constant property of the solid surfaces.

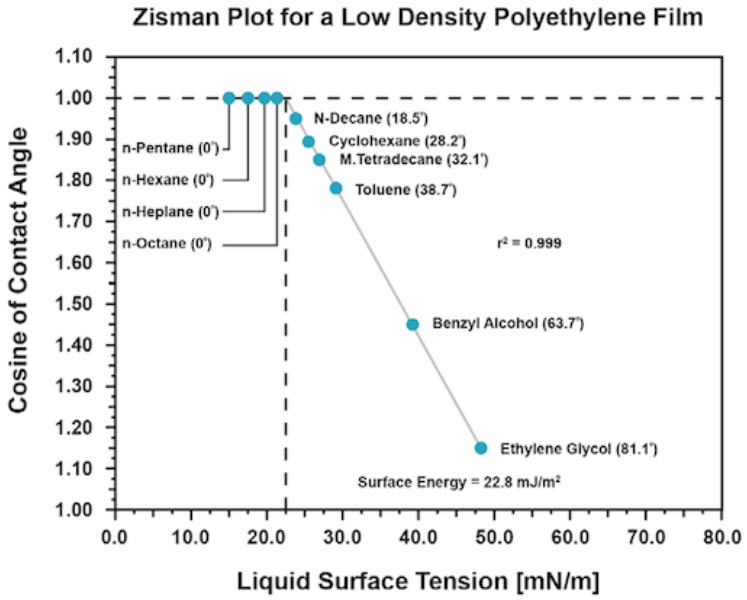

Figure 1.3-6: Zisman diagram of Low Density Polyethylene, it is possible to see the critical surface tension γ_c.

In particular, Zisman realized a diagram relating contact angles of organic solvents with different surface tension deposited over a given substrate and the respective surface energies (as surface tension values), *figure* 1.3-6 is an example of that type of diagram [132]. It identifies the critical surface tension $\boldsymbol{\gamma_c}$ of a non-polar surface, that is an estimated valor because the free surface energy is seen only as a single parameter, instead of considering it as a sum of different factors (active groups on the surface, polar interactions, ect.) that interact together.

Zisman's method assumes that when a liquid has a 0° angle with an underlying surface (i.e., it is completely spread over that surface) its surface tension is either lower or equal to the surface energy of said surface. In this frame, it is possible to determine, with a good level of approximation, the surface energy of a material via measurement of a series of contact angles $\boldsymbol{\alpha}$ established by the considered surface and different liquids (*figure* 1.3-7 "1" and "2"). The cosines of the measured contact angles are then plotted against the surface tensions of the corresponding liquids (*figure* 1.3-7 "3"), which are chosen so to have progressively smaller surface tensions. The intersection between the plotted curve and the line identified by the $\cos(\boldsymbol{\alpha}) = 1$ ($\boldsymbol{\alpha}$ is equal to 0) is then considered as the critical surface tension of a liquid in equilibrium with the considered solid's surface, hence the solid surface energy (*figure* 1.3-7 "3" and *figure* 1.3-6). While this method is very simple and easily applicable, it must be taken some care when interpreting its results, since the plotted curve is sometimes hyperbolic in its final part due to the difficult to estimate the

contact angle when the liquid and the surface have similar energy; this could lead to erroneous estimations of the considered surface energy. If it is necessary to compare different surface treatment to understand which is difference in free surface energy, this method is often perfect, because the error is the same for all the test (if the tests are done at the same conditions), and it is a rapid and low cost method.

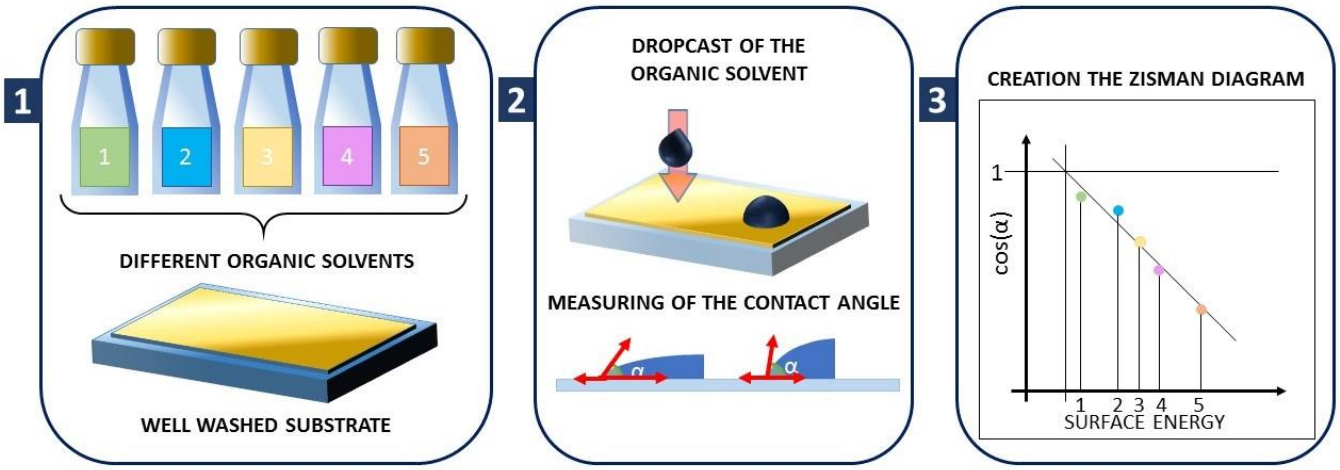

Figure 1.3-7: scheme of the different steps needed to create the Zisman diagram.

1.3.4: SURFACE TREATMENTS

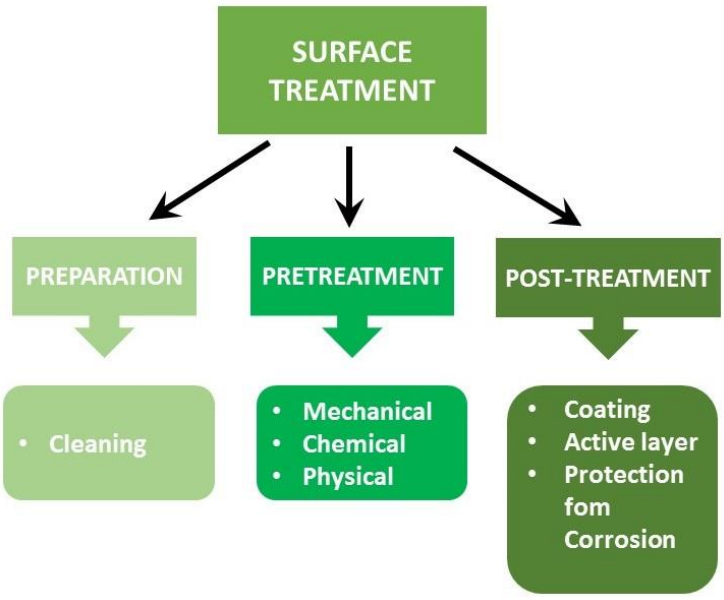

Figure 1.3-8: main groups of the surface treatment to prepare a surface.

The surface is an extremely important part of a considered sample, and indeed in many applications it is the only part of a material worth of actual interest. However, surface treatments are not only aimed to clean it up. Surface treatments can also be used to increase or decrease its

compatibility with other materials, or to modify the charge transfer properties between materials places in contact with the surface itself. Surface treatments can also change the physical properties of a surface, like for example wettability, hardness or friction. A few possible surface treatments are listed in *figure* 1.3-8, and they can be divided in three categories: i) preparations; ii) pretreatment; iii) post treatment before the final use. While Preparation procedures are limited to cleaning methods, already discussed in par. 1.3.2, a brief overview of pre- and post-treatment methods will be given hereafter.

1.3.4.1: Pretreatments

Pretreatments are needed to prepare the surface for subsequent characterization or material deposition steps. They can be mechanical, chemical or physical, depending on the considered material, on its final application and on the desired result.

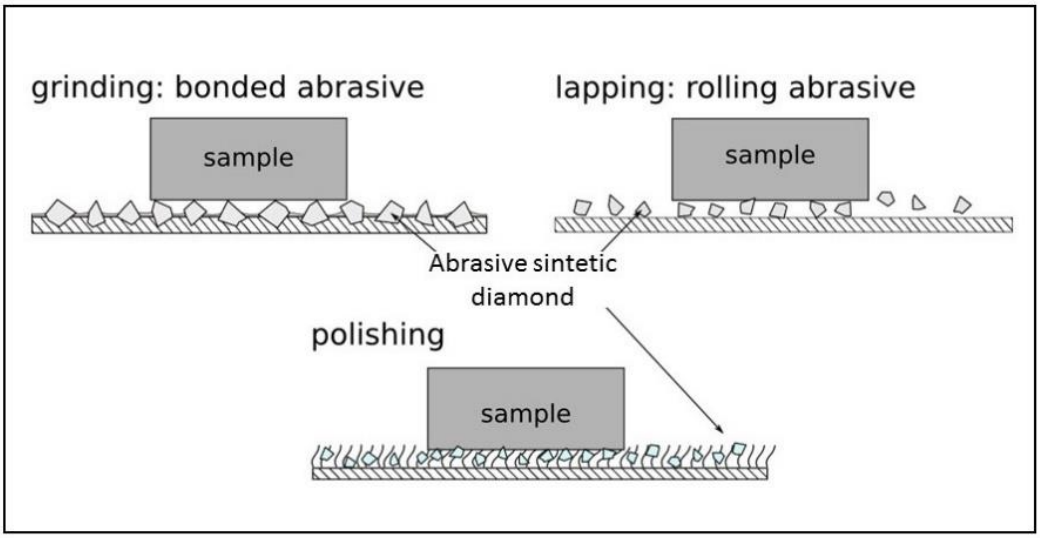

Figure 1.3-9: mechanical pre-treatment with the uses of different sizes of sandpaper, grinding, lapping particles, from millimeters to nanometers.

Mechanical processes are aimed at smoothing a surface, and are generally focused on abrasion approaches, as lapping *figure* 1.3-9, with the uses of different size sandpaper, grinding, lapping particles, from millimeters to nanometers.

Chemical pretreatments usually involve the presence of acids that dissolve part of the surface or transform it. These treatments can modify the shape of the surface or change its chemical nature, for example increasing its hydrophilicity via generation of surface -OH groups. The choice of the acids and of their concentration depends from the needed results and from the considered materials.

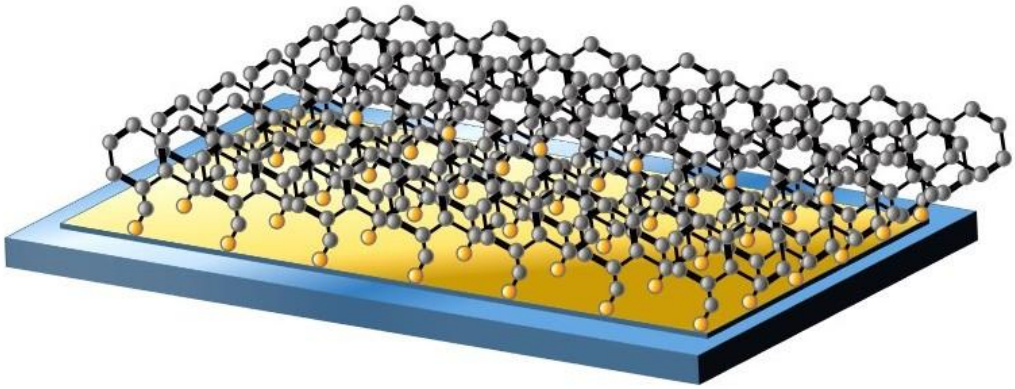

Figure 1.3-10: chemical pretreatment with a monolayer of organic molecules (SAMs) on metals substrate.

Chemical pretreatments can change the chemical and the physical characteristics of the surface at the same time. Among various possible chemical pre-treatments, a particular interest is held by the use of Self Assembled Monolayers (SAMs) (*figure* 1.3-10). They are small organic molecules with two different terminal groups, i.e. a "head" and a functional "tail" group. The description of this type of treatment, and of how it affects the surface properties, is described in more detail in the following paragraph 1.4.

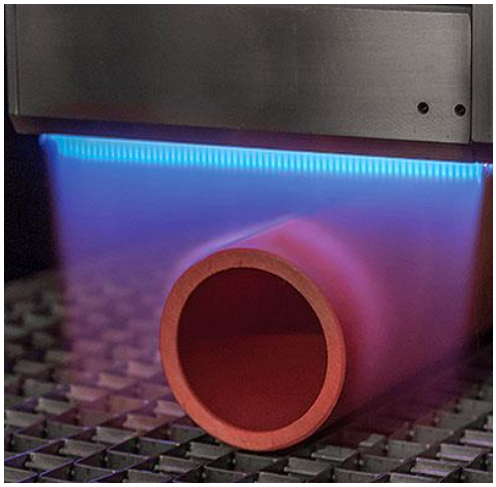

Figure 1.3-11: digital photo of a polymeric tube flame treatment.

Physical pretreatments use highly energetic charges or ionic species to modified the surface of the considered materials. The three most used processes are i) free flames, ii) corona discharge and iii) plasma. The flame treatment (*figure* 1.3-11) uses oxygen mix with propane or acetylene. When applied to organic materials like polymers it must be carried out only for a few seconds, otherwise there is the risk of burning the sample. It improves the wettability and the adhesion of the surface introducing oxygen-based active groups on the surface of the material, like -OH, -COOH, -COH functionalities.

The corona discharge (*figure* 1.3-12) is a method in which two electrodes are placed on top and bottom of the sample to be treated, at atmospheric pressure. A high alternated (high frequency) voltage is then applied between the electrodes, which generates a plasma in the immediate surroundings of the material's surface. This method is usually carried out at ambient pressure and in air, and in this case, is used to increase the surface wettability and adhesion (and crosslinking of polymers and organic materials). However, its effect on the surface is short-living due to the formation of radicals that start immediately to react among them and with all the chemicals present in the atmosphere, so it is important to use the material immediately after the treatment [140].

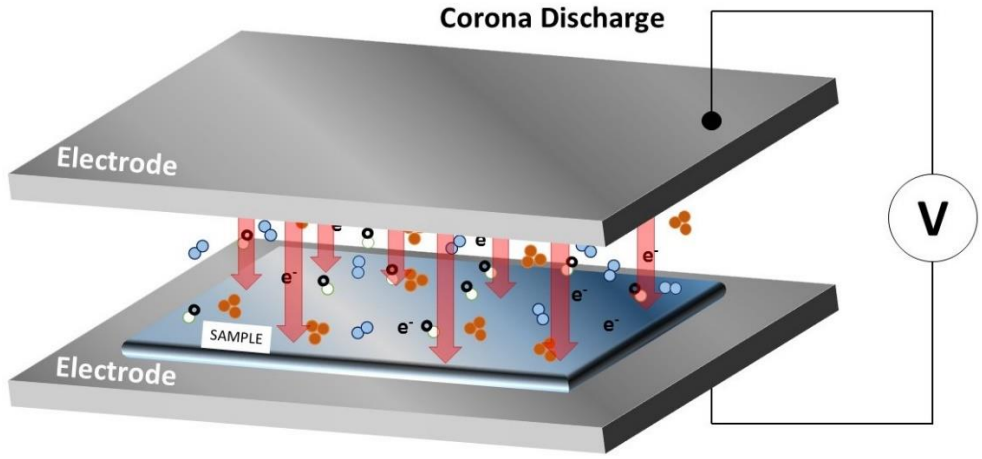

Figure 1.3-12: scheme of a corona discharge of a metallic substrate.

The plasma process (*figure* 1.3-13), takes place in a closed chamber with low pressure (around 10^{-3} to 10^{-4} atm). For this reason, it is usually carried out in batches, even though recent developments allow to carry out plasma treatments even at atmospheric pressure and [141], thus permitting continuous processing. The plasma treatment is very versatile, and it can be used for cleaning, surface activation towards water or other liquids, or for etching purposes, properly varying the chemicals to be transformed into plasma.

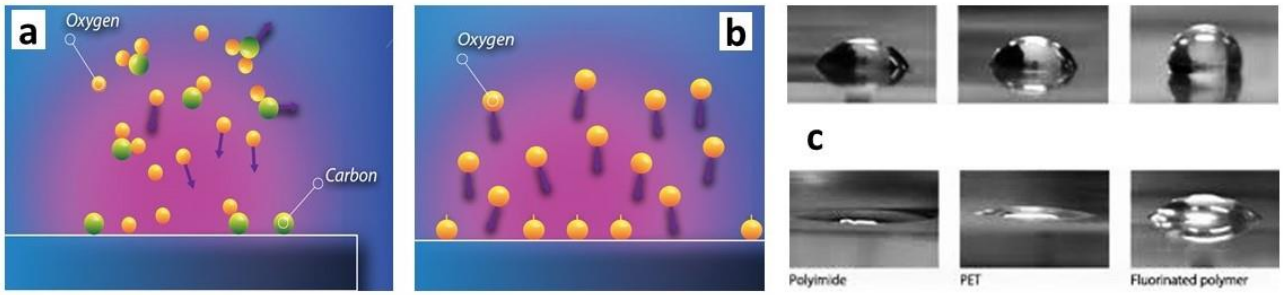

Figure 1.3-13: a) cleaning treatment with plasma method; b) surface activation via plasma treatment methods; c) different surface wettability of different polymers after the plasma treatment.

1.3.4.2: Post-Treatment

Surface Post treatments are sometimes needed for practical applications of the whole device that has been fabricated over a material surface. In particular, they are useful when coating/encapsulation steps are needed to protect the active part of a device, or when several layers must be prepared and treated for achieving one fully operative device, as is often the case for organic electronics. For example, a flexible multi-layers OFET (*figure* 1.3-14) contains several layers, each with a different function.

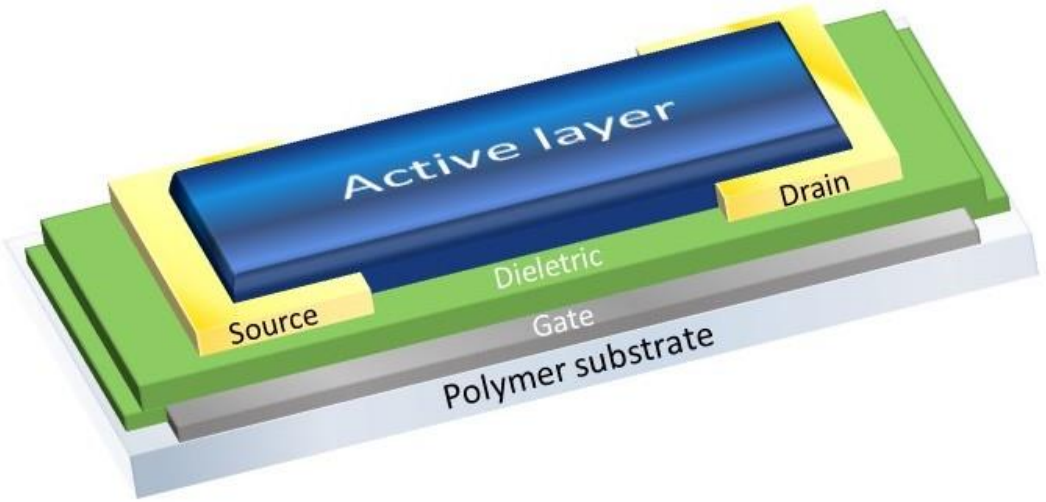

Figure 1.3-14: scheme of a flexible OFET. It is formed by a polymeric substrate, a metallic gate (normally gold, silver, aluminum PVD), dielectric layer that separate the gate from the electrode (source and drain), and an active layer that connects the electrode.

Each of these layers needs a cleaning procedure, a pretreatment and a post-treatment, and the sub-sequent deposition of a new layer on top of the upper one until the device is complete, although not all layers need the same types or number of cleaning and pre/post-treatments, especially considering that some of them can damage the sample.

A typical example of a post-treatment is the coating of the surface with a protection layer against environmental conditions. This is typically used in anti-corrosion protection as the first barrier, which is normally made throughout organic solvents that evaporate living pigments and throughout solid charges that increment the total water and oxygen path until the metallic surfaces. Anti-corrosion coating need a pretreatment of the surface to increase the adhesion, and it is normally used in the naval field against aggressive sea environment. Another example of post treatment before use of the sample is the surface cover with organic molecules that increase the adhesion between organic/inorganic surfaces [142] as show in the *figure* 1.3-15, where the used

molecules increases the wettability of the resin composite and at the same time react with the same resin to generate a strong covalent junction. This technique finds a wide application in the medical field, particularly in the use of orthodontics pins.

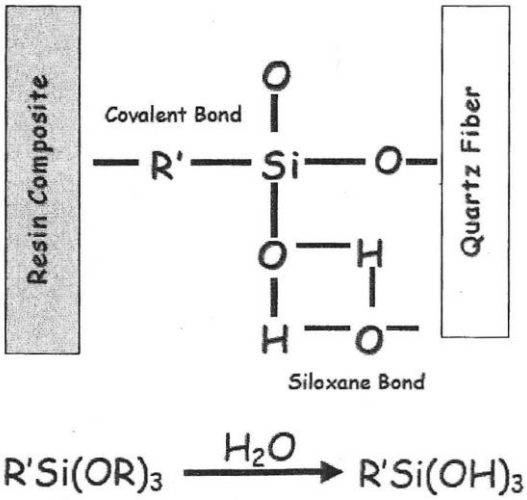

Figure 1.3-15: scheme of the junction between quartz fiber and resin matrix, in which an organic monolayer increases the adhesion.

1.4: SELF ASSEMBLED MONOLAYERS (SAMs)

Nanoscience is the science field that studies materials with sizes in the range from a few to a few hundreds nm. The physical and chemical properties at this scale are completely different from those at the macro/bulk scale, and the surface phenomena become predominant with respect to the volume ones. Also, the gravity force doesn't have the same intensity as in the macro scale. A key role in the development of nanostructures is played by chemistry, that can destroy or create bonds between atoms, create well-ordered or amorphous structures, change the active groups on molecules. Creating nano-crystals, nanowires, nanotubes, specifically tailored polymers. These structures can be used as catalysts, charger transporters, surface modifiers. Research in this field is helped by the development of new tools for the characterization of nanoscale structures. Some of these tools can even manipulate the atoms, move them, and reorganize them on the sample surface. The AFM (Atomic Force Microscopy) and the general class of scanning probe techniques are two examples of these techniques [143]. Among the most studied nanostructures, which can be characterize also with scanning probe techniques, Self-Assembled Monolayers (SAMs) hold a privileged place.

1.4.1: WHAT ARE SELF ASSEMBLED MONOLAYERS?

Self-Assembled Monolayers (SAMs) are monomolecular layers made by organic molecules, with different sizes and functional groups, adsorbed on a surface (usually based on metals or oxides). SAMs have a headgroup with a specific affinity for a substrate, and a functional group that changes the chemical characteristics of the original substrate surface (*figure* 1.4-1). It is possible to change the chemistry of all the surface or only a specific part of it, using proper SAM patterning techniques. SAMs organizes spontaneously in crystalline or semi-crystalline structures after the deposition via solution or gas phase [143]. The average thickness of the organic substrate is in the range of 1-3 nanometers, depending on the size of the used molecule. There are specific headgroups for each type of metal or oxide surface, for example thiols create strong bonds with noble metals as gold [144], platinum [145] and palladium [146], but also they can bond with copper, silver [147], lead and mercury [148].

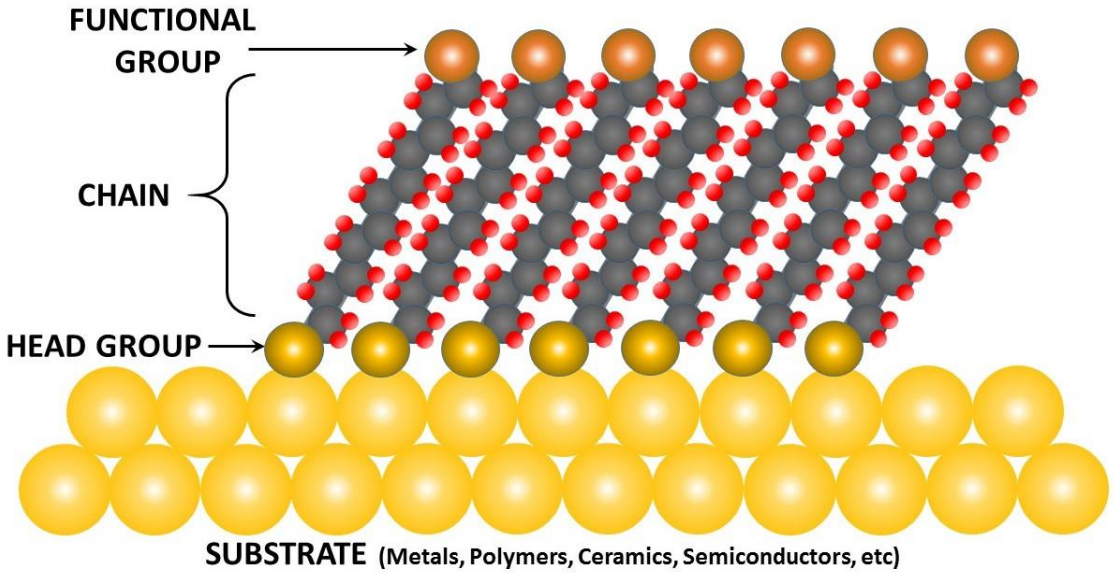

Figure 1.4-1: scheme of the SAMs main part.

SAMs can be easily prepared. Though it is possible to fabricate them in vacuum, they can be deposited also by solution processing or by gas phase [149, 150, 151]. An accurate choice of SAMs can help to protect the substrate from the external environment, and modify the macroscopic physical properties as wettability (*figure* 1.4-2), friction or adhesion. Given the extreme versatility of organic compounds, which structure can be tuned via organic synthesis, SAMs can change a surface from hydrophobic to hydrophilic just varying a functional end group from a polar to an apolar one [152]. On the other hand, this occurs leaving the material's bulk properties unchanged, like for example the transparency for a glass sheet treated with hydrophobic SAMs, that via wettability changes induce self-cleaning properties.

Figure 1.4-2: digital photo of a surface with and without SAMs treatment to decrease the solvent wettability.

1.4.1.1: Key substrate features for proper growth of SAMs

The substrate has a very important role in the choice of the correct headgroup for the SAMs to be used in a surface functionalization. Most often, the substrate choice is a constraint imposed by

the research purpose or by the sample application. The materials used for the substrates are normally metals deposited by PVD or e-beam on a support that can be glass, silica or mica. A particular mention is needed for gold, that is the most used substrate in SAMs research, and became a kind of standard surface for these studies [143].

The motivations for its success are:

1. It is a noble metal, and as such it is inert. Therefore, it does not have any oxide layer on it, and it does not generate any dangerous effect in biological environment. For these reasons, it is historically the most investigated one;
2. It is extremely versatile; it is possible to use it as a colloidal solution of nanocrystals or as thin films deposited by PVD.
3. There are a lot of headgroups that can bond with it, and it doesn't start any secondary chemical reaction.
4. Gold is a standard substrate used also for a huge number of spectroscopic techniques.

The metallic films used for SAMs deposition films have often (1,1,1) dominant textures on glass, or (1,0,0) for gold in specific cases [153], and are rarely perfectly monocrystalline, unless specific deposition techniques are used; indeed, they are usually polycrystalline, with the final grains sizes and structures depending on the type of substrate, on its temperature [154.] and on the incident angle of the metal flux [155]. High temperatures increase the size of the grains and change their shape, from round to square, while an increase of the angle leads to the decrease of their size. Another parameter influencing the grain size is the melting temperature of the materials, especially for metals, that are deposited by PVD. Metals with high melting temperature as palladium (1552°C) or platinum (1772°C) tend to grow small grains, while metals with low melting temperature as gold (1064°C) tend to grow small ones, in the same deposition conditions.

The grain size is very important for the SAMs growth. Substrates with small grains have little roughness, which limits the variability of the outcome of SAMs growth procedures in terms of coverage, time needed for full monolayer coverage, defectivity and general SAMs organization degree. The size of the grains can be modified with different methods to obtain a flat surface: i) Thermal annealing [156]; ii) Chemical recrystallization [157]; iii) Electrochemical polishing [158]. If the support is mica it is possible to use a method called template stripping, that can reduce the surface roughness down to 1 nm [159]. As showed by the *figure* 1.4-3, the mica, that has a

roughness in the range of 0,2 nm [160], is covered by a PVD gold layer, with a thickness in the range of tens of nano-meters. The free metal face is junked via epoxy glue on the substrate, and when the glue is completely dry the mica is removed with mechanical method. Ideally the new gold surface has a roughness down of 1 nm, and it is perfectly clean and flat [161].

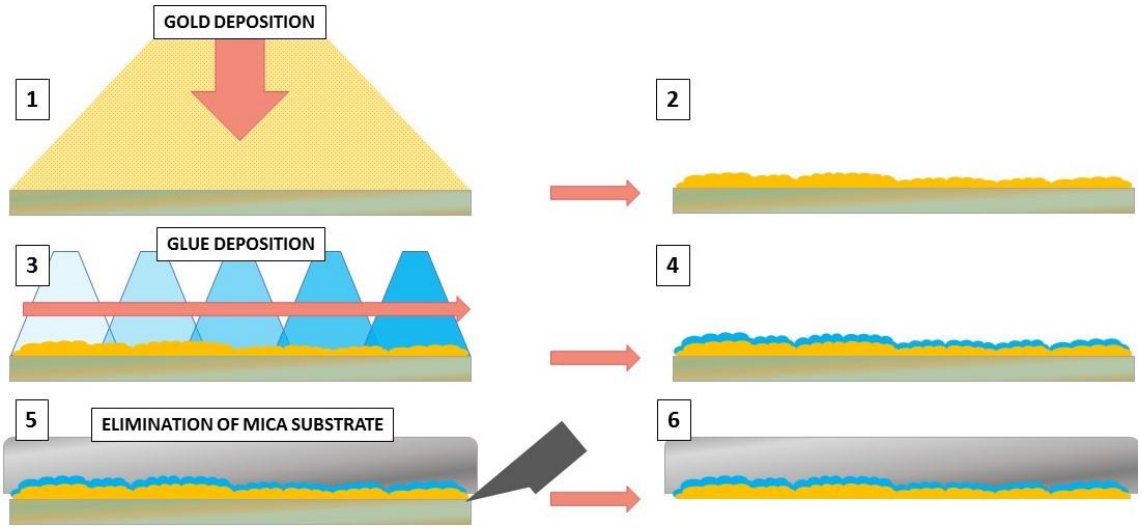

Figure 1.4-3: schematic representation of the template stripping method.

After the surface deposition and possible treatments to decrease its roughness, the last fundamental step prior to SAMs growth is the surface cleaning, which removes the impurities allowing the surface to properly host the SAM. Details about the possible cleaning methods have been given in par. 1.3.

1.4.2: SAMs DEPOSITION

SAMs can be deposited via liquid or gas phase. The gas phase deposition must be carried out under UHV and it is generally used for specific spectroscopic analyses, while the liquid-based deposition is very simple, low cost and does not require any peculiar tool. The Gas Phase approach is carried out in vacuum (usually ultra-high, i.e. 10^{-9} mbar) inside a dedicated chamber, otherwise the organic molecules can interact with atoms, molecules and impurities (normally present in the atmosphere). For the Gas Phase deposition to be effective, the SAM-precursor molecules must have less than 10 carbon atoms (while Liquid Phase deposition does not have this limitation. This

method is mostly used to prepare SAMs aimed at fundamental studies, like the dynamics of the self-assembly phenomena [162].

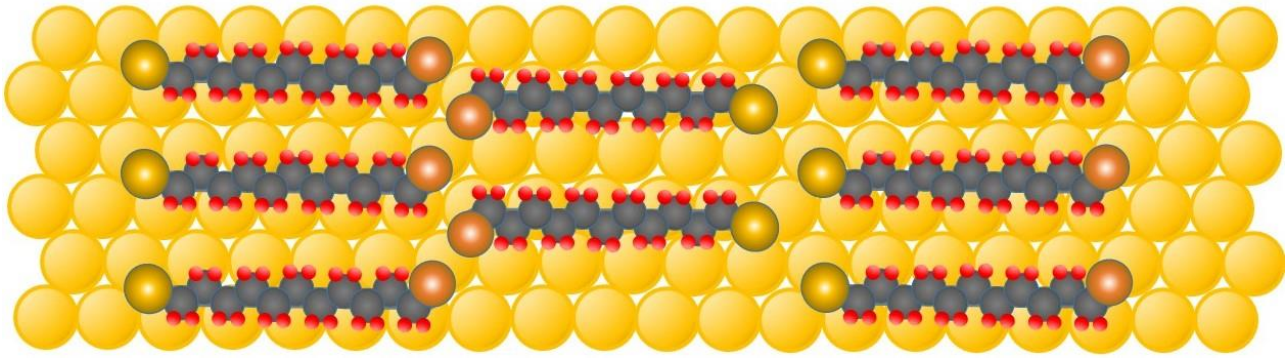

Figure 1.4-4: schematic representation of the SAMs alkane-chain lying flat on the surface.

In gas phase deposition method, normally the SAM has a complex kinetic growth, before a complete and compact mono-layers there are one or more intermediate low-coverage phases so-called striped phases. Here the SAMs, specifically the alkane-chain SAMs, are lying flat on the surface (*figure* 1.4-4). The transition phases between the striped one to the compact layer became a significant kinetic bottleneck at the lengthening of the alkyl chain. The steric hindrance and strong chain-metal interaction reduce the kinetic of the assembly for long chain [163, 164].

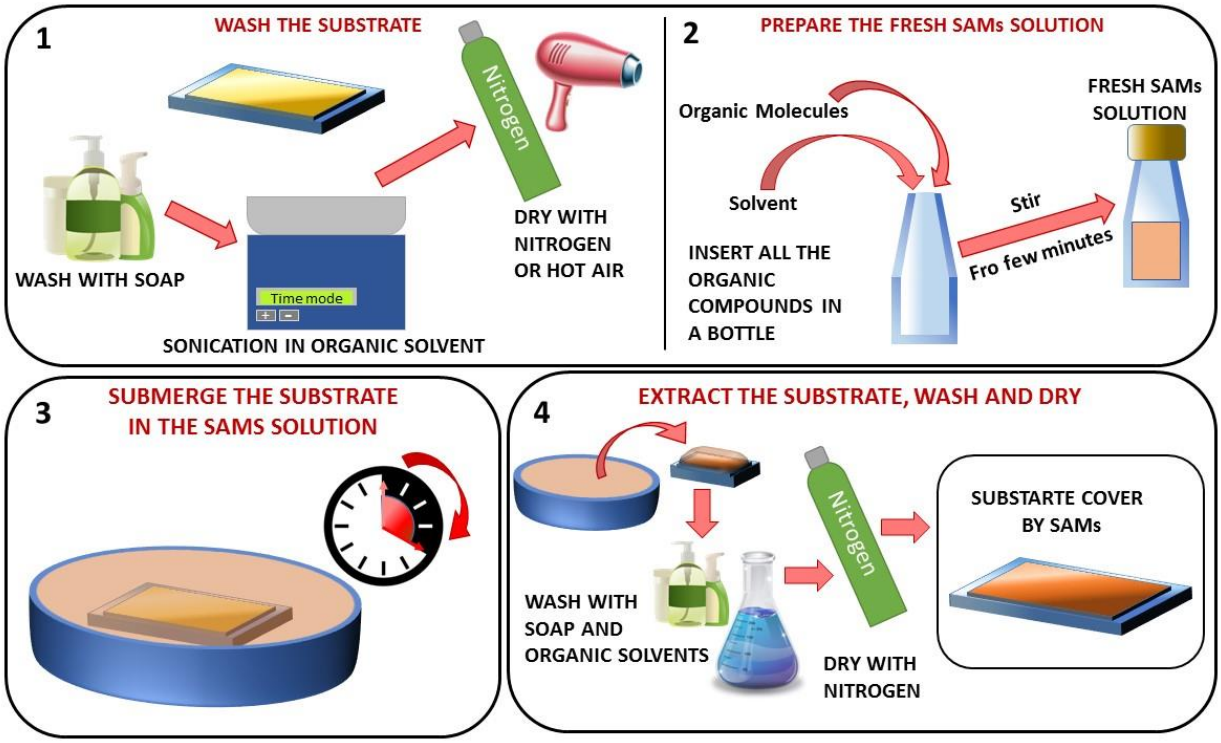

Figure 1.4-5: practical procedure to cover a surface with SAMs via solution method.

The Liquid Phase is the most common method used to deposit SAMs. The organic molecules are dissolved in alcohols, usually it is ethanol because: i) it has low toxicity; ii) It can be solvated the main part of SAMs with complete different polarity od chain length; iii) It is cheap; iv) it is available with high purity. The concentration range is 1 to 10 mM of SAMs molecules. The practical procedure (*figure* 1.4-5) is very simple, involving the submersion of the selected substrate in the SAMs solution. Then the system is left undisturbed for the time needed for the formation of the SAM-surface bond formation (hours/days, depending essentially on the SAM/substrate couple and on the degree of SAM packing perfection required), and the so-treated substrate is extracted, washed to eliminate the unreacted organic molecules and dried. After these operations, the sample is done and ready for the application or the characterization. It is interesting to know that in a few minutes of immersion, the SAM-precursor molecules already cover all the surface. However, after this time they aren't well ordered, and it is necessary from 12 hours to 10 days to obtain a well-organized and compact (almost crystalline) monolayer [165]. In addition to the immersion-time, other parameters influence the outcome of the liquid phase SAM growth procedure. The first and most important variable is the solvent type, as this modifies the kinetics of SAM formation and its assembly mechanism, even though up to now on this point there are only semi-empirical evidences. For example, alkane thiolates have a SAMs formation rate faster in very polar solvents than in alcohols [166, 167], and ethanol solution promotes the formation of compact and order thiols layer better than organic solvents [168]. Moreover, the rate of adsorption of the SAM-precursor molecules on the substrate surface disperse in a hydrocarbon solvent decreases due to the strong solvent-SAM interaction that tend to hinder their access at the surface [168]. In this case the possibility of defects in the film is very high, even though these problems can be minimized increasing the immersion time.

The temperature is another fundamental variable of SAM formation. High temperatures in the first minute of the immersion can support the absorption of the molecules on the substrate and the chains reorganization [169]. In fact, above about 25°C (or 298,15°K) the kinetic energy of organic molecules is sufficient to reduce the number of defects and to increase the growth rate, allowing easier de-absorption of the solvent from the substrate, and the overcoming of the energy barrier of the SAM-surface bonding process [170]**.**

Concentration of the precursor molecule and immersion-time are inversely related. High concentrations allow a short immersion-time to grow monolayers with good surface coverage and arrangement, while low concentration require longer immersion times [171]. The typical surface

density of SAMs having an alkylic chain on gold is about 4,5 x 10^{14} molecules/cm^2 [172], so 1 µM is a typical minimum solution concentration for achieving good quality monolayers. In general, for 1 mM solutions the time needed at room temperature (20°C) for a complete surface cover is in the order of 12 to 18 hours; the maximum immersion-time after which no further meaningful rearrangement is found is about 10 days [165].

The presence of the oxygen inside the solution decreases the SAM formation rate and arrangement reproducibility [146]. The thiols, in specific the alkanethiols, are sensitive to the presence of oxygen inside the solution. The combination between the ambient light and the oxygen promotes the formation of sulfonates or to disulfide bridges introducing defects inside the monolayer [173, 174]. A degassing with inert gas and a following preservation in an inert atmosphere at dark are hence recommended. Apolar solvents as N-hexane or toluene are a good solution to decrease the presence of oxygen inside the solution, but on the other hand the apolar organic solvents can be affected the final SAMs structure and compactness, as said before.

Finally, the purity of the solution/SAMs [146] and the cleanliness of the substrate are the last two most important variables. The presence of impurities in both the solvent and the precursor molecules and on the substrate, can damage the SAM precursor molecules and promote the formation of dimers, as well as cause disorderly arranged layers.

1.4.3: CHARACTERIZATIONS OF SAMs STRUCTURES

The structure of SAMs have been investigated deeply since their discovery, with particular reference to the correlation between their final arrangement and the different variables influencing the self-assembly phenomena. Since SAMs are exquisite nano-sized layers covering often several cm2 of substrate, to thoroughly characterize a SAM it is necessary to combine different complementary techniques, truly ranging from the macro to the nano-scale.

The main tools used to carry out these investigations are scanning probe microscopies such as Atomic Force Microscopy (AFM) or Scanning Tunneling Microscopy (STM) and ultra-sensitive surface characterization techniques, like X-ray Photoelectron Spectroscopy (XPS) or UV Photoelectron Spectroscopy (UPS), as well as humbler but still effective approaches like the determination of contact angles.

AFM and STM create a direct image of the layer structure. With AFM, it is possible to see the defects, the presence of impurities and the crystal organization lattice [175]. The negative point of this technique is its resolution, perfect for the atomic scale but not able to catch the SAM organization over a large surface. The same problem affects STM [176], which has an even better spatial resolution than AFM, down to sub-Å resolutions. Therefore, STM is very useful to study the details of the single molecule-substrate interactions, but ill-suited for broad views of large areas. Moreover, since STM is effective only with conducting or semiconducting materials over large substrate-tip distances, it can be used with insulating SAM-precursor molecules only if chain isn't longer than 12 atoms [176].

Diffraction techniques are used to investigate the 2D structure of SAMs. For example, LEED (Low-energy electron diffraction) [177, 178] can show the reciprocal lattice of SAMs, but its spatial resolution is limited to 100Å. LEAD (Low-energy atomic diffraction) [179, 180] has the same problem of resolution of the LEED but has a greater surface sensitivity and uses a lower X-ray energy. GIXD (grazing-incident X-ray diffraction) [181, 175] has the best resolution compared to the previously mentioned techniques, and the possibility to use a scattering theoretical approach to examine the signal and the surface characteristics. Therefore, it is one of the most used characterization techniques for SAMs.

Spectroscopic methods as Infrared Spectroscopy (IR), Raman Spectroscopy, or XSP combined with diffraction methods, give lots of information about the SAMs structure, characteristics and properties. For example, IR finds information on the structure, as the chain orientation and inclination [182]. XPS can give information about the binding energy and the work function of the new surface, but not only: it is possible to evaluate the atomic composition of the film perpendicularly to the surface [Duwez, A.-S. J. Electron Spectrosc. Relat. Phenom. 2004, 134, 97]. The main problem is the interpretation of the data due to the attenuation of the photoelectron signal of the atoms on the substrate surface by the overlapping organic material. All the diffraction and spectroscopic techniques, in comparison with the scanning probe-based ones, give information about the SAM structure characterized by being averaged over the whole SAM surface, hence including also possible impurities and defects, and therefore they are useful for investigating the general properties of a SAM-covered area, rather than precise parts of the considered monolayer.

1.4.3.1: Contact Angles Measurement

One of the most frequent uses of SAMs is to change the chemistry of a surface, in particular its wettability, to promote or depress the adhesion/contact of a material layer to be put in contact with the surface. The contact angles measurement is an old, rapid and inexpensive macroscopic technique to determine the changes in surface properties occurring upon SAM-functionalization, including the surface energy, via the Young equation (1.3.3 part) [183].

A contact angle definition can be found into the Surface Science Techniques book [184], and it is: "*The contact angle is defined as the angle formed by the intersection of the liquid-solid interface and the liquid-vapor interface (geometrically acquired by applying a tangent line from the contact point along the liquid-vapor interface in the droplet profile)*"; is possible to see the representation of this definition in *figure* 1.4-6.

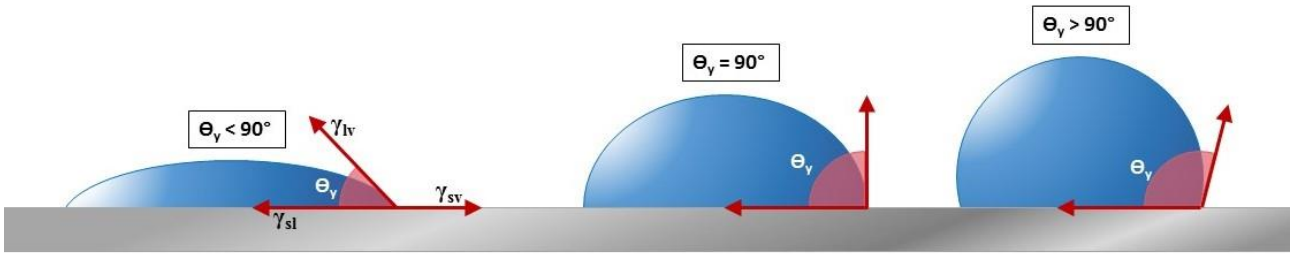

Figure 1.4-6: representation of the contact angle as a tangent line of the drop, with different inclinations. Here γlv, γsv, and γsl represent respectively the liquid-vapor, solid-vapor, and solid-liquid surface tensions; Θy is the contact angle

High wettability surfaces promote extensive spreading of the above lying liquids over it with a resulting small contact angle, near to 0° (*figure* 1.4-6). When the surface is solvo-phobic the final angle has a value over 90°, while in the extreme case of super-solvo-phobicity the angles is over 150° and the drop on the surface shows a near spherical shape [184]. This behavior depends from the interaction between the solid surface atoms, the liquid surface atoms and the liquid vapor in the environment. All the molecules inside the bulk of the liquid drop interact with the neighbors, realizing a force balance equal to zero, while the surface molecules don't have a complete shell of neighbors, generating a not zero force balance (*figure* 1.4-7). This imbalance produced drop contraction: volume is reduced as much as possible and drop assumes the shape of a sphere in order to increase the Volume/Area ratio, and, in consequence, to decrease the total surface tension. This tendency is generally mitigated by the underlying substrate, that can interact with the drop surface molecules, helping the drop contraction (solvophobic surface) or its spreading (solvophylic surface). Therefore, the contact angle gives an average measure of all the forces

involved, internal and external (as gravity), inside a given solid-liquid-vapor system closed in a specific environment/system [185].

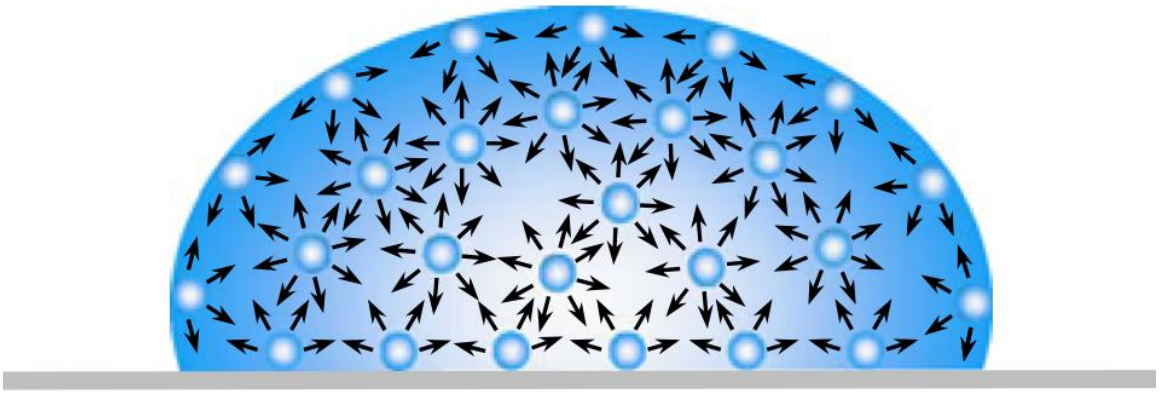

Figure 1.4-7: : schematic representation of the interaction of the molecules inside the bulk of a liquid drop and in the border part where there isn't a complete shell of neighbors molecules.

The Young's equation describes this specific system using a comparison between the cosine of the contact angle and the equilibrium of the three interfacial tensions, as shown in the formulas (12) and:

$$\cos\theta_y = \frac{\gamma_{sv} - \gamma_{sl}}{\gamma_{lv}} \qquad (12)$$

The determination of the solid surface tension is the most important application of the contact angle technique, because this is the easiest indirect method to achieve this valor [186]. Zisman and co-workers were pioneers in the contact angle interpretation (part 1.3.3), and from the combination of the Young and Zisman work numerous methods and theoretical calculations have been developed. One of the most important works in this sense is that made by Kwok and Neumann [186]. They developed a criterion to measure and interpret the contact angle results using the Young's equation. Postulations of the criteria are:

- The reference liquid is always pure;
- The Young's equation is valid for calculating the surface energies starting from experimental contact angles;
- The solid surface tension is always lower than the reference liquid surface tension;
- γ_{lv}, γ_{sv}, and γ_{sl} are considered constant during all the experiment;
- The solid-vapor surface tension is considered constant and independent from the used liquid.

These criteria are perfect for correct and reproducible measures, but the considered solid surface should be inert to the liquid, smooth, rigid and homogeneous, and this doesn't represent a real condition.

The Young's contact angle $\boldsymbol{\Theta_y}$ isn't the only possible contact angle because the Young's experiment provides an ideal system with a smooth surface and static measurements. To have more information about a given surface it is possible to measure the dynamic contact angle, in which a drop of reference liquid is expanded and contracted on the surface (*figure* 1.4-8), giving respectively the advancing $\boldsymbol{\Theta_a}$ and receding $\boldsymbol{\Theta_r}$ contact angle. In this case the difference between the two angles is called hysteresis (***H***) and its formulation is (13):

$$H = \Theta_a - \Theta_r \quad (13)$$

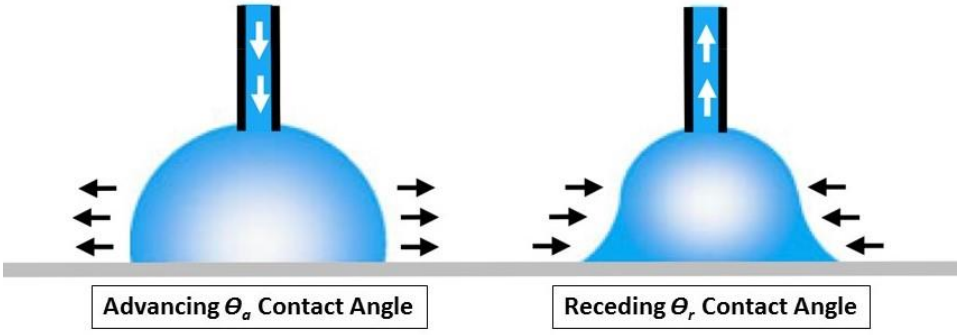

Figure 1.4-8: expansion and contraction of a drop of liquid on a surface for the measures of advancing Θa and receding Θr contact angle.

The hysteresis depends by the roughness and the chemical heterogeneities of the surface that are considered as motion barriers for the drop movements. Recent studies confirm also that the contact angle hysteresis depends by the combination between the nature of the solvent (polar, apolar) and the substrate surface energy [187]. For example, the pinning of the edge drop line on hydrophobic and superhydrophobic surfaces promotse the hysteresis, as Krumpfer and McCarthy showed [188].

A good approximation on contact angle on rough surface can be obtained using the Wenzel [189] or the Cassie-Baxter angles [190], even though there aren't established guidelines to correctly identify the limits for which a surface works perfectly. The essential rules usually followed in these determinations are: i) the surface must be as smooth as possible; ii) all the possible external presence on the surface should be removed (as dust, dirt, ect.); iii) the reference liquid must be inert as possible.

Contact angle measurements can be used to compare different surface treatments comparing the different surface free energy that these substrates have. All the problems about the substrate heterogeneity are bypassed because the only important result is the $\Delta\Theta_y$ between the sample before the surface treatment and that after the surface treatment. For example, it is possible to understand in this way which chemical surface treatment gives the better wettability or the lower surface energy, or if different roughness can appreciably affect the junction between different materials. The strengths of this comparative approach are its easiness, low cost equipment, rapidity in obtaining the results.

Figure 1.4-9: digital photo of a modern telescope-goniometer

The contact angle measuring methods are several, but the most widely used technique is the direct measurement with a telescope-goniometer of the three-phase point on the profile of the sessile drop. Sessile drop means a perfectly blocked drop onto the substrate. The first commercial equipment for these measurements was made by W.A. Zisman in 1960s. The equipment is made by (*figure* 1.4-9): a sample-holder, where it is possible to mount both liquid and solid samples; a microscope with a back illumination source; a micrometer pipette to deposit the drop. The measure is simple: after the drop deposition the drop profile must be aligned with the protractor, and from that it is possible to read the tangent angle. Nowadays the reading, after the correct sample positioning, is carried out by a computer program, decreasing operator error. The advantages of this method are mainly the simplicity and the low amount of wasted materials (only a little drop and a small substrate are needed). On the other hand, there is always the possibility of liquid-surface contamination, that would affect the measurement results, and the quality of the result depend by the operators' abilities. Moreover, this technique hasn't a good accuracy in the case of small angles (below 20°), due to the too flat drop profile, that generates an uncertainty in

assigning the angle tangent [184]. The evaluation of the contact angle depends also from the drop volume [191]. The accuracy of the measure is generally in the range of ±2°, which is acceptable for most applications [192].

1.4.4: STRUCTURE OF SAMs

SAMs are characterized by a head group, that establishes bonds with the substrate, and by a terminal functional group, and both are connected by an intermediate chain, which can be of different chemical nature (*figure* 1.4-10).

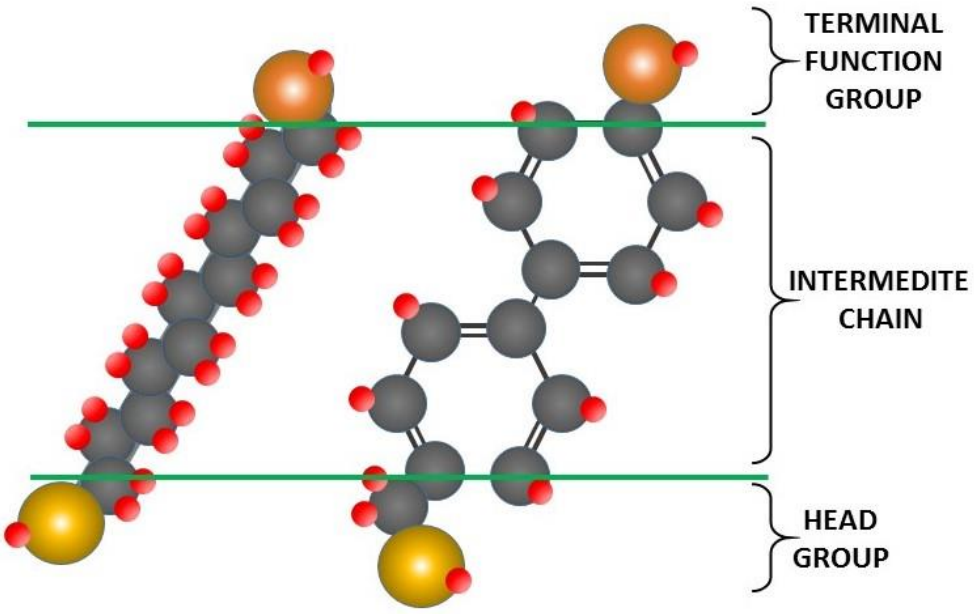

Figure 1.4-10: schematic illustration of two organic molecules with the same functional and head group but different intermediate chains.

The 2D structure of SAMs is described by the packing of the chains, their crystalline order, the symmetry, and the lattice parameters, while the tilt angles (θ), the tilt direction and the twist direction (β) describe the arrangement of molecules inside the structure (*figure* 1.4-11 "a"). As mentioned before, gold became a standard substrate in SAMs description and analysis, and for this reason the here considered substrate is the (1,1,1) gold. Linear alkylic-chains are the simplest type of intermediate chains used in SAMs. In this case, the maximum surface density of molecules (i.e., the best packing) attainable depends on two parameters: i) the distance among the metal atoms on the surface; ii) the position of the head atoms on the metallic lattice. Investigations via diffraction techniques showed that a $(\sqrt{3}\times\sqrt{3})$ R30° (R = rotated) lattice is established on the

surface when the n-alkylic chains are long 10 carbon atoms, that is the shortest chain length which produces to have the n-alkane-chain high-quality packing [193, 194] *figure* 11-1.4 “b”[195].

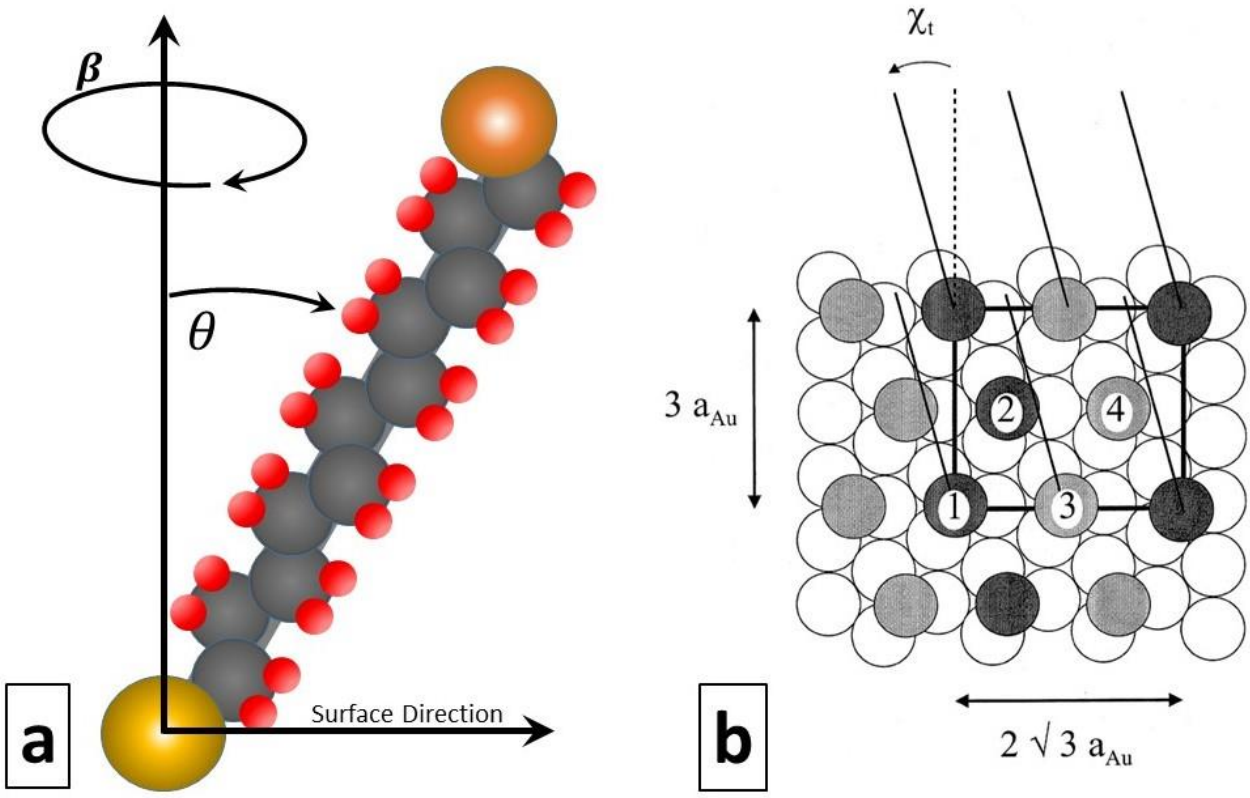

Figure 1.4-11: a) schematic illustration of the tilt angles (ϑ) and the twist direction (ϐ); b) a n-alkylic chain with 10 carbon atoms (√3×√3) R30° (R = rotated) lattice.

A super-lattice structure c(4 x 2) is also found, and its presence is supported by STM investigations [196]. In the ($\sqrt{3}\times\sqrt{3}$) R30° conformation, the area for each molecule is 21,6 Å and the distance among them is around 5 Å. With reference to *figure* 11-1.4 “a”, the average tilt angle θ of molecules is 34°, while the twist angle β is near 50°. θ and β angles are not the same for all the metals surfaces. For example, θ is 10° on silver and 0° on mercury, due to the different lattice characterizing each metal. The intermediate chain type modifies both the tilt and twist angles: in general, the presence of aromatic rings originates a tilt angle smaller than the one produced by alkyic chains [197]. This is due to their steric hindrance and to the rigidity of the chain. The length of the chains can also modify the stability of the SAMs layers. A chain with more than 10 carbon atoms has higher stability then a short one, likely due to the lateral interaction among the molecules.

SAMs can have different structural defects. The main cause of defects is the dynamic nature of the SAMs, the chemical compounds employed and the surface structure. As already mentioned, impurities of the compounds used in SAMs preparation can compete with SAMs precursors for adsorption on the metal surface. In addition, defective metal surfaces can also can be transported to SAMs layers. Polycrystalline structures and surface irregularities modify the structure of SAMs, lowering its compactness *figure* 1.4-12.

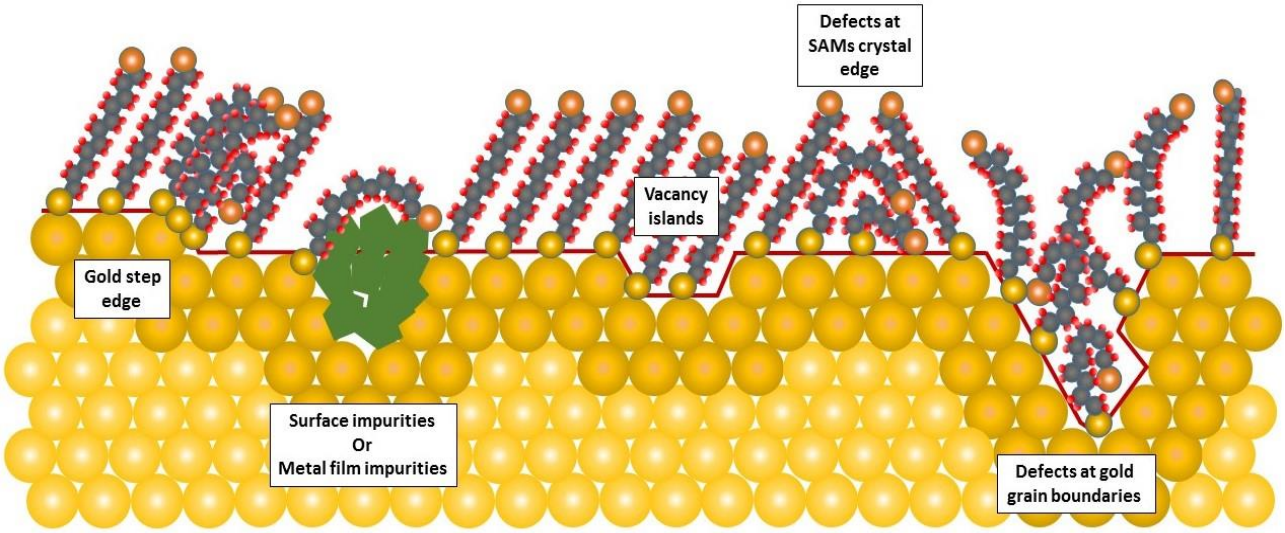

Figure 1.4-12: illustration of the main intrinsic and extrinsic defects present on a polycrystalline substrate covered with SAMs.

1.4.5: APPLICATIONS OF SAMs

SAMs can be used in different technical applications. They can constitute active elements in biological sensors [198], but also SAMs with long alkane-chain (more than 16 carbon atoms) are used as protective coatings against the corrosion [199]. Specific SAMs can change the wettability of the substrate if they expose to a solvo-phobic or solvo-phylic group as shown in *figure* 1.4-13 "a" [200] *figure* 1.4-13 "b" [201]. In the same way, it is possible to modify the friction between two mechanical parts [202]. In certain applications, the presence of SAMs improves the adhesion of completely different materials [203.].

The negative aspect of SAMs is their vulnerability at the degradation, as all organic materials. They don't resist to high temperatures or to strong acid/basic environments, as well as to mechanical solicitations like scratching or relatively high localized pressures. Nonetheless, an

accurate engineering of the device in which they will be inserted (like for example appropriate coating protecting the deposited SAMs) can greatly optimize the final device lifetime.

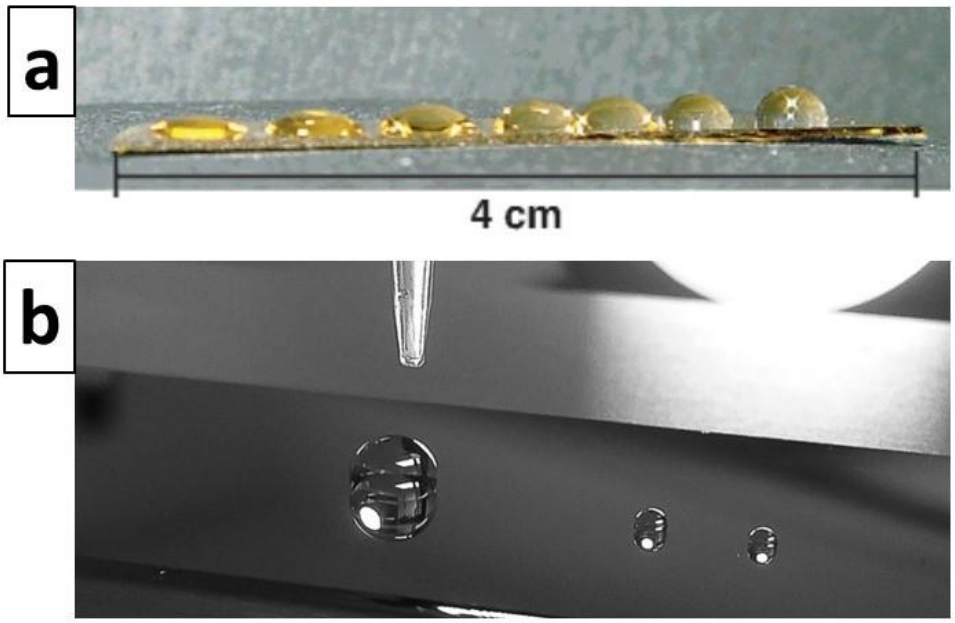

Figure 1.4-13: a) demonstration of a hydrophobicity gradient, measured by the drop spreading; b)high hydrophobic surface made with a complete SAMs coverage.

1.5: GENERAL PROCESSING TECHNIQUES FOR ORGANIC ELECTRONICS

A device is made of different parts and different layers of materials, from conducting to insulating ones, and conductive paths connecting all of them. To deposit each of these parts elements an enormous variety of technologies can be used. Each technology has advantages and drawback, that drive their selection in the device fabrication process. The final structure and the type of materials are the two main constraints in this choice. Also, the economical aspect of a given process, in terms of both capital expenditure and operation costs, must be evaluated in selecting a rational production process.

Leaving aside substrates and finishing steps of a device fabrication, most of the technologies used on organic electronics refer to the deposition of materials, that can be made via vacuum or wet processing. The main differences between these two options are:

- Cost of the equipment: Vacuum processes are more expensive than wet ones;
- Materials: in many cases (excluding most polymers, which can be processed only by wet processing), both processes can deposit the same materials;
- Quality of the materials: In vacuum processes the starting materials must have high purity to obtain a high-quality deposition, while wet processing is a bit more robust in this sense; however, when it comes to the electronic performances of organic semiconductors, high purity is always necessary.
- Cover area: wet processing is better suited than vacuum for covering large areas;
- Precision of the final structure: with some exceptions (like soft lithography), vacuum processes have a better control in the final size and shape of the deposited material

In the following, the most used wet and vacuum processing techniques are described.

1.5.1: VACUUM PROCESSING

1.5.1.1: Chemical Vapor Deposition (CVD)

Chemical Vapor deposition is a technique capable of covering a specific target substrate with a layer/pattern of high quality thin film, based on the reaction of different precursors in gas phase at the interface with the substrate [204]. The reactants in gas phase are mixed together in a reaction chamber, where they react and/or decompose on the substrate and obtain the final solid film. Various types of chemical reactions are utilized in CVD for the formation of solids: pyrolysis, reduction, oxidation, hydrolysis, etc. CVD can create different layer morphologies: monocrystalline, polycrystalline, amorphous, and epitaxial.

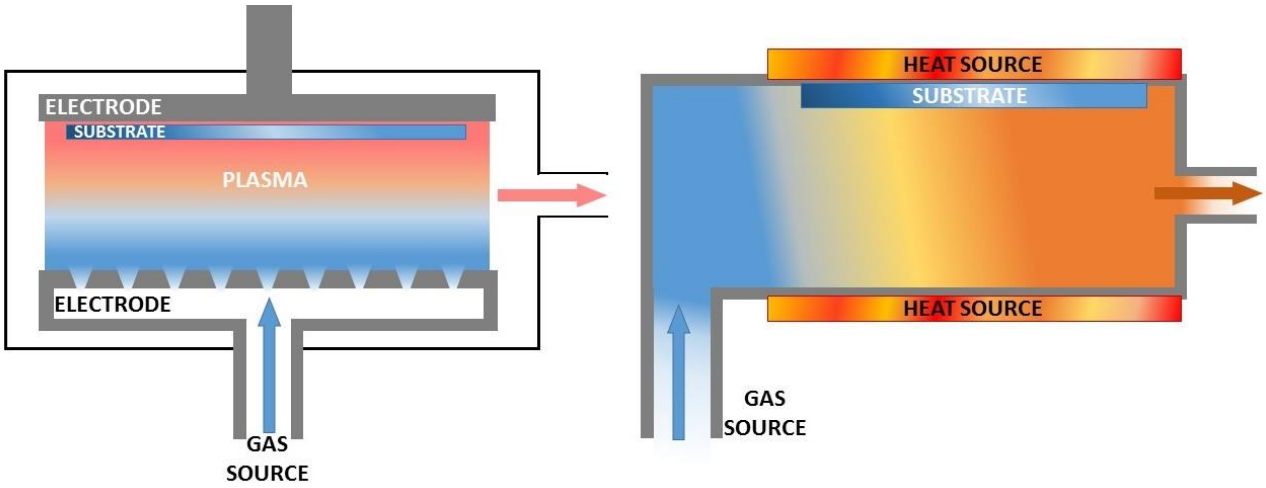

Figure 1.5-1: schematic illustration of the CVD heat and plasma-initiated.

CVD can be classified by the operating pressure inside the reaction chamber at atmospheric, low or ultrahigh vacuum. The choice of one or the other approach depends on the substrate characteristics (lower vacuum usually need higher process temperatures for keeping the chemicals in the gas state, and plastic substrates typically cannot be heated over 150°C without noticeable degradation) and of the type of chemicals used. Heat (plasma, hot filament, combustion CVD) or photo-initiation (UV radiation) are used to start the final decomposition (*figure* 1.5-1).

CVD is normally used to modify the normal characteristics of the surface. Polymer super-thin coating is the most used and versatile process, with which it is possible to obtain lubricity, hydrophobicity, or weather-resistance surfaces in a simple and fast way [205]. In particular, CVD is used to grow the Parylene family polymers, used as encapsulating layers for organic semiconductors. Other common industrial coatings realized by CVD are silicon dioxide, silicon

nitrate, tungsten thin films, diamond. CVD is also a technique of choice for growing carbon nanotubes [206].

1.5.1.2: Physical Vapor Deposition (PVD)

Physical Vapor Deposition is used to deposit thin films of solid/liquid materials on the target substrate via a previous gasification of said materials [207]. The gasification of the material is obtained via physical methods, like i) ion beams, that are directed towards a starting solid material target, that is progressively consumed as the vaporized material leaves it (*figure* 1.5-2) [208], ii) electric evaporation, in which the source materials are evaporated with high power electrical energy (electrical arc); iii) laser pulse, where a high power laser is used to erode and vaporize the source materials. These methods need a high vacuum chamber, not less than 10^{-6} Pa, because the presence of other particles can damage the homogeneity and properties of the thin coating layer.

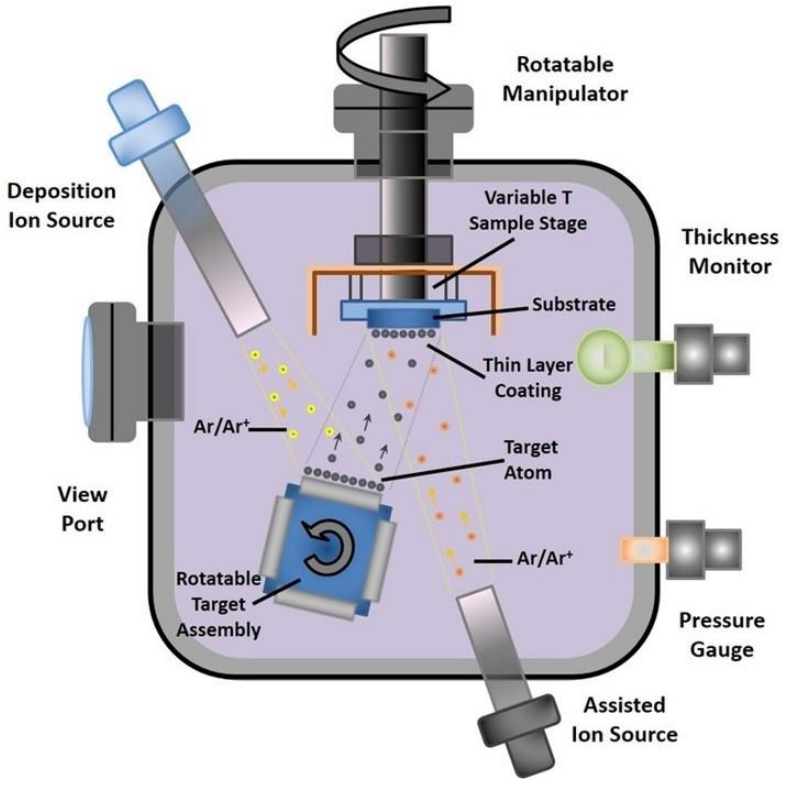

Figure 1.5-2: representation of an ion beam PVD.

PVD is used for coating specific surfaces or part of them for mechanical, optical, chemical or electronic functions. Basically, the choice of coating materials is mainly oriented to metallic-ceramic materials (metals, alloys, semiconductors, metal oxides, carbides, nitrides, cermet, etc), but in recent years also applications realizing PVD of organic semiconductors have been realized, regarding thin films and organic semiconducting single crystals [209]. However, PVD is a high

energy-consuming technique, and a consistent amount of the starting material is wasted (low material yield), especially for organic materials, which are sensitive to thermal degradation. Using appropriate substrate functionalization strategies, it is also possible to use PVD for growing OSSCs in well ordered patterns [210] The adhesion of the so-realized films is usually excellent and it is possible to realize every very thin (down to a few nm) films, with excellent flexibility when deposited on flexible substrates.

The fields of application of PVD are countless, ranging from aerospace (hard and anticorrosion coatings) to biomedicine (coatings for biomedical equipment), as well as in electronics (growth of semiconducting oxide layers).

1.5.1.3: Sputtering

Sputtering is a PVD-type technique where the target material is hit by energized particles [211], and eject the atoms directly against the covered surface (*figure* 1.5-3) [212, 213].

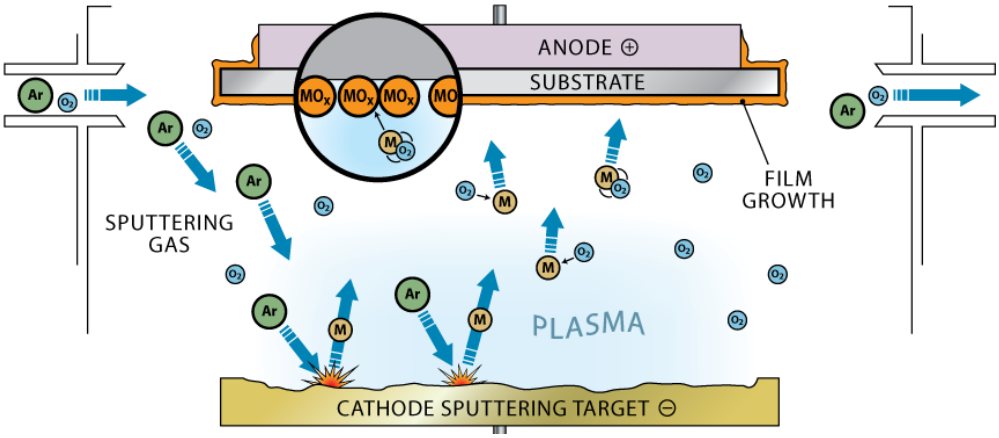

Figure 1.5-3: PVD sputtering method.

The sputtering gases are normally inert gas, as argon, and their choice depends on the atomic weight of the target material. To have a better performance the incident ions should have a comparable mass to the target atoms, and promote the exchange of the kinetic energy among them. Ions can be generated by plasma, ion sources, accelerators or by radioactive materials emitting alpha particles. The ions transfer the energy to the atoms in collision cascade. The sputter yield depends mainly on: i) type of target material; ii) kind and energy of the used ions; iii) angle of ion impingement (*figure* 1.5-4.).

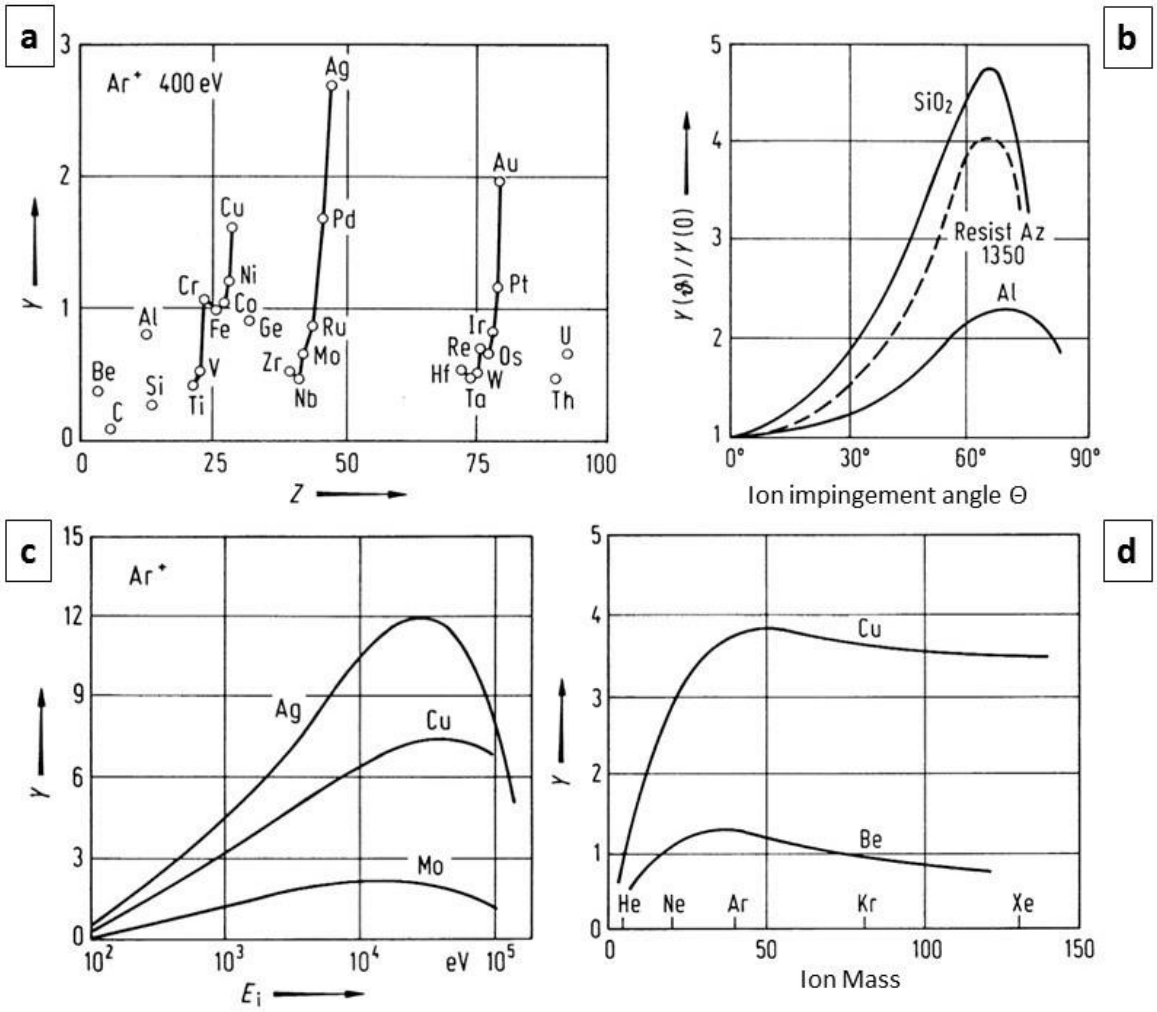

Figure 1.5-4: a) sputter yield Y vs target materials atomic mass Z; b) sputter yield Y vs angle of ion impingement; c) sputter yield Y vs ion energy Ei; d) sputter yield Y vs ion mass.

In organic electronics, the sputtering technique is mainly used in relation with the fabrication of this conducting oxide layers, which are coupled to optoelectronic devices like OLEDs and organic photovoltaic cells.

1.5.2: WET PROCESSING

1.5.2.1: Drop Casting

Drop casting is the simplest method to deposit liquid materials to obtain crystalline, semi-crystalline and amorphous structures. A solution of the material to be deposited is drop on the surface (in the precise position needed), afterwards it is necessary to wait until the solvent evaporates and leaves the material on the substrate (*figure* 1.5-5) [214]. The main advantages are simplicity and material saving. On the contrary, the main limitations are a bad uniformity, poor

thickness control and small area coverage. Thickness mainly depends on solution concentration, while the final morphology depends on solvent evaporation rate, which is influenced by temperature (substrate and environmental) and solvent boiling point.

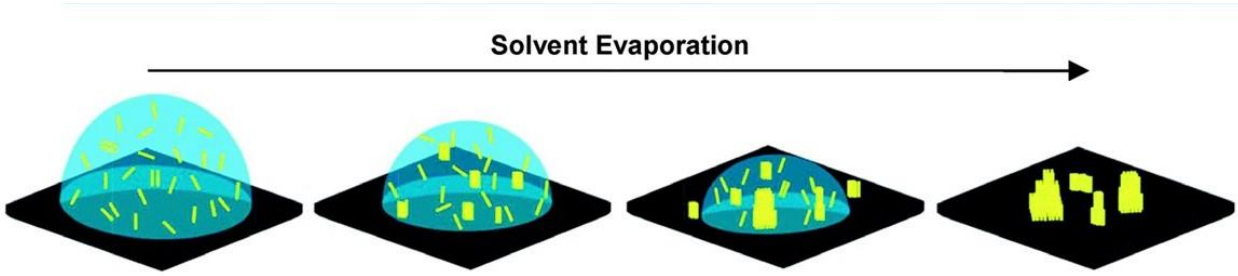

Figure 1.5-5: illustration of material deposition via drop casting method.

1.5.2.2: Spin Coating

Spin coating is a refinement of the drop casting process, used to coat small surfaces with a uniform layer of material. The advantages of spin coating are uniformity, reproducibility and a good thickness control, and with an appropriate optimization it is possible to obtain a thickness lover than 10 nm. The main disadvantages of spin coating are that it is not able to cover large areas and that the greatest part of starting material is wasted.

The process is very simple and it is divided in 3 steps (*figure* 1.5-6) [215]: i) deposition of a drop of the coating material solution onto the substrate, which is fixed to a rotating disc; ii) rotation of the disc onto which the substrate is fixed; during this step the solution spreads on the substrate due to centrifugal force exerted by the disc rotation; iii) evaporation of the solvent (usually during the rotation step, but also after the rotation is stopped).

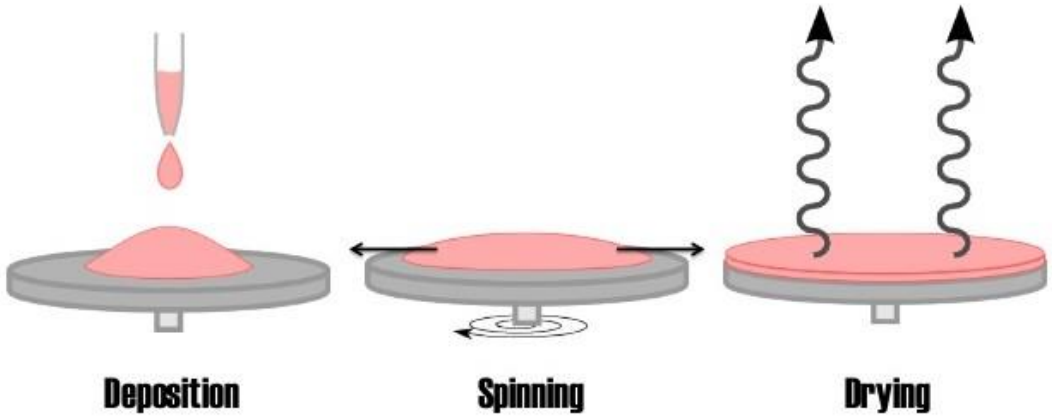

Figure 1.5-6: illustration of the three spin-coating steps, from the left solvent deposition, spinning of the solvent and drying of the resulting material layer.

The main problem of this technique is that the fast solvent evaporation occurring during the rotation step reduces the time for the achieving good molecular ordering in the resulting solid layer. Using a high boiling point solvent during the process allows to overcome this problem [216], and a thermal annealing after the process can help to improve the molecular ordering of the molecules inside the film [217].

The obtained film thickness depends strongly on the fluid viscosity and density, rotation speed, and solvent boiling point. This technique is commonly used in microelectronics industry for the deposition of lithographic masks, and is used in organic electronics to deposit conducting oxide-layers precursors (sol-gel solutions) and organic semiconductors (either polymeric or molecular ones) in thin films. While spin coating allows a very good control over the film thickness down to a few tens of nm and very homogeneous surfaces, it cannot produce material patterns.

1.5.2.3: Spray Coating

Spray coating, as underlined by its name, is a coating technique that covers the substrates with a solution finely dispersed in micro-drops (aerosol) by properly shaped nozzles, thanks to the flow of a carrier gas (*figure* 1.5-7). Once the sprayed solution has dried, a thin solid film is left on the substrate. The film morphology can be controlled by: i) carrier gas pressure inside the nozzles; ii) solution viscosity; iii) solvent boiling point; iv) the nozzles geometry; v) the distance between the nozzles and the substrate. In general, high gas pressures generate small drops of solution, that favor fast solvent evaporation, often occurring directly in the path from the nozzle to the substrate, until reaching the limit of nozzle clogging. If the solution viscosity is increased the size of the drop is increased too; a too large viscosity (exact values depend by a multitude of parameters, ranging from the nozzle diameter to its geometry, and include also the temperature at which the process is carried out) causes nozzles clogging. The choice of a correct main (it is possible to mix several solvents for preparing the solution to be sprayed) solvent can help to avoid clogging, with best options being high boiling point solvents. The geometry of the nozzles can modify the geometry of the flux. Increasing the distance between the substrate and the nozzle enhances the surface area that it is possible to cover with a single spray pass, but decreases the homogeneity and the thickness of the obtained layer.

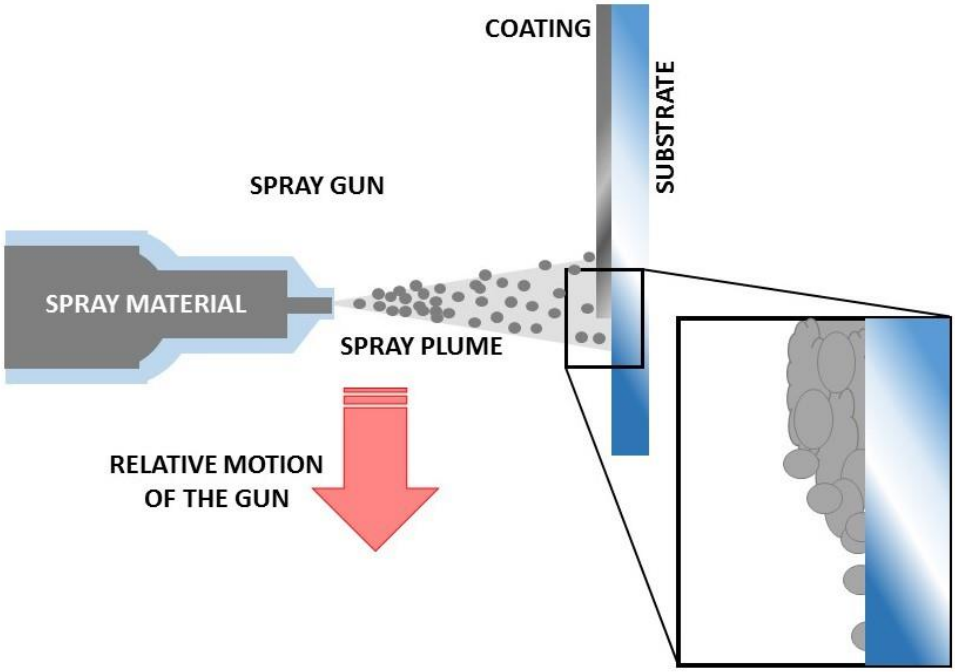

Figure 1.5-7: spray coating schematic illustration.

The main advantages of this technique are: i) high throughput; ii) adjustable film thickness, especially using multi pass approaches; iii) large area coverage; iv) relative independence of the final film topology (for thicknesses higher than a few hundreds of nm) from that of the substrate. Since it is possible that the solution drops arrive onto the substrate being almost dry, the homogeneity of the film is often scarce. In order to avoid this problem, it is necessary to use either high boiling point solvents, or to decrease the substrate-nozzle distance. Another inconvenient of spray coating is that it is not suitable for defining precise material patterns, due to the lack of effective methods to control the actual and precise size of the aerosol cone exiting the nozzle.

Nonetheless, the spray technique is used in almost every industrial field, from packaging to consumer electronics. In organic electronics, it is being explored for plastic solar cells [265], but also applications in the deposition of transparent conducting oxides is being explored. [218]

1.5.2.4: Blade Coating - Die Coating

Blade coating, or knife coating or doctor blading, is a processing method for the fabrication of large area films on rigid or flexible substrates. The ink is placed in front of a fixed blade, and the substrate moves under the blade as in (*figure* 1.5-8 "a"). The thickness of the film is mainly determined by the fixed gap between the blade and the substrate in motion and by the

concentration of the deposited solution layer, that via shrinking due to solvent evaporation defines the final solid film thickness.

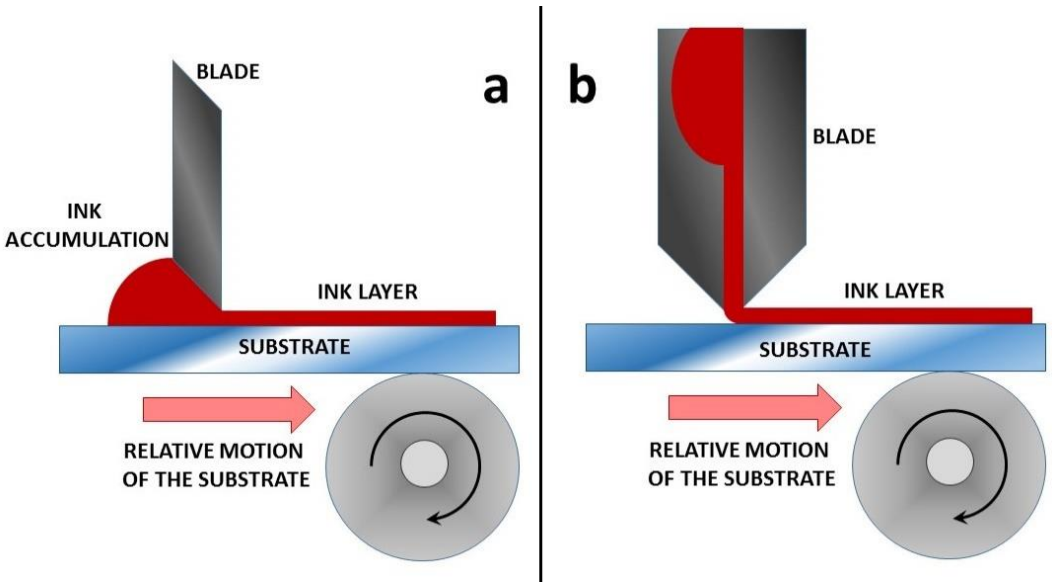

Figure 1.5-8: illustration of a: a) Blade coating: b) Die coating. It is possible to see the main difference between them, the presence of the fluid delivery system inside the die coating that controls the ink release.

The advantages of blade coating are found in a very high throughput, and in the capability to cover very large areas with homogeneous layers. Moreover, in blade coating the material waste is reduced to a minimum. Another positive point is that with this technique it is possible to achieve uniform films with thicknesses as low as 200 nm [219]. It also allows to grow oriented organic semiconductor crystals by controlling the solvent evaporation rate and the solution supply [220]. Difficult in tuning the blade position (the exact planarity with respect to the substrate is hard to obtain) and the viscosity of the ink-solution are the main disadvantages of this technique. In fact, low viscosity solutions do not allow to obtain a uniform layer, while excessive viscosities lead to blade clogging.

The approximate thickness of the dry layer can be calculated with the empirical formula (14)

$$d = (1/2)\cdot g\cdot(c/\rho) \qquad (14)$$

where d is the dry layer thickness, g is the blade gap height, c is the ink concentration, and ρ is the density of the material in the final dry film is g/cm^3.

Die Coating is an evolution of blade coating. In this case the ink is inserted inside a hollow blade, in a fluid delivery system that controls the ink release (figure 1.5-8 "b"). With this approach, it is possible to heat the chamber, thus regulating the ink viscosity, and to insert high viscosity inks,

or even semi-solid inks. The main advantages of this technique are: i) Increase of the production throughput thanks to a well controlled flux of solution and ink viscosity; ii) high degree of control of the coating homogeneity and smoothness; iii) ability to realize layers down to 20 nm-thick with very good uniformity control across the whole coated surface; iv) minimal material waste.

These printing technologies are mainly used for depositing organic semiconductors layers in flat panel displays (LCD, OLED), organic-based photovoltaic panels, OLEDs and LEDs for Solid State Lighting, Polymer Batteries.

1.5.2.5: Dip Coating

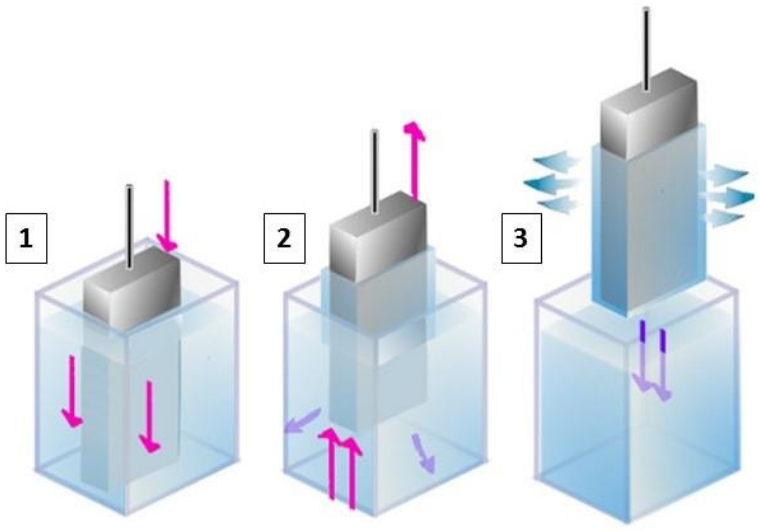

Figure 1.5-9: schematic illustration of the dip coating process: 1) immersion; 2) slow extraction; 3) drying.

Dip Coating is a technique designed to cover substrates with thin films by immersion of the substrate inside a vessel filled with the desired coating solution. The speed of extraction of the substrate must be controlled to form a perfect and homogenous film. The process consists in three distinct phases (figure 1.5-9) [221]: i) immersion of the substrate time needed to favor the coating solution adhesion to the substrate; ii) extraction of the substrate (slow speed), drainage of the excess liquid; iii) evaporation of the solvent. In this way, it is possible to achieve a strict control over the final dry layer thickness [222].

Versatility and ease of implementation represent the main advantages of dip coating technique, as well as the very high uniformity of the film with thicknesses even down to 10 nm, and large area coverages. On the other hand, dip coating is rather time consuming, is a batch technique (i.e., no roll-to-roll is possible, unless very specific and usually poorly effective setups

are used) and delivers a coating layer on both the sides of the substrate. Moreover, it cannot deliver precise patterns, but only uniform coatings.

1.5.2.6: Screen Printing

In Screen Printing the ink solution is squeezed through a screen mask onto the substrate surface, via external pressure applied by means of a squeegee (*figure* 1.5-10) [223]. In some cases, the ink is sprayed instead of being pressed. The ink lying on the mask wets the substrate only in the free apertures of the mesh, originating the desired coating or pattern.

To be effective, the ink must have high viscosity, in order to avoid bleeding through the mask apertures in absence of external pressure. The mask is made by a tensed mesh, fixed to a rigid frame.

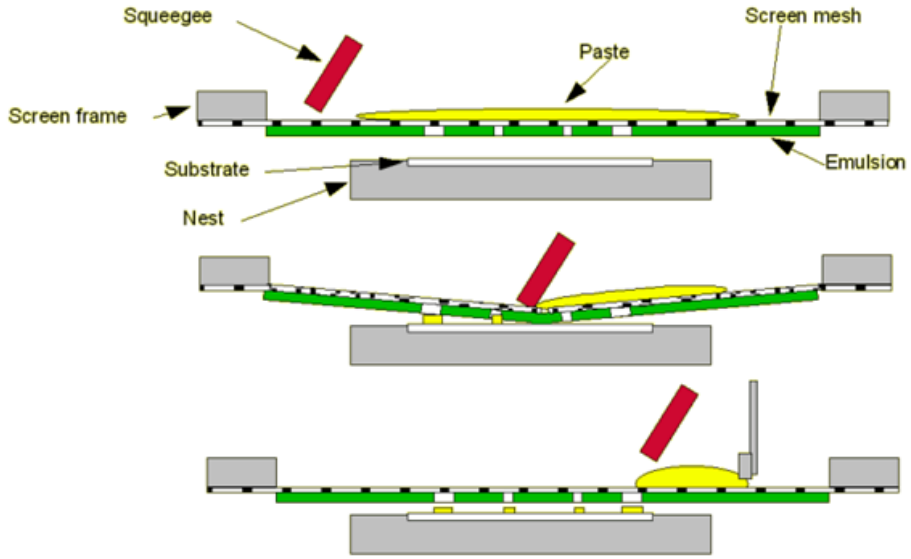

Figure 1.5-10: schematic procedure of screen printing; from the top: i) deposition of the paste on the screen mesh; ii) external pressure applied by means of a squeegee, compressing the paste and the mesh on the substrate; iii) removal of paste in surplus and extraction of the substrate for drying.

The main advantage of this technique is the simplicity of the procedure, while its main limitations are a relatively low resolution (around 50-100 μm) and the high amount of waste material (the viscous ink not pressed through the mask's apertures usually thicken rapidly, and must be periodically removed and thrown away).

Screen printing is very versatile: ink pastes based on conductive, semiconductive or insulating materials can be formulated, based on either inorganic or organic materials. In addition, it is possible to screen print inks on an enormous variety of substrates, including textiles, ceramics, wood, paper, glass, metal, and polymers, and it is usually very inexpensive to implement it. It is

widely used in electronics industry, especially for designing printed Circuit Boards, as well as for all the electronic features (conductive tracks, pads, etc) that do not need fine resolutions. In organic electronics screen printing is being actively investigated for printing organic photovoltaic cells [224].

1.5.2.7: Inkjet Printing

Inkjet printing is based on the controlled ejection of ink drops from a micro-sized nozzle. It is one of the most studied and researched wet processing technologies in the last 30 years. Its success comes from its simplicity of operation, the possibility to deposit several different types of materials (from inorganic to organic ones, and even living cells) with a high precision (down to a few microns). If the ink and the process are perfectly optimized it has a very high throughput. Moreover, the overall printing tools costs are usually much lower than those of instruments exploiting other technologies.

Inkjet printing of organic semiconductors and conductors has been at the center of intense research in the last 20 years [225], and this technique has been central in the development of this PhD thesis work. Therefore, a detailed description of this technique will be given in the next paragraph.

1.6: INKJET PRINTING PROCESS

Nowadays Inkjet Printing (IJP) is one of the most used printing processes in the world, and one of the most patented ones. Inkjet printers are diffused everywhere, for home applications or in high-tech-industries, allowing deposition of biological material as well as traditional inks for typographic printing, with high precision, down to a few tens of microns in terms of lateral resolution (*figure* 1.6-1). IJP has been investigated since 1950's [226] in industrial production, but only since the '80s [227] the real potential of IJP was realized.

Figure 1.6-1: examples of the main applications of the IJP nowadays from books to coins in paper up to clothing.

IJP is considered a simple technology, and the printing head, the substrate and the ink are the main three elements that form the total process. Each of them introduces a set of limitations. The substrate is often constrained by the selected application, and its chemical properties can't be changed, or they can be changed only partially. The print head characteristics depends on the equipment design, and have a limited versatility, unless the whole equipment is changed. The ink is the bridge between the substrate and the final product, and the main rules of ink selection are given by the head and substrate characteristics (chemical compatibility and viscosity for the print head, chemical and physical compatibility for the substrate). IJP is very versatile: it is possible to deposit almost any type of organic or inorganic materials, on virtually any type of substrate.

Among the advantages given by IJP with respect to other printing techniques (screen printing, spraying, roll coating and dip coating) it is possible to mention very low costs (waste of ink is reduced to a minimum), high quality output, the possibility of exploiting digital processes, the possibility to use any type of substrate. Moreover, an inkjet printer may be easily included in complex production lines, and even in highly controlled environments, like clean rooms.

In the following, the different types of printer and printer heads will be described, as well as the main components and chemical-physical characteristics of IJP-compliant inks. The substrate characteristics and properties suitable for IJP are described in the section 1.3 of the chapter.

1.6.1: TYPES OF PRINTER AND PRINTER HEADS

The inkjet printers can be divided in two main groups, depending on characteristic of ejection of the drop:

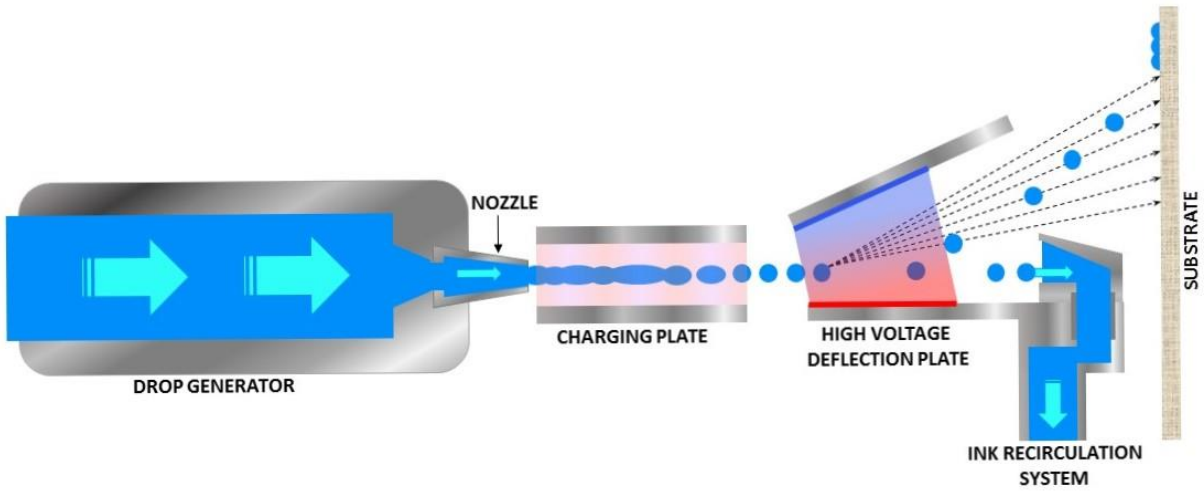

Figure 1.6-2: schematic illustration of the CI printer.

- **Continuous inkjet (CI)**: it is primarily used to mark and code industrial products. Its operation is very simple: a pump pushes the ink from the reservoir to the small nozzles, and creates a continuous stream of drops (*figure* 1.6-2). The operation frequency range is from 50 kHz to 175 kHz, and it is generated by a piezo crystal, which vibrates generating the pressure necessary to eject the ink drops. After the ejection, all the drops are electrically charged and then deflected by an electric field that gives them the right orientation with respect to the substrate. All the unused drops go through a recirculation system for further utilization. CI is a high-speed printing technique, perfect for industrial

applications, and has a high drop velocity, near 25 m/s, required by the high distance between the substrate and the nozzles. Its main advantage with respect to other IJP devices is the possibility to use volatile solvents as ink components, which reduces the drying time. The disadvantages of this technique are a low resolution, the fact that it generally uses environmentally unfriendly inks and a relatively high waste of ink, due to imprecise orientation of the ink drops by the deflecting field.

- **Drop on Demand (DoD)** [228, 229]: In this technique, the ink drops are ejected only if required, as the name suggests; the drop is created by a pressure pulse. There are different possible methods to generate the pulse, each of which has a specific application, as well as advantages and disadvantages. The subcategories of DoD come from the pulse generator types, which can be: i) thermal; ii) piezoelectric; iii) electrostatic. Hereafter a description of each different subcategory is given.

    1. ***Thermal:***

        It is a very diffused technology for home printing applications. In this case the ink pulse is generated by a rapid heating of a small resistive element placed in an ink chamber located before the nozzle (*figure* 1.6-3). Temperature of the heating element rises quickly from room T to 350-400°C, and causes a rapid evaporation of the ink solvent. Rresulting bubble pushes the ink through the nozzle. The void formed by the drop ejection is filled by new ink coming from the reservoir, and the process can restart. Advantages of this type of pulse generator are: i) very small drop size, in the range of picolitres, until 1 pL in the case of high resolution printer for photos; ii) high nozzle density (2400 nozzles per inch) [230]; iii) print head compactness, which reduces the production costs. On the other hand: i) solvent used must be vaporized and it must resist to a high temperature processing without occurring into degradation; ii) all ink components must resist to a high increase in local temperature without the loss of the chemical and physical properties; iii) print head life isn't long, depending on the way which is used, because of the resistive element ink coating.

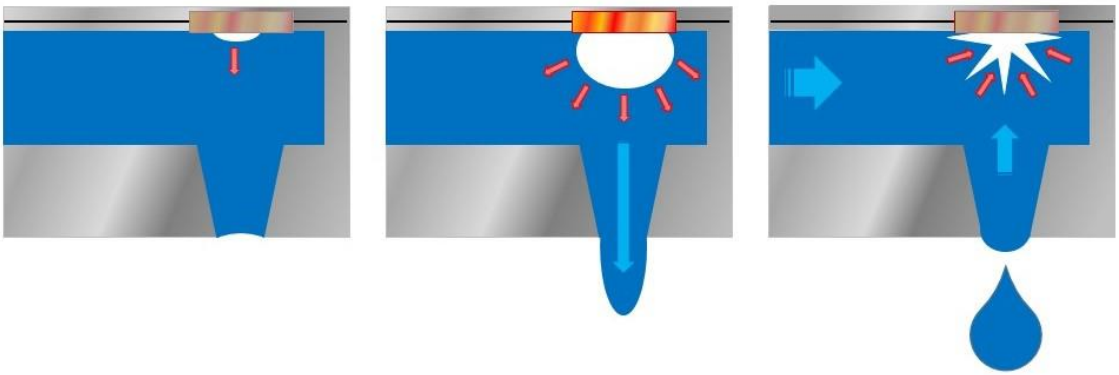

Figure 1.6-3: schematic illustration of how a thermal DoD head works.

2. *Piezoelectric*:

It is the most diffused technology, especially in the industrial field. A piezo-crystal generates the ink pulse, commonly zirconium titanate, deformed by an applied electric field (*figure* 1.6-4). Drop formation is based on four different steps. In the first step, before the ejection of the drop, the ink chamber placed near to the nozzle, is subjected to a small pressure, caused by an appropriate electrical field applied to the piezo element; in the second step the voltage is turned off and the crystal returns in a relaxed position, generating a flux of ink from the reservoir to the nozzle chamber. In the successive phase the crystal is strongly and rapidly warped, producing a pressure pulse that ejects the drop out of the nozzle. The crystal is then subjected to an electric field and the ink chamber returns to a depression state. The advantages of this head type are: i) high freedom in ink design, more than in all the other types of head; ii) long head life. The main disadvantages are: i) the relatively high cost of the head and of the controlling hardware; ii) relative higher cost compared to printers based on thermal print heads.

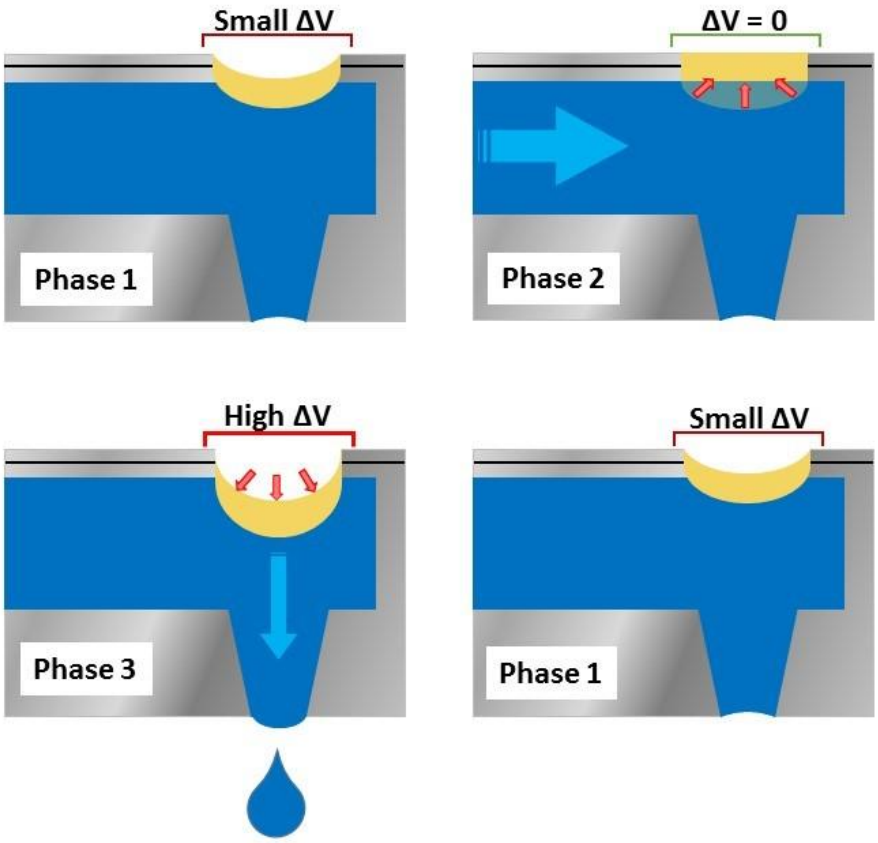

Figure 1.6-4: schematic illustration of how a piezoelectric DoD head works.

3. ***Electrostatic*:**

   There are only few commercial applications for this type of DoD head (*figure* 1.6-5) [231]. The ink is pushed out using a strong electrical field between an internal electrode and the orifice of the nozzle. Free charges inside the ink are attracted to the orifice and generate the drop, which can be ejected only if the electric field force exceeds the surface tension of the ink. The advantages are: i) ink is highly concentrated; ii) resolution doesn't depend on the nozzles diameter; the applied voltage controls the size of the drop, it can arrive until 0.3 pL [231]; iii) it is possible to create highly resolved images (600 x 600 dpi). The disadvantages are: i) ink must contain conductive particles or fluids; ii) relatively high cost in technology implementation.

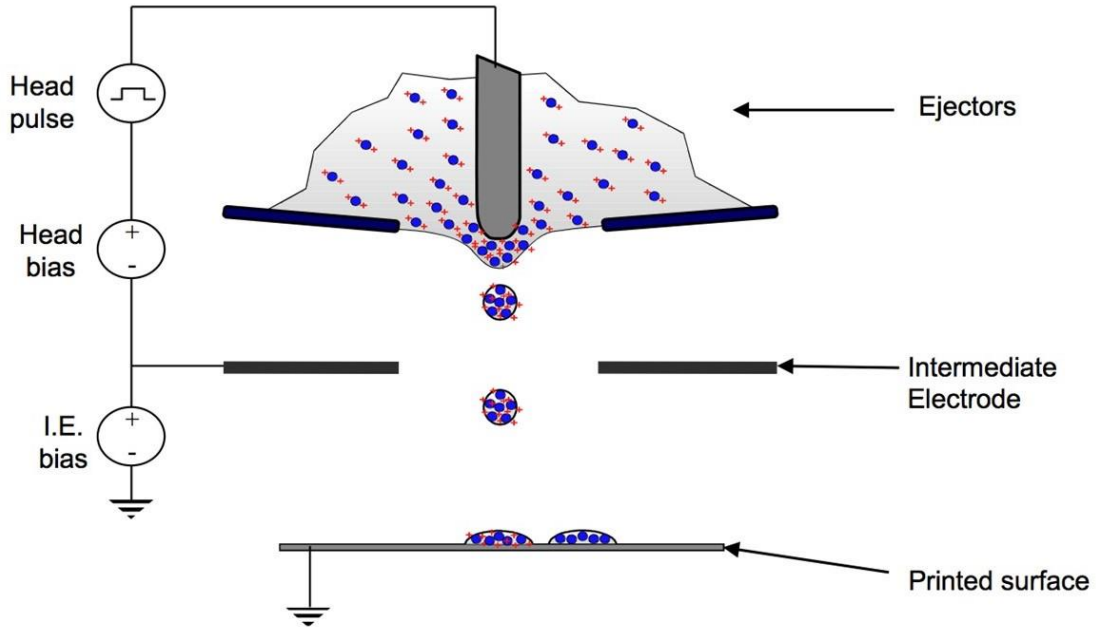

Figure 1.6-5: schematic illustration of how an electrostatic DoD head works.

One major challenge of IJP is the implementation of high throughput, to achieve high quality printing in a time as little as possible. It is possible to achieve this goal via a single print head pass with high jetting speed, but this requires a tight nozzles control, and often pre- and post-surface/ink treatments. Another possibility is to use multiple print head passes, which increases the final print quality and decreases the cost of integrating control systems, but at the same time decreases the total process speed. The reduction of the production time is possible also by cutting the maintenance times, increasing the lifetime of the printing head. Normal life for a DoD piezoelectric head is around 10^{13} drops. This looks like a large number, but for devices working 24 hours a day for seven days a week it could be rather short. Ink self-recovery can be a solution, with a continuous jetting flux to prevent the ink drying and the consequent clogging of the nozzles.

A further challenge introduced by the electronics industry is reduction in size of the drop and the accuracy in drop landing position on the substrate. The size of the drop is directly proportional to the size of the printing shape, but a small drop has a high surface/volume ratio that affects the deceleration, the evaporation and the force to eject the drop. All these factors impact on the head design.

1.6.1.1: Printer Head Performances

The print head performances are strongly connected to the ink properties and characteristics. Before their use, all the finished inks are tested inside printers in order to

understand if the technical requirements are respected. Drop latency is an important parameter for a good ink formulation. it represents the maximum period in which the ink can remain inside the nozzles without jetting, and without changing appreciably the ink properties. The drop latency range is specific for each ink formulation, and can vary from seconds to minutes. The variation of the ink properties is caused by the evaporation of the solvent inside the nozzles. The composition changes in comparison with the original formulation and the solution must be pumped out before the subsequent printing. If there is a long idle time to be waited during the printing process, some components may precipitate inside the nozzle and causing nozzle clogging. Moreover, high concentration of pigments, solubility decrement (due to pH changes or to the viscosity increment) also contribute to nozzle clogging. Latency time may be increased using these precautions during the ink design: i) use of the highest possible amount of high boiling point solvents inside the ink; ii) for water-based ink, addition of high boiling point co-solvents, like glycols is prefers; iii) increase of the solubility of solid, and decrease of its concentration; vi) use of non-volatile pH control agent; v) in pigment-based inks, introduction of stabilizing agents. If the ink, despite these precautions, dries in the nozzle orifice, it is necessary to re-dissolve the ink crust with new ink flux. The ability to eliminate this crust by new ink flux is named "recoverability", and represents the time and total quantity of ink that must be used to reobtain a perfect jetting section.

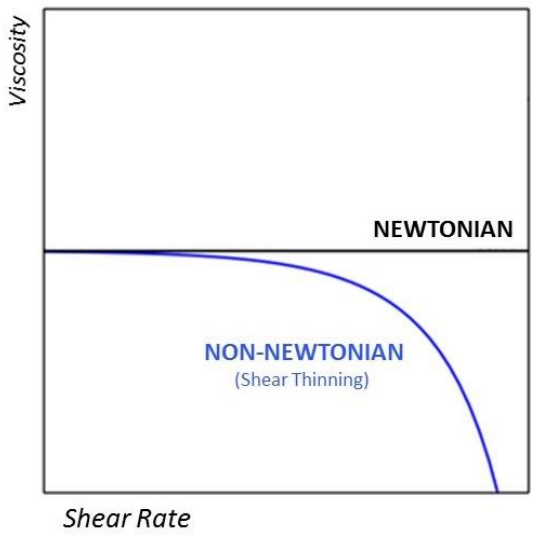

Figure 1.6-6: in the diagram shows the different viscosity trends of a Newtonian fluid and a non-Newtonian fluid with shear stress increasing

Since within the printer there are numerous tubes and filters in which the ink should flow from the cartridge container to the nozzles orifices, the pigments concentration and the fluid rheology are two fundamental parameters allowing a correct ink flow from the reservoir to the

print head. Inks with high particles concentration can block the internal filters, while highly viscous inks need high temperatures to work. In rare cases inks may have a non-Newtonian (*figure* 1.6-6) rheological behavior, that may result in viscosity increases inside the channels in which the shear stress is low, causing the ink to not flow properly. There are two main parameters to consider during ink formulation in order to avoid these problems and to promote a good ink flow:

1. *Particles size*: for inks including solid particles, the particles diameter should be 100 time less than the nozzle orifice. For example, for a 40 μm orifice the particles size maximum limit is 400 nm.
2. *Rheologic Control*: in this case the ink rheological properties are finely tuned via selecting and testing the proper ink components and their concentration, as well as adding compounds like polymers and viscosity regulators.

During the printing process, the formation of many small drops instead of a single one decreases the printing quality. The combination of ink viscosity, surface tension and density with head orifice diameter and pulse force is strictly related to the shape of the drop, and defines an operational window to optimize the ink formulation. Typically, an inkjet ink has its viscosity in the range of 3 to 25 cP, and its surface tension from 25 to 50 dyne/cm. The Ohnesorge (Oh) dimensionless number (15) [232] is the relation between viscosity and surface tension with the Reynolds and Weber numbers:

$$Oh = \frac{\sqrt{w_e}}{R_e} = \frac{\eta}{\sqrt{\rho D \sigma}} \qquad (15)$$

where ***η*** is the viscosity, ***ρ*** is the density of the ink, ***σ*** is the surface tension and ***D*** is the orifice diameter. ***We*** represent the Weber number: $w_e = \frac{\rho V^2 D}{\sigma}$, the ratio between the internal forces and the surface tension. ***Re*** stands for the Reynolds number: $R_e = \frac{\rho V D}{\eta}$, the ratio between internal force and the viscous force. In both cases ***V*** indicates the velocity of the ejected drop. Sometimes the Z number, which is the inverse of the Oh number, is used in literature [233, 234, 235]; if Z is included between 1 and 10, the drop formation is guaranteed. A value of Z lower than 1 indicates high viscosity and a possible occlusion of the orifice, while if it is larger 10 it indicates the formation of satellite small drops, rather than that of a single, compact drop.

1.6.2 INK: TYPES, CHARACTERISTICS, AND FORMULATION

The ink formulation requires a lot of research and a considerable number of practical attempts before achieving optimized results. The ink is most often a complex solution of different materials, that can include inorganic particles, ions, organic materials, highly viscous compounds. All the components must be perfectly balanced in the ink formulation to achieve the desired result. After having satisfied the major ink requirement, which is the chemical and physical compatibility with the print head in use, the main physical characteristics to be considered are viscosity and surface tension. A lot of other aspects must be considered during an ink preparation such as generated pollution, performance of the ink, shelf life of the ink, jetting behavior, etc.

There are four main types of ink: phase-change, solvent-based, water-based, UV curable.

- **Phase-change** [236]:

  These inks are known also as hot melt inks. They are in solid form and are melted only before the printing process. They dry quickly and don't spread on the surface, which is perfect for a high-quality printing. Among the other characteristics, they have good opacity and ambient friendliness; however, they have a poor abrasion resistance and low durability.

- **Solvent-based** [237]:

  They are the most used types of ink, and they are characterized by an enhanced versatility, with almost infinite possible formulations. Their cost is low, and the resulting print quality and durability are high for a wide range of substrates. Adhesion to the substrate and fast drying times are usually good. The main disadvantages are environmental unfriendliness and the possible clogging of the nozzles caused by a too fast drying.

- **Water-based** [238]:

  Water is the main solvent present inside these types of ink, which are environmentally friendly and inexpensive. The main problem blocking their penetration in the industrial field is their low adhesion to non-porous substrates. Furthermore, they often require a pre- or post- surface treatment to implement print durability.

- ***UV curable*** [239]:

  Inks of this type are designed to remain fluid until the action of UV irradiation, that promotes their solidification. After some recent strong investments in research, these inks and the related printing technique has entered the coating industrial field. The main benefit is the reduction in time production also of 90% compared with the classic coating procedure. This reduces the pollution due to the solvent present in the paint because this process is based on the UV polymerization and not on the solvent evaporations to became a rigid layer. The main disadvantages are the high cost of the related hardware and the short shelf life of the inks, combined with incompatibilities with food products; for this reason they are extensively used in automotive industry.

1.6.2.1: Ink Composition

An ink is made of two main components: the vehicle, which is the fluid carrier and it is composed of one or more solvents, and the deposited material. The latter may be a floating solid (for example metallic or semi-metallic particles, organic nanocrystals, pigments) or a solvated compound (typically, dyes). The mix of these components gives the ink its chemical and physical properties, and is responsible of its behavior when it touches the surface of the printed samples. The main characteristics of an ink are viscosity, surface tension and stability. Moreover, pH and possible presence of electrolytes or dye/pigments impact on the ink behavior, as well as its, dielectric or conductive properties and the presence of foaming-defoaming additives. A brief overview of the effect of these compounds on the ink properties is hereby given.

1.6.2.2: Viscosity

The normal range of ink viscosity for inkjet printing is from 3 to 25 cP. Viscosity affects the jetting performance and the spreading of the ink on the substrate. The required viscosity is strongly connected with the printer head type: for example, a thermal one can work with only 3 cP, while in the case of a piezoelectric one the value must be higher, up to 20 cP. During ink storage, the viscosity may change due to the aggregation of particles or to unwanted pre-curing of UV inks. It is extremely important to pay attention to these situations and to change the ink (for a new ink, or a new formulation) if necessary, to prevent damage to the print head. The presence of pigments, particles or crystals can promote the aggregation phenomena if they are in high

concentration and/or they are large. In general, it is preferable to have solid components as small as possible to obtain a stable colloidal solution.

It is possible to change the viscosity also during the printing process, like for melt inks, if the printer head has gotten a resistive heater inside the nozzles. This configuration makes it possible to heat inks with higher viscosity, optimized for the substrate interaction after the jetting, allowing suitable rheological behavior in the printing head. In fact, the viscosity depends on the temperature: when the temperature increases, the viscosity decreases and vice versa; in addition, a little variation in temperature can result in a high variation in viscosity (*figure* 1.6-7).

Dynamic Viscosity of Water

Temperature [°C]	Viscosity [mPa·s]
10	1.308
20	1.002
30	0.7978
40	0.6531
50	0.5471
60	0.4658
70	0.4044
80	0.3550
90	0.3150
100	0.2822

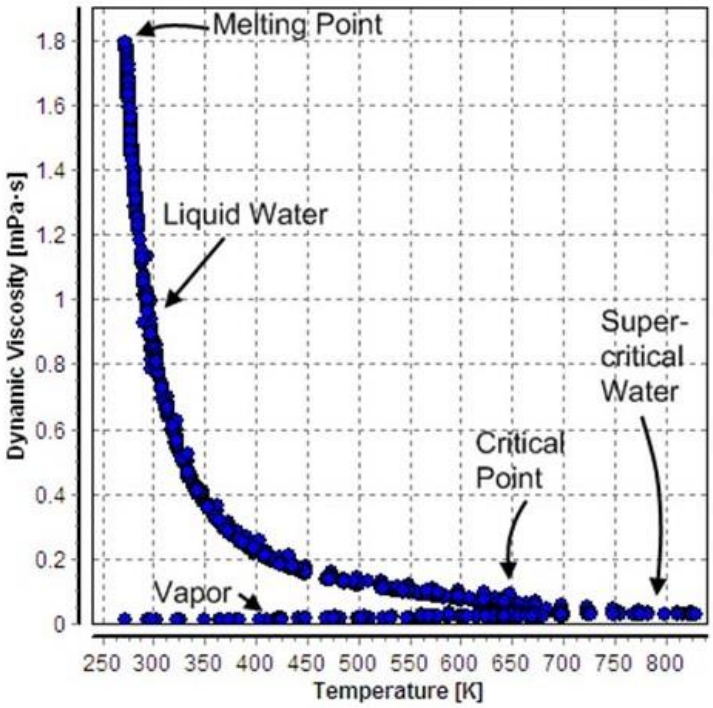

Figure 1.6-7: example of viscosity variation with the variation of the temperature, specifically the variation of the dynamic viscosity of water [240]

The viscosity of the inks is influenced by the presence of particles (metals crystals, ceramic particles, CNTs, pigments, etc.), and especially by the presence of the dispersant compounds used to avoid the aggregation phenomena. Each type of particle has a most suitable group of dispersants, and an optimal concentration for ensuring optimal viscosity. In fact, the viscosity of the dispersion decreases with the increase in dispersant concentration, until a minimum, after which it starts to increase again (*figure* 1.6-8).

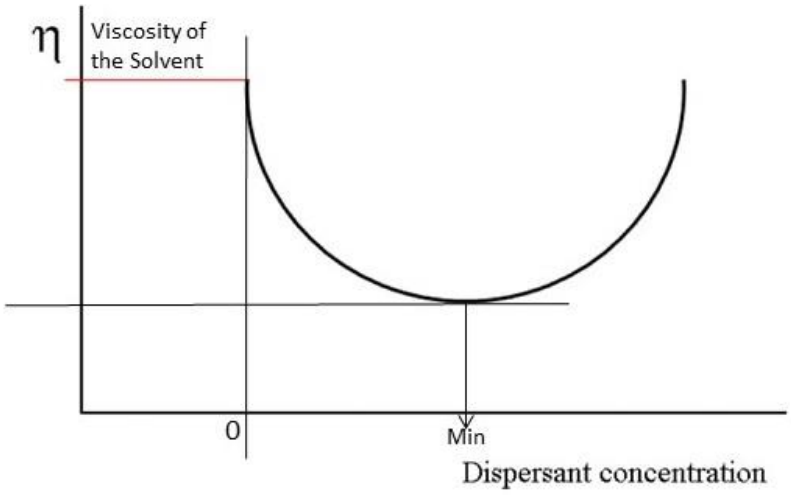

Figure 1.6-8: diagram of the viscosity variation in function of the particles concentration

1.6.2.3: Surface Tension

Surfactants and a correct mix of solvents determine the surface tension of the inks, a fundamental characteristic together with the viscosity, which affects the drop formation and its spreading on the substrate. The surface tension is the required energy to increase a liquid area by a unit of area, it depends by the attraction of liquid molecules, and the liquid surface acts as an elastic foil. It can be measured using Nouy ring or Wilhelmy plate methods [241]. For adjusting surface tension, it is possible to use surfactants. The concentration of a surfactant in a typical ink is usually below 1% w/w, most often around 0,1 % w/w. A little variation of the surfactant concentration may cause a significant change in the surface tension. During the printing process, there is dynamic surface tension, and it should also be considered. This parameter is present during the formation of a new surface, in the intermediate moment between the total absence of surfactants on the new surface and their complete coverage. Some examples are given by, the drop formation during the jetting moment, and the drop spreading on the substrate. Initially, the surface has a high surface tension, but after the diffusion of the surfactants it decreases until reaching its equilibrium.

The resulting static and dynamic surface tensions are affected by the interaction and the changing in the equilibrium of all the compounds in the solution.

1.6.2.4: Ink Stability

An ink is considered stable only if all its properties do not change in a determinate time, or rather the ink life time. There are three main problems concerning the ink stability precipitation,

phase separation and polymerization; another problem, rarely occurring, is due to the ink container walls, that may introduce new elements like metal ions or promote a phase separation caused by the temperature gradient between the wall and the center.

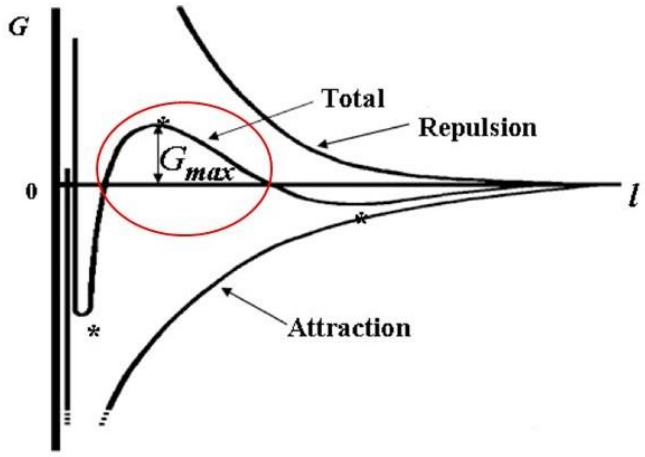

Figure 1.6: diagram of total interaction forces in a colloidal system

a) Precipitation: it happens only if not all the ink components are soluble in the main solvent and no aggregation occurs. Particles come near each other and start to interact due to intermolecular forces, like Van der Waal or induced dipoles. The final free energy of the aggregate is less than the sum of all the particles free energy, and reaches the minimum potential energy as in *figure* 1.6-9. A barrier able to prevent particles from getting in touch with each other, overcoming the attraction mechanism, is hence used.

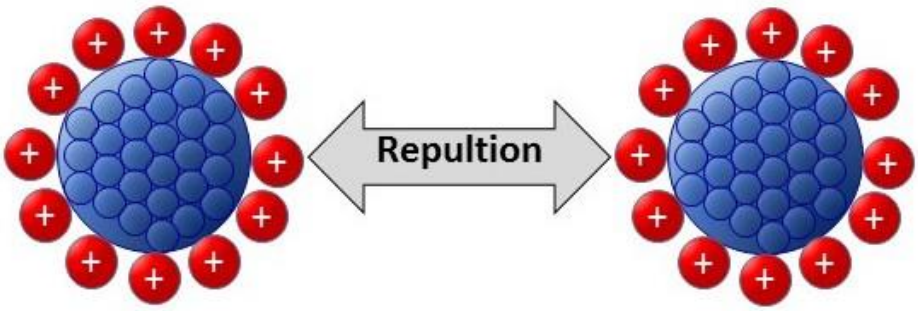

Figure 1.6-10: Schematic illustration of the repulsion between two particles stabilized by anionic or cationic elements adsorbed on the surface.

The choice of the barrier type depends on the nature of the solvents, since water or organic solvents have different properties, and the barrier must be different. In the case of water-based solvents, or more generally in high dielectric constant fluids, ink electrical repulsion is one of the most used solutions; to this end, particles are covered with

anionic or cationic elements (*figure* 1.6-10). to generate a repulsion when the distance between them decreases.

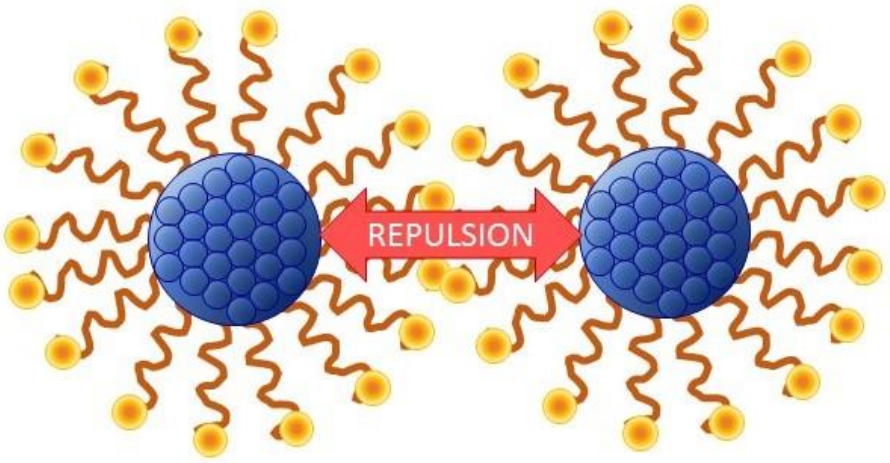

Figure 1.6-11: Schematic illustration of the repulsion between two particles stabilized by organic molecules adsorbed on the surface

Steric mechanism is the best choice for organic-based inks, by means of long molecules or polymers adsorbed on the particles surface. The molecules create a mechanical wall and work as "spacers" that block the contact and pushes away all from each other particles (*figure* 1.6-11). The choice of the steric hindering molecules is important because their behavior depends on the interaction with the solvent; anyway, often a correct concentration of the selected molecules can stop the aggregation also if the solvent is not perfectly appropriate for those molecules. As is visible in *figure* 1.6-12, the combination of ‘‘solvent quality’’, which can be good or bad, and ‘‘concentration of the dispersant’’ can be essentially reduced to four different possibilities. In the first three (*figure* 1.6-12 ‘‘a’’, ‘‘b’’, ‘‘c’’), the aggregation is blocked or reduced at the minimum, while in the fourth case (*figure* 1.6-12 ‘‘d’’), there is still aggregation.

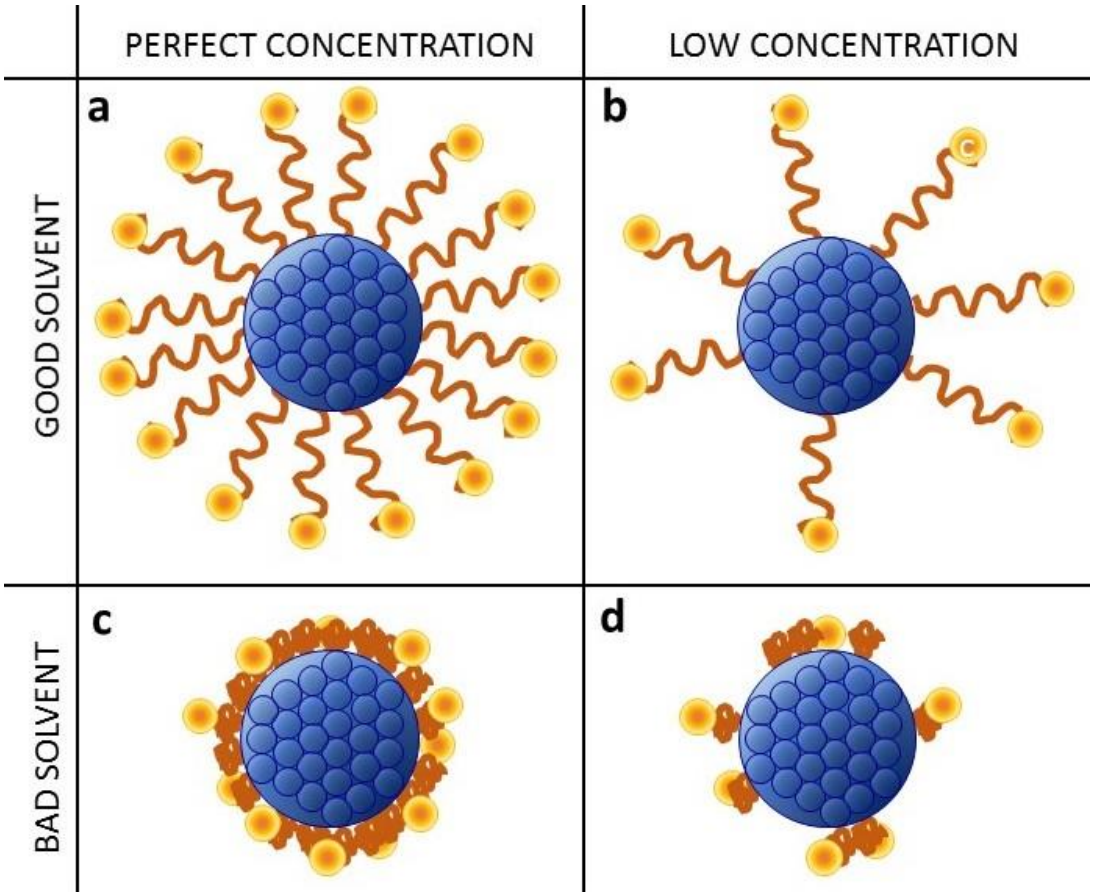

Figure 1.6-12: schematic illustrated table of the four possible combinations between the affinity of the main solvent with the organic capping and the quality of the particle covered with the same capping.

b) Phase separation: it can derive from an incorrect use of defoaming compounds or from a wrong ink design. In the first case, one possible solution is to decrease the concentration of the defoaming compounds, or changing the chemical nature of such compounds (using different chemical moieties); in the second case, the ink formulation must be redesigned.

c) Polymerization: it can happen only for UV-curable inks. Since the curing reaction is promoted by UV light, this problem can be prevented by simply shielding the ink from light before the deposition.

1.6.2.5: pH and Electrolytes

The pH is important only in water-based ink, and only if in the ink is present a compound that changes its solubility and stability upon pH variation. For example, acrylic resins are insoluble in low pH solutions.

To keep the ink pH constant, an often used strategy is that of adding buffers, which decrease the ink vulnerability. The electrolytes that may be present in the ink can cause stability problems during a prolonged storage, as phase separation and flocculation. Therefore, the concentration of electrolytes must be kept to a minimum. In this view, the quality of the water for the ink is essential, because a too high ionic concentrations can introduce unwanted electrolytes in the ink.

1.6.2.6: Dielectric Properties and Conductivity

The electrical properties of the ink are fundamental for Continuous Inkjet, where the drop position is controlled by a deflection field, but also for conductive inks for electrical applications. Moreover, the ink conductivity must be kept constant during all the ink life and storage (the later can modify the ink electrical characteristics via the interaction with the container materials). These properties can be tuned by adding to the ink electrolytes and/or ionic surfactants.

1.6.2.7: Dye and Pigment

Between dye and pigment there is a precise distinction: dye is a molecule soluble in the ink medium, while the pigment is not soluble, it is just dispersed. Dye-based inks are more stable than pigment-based ones. In general, a dye is a specific molecule that gives a color to the ink, and its concentration must be low to prevent any precipitation at the bottom of the container, especially at low temperatures (typical of winter storage conditions). The optical properties of the dye are affected by the pH, the electrolyte presence, the medium polarity and surfactant traces. Pigment concentration is normally below 10% w/w, to avoid aggregation and precipitation. In some cases, for conductive or ceramic inks the pigment can have also a 50% w/w concentration. The main problem for the pigment-based inks concern precipitation and formation of agglomerates induces decrement in optical density and the nozzles clogging during the printing process. A correct ink formulation can help to avoid the problem, and a continuous ink containers monitoring can identify unusable ink.

1.6.2.8: Foaming and Defoaming

Bubbles inside the ink can be a substantial printing problem, as they can damage the printer head or block the normal work of the nozzles. The introduction of defoaming compounds helps to minimize this phenomenon. The defoamers are compounds that decrease the ink surface tension and facilitate the elimination of bubbles. However, defoamers promote the phase separation

inside a solution, causing ink storage problems, and for this reason their concentration must be as low as possible.

1.6.3: INK ON SUBSTRATE

When the drop impacts on the substrate, it usually creates a flat dot. The size of the dot depends on different parameters, in turn depending on the printer characteristics, such as drop volume and velocity, and from the physical properties of the substrate and ink. The interaction between the ink and the substrate determinates the ink wettability and the evaporation process.

As a general rule, the printed shape can be tuned changing the ink and the substrate surface tension. An ink surface tension lower than that of the surface promotes a complete spreading of the drop; vice versa, with ink surface tension higher than that of the surface the drop tends to retain its shape [242]. The use of a low boiling point solvent, which in general has a low surface energy, increases the ability of the drop to wet the surface, but this is not the most convenient solution since low boiling point solvents can evaporate inside the nozzles and clog them. Therefore, substrate wettability is usually increased by using additives to achieve a low ink surface tension, taking care for a proper trade off with the jettability parameters.

The spreading of the drop on the substrate depends also on the substrate morphology: for example, porous or high roughness surfaces tend to block the dot expansion.

As the drop approaches the target surface, three different stages can be identified: i) the drop hits the target surface; ii) the fluid inside the drop expands radially and covers a surface that has a diameter of about one order of magnitude more than that of the free-floating spherical drop. All the drop mass is accumulated on the ring boundary, and the kinetic energy is dissipated partly due to the viscous flow; iii) the fluid starts to recoil toward the center when the maximum of expansion is reached. The fluid experience hence internal oscillations due to viscous dissipation before equilibrating on the surface (*figure* 1.6-13) [243].

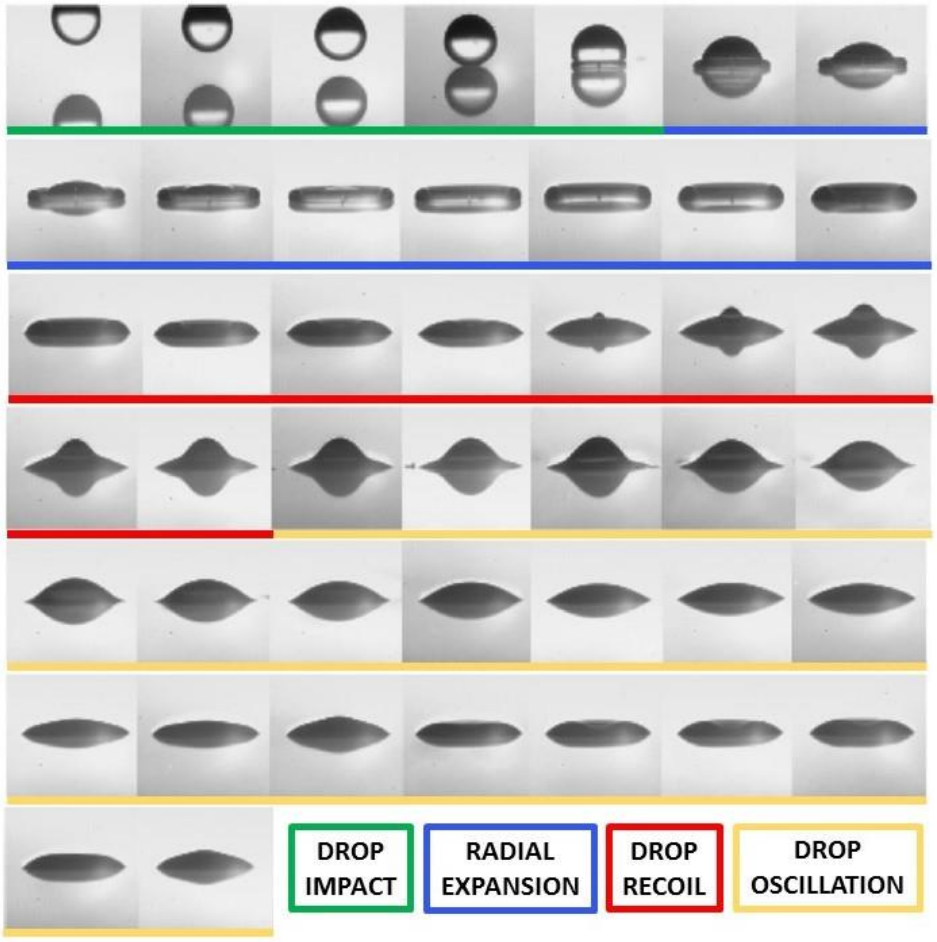

Figure 1.6-13: sequence of photos of the impact of a water drop on a surface. The four steps are clearly visible: i) drop impact-green; ii) radial expansion of the drop-blue; iii) Drop recoil-red; iv) drop oscillation-yellow. Between the photos there is a time delay of 3 μs.

It is possible to elaborate a diagram of the drop spreading phase against time. To this end, it is possible to define a spreading factor d* (equation 16):

$$d^* = D_{sp} / D \qquad (16)$$

where $\boldsymbol{D_{sp}}$ is, the substrate contact zone diameter, and $\boldsymbol{D}$ is the initial drop diameter.

The time elapsed after the drop impact can be calculated as $\boldsymbol{t^*}$ from the following equation (17):

$$t^* = \frac{Vt}{D} \qquad (17)$$

where $\boldsymbol{V}$ is the drop velocity, $\boldsymbol{D}$ is the drop diameter and $\boldsymbol{t}$ is the time.

The resulting plot $\boldsymbol{t^*/d^*}$ can be divided into four different zones (*figure* 14-1.6). [244, 245]. In this graph, time $\boldsymbol{t^*} = 0$ identifies the drop touch on the surface.

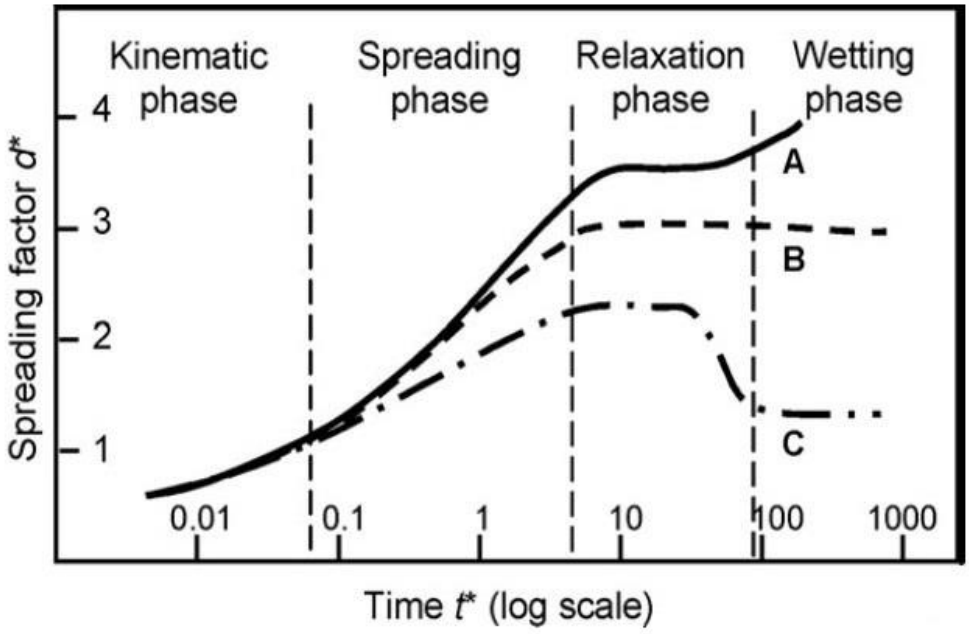

Figure 1.6-14: spreading of the drop on a surface after the impact. The three curves represent three different types of substrate: A high wettability substrate, C low wettability substrate and B intermediate wettability substrate.

In this graph, it is possible to identify the following zones:

- Kinematic phase: the spreading factor increases with a law $d^* \sim t^{*1/2.}$

- Spreading phase: a constant increase in the d* with t* is found; in the initial part of this phase the ink viscosity strongly affects the expansion. A low viscosity promotes a great radial flux, and the surface tension does not give any important contribution.

- Relaxation phase: the surface tension is the most important factor in this phase because it determines the wettability of the surface. The balance between viscous and internal forces defines the contact angles of the printed drop.

- Wetting Phase: during this phase the drop expands until its maximum, determined by the surface energies ratio. There are six possible drop impact modes, as it is possible to see in *figure* 1.6-15 [245]. In some of these modes small bubble of air can be trapped between the fallen drop and the substrate, due to the high drop velocity and the large Weber numbers, while the surface energy does not affect the phenomenon.

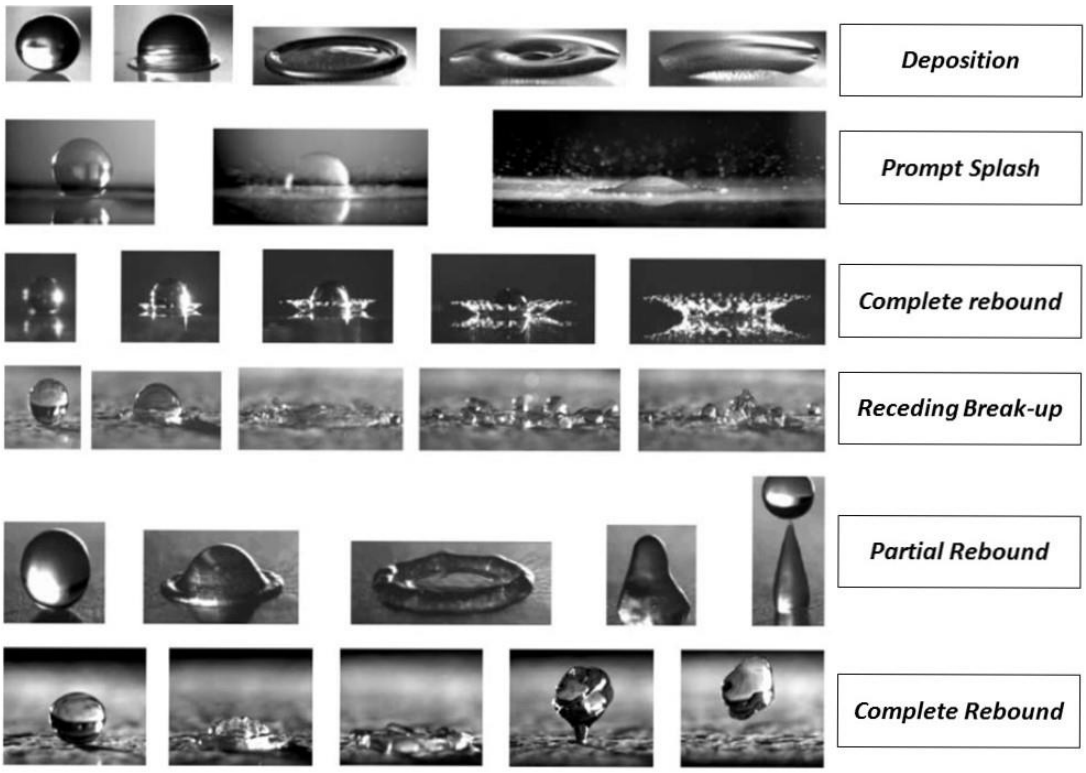

Figure 1.6-15: possible morphology of the ink drop impact on the substrate.

1.7: COMBUSTION PROCESS FOR INKJET FABRICATION OF NANOTHIN ALUMINUM OXIDE DIELECTRICS

Solution based processing can produce low-cost and flexible electronics and it can be applied to the fabrication of TFTs [246]. The recent development of high-performance semiconducting inorganic metal oxides further promoted research in this science field [247]. Gallium/indium free semiconductors based on non-toxic and abundant materials, like Zinc and Tin, can be obtained using liquid precursor-based processes. For example, Zinc Tin Oxide (ZTO) active layers can be produced with this approach [248, 249].

Solution-based processes reported in literature [250, 251, 252] normally uses toxic solvents as acetonitrile, 2-ethoxyethanol or 2-methoxyethanol, with a further thermal step reaching temperature of 400°C, even though a few articles about the use of aqueous solutions for the fabrication of ZTO TFTs are reported [253]. The main problem of these researches is the junction among metal oxide semiconductor, gate insulator and substrate. In particular, there aren't flexible substrates, usually made of polymer films, that can resist at such high temperatures without any damage and/or decomposition. The insulator-semiconductor junction is also a problem, since insulators for flexible devices are usually made of organic films, that can't resist to the heat treatment. A possible solution to this problem is to use thin metal oxide layers as dielectrics, conserving the possibility to use solution processing wherever possible.

In order to circumvent the need for very high temperatures for the formation of performing oxide layers it is possible to use a strategy based on local combustion within the forming oxide layer. In particular, low temperature combustion is possible for the synthesis of indium, yttrium, zinc, tin and gallium based multicomponent oxides layer. The energy source coming from a combustion chemical reaction occurring within the deposited layer provides heat to the system and promotes a homogenous conversion of the precursors to the desired oxide at temperatures much lower than those normally needed for the task. To take advantage from this strategy the precursors are made of three components: i) a metal salt, usually a nitrate Me-NO_3; ii) an organic fuel, usually urea or glycine; iii) an organic solvent, that doesn't take part in the reaction *figure* 1.7-1.

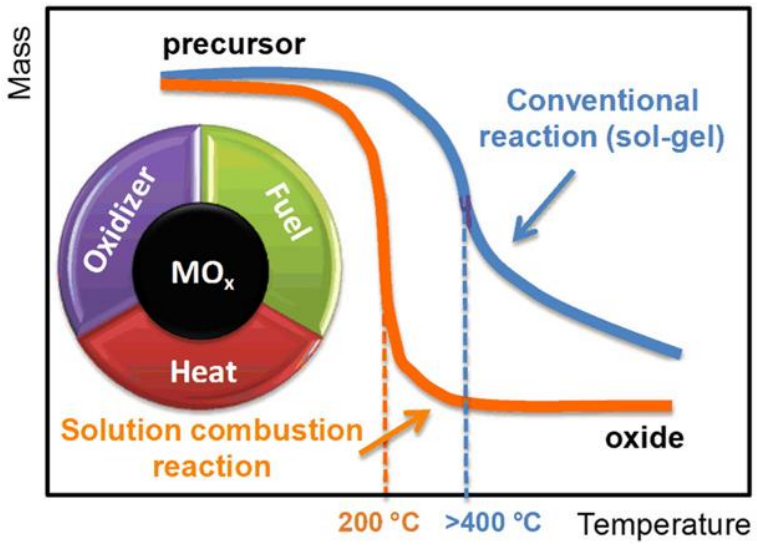

Figure 1.7-1: schematic representation of the three important constituents of the combustion process (heat, oxidizer and fuel), and the temperature comparison between a sol-gel conventional reaction with the solution combustion reaction. The decrease in heating temperature is evident [254].

The fuel is an important element for this chemical reaction not only for the combustion itself, but because it prevents the selective metal ions precipitation creating stable molecular complexes [255]. The fuel usually is an organic compound exploited as reduction agent, while the metal nitrate is the oxidizing element. The final products are nano-size crystal clusters, that are sintered together by both the combustion heat and additional heat provided from the external environment. Jain et al. [256] used a simple method to calculate the stochiometric equilibrium of the reaction based on fuel chemistry. To determinate the total fuel moles needed for a given number of moles of oxidizer is necessary to use a thermodynamic approach, and to calculate the Fuel/oxidizer ratio (Φ) (18):

$$\Phi = \frac{RV}{OV} n \qquad (18)$$

where ***RV*** is reducing valence, ***OV*** is an oxidizing valence, ***n*** is the number of moles of fuel per mole of oxidizer. The optimal stoichiometry composition of the redox mixture is obtained for Φ = 1. This means that additional oxygen molecules aren't required and "n" is the searched value. Metal ions, carbon and hydrogen are considered as reducing elements with the corresponding valence of metal, +4 for carbon and +1 for hydrogen. Oxygen and nitrogen are oxidizer elements with the corresponding valence of -2 and 0. The urea (CH_4N_2O), that is considered as a fuel, has a reducing valence equal to +6 as calculated from the RV (Reduction Valence) calculation: RV = 4 + (4x1) + (2x0) - 2 = +6 [C + (Hx4) + (Nx2) + O]. The presence of the solvent, either organic or aqueous, doesn't affect the redox reaction. As an example, to simplifies the comprehension can be

the calculation of the Al2O3 synthesis from the combination of aluminum nitrate decomposition and urea oxidation. The complete reaction is:

$2Al(NO_3)_3.\ 9H_20 + CO(NH_2)_2 \rightarrow Al_2O_3 + 20H_20 + 4N_2 + CO_2 + 6O_2$

where RV of the fuel (urea) is equal to +6, and OV of the aluminum nitrate is equal to -15, considering Φ = 1, "n" has a valor of 2,5. Therefore, 2,5 moles of urea are needed to reduce a mole of aluminum nitrate to Al_2O_3 [257].

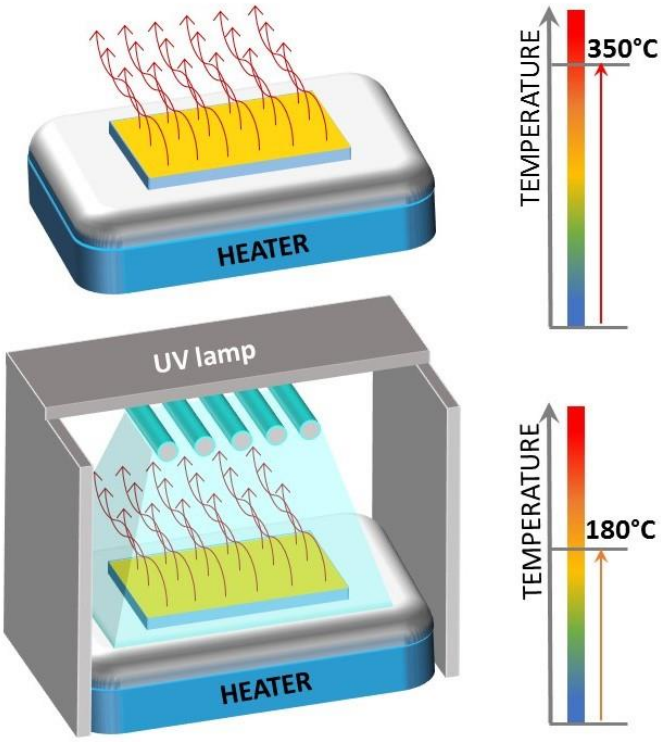

Figure 1.7-2: schematic comparison between a substrate using only annealing to activate the combustion reaction and one in which there are two different energy sources. In the second case the temperature is decreased of 170°C.

Another important element involved in the chemical reaction is the continuous heating of the substrate (*figure* 1.7-2). Heat increases the energy inside the solution layers, and promotes the combustion process initialization, favoring the solvent evaporation. The increase of the temperature leads to an increases in the quality of the thin layer formation; but the energy given to the system can be thermal or photonic (UV light). The introduction of a second energy supplier can decrease the intensity needed from of the first one, which in this case is equivalent to a temperature reduction. In turn, the low temperature allows the utilization of polymeric substrates, that is the final goal for this application.

The time allowed for the heat or heat/UV treatment of the layer within which one wants to depends on the temperature of the heater, or from another point of view, on the total amount of

energy given to the system. High temperature, low treatment time and the combination of two different energy sources can further decrease the overall time needed for the layer synthesis. The limitations of low temperature combustion are mainly three:

1. Solvent choice: the total amount of moles of fuel and the Me-nitrate must be completely dissolved inside the solvent: this is the first and the most important limitation for the choice of the solvent.

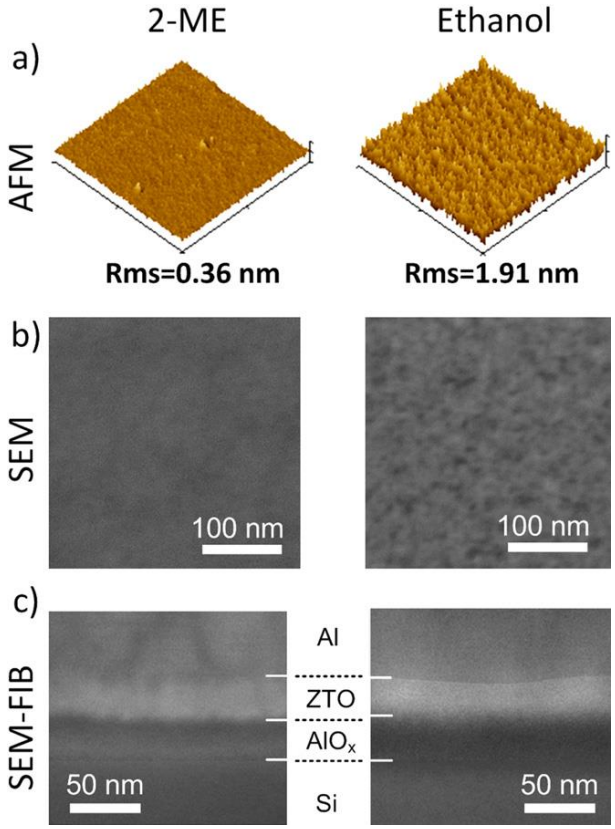

Figure 1.7-3: roughness comparison between two different samples made with solvents having different viscosity. The less viscous (ethanol) shows a very low roughness compared with the more viscous [254].

2. The production process is the second limitation: spin coating requires low viscosity solvents, but others as inkjet printing processes need high viscosity solvents. High viscosity solvents have a high boiling point. They aren't the best choice because traces of them can remain inside the deposited material, and decrease the electrical properties of the device. It is hence necessary an equilibrium among the viscosity of the solvent, the characteristics required for the solution, for the production process, and the heating sources. The viscosity is a fundamental parameter for the solvent choice as the *figure* 1.7-3 shows. In particular, it is possible to see a comparison

between the morphological characteristics of two different layers of ZTO deriving from solvents having different boiling points and viscosity. The two layers have a very different roughness, while the thicknesses are roughly the same, as well as their conductive properties. However, the ethanol solvent is much more environmental friendly than 2-Metoxyethanol.

3. Energy sources: The most used energy source is a heater placed under the substrate. It is possible to introduce in the system also a UV-lamp to decrease the total amount of energy (i.e., of temperature) administered to the substrate. In general, the energies supply can be provided either from the bottom or from the top of the sample. In the second case, due to solvent evaporation, it is possible to grow a "skin" of material that blocks an effective solvent evaporation. The result of this situation is invariably a layer with low conductive properties and a huge number of holes. There are a lot of possibilities to solve this problem, from high temperature to low energy UV-lamp:the optimal choice is based on the selection of the final use of the device.

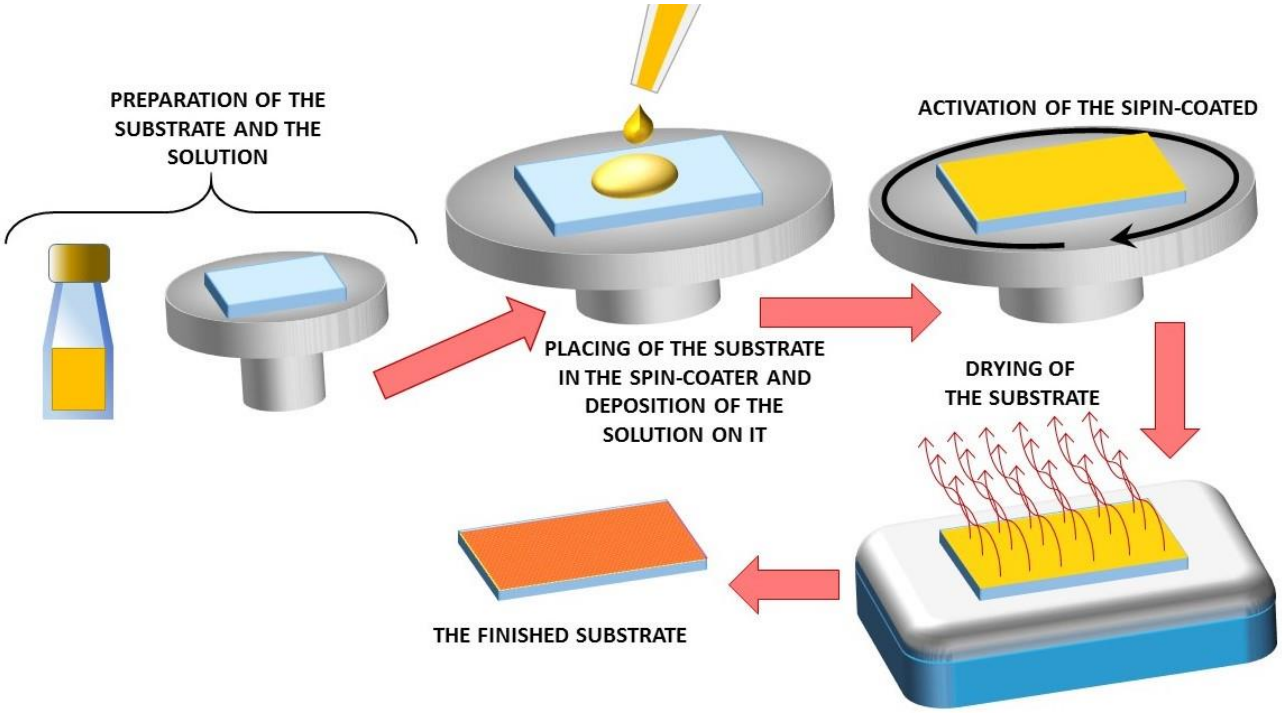

Figure 1.7-4: schematic representation of the spin-coating deposition procedure.

Spin-coating is the main production method used up to now in order to deposit the solution layer for chemical combustion processes *figure* 1.7-4. With this technique, it is possible to have a high degree of control on the resulting layer thickness, but sometimes spin coating fails to deliver

i) a morphologically homogeneous and compact layer; ii) a layer with the required thickness. For this reason, a pre-annealing treatment to dry the material and allow a second deposition is made. The sample can be subjected to the heat treatment also after the last layer.

Another possible processing technique to deposit the combustion solution is the IJPP *figure* 1.7-5. In this case the solution requires a specific optimization to become jettable. In particular, the solution viscosity and the substrate wettability (compatibility between superficial tension of ink and substrate surface) must be optimized for achieving good results. On the other hand, Inkjet printing allow a very low waste of material, a high precision in the deposition of the layers, and the possibility to realize computer-defined patterns, which is precluded to spin coating (see par. 1.5).

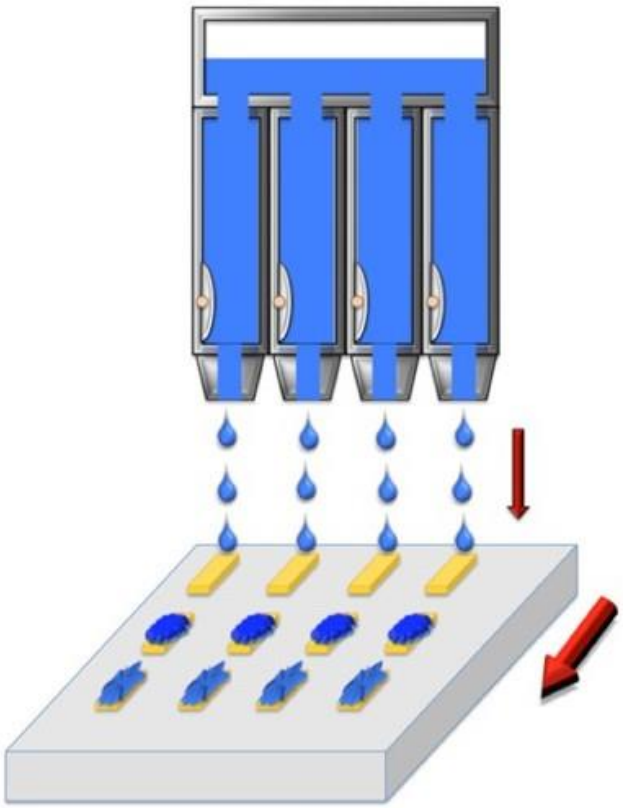

Figure 1.7-5: schematic representation of the IJPP deposition procedure.

1.8: THIN FILM TRANSISTOR

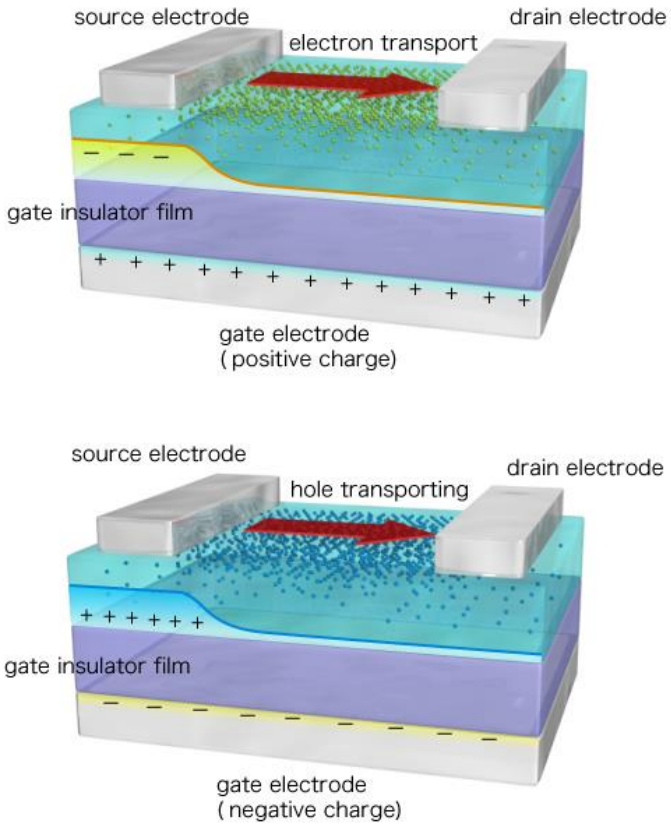

Figure 1.8-1: schematic illustration of a FETs and its operation after the application of a bias between the source and drain (motion of electrons and holes) [258].

Thin Film Transistors (TFTs) have the same architecture of field effect transistors (FETs), but they are characterized by a very small "z" (height) dimension of the whole device, allowing in principle even its flexibility. A TFT is composed by three main parts: i) source; ii) drain; iii) gate. A dielectric layer isolates the gate from source and drain, and the latter are connected via an ohmic contact to an active semiconductor channel [259]. When a bias between source and drain is applied, the carriers flow from drain to source through the channel creating, a current I_{DS} (*figure* 1-1.8). Modulating a potential V_{GS} between gate and source it is possible to attract or repel charges at the interface between the channel and the dielectric selecting the type of charge allowed to travel through the channel depending on the bias polarity, and tuning the amount of free charges depending on the bias intensity (*figure* 1.8-1).

In this way, it is possible to modulate the current I_{DS} because the conduction is a direct function of V_{GS} and density of charge carriers.

Since the conduction involves only a single type of charge transport, the transistor is considered unipolar. The zone formed by the gate-dielectric-semiconductor acts as a capacitor useful to increase the carrier concentration affected by the electric field. High dielectric constant and thin layer of the dielectric increases the semiconductor coupling.

The main geometrical parameters of the gate are (*figure* 1.8-2) : i) length (L), the distance between the source and the drain; ii) the total width (W) of the gate; iii) the ratio between W/L. Small lengths facilitate the passage of the carriers through the channel to the drain.

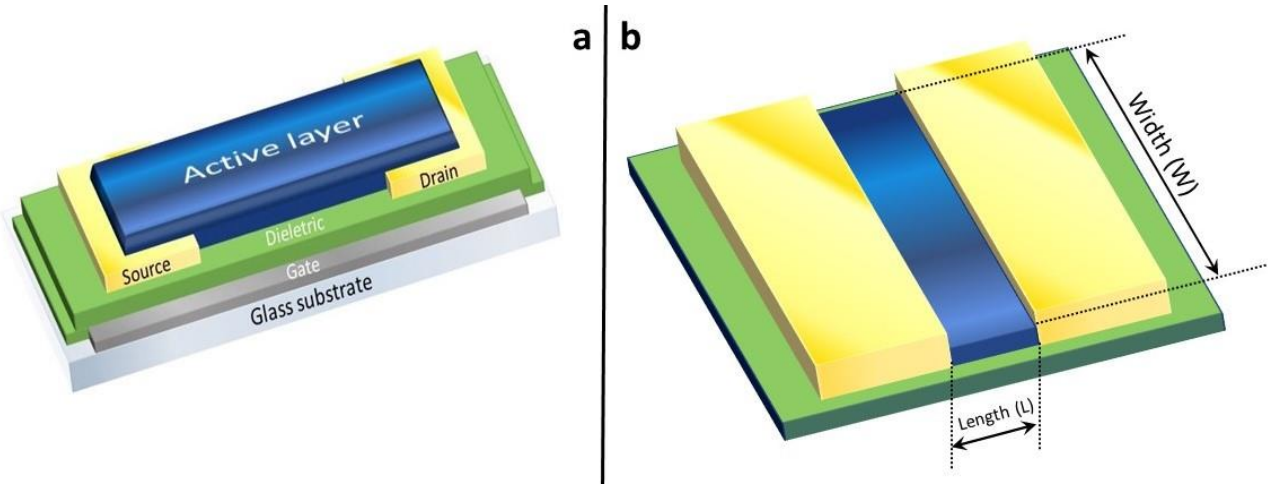

Figure 1.8-2: a) schematic representation of a TFT structure; b) the main geometrical parameters of the gate.

The TFT is usually made film deposing a film on a non-conductive substrate, amorphous or polycrystalline and can be flexible (polymeric substrate). When using flexible substrates, the device fabrication temperature is limited by the thermal resistance of the used materials. For example, polymeric films degrade in a range of temperature around 150-250°C.

There are two main possible TFT configurations: i) top-gate/bottom-contact; ii) top-contact/bottom-gate. For each of the two main groups of structure: coplanar and staggered (*figure* 1.8-3). The choice among these structures depends on the targeted device production parameters and application. For example, in some cases it is better to deposit all the layers (source and drain, dielectric and gate) on the semiconductor channel to promote an intimate contact between the layers. If the semiconductor can damage its properties during the coating process caused by, for example, high temperature or vacuum, it is better to adopt a coplanar

bottom contact top gate. In this case the semiconductor is the latest layer deposited. Also, roughness is an important property of the surface that can change the order of the layers. Irregularities of lower layers, introduced by a different wettability characteristic for each material constituting the device, directly impact the coverage uniformity, possibly creating pinholes. A homogenous steps coverage is crucial to obtain a working device. For this reason, an effective layer-to-layer optimization, in terms of roughness and wetting, is required [260, 261].

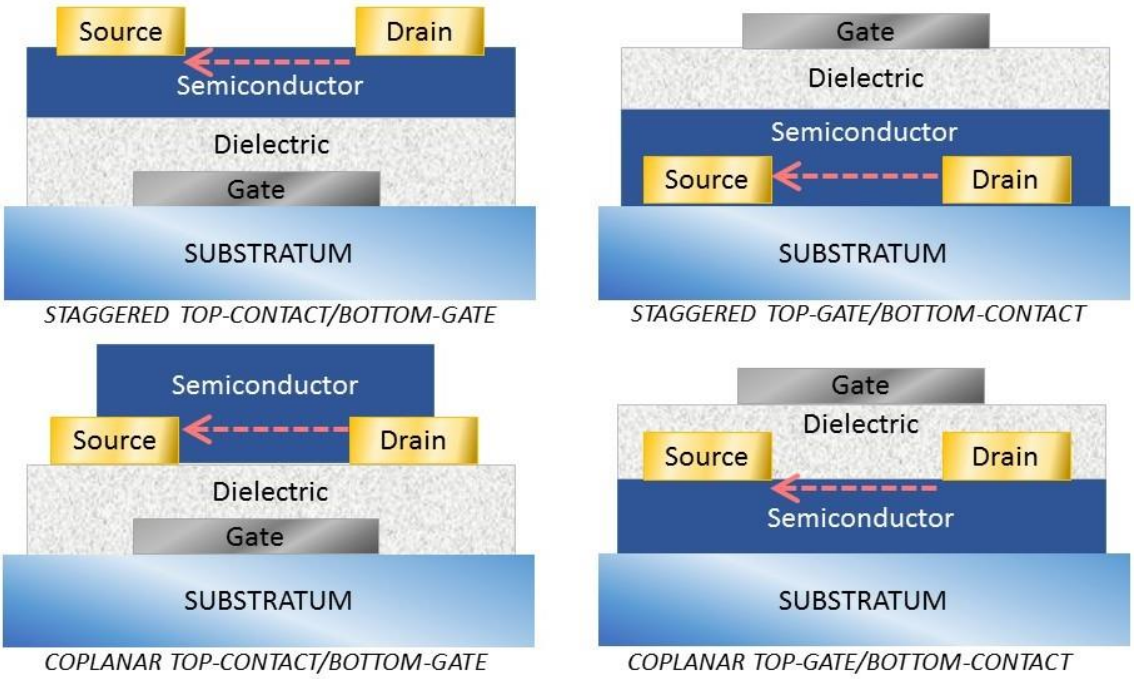

Figure 1.8-3: schematic illustration of the four possible combinations between the two-main possible TFT configurations: i) top-gate/bottom-contact; ii) top-contact/bottom-gate, and the two main groups of structure: coplanar and staggered

1.8.1: FET ELECTRICAL CHARACTERISTIC

The FET behavior changes with the variation of applied gate bias. There are three different regions in which it is possible to divide its electrical response (*figure* 1.8-4) [262]. For p-type or n-type channel the charge distribution is opposite, but the description of the channel modulation is the same.

- Cut-off region: here if V_{GS} (gate-source voltage) is lower than V_{TN} (threshold voltage, that is the lower bias needed to switch on the charge transport in the channel), the transistor is off because the total concentration of charges in the channel is low and does not allow the formation of a meaningful drain current.

- Linear (Ohmic) region: here $V_{GS} > V_{TN}$ and $V_{DS} < (V_{GS} - V_{TN})$, in this case the current is flowing in the channel controlled by V_G, the current I_{DS} can be calculated with the equation (19), and the transistor is on. FET has a resistive behavior in this region and works as a resistor.

$$I_{DS} = \left(W/L\right) C_i \mu_{FE} \left[(V_{GS} - V_{TN}) V_{DS} - \tfrac{1}{2} V_{DS}^2 \right] \qquad (19)$$

where ***W*** is width of the channel, ***L*** is the length of the channel, C_i is the gate capacity per unit area, and μ_{FE} is the field-effect mobility.

The field effect mobility μ_{FE} (20) is obtained from the transconductance (g_m) at low V_{DS}:

$$\mu_{FE} = \frac{g_m}{\frac{W}{L} C_i V_{DS}} \qquad (20)$$

- Saturation region: the increase of V_{DS} is less and less capable of increasing the amount of free carriers in the channel, delivering an almost constant I_{DS}. Increasing the VGS the value of the saturation current increases due to the higher number of available carriers allowed by the higher gate polarization. The current I_{DS} in this region can be calculated with the equation (21):

$$I_{DS} = \left(W/L\right) C_i \mu_{sat} (V_{GS} - V_{TN})^2 \qquad (21)$$

where ***W*** is width of the channel, ***L*** is the length of the channel, C_i is the gate capacity per unit area, and μ_{sat} is the saturation mobility.

Saturation mobility μ_{sat} (22) is obtained from g_m with high V_{DS}:

$$\mu_{sat} = \frac{\left(\frac{\partial \sqrt{I_{DS}}}{\partial V_{GS}}\right)^2}{\frac{W}{2L} C_i} \qquad (22)$$

The transconductance "g_m" is the ratio between a changing in the I_{DS} and the consequence changing in the V_{GS} at constant V_{DS}, equation (23) [263]:

$$g_m = \frac{\Delta I_D}{\Delta V_{GS}} \qquad (23)$$

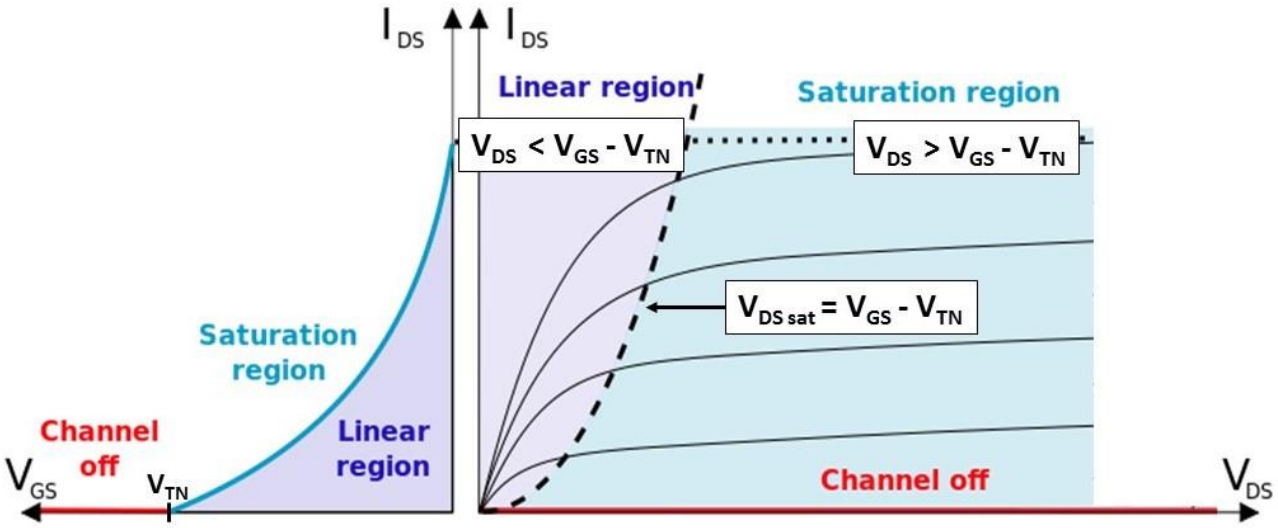

Figure 1.8-4: on the left, the transfer characteristic of FET with the three regions. On the right, family of IDS curve for a n-type FET, it is possible to distinguish between the linear and the saturation region.

1.8.2: TFT CHARACTERIZATION CURVE

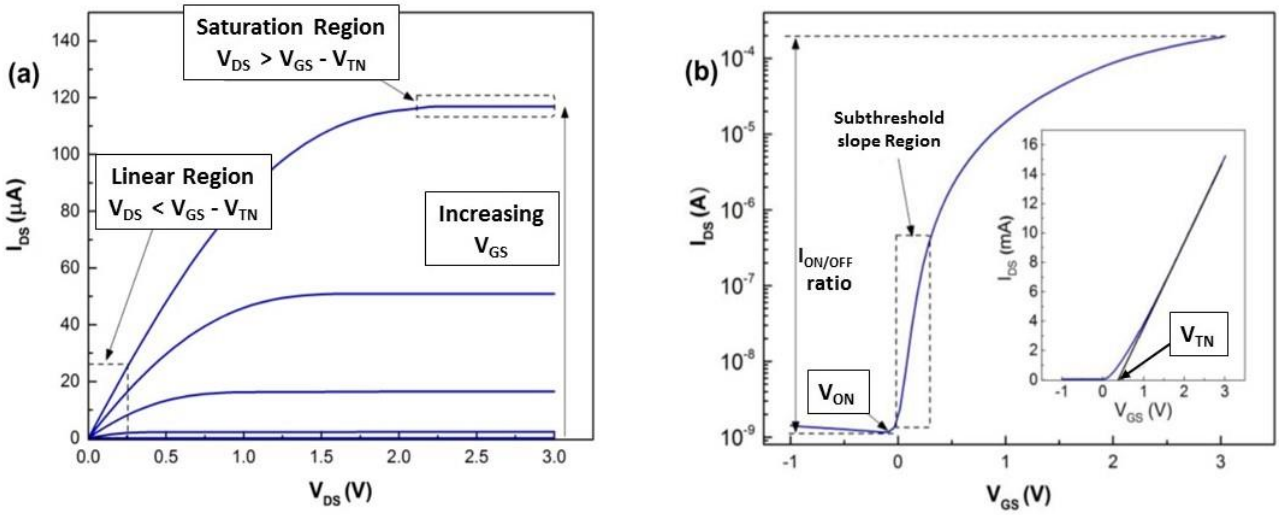

Figure 1.8-5: output (a) and transfer (b) curves for n-type oxide TFT.

A typical characterization of TFTs involves static-current voltage measurements where output and transfer curves are obtained. Output curve provides mostly a qualitative information regarding the effectiveness of channel saturation and contact resistance, by sweeping V_{DS} for different V_{GS} values (*figure* 1.8-5 "a"). Transfer curve, obtained by sweeping V_{GS} at constant V_{DS}, offers a quantitative analysis where specific electrical parameters can be determined (*figure* 1.8-5 "b"):

- On/Off ratio: ratio of the maximum to minimum I_{DS}. A higher "on" current offers better driving capability, while a lower "off" current results in low leakage current. Consequently, a higher ratio is preferable;
- Threshold voltage V_{TN}: corresponds to the V_{GS} at which a significant charge is accumulated close to the semiconductor-dielectric interface. A possible methodology to determine this value consists in using a linear extrapolation of the $I_{DS} - V_{GS}$ at low V_{DS};
- Turn-on voltage V_{on}: it is the V_{GS} at which I_{DS} starts to increase. It is visible in the $\log I_{DS} - V_{GS}$ graph;
- Subthreshold swing "S": it indicates the V_{GS} required to increase I_{DS} by one decade, as seen in the subthreshold region. It is defined in V/decade as:

  $S = (\frac{d \log I_{DS}}{dV_{GS}} | max)^{-1}$. A smaller S is preferable, resulting in lower power consumption and higher speed.

BIBLIOGRAPHY CHAPTER 1

1.1 - ORGANIC ELECTRONICS

1. R. G. Kepler, *Phys. Rev*., **1960**, 119, 1226
2. O. H. LeBlanc, *J. Chem. Phys*., **1960**, 33, 626
3. L. M. Schwartz et al., *Mol. Cryst*., **1967**, 2, 379
4. C. K. Chiang et al*., J. Am. Chem. Soc.,* **1978**, 100, 1013
5. C. K., Chiang et al., *Phys. Rev. Lett*., **1977**, 39, 1098
6. H. Shirakawa et al., *J. Chem. Soc. Chem. Com- mun*., **1977**, 579
7. C. W. Tang et al*., Appl. Phys. Lett.,* **1987**, 51, 913
8. W. Tang, *Appl. Phys. Lett*. **1986**, 48, 183.
9. A. Tsumura et al., *Appl. Phys. Lett*. **1986**, 49, 1210
10. Akerfeldt M., *Swedish School of Textiles*, **2015**
11. Brett H. Robinson, *Science of the Total Environment*, **2009**, 408, 183
12. Samsung // http://www. rinnovabili.it /energia/ efficienza-energetica/ fast2light-oled-illuminazione-356/
13. https://www.kickstarter.com/projects/infinitypv/heli-on
14. Galagan Y et al., Dr. Vasilis Fthenakis (Ed.), InTech, DOI: 10.5772/25901
15. Isobe M, Takiguchi H, Kiguchi H, Shibatani M. (**2008**) *Japan Patent No. 2008233572 A.*

1.2 ORGANIC SEMICONDUCTORS (OS)

16. D. Gamota et al., Printed Organic and Molecular Electronics, *Springer*, Berlin, **2005**
17. H.Sirringhaus ,*Adv.Mater*, **2005**, 17, 2411
18. A.Facchetti, *Mater.Today*, **2007**, 10, 28
19. F. Würthner, R. Schmidt, *ChemPhysChem*, **2006**, 7, 793
20. G. Witte, C. Wöll, J. Mater. Res., **2004**, 19, 1889
21. C. Ziegler, D. Fichou Handbook of Oligo- and Polythiophenes, *Wiley-VCH*, Weinheim, **1999**, pp. 183 – 282

22. Crone, B. K. et al., *J. Appl. Phys*., **2002**, 91, 10140
23. Crone, B. et al., *Appl. Phys. Lett*., **2001**, 78, 2229
24. Zhu, Z.-T. et al., *Appl. Phys. Lett*., **2002**, 81, 4643
25. Bowring J., Intel steps up polymer memory modules research, www.fabtech.org, Jan 28, **2002**
26. Mehta V. K., Principles of Electronics., S. Chand., **2008**, 56
27. A. Einstein, On the Electrodynamics of moving bodies, june 30 **1905**
28. Transistor Wikipedia English version
29. Peng et al., *Nature*, **2000**, 4, 59
30. Braun, Ernest; Stuart MacDonald, Revolution in Miniature: The history and impact of semiconductor electronics, *2nd Ed. UK: Cambridge Univ. Press*., **1982**, pp. 11–12
31. Shockley, William (**1950**). Electrons and holes in semiconductors with applications to transistor electronics. *R. E. Krieger Pub. Co*.
32. The Chip that Jack Built, (HTML), *Texas Instruments*, Retrieved 29 May **2008**
33. Jack S. Kilby, Miniaturized Electronic Circuits, *United States Patent Office*, US Patent 3,138,743, filed 6 February **1959**
34. Rothberg L., Photophysics of conju- gated polymers, in Semiconducting Polymers (*eds G. Hadziioannou and G.G. Malliaras), Wiley-VCH Verlag GmbH*, Weinheim, **2006**
35. Ariu, M. et al., *J. Phys. Condens. Matter*, **2002**, 14, 9975
36. Hayer, A. et al., *Phys. Rev. B*, **2005**, 71, 241302
37. Mauer R. et al., *Adv. Funct. Mater*., **2010**, 20, 2085
38. Heeger A.J., (*Nobel lecture*). *Angew.Chem. Int. Ed*., **2001**, 40, 2591.
39. Chiang, C.K. et al., *Phys. Rev. Lett*., **1977**, 39, 1098
40. Silinsh E.A, and Capek V.,Organic Molecular Crystals, *AIP Press*, New York, **1994**
41. Wright J.D., (ed.) Molecular Crystals, *Cambridge University Press*, **1994**
42. Kitaigorodskii A.I., Molecular Crystals and Molecules, *Academic Press*, New York, **1973**
43. Schwoerer M. and Wolf H.C.,Organic Molecular Solids, *Wiley-VCH Verlag GmbH*, Weinheim, **2007**
44. Pope M. and Swenberg C.E., Eletronic Processes in Organic Crystals and Polymers, *Clarendon Press*, Oxford, **1999**
45. Hasegawa T. et al., *Sci. Technol. Adv. Mater*., **2009**, 10, 024314
46. Podzorov,V. et al., *Phys. Rev. Lett*., **2004**, 93, 086602

47. Zeis, R. et al., *Chem. Mater*., **2006**, 18 (2), 244

48. Wang, L. et al., *J. Appl. Phys*., **2007**, 101, 054515

49. Minari T. et al*., J. Appl. Phys*., **2006**, 99, 034506

50. Bässler H. and Köhler A.,*Top. Curr. Chem*., **2012**, 312, 1

51. Kroto H.W. et al., *Nature,* **1985**, 318, 162−163

52. Wilson, R. J. et al., *Nature*, **1990**, 348, 621−622

53. Guldi D. M. et al., *Acc. Chem. Res*, **2000**, 33, 695−703

54. Kirner S.et al., *Chemistry. Adv. Mater*., **2014**, 26, 1482−1493

55. Jensen A. W. et al., *Med. Chem*., **1996**, 4, 767−779

56. Anthony J. E. et al., *Adv. Mater*., **2010**, 22, 3876−3892

57. Gaudiana R. et al., *Nat. Photonics*, **2008**, 2, 287−289

58. Iijima, S., *Nature*, **1991**, 354, 56−58

59. Iijima, S. et al., *Nature*, **1993**, 363, 603−605

60. Krishnan A et al., *Phys. Rev. B*, **1998**, 58, 14013−14019

61. Yu M. F. et al, *Phys. Rev. Lett*., **2000**, 84, 5552−5555

62. Yu M. F. et al., *Science*, **2000**, 287, 637−640

63. Odom, T. W. et al., *Nature*, **1998**, 391, 62−64

64. Samsung web site

65. Freek J. M. et al., *Chem. Rev*., **2005**, 105, 1491-1546

66. Warta W. et al., *Phys. ReV. B*, **1985**, 32, 1172.

67. Podzorov V. et al., *Appl. Phys. Lett*., **2003**, 82, 1739

68. Shirota Y. J., *Mater. Chem*., **2005**, 15, 75.

69. Kreouzis T. et al., *Phys. ReV. B*, **2006**, 73, 235201

70. Bao, Z.; Locklin, J. J. Organic field-effect transistors CRC Press: Boca Raton, **2007**

71. Tessler N. et al., *Adv. Mater*., **2009**, 21, 2741-2761

72. Juchescu et all., *Appl. Phys. Lett*., **2004**, 84, 3061

73. de Boer et all, *Phys. Status Solidi A*, **2004**, 201, 1302

74. D. Fichou*, j.* mater. Chem., **2000**, 10, 571

75. P.C. Chang et all, *Chem. Mater*., **2004**, 16, 4783

76. D. Fichou, *Adv. Mater*., **1996**, 8, 500

77. Y. Sakamoto et al., *J. Am. Chem So*c. **2004**, 126, 8138.

78. C.R. Newman et al., *Chem. Mater*. **2004**, 42, 6363

79. R.C. Haddon et al., *Appl. Phys. Lett*., **1995**, 67, 121

80. E. Frankevich et al., *Solid State Commun*., **1993**, 88, 177

81. P.V. Pesavento et al*., J. Appl. Phys*., 2004**,** 96, 7312

82. D. Adam et al., *Nature*, **1994**, 371, 141

83. A.M. van der Craats et al., *Adv. Mater*., **1999**, 11, 1469

84. Y. Shirota, *J. Mater. Chem*., **2005**, 15, 75

85. Horowitz G*., AdV. Mater*., **1998**, 10, 365

86. C.D. Sheraw et al., *AdV.Mater*., **2003**, 15, 2009.

87. Mas-Torrent et al., *J. Am. Chem. Soc*., **2004**, 126, 8546

88. Kazmaier et al., *J. Am. Chem. Soc*., **1994**, 116, 9684

89. F. Wurthner *Chem. Commun*., **2004**, 1564

90. D.H. Dunlap et al., *Phys. ReV. Lett*., **1996**, 77, 542.

91. S.V. Novikov *J. Polym. Sci., Part B: Polym. Phys*., **2003**, 41, 2584.

92. P.G. Lecomber et al*., Phys. ReV. Lett.,* **1970**, 25, 509.

93. Scher H. et al., *Phys. ReV. B*, **1973**, 7, 4491

94. Horowitz G.; Hajlaoui, M. E., *AdV. Mater*., **2000**, 12, 1046

95. Schein L. B.; Mcghie, A. R., *Phys. ReV. B*, **1979**, 20, 1631

96. Warta, W.; Karl, N., *Phys. ReV. B*, **1985**, 32, 1172

97. Gill W. D., *J. Appl. Phys*., **1972**, 43, 5033

98. Pai D. M*., J. Chem. Phys*., **1970**, 52, 2285

99. Mozer A. J.; Sariciftci, N. S., *Chem. Phys. Lett*., **2004**, 389, 438

100. Z. Rang et al., *Appl. Phys. Lett*., **2001**, 79, 2731

101. C. Gohet al*., J. Appl. Phys. Lett.*, **2005**, 86, 122110.

102. A. Zen et al., *AdV. Funct. Mater*., **2004**, 14, 757

103. Eley D. D., *Nature*, **1948**, 162, 819

104. Akamats, H., Inokuchi H., *J. Chem. Phys*., **1952**, 20, 1481

105. Inokuchi H., Harada Y., *Nature*, **1963**, 198, 477

106. Schein L. B., *Chem. Phys. Lett*., **1977**, 48, 571

107. Schein L. B. et al., *Phys. ReV. Lett*., **1978**, 40, 197

108. Braun, C. L., Scott, T. W. *J. Phys. Chem*,. **1983**, 87, 4776

109. Scher, H., Lax, M. *Phys. ReV. B*, **1973**, 7, 4491

110. Silinsh, E., Ca´pek, V., *American Institute of Physics*, New York, **1994**

111. Glaeser, R. M.; Berry, R. S., *J. Chem. Phys*., **1966**, 44, 3797

112. R. S. Knox, Theory of excitons, Solid state physics (*Ed. by Seitz and Turnbul, Academic, NY*), 5, **1963**

113. R. H. Friend et al., *Nature*, **1999**, 397

114. D. P. Craig and S. H. Walmsley, Excitons in molecular crystals: Theory and Applications; Amsterdam: *W. A. Benjamin, Inc*., **1968**

115. M. Hoffmann et al., *Chemical Physics*, **2000**, 258, 73-96

116. Pope M., *Molecular Crystals*, **1968**, 4, 183-190

117. Vitaly and Podzorov, Organic single crystals: Addressing the fundamentals of organic electronics, MRS *Bulletin*, **2013**, 38, 15-24

118. Karen K. GleasonCVD Polymers: Fabrication of Organic Surfaces and Devices, First Edition. Edited by Karen K. Gleason. © **2015** *Wiley-VCH Verlag GmbH & Co. KGaA*

1.3: SURFACE

119. C. Neinhuis et al., *Annals of Botany*, **1997**, 79, 667.

120. Anonymous (**1975**), Instruments for the Measurement of Surface Roughness by Profile Methods, ISO3274, *International Standardization Organization*.

121. Anonymous (**1985**), Surface Texture (Surface Roughness, Waviness and Lay), *ANSI/ASME B46.1, ASME*, New York.

122. Degarmo, E. Paul et al., Materials and Processes in Manufacturing (9th ed.), *Wiley*, **2003**, 223.

123. J.C.Norris, surface free energy of smective clay minerals, *in SUNY*, **1993**, Buffalo.

124. Duncan B. et al., *NPL REPORT DEPC MPR 020*, **2005**.

125. Daniel Bonn, *Rev. Mod. Phys*., **2009**, 81(2), 739.

126. Hansen F.K., Surface Energy of Polymers, *University of Oslo*, **2004**.

127. https://theses.lib.vt.edu/theses/ available/ etd-05042001-163337/unrestricted/03Chapter2.pdf.

128. T.Young, An essay on the cohesion of fluids. *Philosophical Transactions of the Royal Society of London*, **1805**. 95: p.65-87.

129. Kabza K. et al., *J. of Chem. Edu*., **2000**, 77(1), 63.

130. Daniel Bonn, *Rev. Mod. Phys*., **2009**, 81(2), 739.

131. H. W. Fox and A. Zisman*, J. Colloid Sci*.,**1952**, 7, 428.

132. http:// www.biolinscientific.com/ application/surface-free-energy- measurement/.

133. Lang, N. et all, "Theory of Metal Surfaces: Work Function", *Phys Rev B*, **1971**, 3 (4), 1215

134. Gauyacq, J.P., Borisov, A.G., Charge transfer in atom-surface collisions: Effect of the presence of adsorbates on the surface, *Journal of Physics Condensed Matter*, **1998**, 10 (30), 6585.

135. Inglesfield J.E, Surface electronic structure, *Reports on Progress in Physics* , **1982**, 45(3), 223.

136. Young Keun Lee et al., *Nano Lett*., **2011**, 11, 4251–4255.

137. M.C. Teich, G.J. Wolga*, J. of the Optical Soc. Of Am*., **1966**, 57(4), 542.

138. Cardona M., Ley L., Photoemission in Solids, *Eds: Springer, Berlin, Germany*, **1978**.

139. Crowell C. R., *Solid-State Electronics*, **1965**, 8(4), 395.

140. M. Goldman et al., *Pure & Appi. Chem*., **1985**, 57(9), 1353.

141. http://www.tappi.org/content/events/07europlace/presentation/07europl51.pdf.

142. Monticelli F. et al., *Operative Dentistry*, **2008**, 33(3), 346.

1.4: SELF ASSEMBLED MONOLAYERS (SAMs)

143. J.C. Love et al., *Chem. Rev*., **2005**, 105, 1103-1169.

144. Poirier et al., *Science (Washington, D.C*.), **1996**, 272, 1145.

145. Li et al., *Langmuir*, **2003**, 19, 6744.

146. Love et al., *J. Am. Chem. Soc*, **2003**, 125, 2597.

147. Laibinis et al., *J. Am. Chem. Soc*., **1991**, 113, 7152.

148. Muskal et al., *Electroanal. Chem*., **1996**, 409, 131.

149. Nuzzo et al., *J. Am. Chem. Soc*., **1983**, 105, 4481.

150. Fenter et al., *Langmuir*, **1991**, 7, 2013.

151. Troughton et al., *Langmuir*, **1988**, 4, 365.

152. F. Schreiber, *Progress in Surface Science 65*, (**2000**) 151-256.

153. Schweizer et al., *Surf. Sci*., **2001**, 490, L627.

154. Semaltianos et al., *Thin Solid Films*, **2000**, 366, 111.

155. Skaife et al., *Langmui*r, **2001**, 17, 5448.

156. Hou et al., *Langmui*r, **1998**, 14, 3287.

157. Twardowski et al., *Langmuir* **2002**, 18, 5529.

158. Gutmann, Chemical mechanical planarization of microelectronic materials; *JohnWiley & Sons*: NewYork, **1996**.

159. Hegner et al., *Surf. Sci*., **1993**, 291, 39.

160. T.J. Senden and W.A. Duker, *Langmuir*, **1992**, 8, 733.

161. F.F Rossetti, *Langmuir*, **2003**, 19(24), 10116.

162. Schreiber, *F. Prog. Surf. Sci.,* **2000**, 65, 151.

163. Poirier, *G. E. Chem. Rev*., **1997**, 97, 1117.

164. Dubois, L. H. et al., *J. Chem. Phys*., **1993**, 98, 678.

165. Terrill, R. H et al., *Langmuir,* **1998**, 14, 845.

166. Peterlinz et al., *Langmuir*, **1996**, 12, 4731, (225).

167. Dannenberger et al., *Langmuir,* **1998**, 14, 4679.

168. Yamada, R. et al., *Chem. Lett*., **1999**, 667.

169. Yamada et al., *Lagmuir,* **2000**, 16, 5523.

170. Kawasaki, M.et al., *Langmuir,* **2000,**16, 1719.

171. Bain, C. D. et al., *J. Am. Chem. Soc*., **1989**, 111, 321.

172. Dubois, L. H. et al., *Annu. Rev. Phys. Chem*., **1992**, 43, 437.

173. Hicham Hamoudi et al., *Phys. Chem*. Chem. Phys., **2008**, 10, 6836.

174. M.A.D. Millone et al., *Langmuir,* **2009**, 25(22), 12945.

175. A. Ulman , Self-assembled monolayers of thiols, Thin Films, vol. 24, *Academic Press, San Diego*, **1998**.

176. G.E. Poirier, *Chem. Rev*., **1997**, 97, 1117.

177. H. Luth, Surfaces and Interfaces of Solids, *Springer, Berlin*, **1993**

178. L.H. Dubois et al., *J. Phys. Chem*., **1993**, 98, 678.

179. G. Scoles (Ed.), Atomic and Molecular Beam Methods, vols. 1 and 2, Oxford *University Press, Oxford*, **1992**

180. C.E.D. Chidsey et al., *J. Chem. Phys*., **1989**, 91, 4421.

181. R. Feidenhans'l, *Surf. Sci. Rep*., **1989**, 10, 105.

182. Roy D. Fendler*, J. Adv. Mater*. **2004**, 16, 479.

183. Young T., *Philos. Trans. R. Soc. (London)*, **1805**, 95, 65-87.

184. G. Bracco, B. Holst, Surface Science Techniques, *Springer Series in Surface Sciences*, 51, **2013**, Springer-Verlag Berlin Heidelberg.

185. J.H. Snoeijer, B. Andreotti, *Phys. Fluids*, **2008**, 20, 057101.

186. D.Y. Kwok, A.W. Neumann, in Contact Angle, Wettability and Adhesion, vol. 3, ed. by *K.L. Mittal (VSP International Science, Boston*, **2003**), p. 117.

187. Chibowski E., Malgorzata J., *Colloid Polym Sci*, **2013**, 291, 391.

188. Krumpfer JW, McCarthy TJ, *Faraday Discuss*, **2012**, 146, 103.

189. R.N. Wenzel, *Ind. Eng. Chem*., **1936**, 28, 988.

190. S. Baxer, A.B.D.J. Cassie, *Tex. Inst*., **1945**, 36, 67.

191. P. Letellier et al., *J. Colloid Interface Sci*., **2007**, 314, 604.

192. A.W. Neumann, R.J. Good, Surface and Colloid Science: Experimental Methods, vol. 11, ed. by *R.J. Good, R.R. Stromberg (Plenum Publishing, New York*, **1979**), p. 31].

193. L. Strong et all, *Langmuir*, **1988**, 4, 546.

194. C.E.D. Chidsey et all, *Langmuir*, **1990**, 6, 682.

195. F. Schreiber, *Progress in Surface Science*, **2000**, 65, 151.

196. Poirier, *Langmuir*, **1997**, 13, 2019.

197. Stapleton et al., *Langmuir*, **2003**, 19, 8245.

198. [J. Homola, *Chem. Rev*., **2008**, 108, 462.

199. Xia, Y. et al., *Microelectron. Eng*., **1996**, 32, 255.

200. Morgenthaler, S. et al., *Langmuir*, **2003**, 19, 10459.

201. http://www.cambridgenanotechald.com/applications/sams.shtml.

202. H.I. Kim et al., *Langmuir*, **1999**, 15, 3179.

203. Petrenko, V. F. et al., *Can. J. Phys*., **2003**, 81, 387.

1.5: GENERAL PROCESSING TECHNIQUES FOR ORGANIC ELECTRONICS

204. Daniel Dobkin, M.K. Zuraw, Principles of Chemical Vapor Deposition, *Springer Science & Business Media*, **2003**.

205. Gleason et al., *Materials Today*, **2010**, 26

206. Prasek J. et al., *J. of Mater. Chem.*, **2011**, 21 (40), 15872.

207. D. M. Maddox and William Andrew, Handbook of Physical Vapor Deposition (PVD) Processing, *Second Edition, Elsevier*, **2010**.

208. www.adnano-tek.com.

209. Laudise R.A. et al., *J.l of Cry. Growth*, **1998**, 187 (3-4), 449.

210. A. Briseno et al., *Nature*, **2006**, 444, 913.

211. R. Behrisch, Sputtering by Particle bombardment, *Springer, berlin*, **1981**.

212. http://lnf-wiki.eecs.umich.edu/wiki/Sputter_deposition.

213. http://static.ifp.tuwien.ac.at/homepages/Personen/duenne_schichten/pdf/t_p_ds_chapter2.pdf.

214. Shuang-Yuan Zhang et al., *Chem. Soc. Rev*., **2014**, 43, 2301.

215. http://www.slideshare.net/seta667/hints-elfos-forslidesahre.

216. Chang et al., *Chem. Mater*., **2004**, 16, 23.

217. McCulloch et al*., Nat. Mater.,* **2006**, 5, 328.

218. Al-Dahoudi N. et al., *Thin Solid Films*, **2001**, 392(2), 299.

219. W.-B. Byun et al., *Current Appl. Phys.*, **2011**, 11.

220. Z. Bao, *Adv. Mater*., **2009**, 21, 1217.

221. http://www.toa-optical.com/.

222. Sandberg et al., *Langmuir*, **2002,** 18, 26.

223. http://www.gwent.org/gem_screen_printing.html.

224. F. C. Krebs et al., *Solar Energy Materials & Solar Cells*, **2009**, 93, 422.

225. Anke Teichler et al., *J. Mater. Chem*. *C*, **2013**, 1, 1910.

1.6: INKJET PRINTING PROCESS

226. Elmqvist R., *US Patent No. 2566443*, **1951**.

227. Sweet R., *US Patent No 3596275*, **1971**.

228. Zoltan S., *US Patent No. 3683212*, **1972**.

229. Stemme N., *US Patente No. 3747120*, **1972**.

230. http://www8.hp.com/h20195/v2/GetPDF.aspx/4AA6-1075ENW.pdf

231. http://www.tonejet.com/content/4-downloads/20160812-the-ijc-electrostatic-jetting/ijc2015-tonejet.pdf.

232. W. Ohnesorge*, J. Appl. Math. Mech*., **1936**, 16, 355.

233. N. Reis et al., *Mater. Res. Soc. Symp. Proc*., **2000**, 625, 117

234. N. Reis, C. Ainsley et al., *J. Appl. Phys*., **2005**, 97, 094903

235. B. Derby et al., *MRS Bull*., **2003**, 28, 815-818.

236. Berry JM, Corpon GP, *UN Patent No., 3653932*, **1972.**

237. Bhatia YR, Stallworth H., *US Patent No. 4567213,* **1986.**

238. Chandrasekaran CK, Ahmed A, Henzeler TE, Eu*ropean Patent WO 2003076532 A1,* **2003.**

239. Noguchi H et al., *RadTech Report*, **2001**, 15(2), 22-25.

240. https://en.wikipedia.org/wiki/Viscosity.

241. Adamson AW., Physical Chemistry of Surface, *5th ed., Wiley Interscience, New York*, **1990**.

242. Roren MJ, Surface and Interfacial Phenomena, 3RD ed., *Wiley Interscience*, **2004**, 243-276

243. Van Dam DB et al., *Phys Fluids*, **2004**, 16, 3403-3414.

244. K. K. B. Hon et al., *CIRP Annals - Manufacturing Technology*, **2008**, 57, 601-620.

245. R. Rioobo et al., *Exp. Fluids*, **2002**, 33, 112-124.

1.7: COMBUSTION PROCESS FOR INKJET FABRICATION OF NANOTHIN ALUMINUM OXIDE DIELECTRICS

246. Park et al., *Thin Solid Films*, **2012**, 520, 1679–1693.

247. Fortunato et al., *Adv. Mater*., **2012**, 24, 2945–2986.

248. Han S-Y et al., *J. Am. Chem. Soc*., **2011**, 133, 5166–5169.

249. Lee J S et al., *J. Korean Phys. Soc*., **2011**, 59, 3055.

250. Avis C and Jang J, *J. Mater. Chem*., **2011**, 21, 10649.

251. Ahn B et al., *ACS Appl. Mater. Interfaces*, **2014**, 6, 9228.

252. Kim C et al., *Thin Solid Films*, **2013**, 544, 129.

253. Park J. H. et al., *Appl. Phys*., **2011**, 50, 070201.

254. Rita Branquinho et al., *Semicond. Sci. Technol*., **2015**, 30, 024007.

255. Zongping Shao et al., *Progress in Materials Science*, **2012**, 57, 804.

256. S.R. Jain et al., *Combust. Flame*, **1981**, 40, 71.

257. Rita Branquinho et al., *ACS Appl. Mater. Interfaces*, **2014**, 6, 19592.

1.8: THIN FILM TRANSISTOR

258. http://www.cstf.kyushu-u.ac.jp/~adachilab/lab/?page_id=3898.

259. B. Chandar Shekar et al*., Korean J. Chem. Eng.,* **2004**, 21(1), 267.

260. E. Fortunato ey al., *Adv. Mater*., **2012**, 24(22), 2945.

261. A. P. P. Correia, P. Barquinha, and J. C. da P. Goes, A Second-Order ΣΔ ADC Using Sputtered IGZO TFTs, *springer, Cham* **2016**.

262. T.Fet et al., "field effect transistor", pp. 1-7.

263. http://www.eng.uokufa.edu.iq/staff/alikassim/lectures/CH-6.pdf.

264. Eric A. Schiff, *Mater. Res. Soc. Symp. Proc*., **2009**, 1153,

265. Spray coating methods for polymer solar cells fabrication: A review, Aziz, F., Ismail, A.F., **2015**, *Materials Science in Semiconductor Processing*.

CHAPTER – 2

RESULTS, DISCUSSIONS AND MATERIALS & METHDOS

2.1 PRELIMINARY SCREENING OF OSSC OF INTEREST

Nowadays OSs materials are present as active layers in numerous applications, including field effect transistors, light-emitting diodes, photovoltaic cells, and radiation sensors. The most important application of OSs materials connected to this PhD work is the possibility to directly detect high energy photons, as X- or Gamma-rays [1]. The first report that suggests the use of OSs materials for this purpose was in the early 60s [2, 3, 4], as scintillators in indirect detectors, dispersed in polymeric matrices or in liquids. Among the characteristics of the OSSCs there is an intrinsic order of the crystalline lattice. This gives translational symmetry and also has a positive impact on the transport properties of the charge because it removes grain boundaries, that reduce the transport of charge in the materials [5]. For this reason, OSSCs are perfect candidates for a key role in organic semiconductors for the XXI century. Indeed, OSSCs recently showed properties of direct detection for ionizing radiation (i.e., direct conversion of high energy photons into electrical charges collectable at properly designed electrodes, without the need for a second device, like a photodiode, coupled to the detecting element) [6, 7]. Moreover, their density is similar to that of the human body tissue, making them perfect for medical applications [8]. OSSCs can be grown via solution methods, that allow the realization of large, high quality single crystals at low production costs. Until now there have not been large area detectors based on organic single crystals technology aren't available on the market, due to their intrinsic problem as stability, reproducibility and time-dependent degradation caused by environmental conditions (humidity, temperature oscillations, mechanical stress). Since there is plenty of organic molecules able to form crystals, before starting to print solutions for OSSCs direct growth on substrate a screening of possible molecules of interest has been carried out, as hereafter described.

2.1.1: TESTED ORGANIC MOLECULES

A first selection of suitable molecules has been made by extensive screening of commercially available molecules and related crystallization tests, to which X-rays response tests followed. This screening activity has been carried out by another researcher in the frame of a parallel PhD work [9] developed in collaboration with the department of Physics and Astrophysics of UniBo, with which my PhD project has been developed in the frame of the European Project i-FLEXIS.

Upon the above mentioned preliminary screening, the most interesting molecules resulted to be: 4-hydroxycyanobenzene (4HCB), 1,8-Naphthalimide (NTI), 1,5-dinitronaftalene (DNN), 6,13-Bis-triisopropylsilylethynyl-pentacene (TIPS). Hereafter a brief overview of each molecule's properties is given.

4HCB

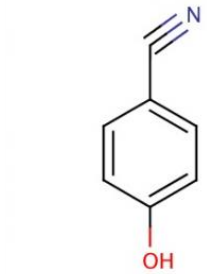	**4-hydroxycyanobenzene (4HCB)**	
	CAS	767-00-0
	Molecular Weight [g/mol]	119.121
	Melting Point [°C]	110
	Solubility	Ethylic ether, toluene
	Density [g/cm^3]	1

4HCB single crystals can be grown in tunable-size by solution grow methods. They have anisotropic electronic transport properties along the tree main crystallographic axes dimensions [10]. The habit of 4HCB crystals is platelet-like. Among the tested OSSCs, 4HCB showed the best X-rays detection properties [6, 7]. However, due to the low molecular weight, 4HCB crystals tend to sublimate even at room temperature, although at a very slow rate (not perceptible in macroscopic crystals). While this is not a particular problem for laboratory experiments, in practical applications this tendency hinders a full industrial applicability of 4HCB.

NTI

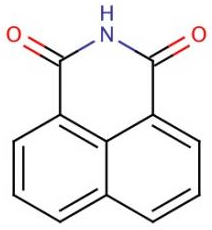	**1,8-Naphthalimide (NTI)**	
	CAS	81-83-4
	Molecular Weight [g/mol]	197.19
	Melting Point [°C]	300
	Solubility	THF, Chloroform
	Density [g/cm^3]	1.47930

NTI has a good response to X-rays [6]. The habit of NTI crystals is needle-like, characterized by an aspect ratio of about 1:20. Rapid evaporation of the solvent from a casted solution does not lead to formation of single crystals, determining instead the growth of a polycrystalline layer.

DNN

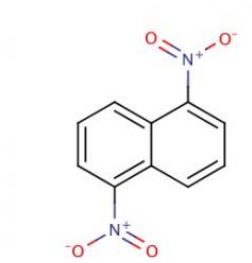	**1,5-dinitronaftalene (DNN)**	
	CAS	605-71-0
	Molecular Weight [g/mol]	218.17
	Melting Point [°C]	213
	Solubility	CHCl3, Toluene
	Density [g/cm^3]	1.481

DNN showed a good response to X-rays [11], and it forms cylinder-like crystals whose aspect ratio is about 1:5.

TIPS

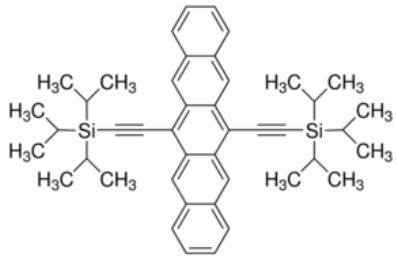	**6,13-Bis-triisopropylsilylethynyl-pentacene (TIPS)**	
	CAS	373596-08-8
	Molecular Weight [g/mol]	639.07
	Melting Point [°C]	276
	Solubility	aceton, anisole, toluene, tetralin
	Density [g/cm^3]	1.104

TIPS is one of the most interesting organic semiconducting molecules available in commerce. The presence of the isopropyl groups increases its solubility in organic solvents, and its pentacenic core allows to reach charge carrier mobilities as high as a few cm2/Vs [12, 13]. It generally forms polycrystalline thin layers that showed very good X-rays detection properties [8].

2.1.2: PRELIMINARY CRYSTALLIZATION TESTS

There are a lot of methods that can be used to produce high purity, low density of defects and high performances OSSCs. Physical Vapor Deposition (PVD) is one of the most used techniques for this purpose. In PVD, organic molecules are inserted in an oven to sublimate them. The generated vapor is then carried along the oven (usually a tubular one) by an inert gas, until

reaching a cold wall, where molecules reorganize themselves to form crystalline structures. The temperature of the process can be relatively low, so the insertion of the target surface directly inside the evaporation chamber is allowed. Thus, also paper-based or polymeric substrates can be used, without the risk of damaging the substrate [14, 15]. PVD is a suitable method to deposit OSSCs in optoelectronic applications, on flexible substrate thanks to the small thickness obtained through a careful optimization of the deposition parameters [16]. One of the problems of this technique is the high cost of the equipment, in addition to the very slow throughput. Then, the size of the final crystals is small, in the order or hundreds of microns, and this fact limits the possibility to use OSSCs from PVD as scintillators in indirect x-ray detectors.

Solution growth is a very interesting technique, able to directly grow the crystals onto devices in a fast and inexpensive way. At the same time, solution growth can be used to produce a considerable amount of large, self-standing OSSCs [17] which can be used for preliminary test in research activities. It is a very simple and direct technique, in which organic molecules are dissolved in a medium constituted by an organic solvent or by a mix of two or more ones. There are four different possible crystal growth process ,figure 2.1-1 [18]: i) solvent evaporation, wherein the solvent is allowed to evaporate in a temperature and saturation controlled environment, it disappears completely; ii) Temperature reduction, in which the low temperature promotes the decrease of organic molecule solubility and the crystals formation on the bottom of the vessel; iii) antisolvent vapor diffusion, in which the open vessel is inserted in a secondary vessel containing an appropriate antisolvent which promotes the formation of the crystals through its vapor diffusion; iv) antisolvent liquid diffusion, wherein inside the same vessel a solvent and an antisolvent are placed, one on the top of the other. The antisolvent diffusion inside the solvent promotes the decrease of the solubility of the organic molecules and the formation of the crystals. In literature, one of the first described attempts to grow OSSCs from solution was made using the solvent evaporation method [19], but the result was a polycrystalline film. The first successes in solution growth was the production of TIPS-pentacene crystals composed by a several micro-crystals with the size in the order of 10 µm [20, 21].

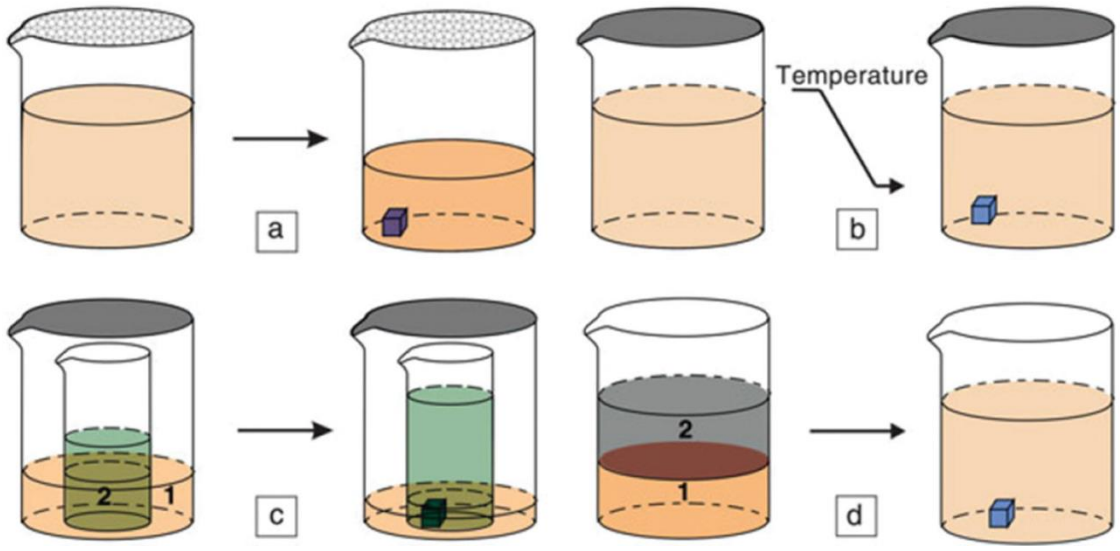

Figure 2.1-1: a) slow solvent evaporation; b) slow cooling; c) antisolvent (1)-solvent (2) vapor diffusion; d) antisolvent liquid diffusion.

The aim of this research work was to grow OSSCs using Inkjet Printing process on interdigitated electrodes, at room temperature. This growth process is essentially based on the slow solvent evaporation method, as the printed drop is exposed to external atmosphere until complete solvent evaporation and crystal formation. In this process, the velocity of evaporation of the printed drop is limited only by the solvent boiling point (a proxy of its vapor pressure). The higher the boiling point, the slower the whole solvent evaporation process, and the better the grown crystal morphology. Therefore, all the inks used in this research have been tested before printing in order to understand if the selected solutions could generate organic crystals; specific tests have been performed to identify the proper solvents to be used for each above reported molecule. Preparation methods and crystal growth will be discussed in the next chapter.

One of the major constraints in formulating a jettable ink is the ink viscosity. The limit for the ink viscosity is fixed by the used printer cartridge, in the range from 10 cP to 12 cP (Dimatix DMP 2831 printer, cartridge model DMC-11610, 10 pL).

In view of the above-mentioned characteristics of the work to be carried out, important selection criteria for organic solvents were their intrinsic viscosity and their boiling points, which are two different but connected parameters depending on the intermolecular forces at work in the liquid. Low boiling point solvents can be used only in a low temperature environment, where evaporation rate and viscosity are reduced. Solvents characterized with high boiling point are usually a good choice for the ink formulation because they have a good viscosity, suitable for the ink jet printing process, and a low evaporation rate, reducing the risks of nozzle clogging.

Moreover, high boiling point solvents reduce the evaporation rate, promoting the growth of large and defect-free crystals.

Also the concentration of the molecule to be crystallized in the ink has a strong influence on the size of the crystal to be grown: high concentration solutions promote the formation of large crystals, but only in connection with a low evaporation rate (otherwise extended nucleation, hence formation of amorphous material or poly-crystals occurs).

In order to properly identify the correct ink formulations, preliminary crystallizations of molecules of interest have been carried out on model substrates, as for the following table 2.1-1. The systems giving the most interesting results in terms of quality of the so-grown crystals have been considered for moving to the printing step.

Table 2.1-1

ORGANIC MOLECULE	SOLVENT	CONCENTRATION [mg/mL]	MOVE TO THE PRINTING STEP
4HCB	Nitrobenzene	8	Yes, only for a short period
NTI	DMSO	5	Yes, only for one time
DNN	Dichlorobenzene	3.5	No, only Drop Cast
DNN	Dichlorobenzene	20	Yes, only for one time
TIPS	Aceton	2	No, only Drop Cast
TIPS	Benzonitrile	4	No, only Drop Cast
TIPS	Nitobenzene	4	Yes, only for a short period
TIPS	Toluen	6	No, only Drop Cast
TIPS	Toluen	20	Yes, only for one time
TIPS	Dichlorobenezene	6	Yes, only for a short period
TIPS	Dichlorobenzene – 60% Chloroform – 40%	6	No, only Drop Cast
TIPS	Dichlorobenzene – 80% Chloroform – 20%	6	No, only Drop Cast
TIPS	Anisole	10	Yes, only for one time
TIPS	Trichlorobenzene	6	Yes, only for one time
TIPS	Trichlorobenzene – 60% Dichlorobenzene – 40%	6	No, only Drop Cast

TIPS	Trichlorobenzene – 90% Chloroform – 10%	6	No, only Drop Cast
TIPS	Tetralin	5.75	Yes, main ink, first version
TIPS	Tetralin	20	Yes, main ink, second version

As it can be seen, except for TIPS, all the tested crystals evidenced one or more practical problems: 4HCB is too prone to sublimation; NTI and DNN are more robust and do not sublimate at room temperature, but they do not deliver good quality crystals with the considered inks upon inkjet printing, and their X-rays response is less effective than that of TIPS.

The crystals for this screening phase have been grown on different types of substrate. Teflon had been chosen as substrate for first tests because of its low surface energy that promotes the shrinking of the deposited drop and, at the same time, the decreasing of the coffee-ring formation. For successive tests, different materials were used as substrate: PET, PEN and Kapton; only during some first trials, also glass had been used, but later its usage has been abandoned because it is not suitable to realize flexible devices. The main features of each used substrate are hereby reported.

PET – Polyethylene Terephthalate

Figure 2.1-2 shows the chemical structure of PET, which is a biaxial oriented thermoplastic polymer, and in this specific case it is biaxially oriented. The average sheet thickness is around 175 µm. Its main proprieties are: dimensional stability, good chemical resistance (except to alkalis that make it hydrolyze), high transparency when processed in thin films. It can operate in the range of 115°C to 150°C but geometrical distortion of PET film occurs starting from 60°. Finally, it has good flexibility - tensile strength in the range 190-260 MPa.

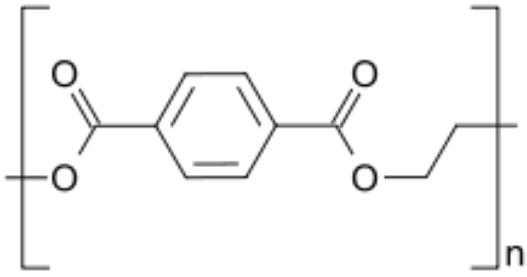

Figure 2.1-2: PET structure.

PEN – Polyethylene Naphtalate

PEN, figure 2.1-3, has a chemical structure similar to that of PET but it has a better temperature resistance due to the presence of a second aromatic ring. It can be biaxially oriented and an average sheet thickness is around 125 µm. The main differences between the PET and PEN are the maximum work temperature, which for PEN is 190°C against the only 150°C for PET, and a higher stretch resistance than PET in the region of 100°C to 150°C. PEN is a perfect polymer for the processes that require a post temperature treatment. On the other hand, its surface can be damaged more easily.

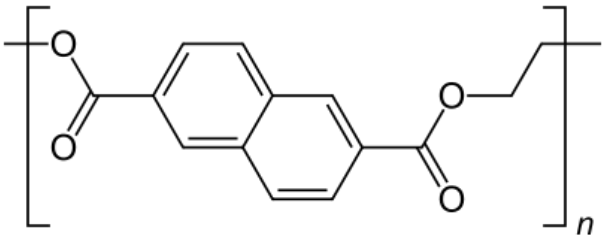

Figure 2.1-3: PEN structure.

Kapton – Polyimide film

Poly(4,4'-oxydiphenylene-pyromellitimide) or Kapton, figure 2.1-4, is normally used in flexible electronic applications, as substrate for printed circuits; it is also used to realize devices for aerospace industry. It has low flammability and smoke emission, it has a high resistance to thermal shock and to strongly ionizing radiations without any degradation. The thickness of the film is 125 µm and the temperature working range is from -270°C to 320°C. Anyway, it can be easily scratched and it poorly resist to alcohols.

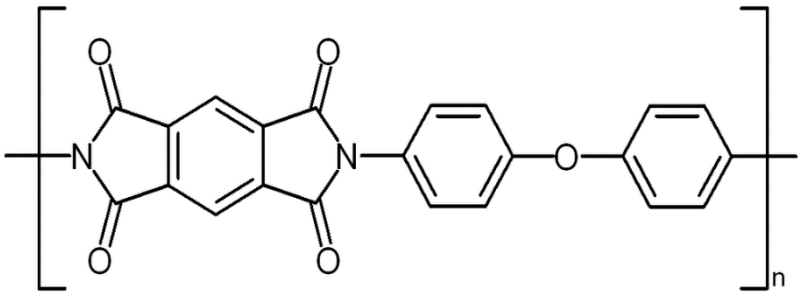

Figure 2.1-4: Kapton structure.

TEFLON® - Polytetrafluoroethylene

TEFLON, figure 2.1-5, has the same chemical structure of the polyethylene but with fluorine instead to hydrogen atoms. It has been used as substrate during preliminary crystallization tests. Its main characteristics are: i) complete chemical inertia, only alkaline melted metals can damage it; ii) fluids do not change their properties when put in contact with it; iii fire resistance: it does not allow flame propagation; iv) it is a perfect dielectric layer; v) low surface tension, 20 mN/m; vi) low friction; vii) high temperature resistance from -270°C to 327°C.

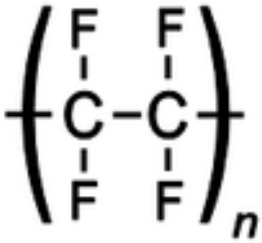

Figure 2.1-5: TEFLON structure.

Also the effect of temperature on the crystal development has been briefly explored. As is visible in table 2.1-2, a lower growth temperature affects both the crystal growth time and the final crystal sizes. Even though lower temperatures are able to deliver larger (and more morphologically perfect) crystals, the difference with room temperature in terms of obtained crystal sizes is not dramatic. On the other hand, the lower temperature increases dramatically the time needed for the crystal development. For this reason, all the printing experiments have been carried out at room temperature, placing the printer under a fume hood in order to avoid as much as possible the contamination of the substrate from dust. The error is calculated via standard deviation.

Table 2.1-2

FINAL SIZE [mm]					
TYPE OF SOLVENT		TEMPERATURE			
		4°C		ROOM (21°C)	
		Approx. time to achieve crystal growth	Average crystal size (mm)	Approx. time to achieve crystal growth	Average crystal size (mm)
Tetralin	Length	From 3 to 4 days	2.7 ± 0.8	From 24 to 36 hours	2. ± 0.6
	Width		1. ± 0.3		0.8 ± 0.2

Toluene	Length Width	From 4 to 5 hours	0.8 ± 0.1 0.4 ± 0.2	From 35 to 45 minutes	0.514 ± 0.1 0.17 ± 0.1

Upon the above mentioned findings, only TIPS was further considered for inkjet printing, together with tetralin as a solvent, at different concentrations.

2.2 PRINTING OF INKS BASED ON ORGANIC SEMICONDUCTOR MOLECULES

The IJP technique seems to satisfy all the requirements for achieving a prominent position in the micro-electronic production sector. In particular, IJP allows covering a large area with a single deposition step, and different layers of the same material or of different ones can be deposited by using different print heads in a continuous printing process. These characteristics, together with the limited waste of printed material, makes IJP very attractive and cost-competitive for mass production of electronic devices. In this frame, organic electronics ideally pairs with the IJP-based fabrication paradigm. In fact, the synergy between IJP and organic electronics allows to realize well defined patterns and to use a wide number of compounds with reduced costs [22,23].

Only in the last few years the interest in printed OSs has been focused on the production of semiconducting single crystals. In fact, IJP devices base on OSs have been long based on semiconducting polymers [24]. In 2011 Minemawari et al. combined the printing process with the solvent/antisolvent growing technique, in which a double printing sequence, first with a crystal-precursor molecule dissolved in an appropriate solvent, and then with anti-solvent, promoted the growth of crystals on top of the substrates [25].

The growth of OSSCs from inkjet printed solutions has a series of issues, starting from the evaporation of the solvent. In fact, printed solvents start evaporating immediately after the drop has left the nozzle; this makes the concentration of the deposited solution rapidly increasing, causing in turn the reaching of critical saturation, upon which nucleation seeds start being created. Since the printed drops have a very small volume (a few tens of pL), the whole solvent evaporation phenomenon is very fast, and usually a polycrystalline layer, instead of a single crystal, is produced. Another common problem generating poly-crystals instead of single ones is related to heterogeneous surfaces (i.e., different materials lying besides each other on the substrate) and/or nanostructured interfaces. These abrupt changes of surface energy, typically found for example in lithographically defined interdigitated electrodes on plastic substrates, create the conditions for fast and sudden nucleation, further increasing the tendency to create polycrystalline materials instead of single crystals. However, poly-crystals should be avoided for electronic applications. In fact, the presence of polycrystalline domains favor the electron-hole recombination inside the grain boundaries, reducing the amount of charges collected at the electrodes [26].

For these reasons, the core of the research activity hereafter described is related to the modification and optimization of inks and substrates in order to print solutions able to generate OSSCs directly onto interdigitated electrodes.

2.2.1: PRINTING TESTS

First printing tests have been performed using TIPS-Pentacene as the OS and tetralin as the solvents (*figure* 2.2-1).

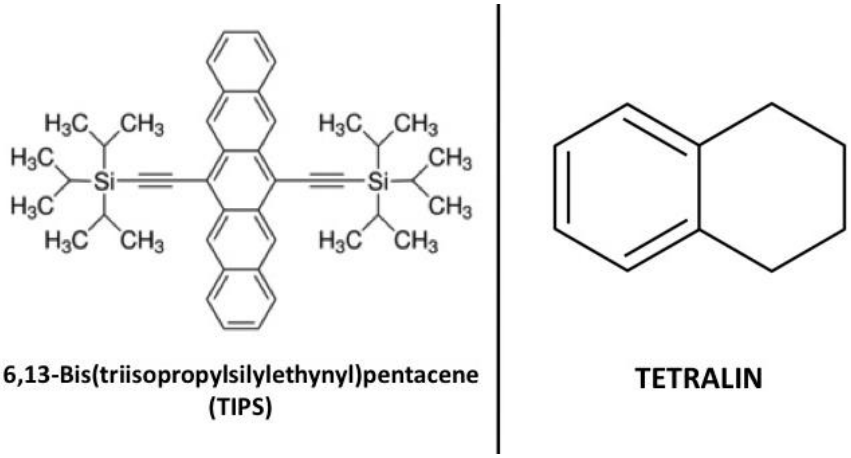

Figure 2.2-1: TIPS-pentacene structure on the left and Tetralin structure on the right.

Tests were performed varying the concentration of this solution from 5 to 30 mg/ml. At the higher concentration, no precipitate was observed when the solution was left undisturbed for more than 1 month at room temperature. To be sure that no precipitation occurred within the printer cartridge, it was decided to limit the ink concentration at 20 mg/mL.

The viscosity of the solutions was studied only in the first research period (with the HAAKE RS 150 Rheo Stress at 20°C). The change in viscosity due to the addition of TIPS molecules is under 1% respect the viscosity of the pure solvent, therefore it was decided to consider the inks viscosity equal to that of the pure solvents, that in the specific case of tetralin it is 2,02 at 25°C [27]. Tetralin has a high boiling point (207°C) that allows a slow evaporation of the solvent, in turn both reducing the possibility of nozzle clogging to occur and slowening the solvent evaporation process, which is beneficial for better crystallization of TIPS. Ink lifetime has been assessed to be of two days, and each of the hereafter-presented samples has been obtained with inks no more than two days old, to avoid any degradation of the semiconductor molecule caused by its interaction with light, and its consequence dimerization [58].

Printing experiments have been carried onto different substrates, including glass, silicon/silicon oxide chips and interdigitated gold electrodes lithographically defined on PEN made at the University of Cagliari (more details in “Materials and Methods” ,2.7.3).

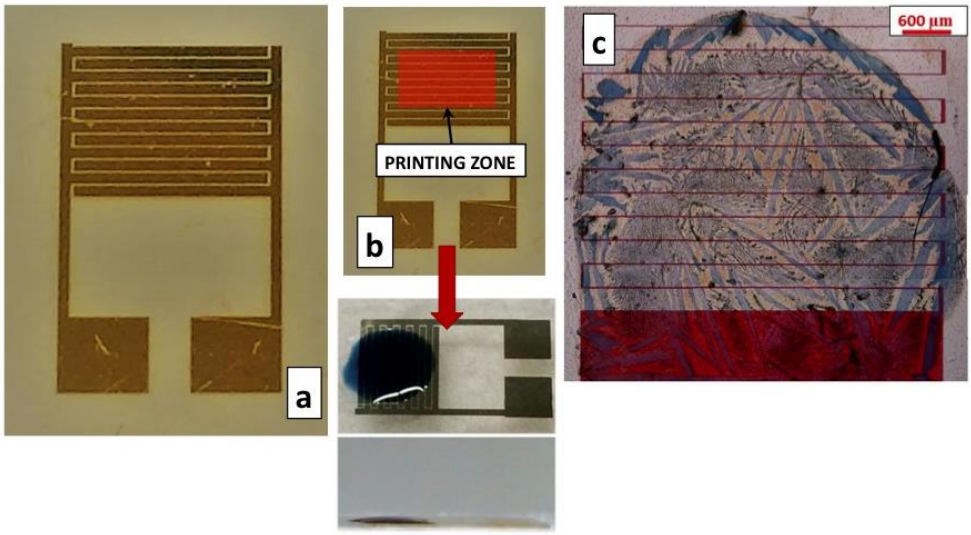

Figure 2.2-2: a) digital photo of a PVD gold electrode on PEN at UniCa; b) indication of the printing zone (upper part) and digital photos of an inkjet printed drop on bare gold; c) crystals grown from a spreading inkjet printed drop.

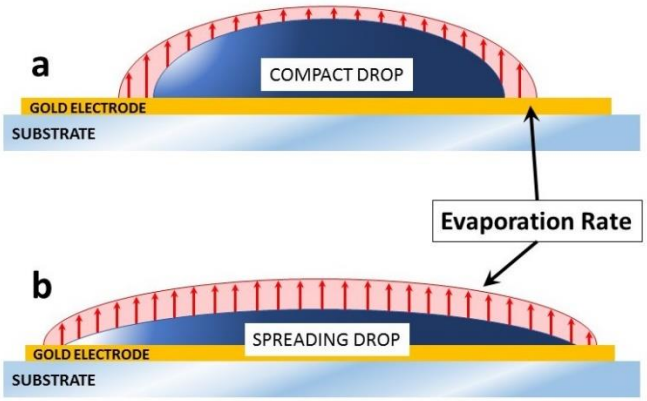

Figure 2.2-3: scheme of different evaporation rates between a spreading drop and a compact one.

As described in par. 1.3 and 1.6, the wettability of ink printed onto a substrate depends strongly from the substrate roughness and surface energy. The high surface energy of gold (1,8 N/m) promotes the complete spreading of the tetralin (35,5 mN/m at 25°C) based ink on the electrode surface (figure 2.2-2 “b”). However, the excessive spreading of the printed drop is to avoid, because spreaded drops are characterized by high evaporation rates (*figure* 2.2-3), that leads to the formation of small, ill-defined and dispersed polycrystals (*figure* 2.2-2 “c”)

Another phenomenon related to high evaporation rates is the coffee ring effect: the highest evaporation rate occurring at the border of the drop causes the primary growth of the crystal at and from the drop border. This causes the majority of the solid material originally present in the ink to disorderly accumulate in the coffee ring, while the small amount of material remaining at the center of the drop is only able to create a discontinuous layer of polycrystalline domains (figure 2.2-4) [28].

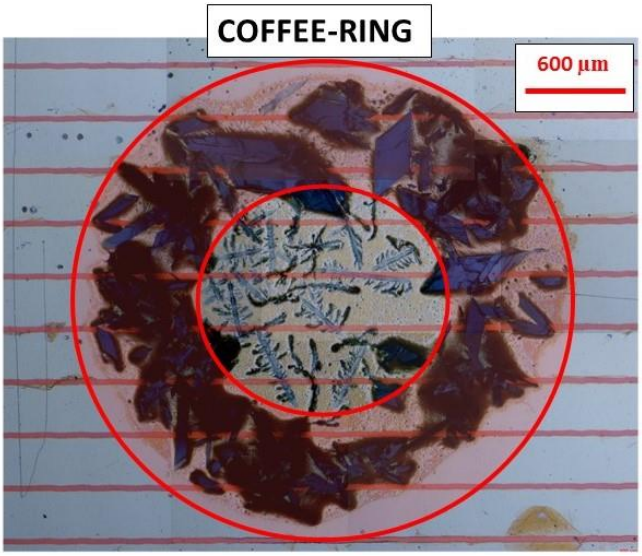

Figure 2.2-4: coffee-ring effect of printed drops. The red ring underlines the crystals present on the coffee-ring that contains the major amount of material in comparison with the discontinuity center coverage.

When this coffee ring phenomenon takes place on heterogeneous substrates like the here used interdigitated gold electrodes on PEN, the final result in terms of highly polycrystalline and disordered layers is ensured.

In order to stimulate single crystal formation, it is thus required to limit the spreading of the drop. In literature, several solutions to this issue have been proposed, as follows:

i) use of solvents/anti-solvents interaction [25] to generate a homogenous poly-crystalline surface;

ii) double solvents approach [29];

iii) physical surface modification via UV treatment [30];

iv) chemical surface modification using SAMs [31];

v) chemical surface modification with partial covering by means of polymers [32]

In this work, it has been chosen to adopt the chemical surface modification approach, by printing a fluorinated SAM onto the substrate. The detailed description of this process will be

given in paragraph 2.3. In the following a detailed description of the inkjet printer used for these studies is given.

2.2.2: INKJET PRINTER DIMATIX - 2831

DIMATIX inkjet printer series 2831 (*figure* 2.2-5) is a widely used semi-industrial printer for research activities aimed to develop and optimize inks. It allows to easily changes the printed ink and it is can pint features with high resolution and the drop depositing is controlled from piezoelectric actuators; the main components of the printer are shown in *figure* 2.2-5.

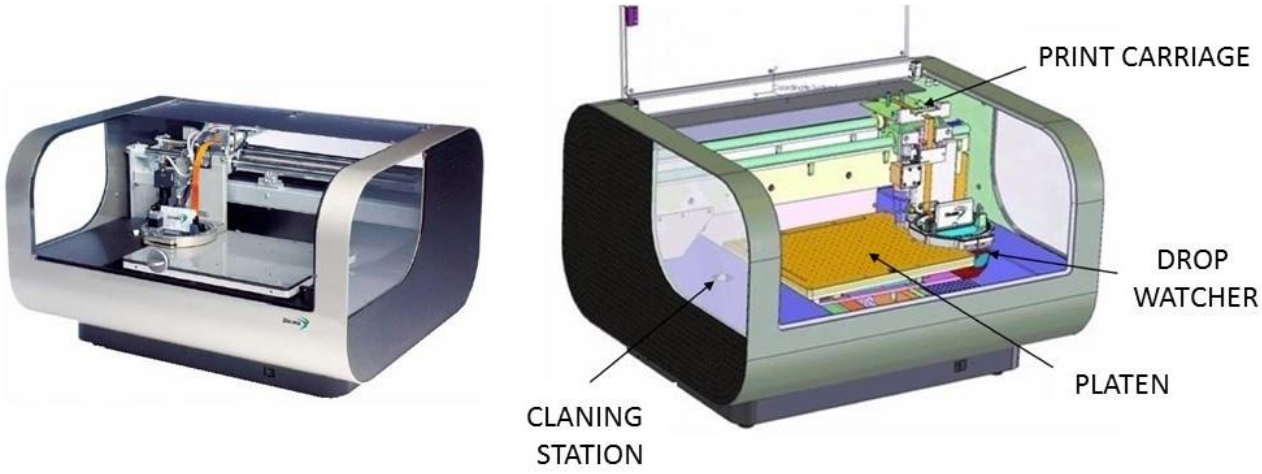

Figure 2.2-5: Digital photo of DIMATIX Inkjet Printer Series 2831 on the left and a scheme of the main components on the right.

The Printer Carriage is the cartridge support and is the core of the printer, because it positions the cartridge with high precision and move all the part over the substrate with 1μm precision, along the metallic plate and in height. The only constraint is related to the height of the substrate, which it can be at maximum of 25mm. The Platen is the support for the substrate, it has a vacuum system to block the sample and a heater system in case it would be required printing onto hot substrates till 60°C. Room temperature sets the lower temperature operating limit, because there isn't a cooling system. On the left side of the printer there is a cleaning station, where the nozzles can be cleaned onto a dedicated pad; here it is then set the home position for the cartridge. At the opposite site, there is the Drop Watcher system: a camera and a mirror allow

to watch the status of the nozzles and to control the size of the drops; in this way, it is possible to select the nozzles to be used and to exclude from printing the clogged ones.

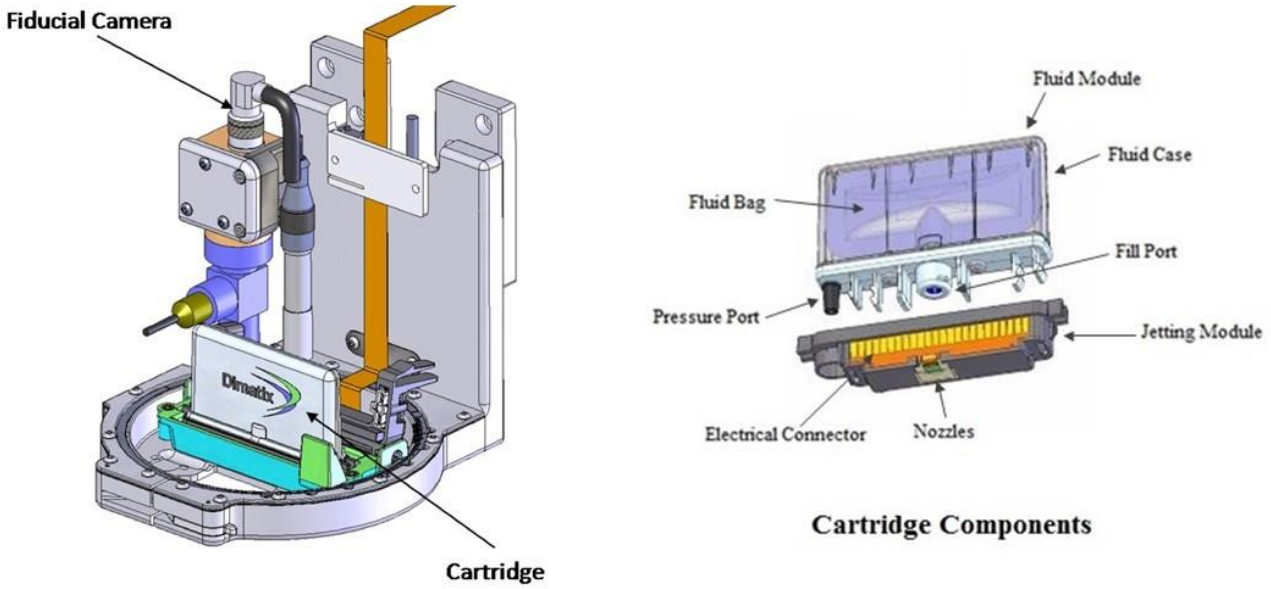

Figure 2.2-6: on the left, scheme of the printing carriage that shows where the cartridge is located, and on the right the cartridge components.

The Printing Carriage *figure* 2.2-6 is the core of the printer, also because it is here hosted the Fiducial Camera, a camera used to supervise monitor printing results, and to control the alignment of the substrate. Carriage moves above the substrate along x axis, while the platen moves along y one. Printing process takes place from the upper part to the bottom of the feature which has to be printed and from the left to the right. It is important to take it in account in order to achieve optimal printing results. Cartridges are composed by two different parts: the fluid module is made by a rigid skin and a soft bag, which acts as 3 mL ink reservoir and it is made in order to be robust to organic solvents. The second part is the jetting module in which in which 16 nozzles are distributed in line; the distance between the nozzles is 254 µm and the diameter of each nozzle is 21.5 µm. Nozzles can be heated till 70°C in order to decrease viscosity of the inks whether fluid viscosity should be too high or if it was required to print hot ink. The characteristics of the fluid to be injected inside the cartridge must comply with the following specifications:

- Viscosity: 10 - 12 cps at jetting temperature;
- Surface Tension: 28 - 33 dyne/cm at jetting temperature;
- Low Volatility: Boiling points higher than 100°C;
- Degassing: Degassing can be done with a vacuum system, by ultrasonic baths or by spinning;

- Filtering: it is recommended to filter the fluids with a 0,2 µm porosity filter;
- Acidity: pH range from 4 to 9.

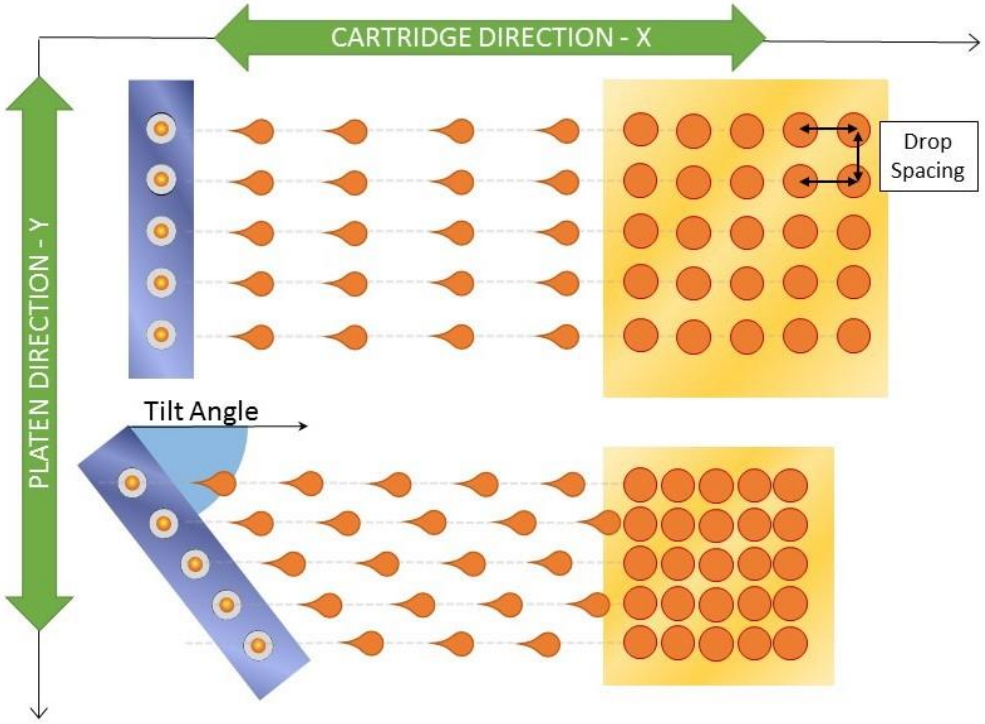

Figure 2.2-7: The printing resolution depends on the drop spacings between the drops, by changing the angle of the cartridge (changing the tilt angle) it is possible to obtain different drop spacing and therefore different resolutions.

Drop Spacing and Resolution (*figure* 2.2-7) are two fundamental parameters, which must be taken in account during the printing process. Drop Spacing is the distance between the center of two drops along the X and Y axes that the printer has deposited on the target substrate and it is the main parameter, which affects printing resolution. Then, drop spacing is related to the total amount of material, which is deposited after a printing session. DIMATIX printer is provided with two different jetting modules: 10pL or 1pL. So, printing resolution depends also on the kind of cartridge used. Thus, smaller spot increase the resolution and the possibility to print higher quality details; anyway, these details cannot be smaller than a singular drop size. Generally, a drop of 10pL of volume produces a spot of around 40um if deposited onto a polymeric or a gold substrate at 28°C.

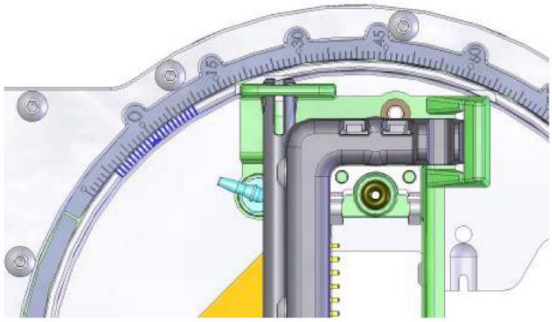

Figure 2.2-8: cartridge-mounting angle scales. It is used to modify the drop spacing.

For DIMATIX 2831 the drop spacing range extends from 5 to 254 µm, and depends on the cartridge-mounting angle, as shown in *figure* 2.2-8. Changing this angle causes the change of the relative distance between the nozzles with the consequence of an increased resolution. Such angle must be manually set by rotating the cartridge support. The most used angles related to the most common drop spacing values are listed in the datasheet of the printer. Relation between the resolution and the drop spacing is: $Drop\ Spacing[\mu m] = \frac{25400}{Resolution\ [dpi]}$ Thus, the choice of the correct drop space value strongly depends on the size of the spot, which can be anyway measured by using the fiducial camera.

Figure 2.2-9: drop watcher window on the left, and not ideal drop falling effects: misdirected jets, tails and not matched velocities.

The last important step before start printing is the “drop watcher” procedure, which allows watching and optimizing the shape of the drops and how drops are leaving from the nozzles (*figure* 2.2-9). In this section of the printing process, it is possible to identify the clogged nozzles, in order to exclude them from the printing of ink (together with nozzles not printing properly). The procedure is quite simple and at the same time extremely important. The drops fall continually

from the nozzles, in this way it is possible to find the not clogged, the misdirect drop and the drop velocity. Changing the printhead potential, which is used to control piezoelectric actuators, the jetting frequency, and the firing voltage it is possible to optimize the printing process.

2.3 CHEMICAL MODIFICATION OF THE SURFACE VIA SAMs

As mentioned in paragraph 2.2, drop spreading is the main problem leading to the formation of polycrystalline areas; drop spreading can in addition induce crystallization outside the desired areas.

After having formulated the first TIPS-tetralin jettable ink, first attempts have been made to print this ink onto interdigitated gold electrodes deposited on PEN (from now on, briefly IDTs). As expected, the printed ink rapidly showed extended spreading of the drop onto the IDT surface, even though a few elongated single crystals were visible in the coffee ring zone of the deposition (*figure* 2.3-1), whose formation was probably favored by the high boiling point of tetralin.

Figure 2.3-1: crystals growth after the spreading of a printed drop. It is possible to see the coffee-ring formation.

In order to try to solve this problem, it has been observed that drop spreading on Teflon surfaces, used for preliminary drop casting tests made during the TIPS ink formulation phase, didn't occur. This phenomenon was due to the low surface energy of Teflon, which ensured the surface tension of the ink solvent (tetralin in most formulations was the by far major component) to prevail on the substrate/liquid interactions. This, in turn, led invariably to the growth of large and high quality crystals. Unfortunately, the wettability of bare gold in standard conditions (i.e., room temperature and normal atmosphere) is much higher than that of Teflon. To overcome this problem, it has been devised to modify the wettability of the gold surface by using a fluorinated SAM, so to mimic the low surface energy of Teflon also on gold. The choice of the most appropriate SAM precursor molecule has been done using the Zisman diagram, a tool which allows

to determine an approximate surface energy value for a material via simple measurement of its contact angles with different liquids (see par. 1.3).

A survey of possibly suitable compounds was made for a series of thiols (namely 1,2,4,5-tetrafluorobenzenethiol, TFT; 2-trifluoroethylthiol, TriFET; 1H,1H,2H,2H-Perfluorodecanethiol, DFT; mercaptobenzene, MB; see table 2.3-1. The resulting Zisman diagram (*figure* 2.3-2) showed that the molecule most effective in delivering a low energy surface, necessary for limiting the spreading of the printed tetralin-based ink drop, is DFT, as expected due to its extensive fluorination degree.

Table 2.3-1

MOLECULE NAME	ABBREVIATION	MOLECULE STRUCTURE
1H,1H,2H,2H-Perfluorodecanethiol	DFT	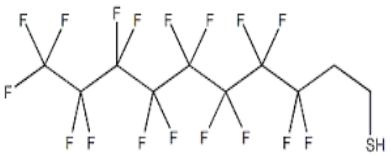
2,3,5,6-Tetrafluorobenzenethiol	TFT	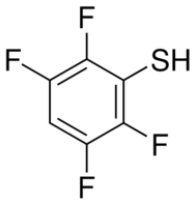
2,2,2-Trifluoroethanethiol	TriFET	CF_3CH_2SH
Mercaptobenzene	MB	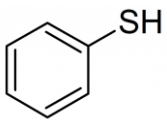

DFT can be easily dissolved in alcohols. After some tests, a first DFT-based ink was formulated dissolving the thiol in 1-hexanol (3% w/w). However, although this ink allowed to print well defined features, its stability in time was very limited, in the order of a few hours, due to the formation of a solid phase observed inside any type of ink container (i.e., inside glass vials or the

printer plastic cartridges). This issue, likely due to thiol dimerization, has been deemed not compatible with the project, which aimed at finding an industrially compatible process. Using longer linear alkylic chains for the alcoholic solvent, the ink lifetime further reduced, down to the order of minutes. Therefore, the ink has been re-formulated with 60% of 1-pentanol and 40% of 1-hexanol, still with 3% w/w DFT (tests carried out using only 1-pentanol as solvent delivered several unwanted satellite drops during printing, as shown in *figure* 2.3-3). The lifetime of this formulation was found to be of around 3 days, judged satisfactory for our purposes. Upon these first results, this optimized alcohol-based ink had been hence adopted.

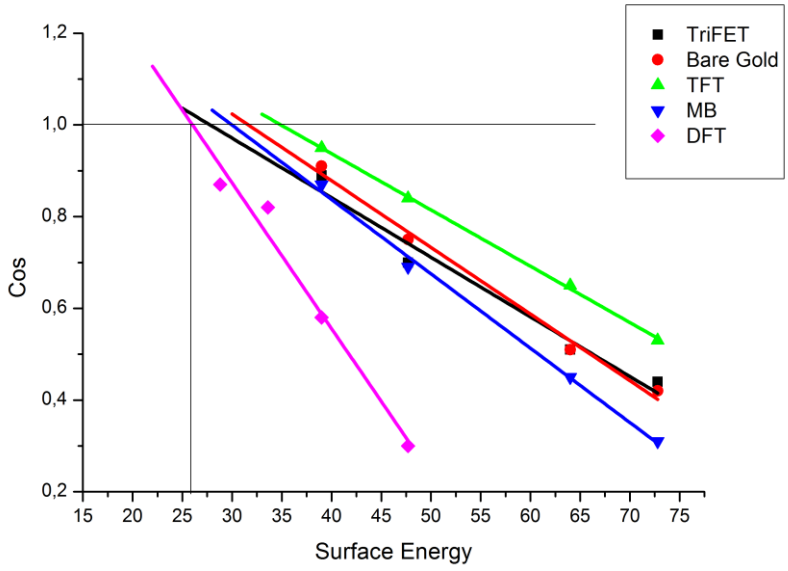

Figure 2.3-2: Zisman diagram about the tested SAMs

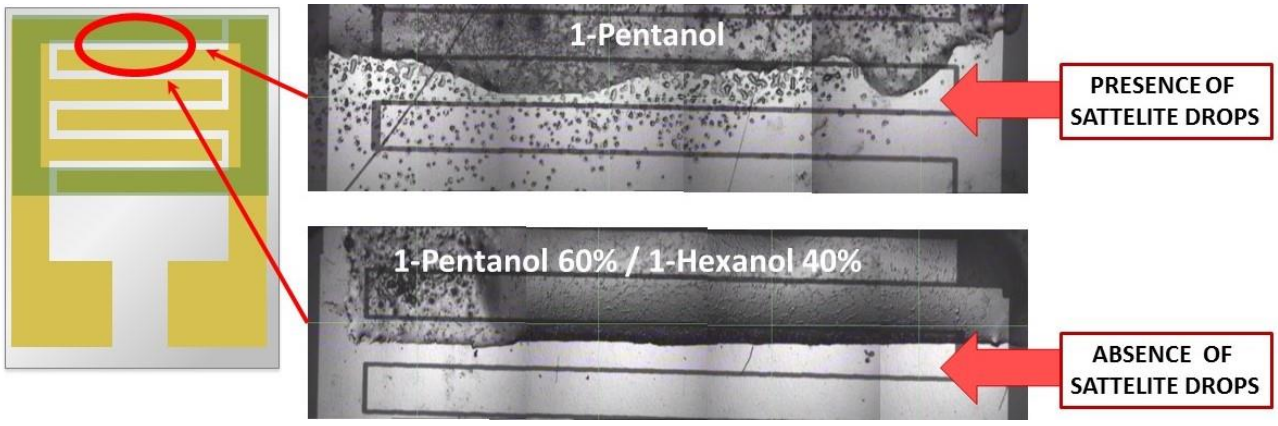

Figure 2.3-3: comparison between corrals printed with 1-pentanol and the mix of solvents, it is possible to see the disappearance of the satellite drops.

On this basis, IDTs have been functionalized by full immersion in the formulated DFT/alcohol mixture ink. As a result, inkjet printed TIPS-tetralin ink drops actually showed a very limited tendency to spread over the substrate, and remained well positioned in the exact point of the substrate onto which the ink was deposited, *figure* 2.3-4. The contact angle for the ink printed on the so-modified surface was found to be of 20.6° (*figure* 2.3-4-b), which represented a remarkable improvement with respect to the complete spreading experienced by the same amount of ink deposited onto bare IDTs (*figure* 2.3-4-a), for which a contact angle was not determinable. The crystals grown on the so-treated IDTs also had a much better morphology than those grown without SAM (compare *figure* 2.3-1 with *figure*).

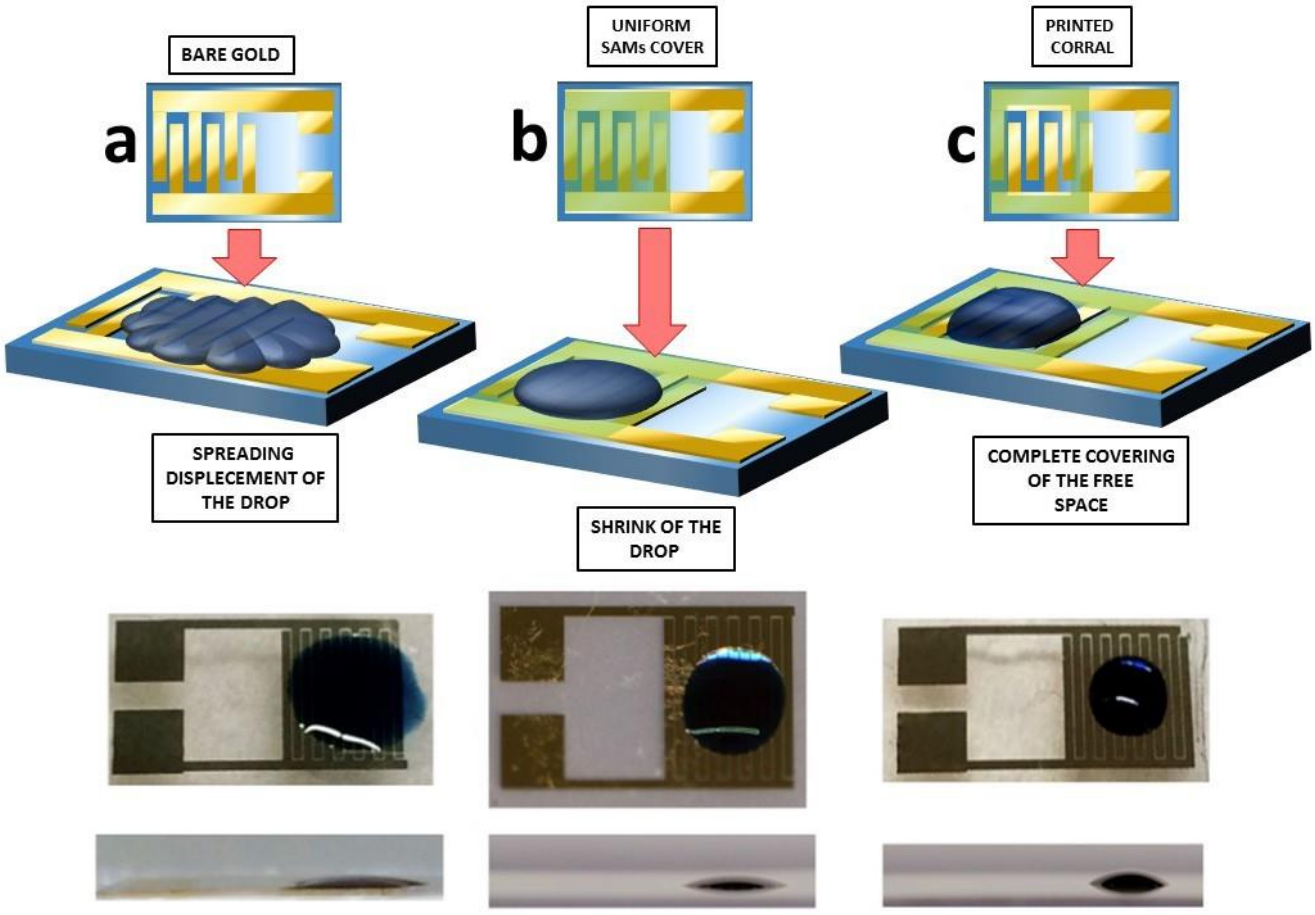

Figure 2.3-4: comparison between a schematic behavior (at the top) with the real behavior (at the bottom), of the printed drop on different substrates: a) bare gold; b) uniform SAMs cover; c) printed corral.

However, it is known that, from an electrical point of view, long chain alkylic and fluorinated SAMs act as an insulating materials [33, 34, 35]. Indeed, attempts to measure the electrical characteristics of the device made by the i-FLEXIS project partners in Bologna showed negligible, if any, current transfer between the two functionalized electrodes (*figure* 2.3-5*,* 2.3-6).

Figure 2.3-5: the crystals shown in the photo were grown on a substrate completely covered by SAMs.

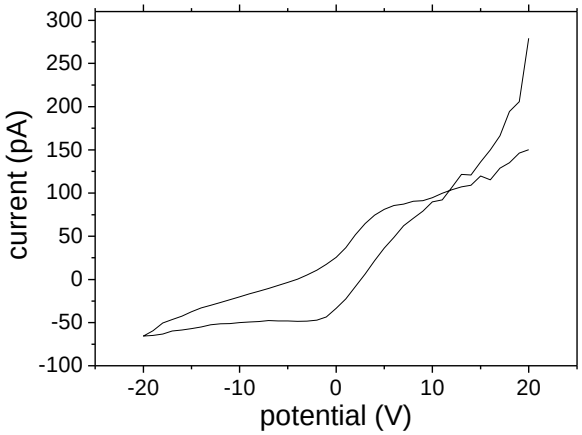

Figure 2.3-6: I-V diagram of the printed crystals electrical behavior made at the University of Bologna.

Therefore, the use of DFT as a SAM placed between the IDTs and the grown TIPS crystals is deleterious with respect to the electrical injection properties of the resulting device, and several other similar tests confirmed the above described result.

In order to circumvent this problem, it has been devised a further approach aimed at placing the fluorinated SAM just as a "fence" around the central zone of the IDT, creating a sort of "solvophobic corral", and not also beneath the printed TIPS solution. In this way, the solvo-phobic effect introduced by DFT molecules is confined just to the lateral edges of the IDT zone onto which the TIPS solution is printed, leaving in principle the charge transfer proprieties of the gold/TIPS crystals interface preserved.

This strategy worked very well to contain the drop, as is visible in *figure* 2.3-7. Interestingly, the contact angle between the corralled IDTs and the tetralin solution (about 31.8°) was higher than that of the fully DFT-covered gold IDTs (about 20.6°)

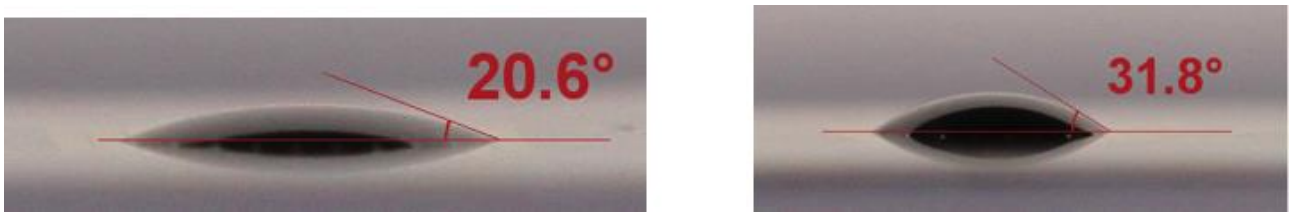

Figure 2.3-7: contact angle measurment between the corralled IDTs and the fully DFT-covered gold IDTs.

This finding evidences that the corral strategy, though not directly lowering the surface energy of the substrate underlying the printed drop, is extremely effective in confining the latter in the desired position (no drop displacement was observed after deposition) and in avoiding extensive wetting. At the same time, this chemical confinement approach allowed to exploit the benefits of a controlled surface wetting without the need for an actual full functionalization with the solvo-phobic compound of the whole surface underlying the drop, that would have inevitably led to drastically decreased carrier injection properties. Moreover, the compact drop achieved with this approach allowed to carry out the solvent evaporation phase with a much slower rate than that of the bare substrate, leading to well defined true single crystals directly grown on the interdigitated electrodes (the term “printed” will be used from now on to identify the TIPS crystals grown upon this chemical confinement strategy), as is visible in *figure* 2.3-8. This is even more important when considering that the substrate, as already mentioned, is highly heterogeneous, since it includes the PEN substrate and several PEN-gold discontinuities (the gold layer is about 100 nm-thick) given by the interdigitated electrodes. Moreover, as the used substrates were based on the flexible PEN plastic, which is known to be scarcely planar, these results are even more significant.

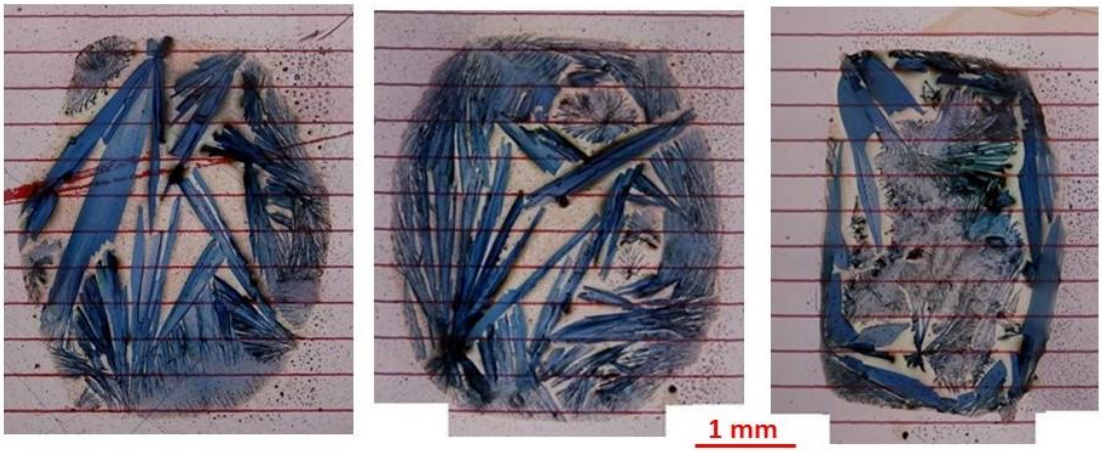

Figure 2.3-8: crystals growth inside a SAMs printed corral on heterogeneous surface.

Figure 2.3-8 shows the visual aspect of TIPS crystals grown inside effective corrals. The internal IDTs surface defined by corrals is around 6 mm^2, and crystal growth took place at room temperature. As it can be seen, TIPS elongated single crystals coexist with more disordered polycrystals and even powdery material. The size of the larger crystals inside the photos is around 1 to 2,5 mm in length and around 0,15 to 0,5 mm in width.

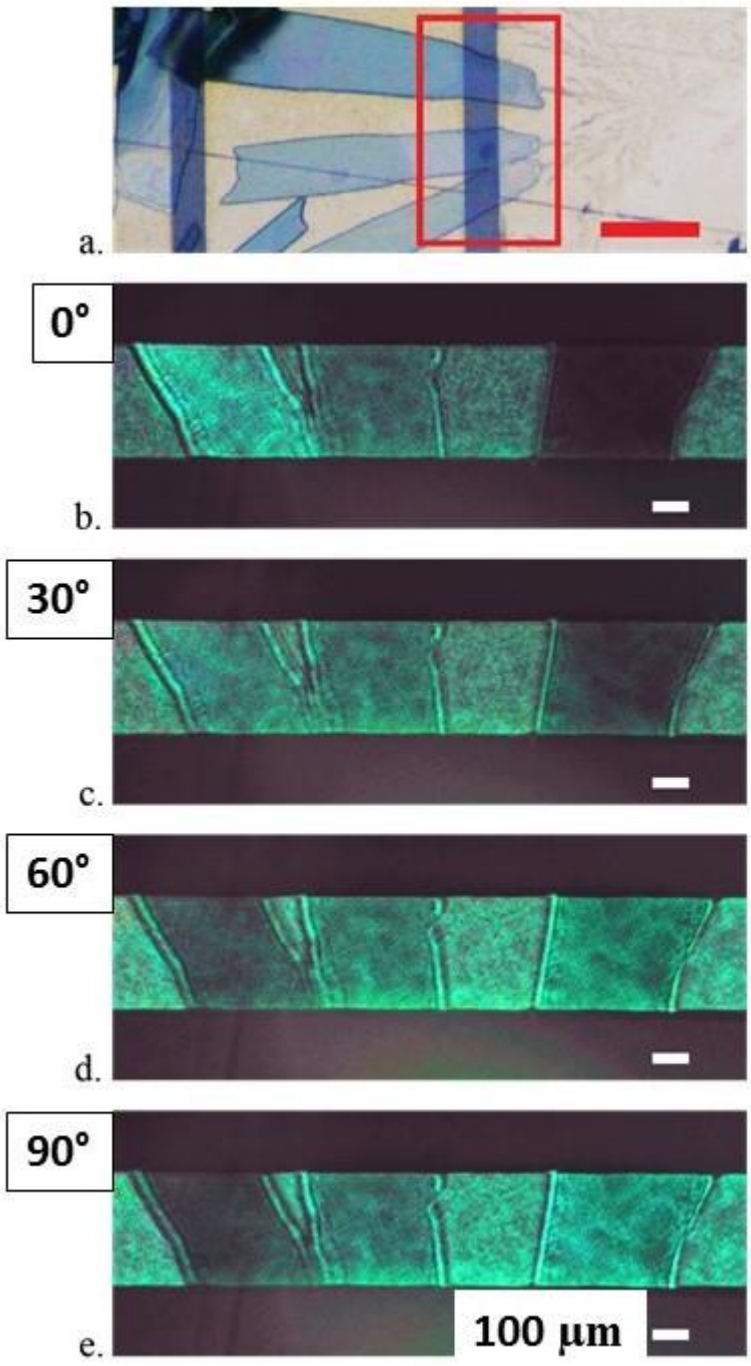

Figure 2.3-9:a) tested crystals. The sequence (b-e) shows a polarized light microscopy of the crystals in (a) taken from the bottom of the sample, at different polarization angles, as labeled in the upper left of each photo.

A direct XRD characterization of the printed crystals was attempted, but with no success, due to the substrate heterogeneity. However, to ensure that the large crystals are actually single crystals, microscope photos of the printed crystals under polarized light have been taken from the bottom of the substrate [36] (*figure* 2.3-9). As is visible, varying the polarization angle, the printed crystas experience uniform light rotation, getting progressively darker/lighter depending on the considered single crystal, with no recognizable crystal domain border in the imaged zone.

The SAM-based corral was inkjet printed using the above reported formulation. The most efficient corral wall width was established being of about 1 mm. The importance of finding the right corral wall width can be better appreciated looking at *figure* 2.3-10 which summarizes the tests made to find the optimum corral wall width. The scarce efficacy of thinner corrals in containing the TIPS solution can be ascribed to the fact that i) the DFT SAM was not allowed to rest for more than a couple of hours before being washed to eliminate ill-attached molecules, hence it did not have the possibility to self-organize properly, and ii) the PEN substrates had a high roughness (the smoothest substrates obtained after careful and lengthy cleaning) and chemical planarizing treatments achieved a R_a of about 3 nm [9], creating the physical impossibility for the formation of a homogeneous and compact SAM. Therefore, SAM "walls" narrower than 1 mm were found to be less effective in confining the TIPS solution.

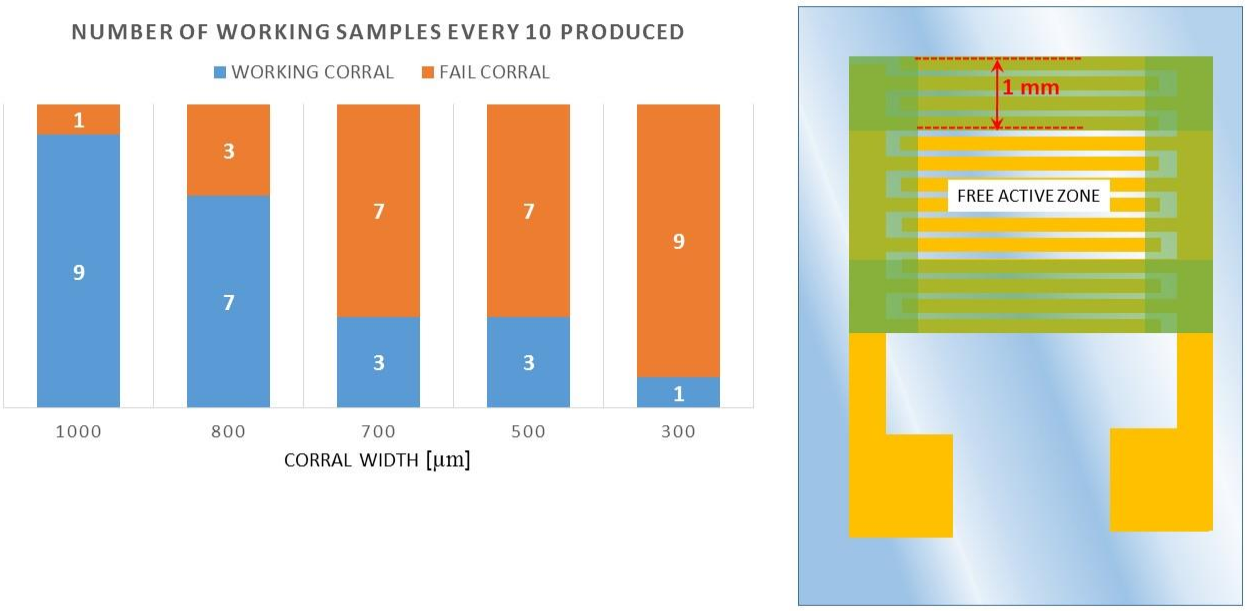

Figure 2.3-10: on the left, there is the diagram of the working samples every ten samples produced; on the right, a scheme of the printed corral is shown.

As is visible in *figure* 2.3-8, small crystals and polycrystalline areas found inside the corral are more frequentely found at the corral borders, and also the largest crystals usually have at least one end in correspondence of the corral wall. These evidences suggest that the corral walls act as nucleation points, a hypothesis that finds support in the known nucleation-inducing effect of micropatterned SAMs [37, 38, 39] Since DFT molecules are likely uniformly distributed, at a large scale, along the corral wall, the overall orientation of the grown crystal is random. This type of

growth can be also helped by the conbination of Marangoni and coffee-ring effect [40] , in which the pinning of the organic semiconducting molecules to the SAM molecules can start local nucleation, which in turn induces a difference of concentration between the edge and the centre of the drop. This concentration gradient leads to the creation of a driving force moving the concentrated solution from the drop center to its edge in an attempt to reestablish a homogeneous concentration (*figure* 2.3-11)[40] . This cycle continues until the solution is completely dried and crystals are formed.

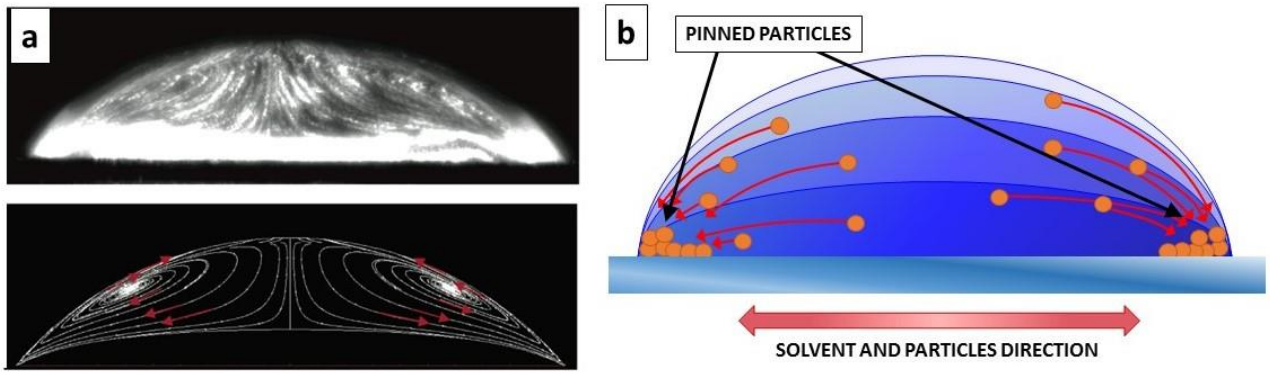

Figure 2.3-11: On the left (a), there is the photo and the scheme of the fluid motion inside a printed drop due to the Marangoni effect. On the right (b), the scheme of the particles motion from the center to the edge of the printed drop generating the coffee-ring.

2.4 CRYSTALS ALIGNMENT

The electrical properties and performances of OSs are strongly dependent on their internal structure. For example, ordered crystalline domains promote a better charge transport both for holes and electrons, due to the reduction the number of grain boundaries, which is known to be a cause of a bad charge transport.

When considering solution processing, from literature it is well known that depending on the way the solvent evaporation takes place, crystal orientation, structure and size may change [41, 42, 43]. Therefore, the possibility of controlling the crystal habit of OSSCs, the most performing OSs, in terms of precisely dictating the growth direction of the crystal, is particularly appealing. In this view, activities about the possibility of guiding the crystallization direction for crystals grown from solution, modifying different growth parameters, have been recently reported. Byung ju Kang et al. [44] showed how it is possible to control crystal growth in order to realize a TIPS-based printed active layer of an Organic Thin Film Transistor. In particular, this work showed that it is possible to control the orientation of the crystals by means of substrates at different temperature, and by properly overlapping printing passes. Thus, crystals are forced to grow along the evaporation direction and over the free space between the source and drain electrodes, contacting them (*figure* 2.4-1).

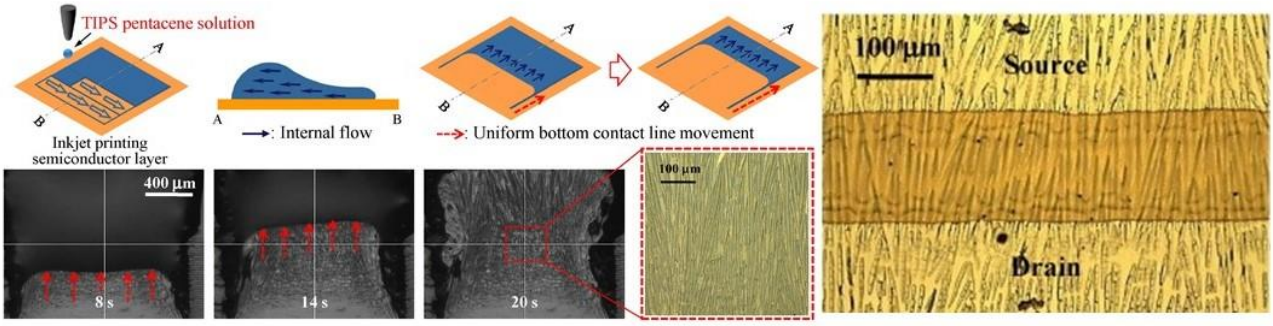

Figure 2.4-1: figure of the Byung ju Kang et al. (from left to right): schematic diagrams and sequential images of the evaporation behavior of drying semiconductor layers inkjet-printed; schematic diagrams and sequential images of the evaporation behavior at 30°C.

Another technique used to control crystal orientation growth was developed by Min Jung Kim et al. in 2011 [45] and Zhengran He et al. in 2012 [46]; they had been able to use a flux of inert gas, such as argon or air, in order to control the orientation of growth of a crystal drop cast from a solution (*figure* 2.4-2).

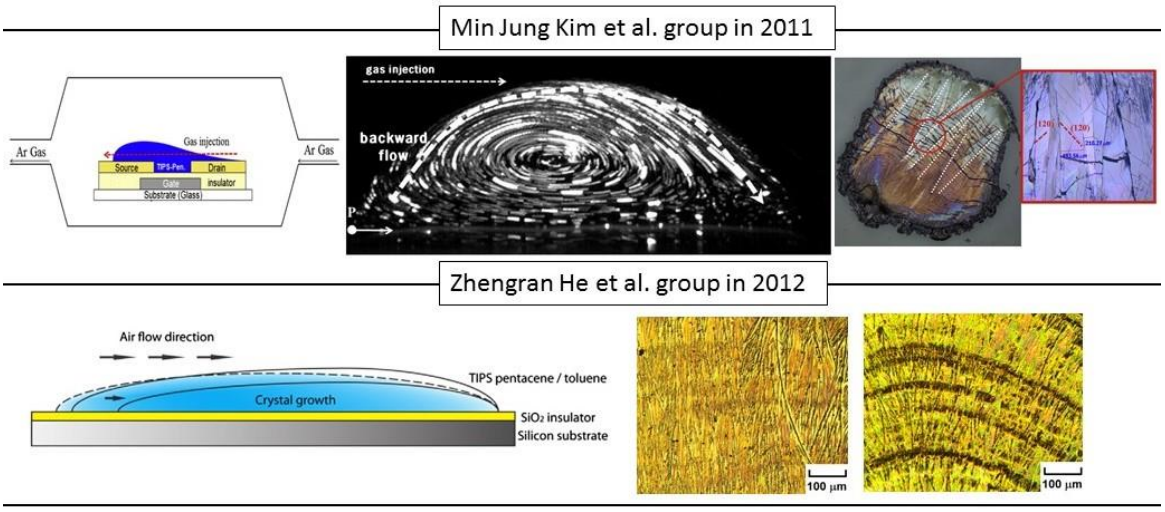

Figure2.4-2: Min Jung Kim et al. in 2011 (from left to right): schematic illustration of the gas (argon) alienation method; convection movement of the liquid inside the drop due to the gas flow; crystals growth with 1000 sccm and a magnification showing the grains alignment. Zhengran He et al. (from left to right): Schematic drawing of the crystal growth with air-flow navigation, optical images of TIPS pentacene thin films oriented with air-flow at difference speed (2L/min and 1L/min respectively).

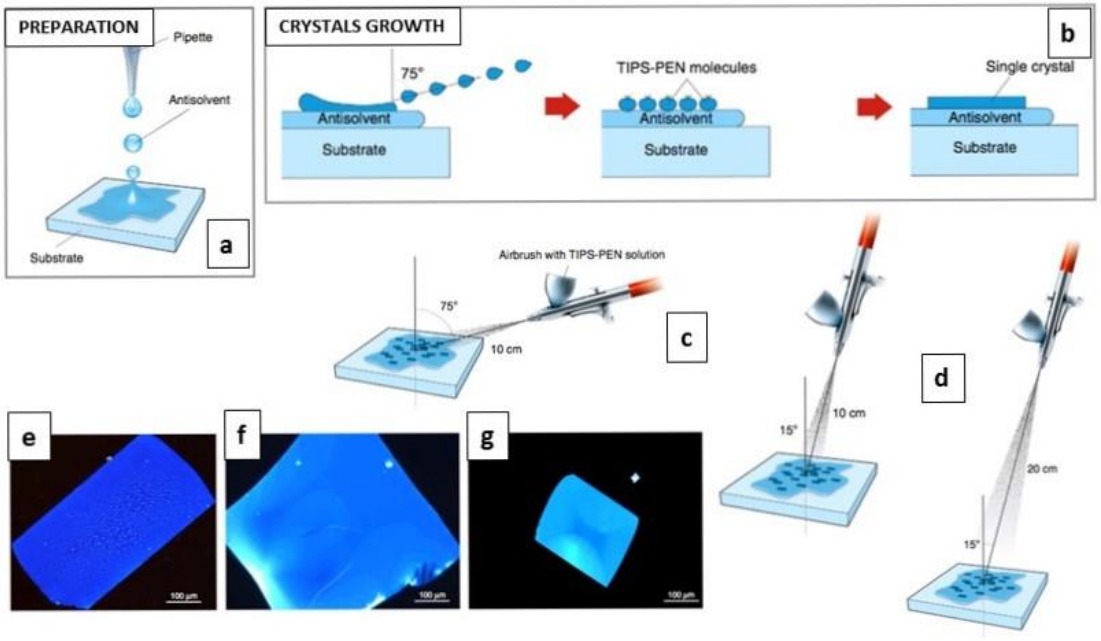

Figure 2.4-3: a) preparation of the substrate with the anti-solvent deposition; b) schematic illustration of the drop deposition via aerograph and the single crystals growth; c-d) indication of the three different aerograph position, different inclination and different distance from the substrate; e-f-g) example of the crystals growth from the three different air brush position: (e) 75° at 10 cm, (f) 15° at 10 cm and (g) 15° at 20 cm.

Panagiotis et al. [47] aligns organic semiconductor crystals using a tilted spray printing with a commercial aerograph on a substrate cover by antisolvent (*figure* 2.4-3). He demonstrated the possibility to grow single crystals of TIPS-pentacene, in different sizes, shapes and orientations, only tilting the aerograph and placing it at a specific distance away from the substrate.

The crystals of 2,5 - Di - (2 - ethylhexyl) - 3,6 - bis (5'' - n – hexyl - 2,2',5',2''] terthiophene – 5 – yl) – pyrrolo [3,4-c] pyrrole - 1,4 - dione (SMDPPEH) were aligned by Sheng Bi et al. [48] using the "controlled evaporative self-assembly (CESA)" method [49] as shows in *figure* 2.4-4. A cylinder is placed in contact with the solution giving rise to capillary forces that attract the solution toward the cylinder. The contact line of the drop is pinned to the substrate and starts to evaporate generating crystals seed. The crystallization of the molecules starts from the seed in the direction of the cylinder, thus aligning the crystals.

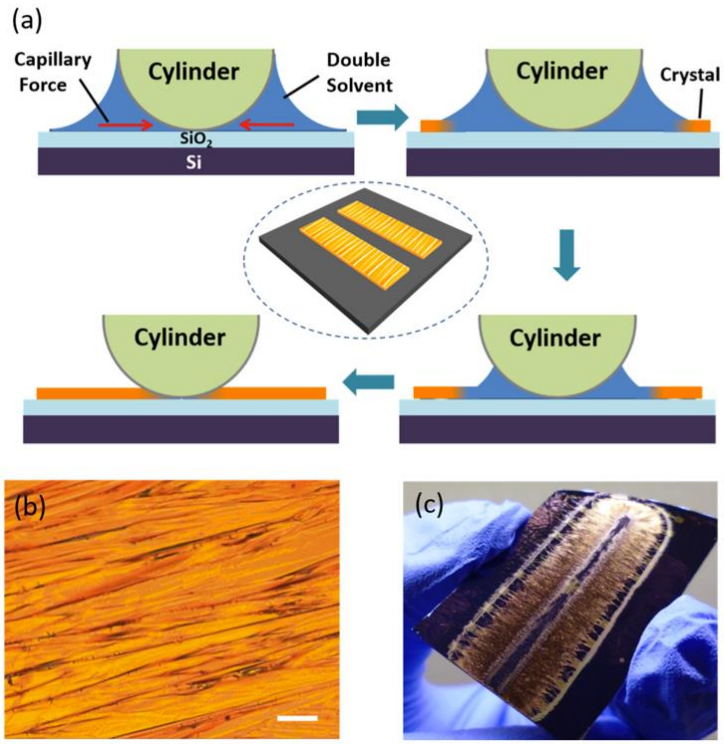

Figure 2.4-4: a) schematic illustration of the CESA method; b) optical magnification of SMDPPEH films, oriented crystals are clearly visible (scale bar 50 µm), the surface is perfectly covered; c) digital image of a crystal growth example with the use of CESA method.

2.4.1: CRYSTALS ALIGNMENT VIA CHEMICAL CONFINEMENT

The chemical confinement strategy discussed in par. 2.3 was explored as a way to impart directional alignment to TIPS crystals. To this aim rectangular corrals with different aspect ratios have been fabricated onto uniformly gold-coated PEN substrates (*figure* 2.4-5), in order to evaluate the effectiveness of this technique.

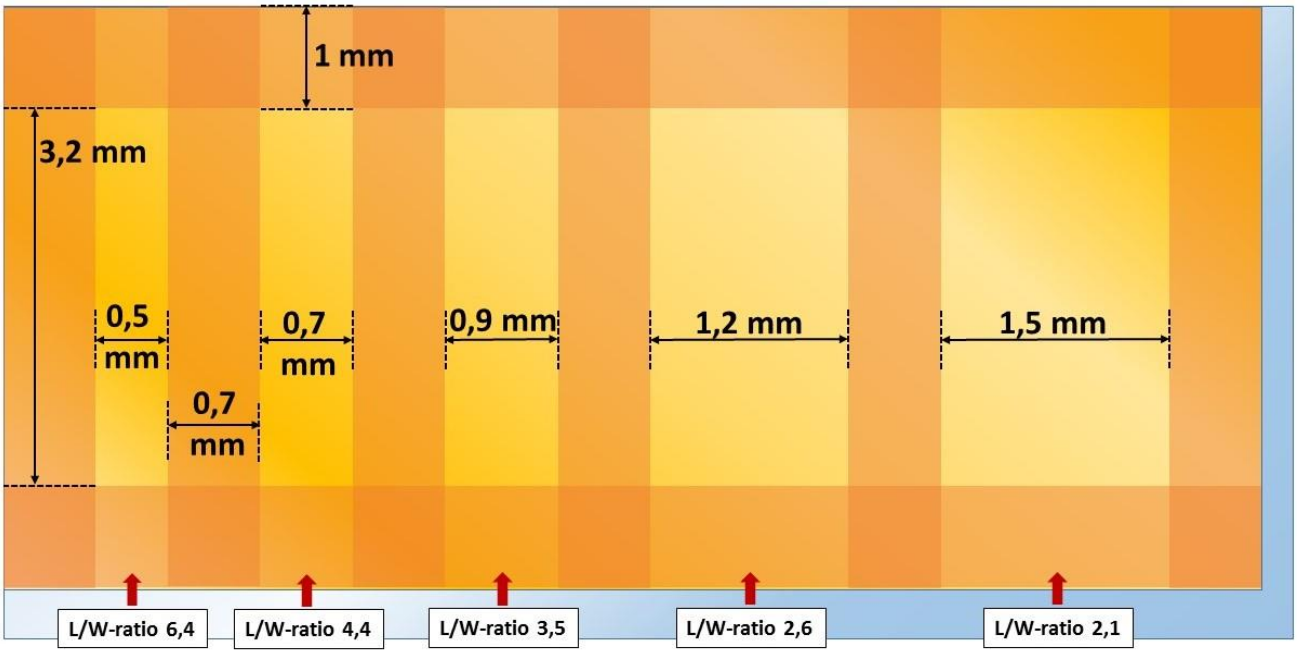

Figure 2.4-5: schematic illustration of the rectangular corrals with the different aspect ratios. The orange part indicates the SAMs corral printed on a gold pad PVD on PEN substrate

As is visible from *figure* 2.4-6, the progressive increase of the aspect ratio of the corrals (going from 2.6 (*figure* 2.4-6 "a") to 4.4 (*figure* 2.4-6 "b") to 6.4 (*figure* 2.4-6 "c")) results in i) formation of crystals more and more oriented according to the longitudinal axis of the rectangle; ii) a marked decrease of the presence of poly-crystals (likely due to optimized solution flow within the more narrow corrals, that tend to minimize convective motion orthogonal to the main rectangle axis); iii) a better morphology of the grown crystals.

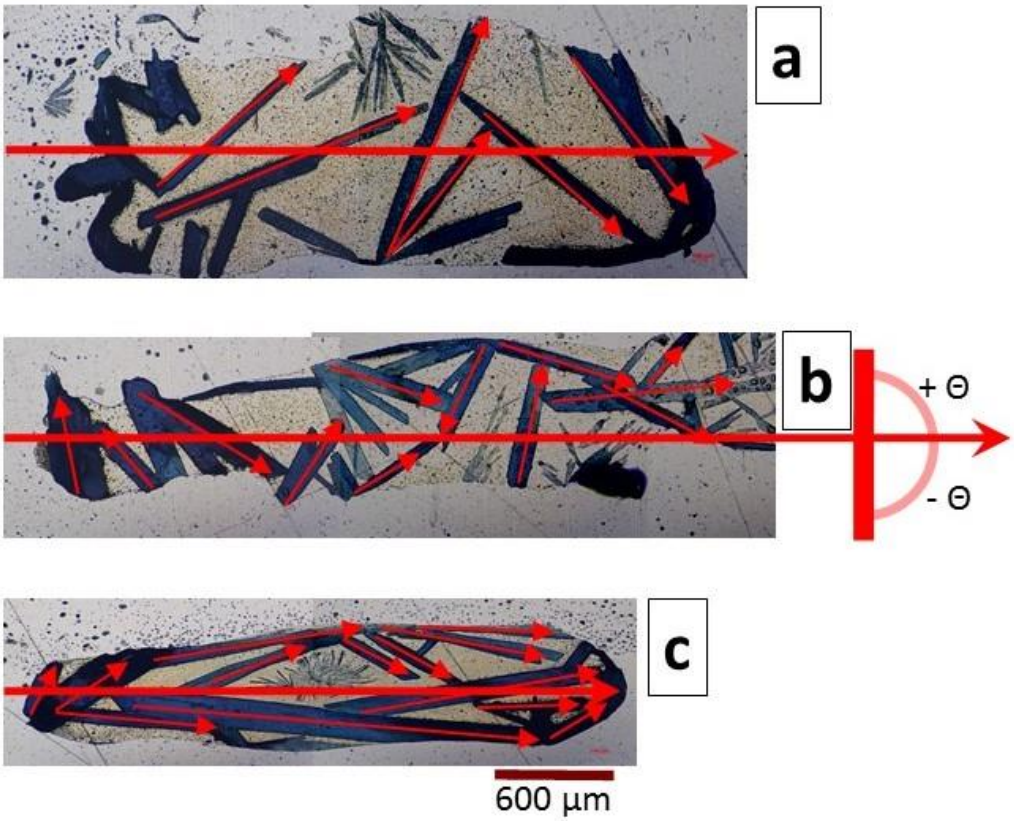

Figure 2.4-6: photos of crystals oriented by the chemical confinement method with different L/W-ratio: a)2.6; b)4.4; c)6.4

In the following *figure* 2.4-7 the absolute angle of the single crystals shown in figure 2.4-6 with respect to the longer axis of the corral is reported.

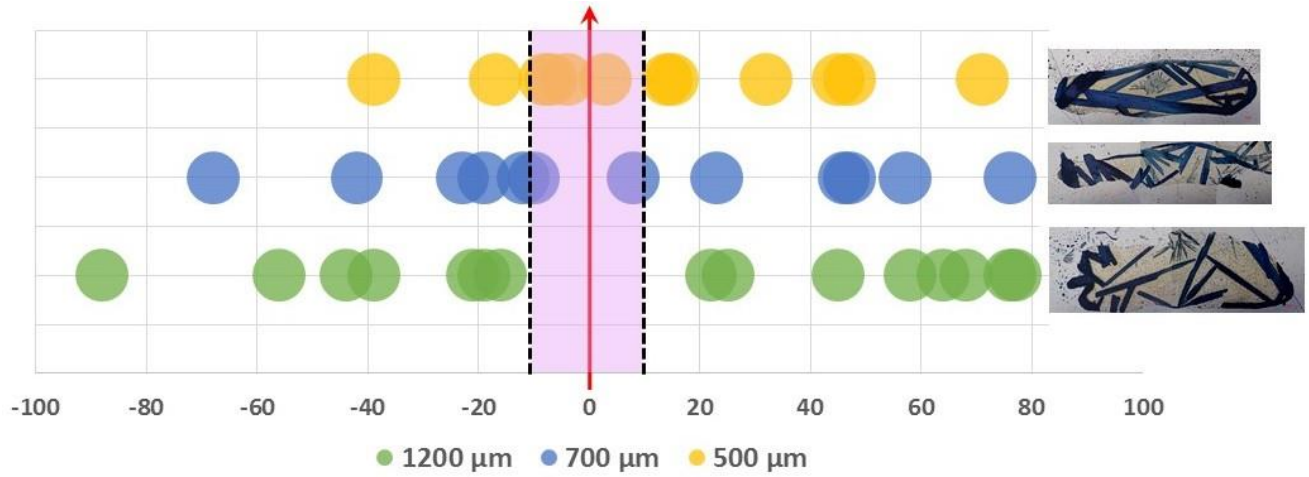

Figure2.4-7: photos of oriented crystals by geometrical method and different L/W-ratio: a)2,6; b)4,4; c)6,4. The ball diagram stresses the increase of crystals alignment at the L/W-ratio increment.

As it can be seen, from a value of 2.1 L/W-ratio to a 6.4 L/W-ratio a progressive increment of the number of crystals describing an angle of ± 10 degrees with the longer rectangle axis is observed. Average orientation improvement has been evaluated being around 49%; this value has

been calculated taking in account only crystals with length of more than 150 μm. Anyway, if only crystals with lengths higher than 1.5 mm are taken in account, this percentage rises up to 66%.

These data demonstrate that it is possible to control the crystal alignment over planar gold surface using the chemical confinement strategy. This possibility was verified also on interdigitated gold electrodes lithographically defined on PET, where the highly heterogeneous nature of the substrate (different materials, i.e. gold and PET, several geometrical edges, i.e. the gold electrodes discontinuities with respect to the PET substrate, and the intrinsic PET roughness) create a difficult environment for an ideal crystallization process. In fact, as described before (chapter 2.3), surface discontinuities act as nucleation points: thus, a polycrystalline growth from solution was expected to be preponderant, as it is shown in *figure* 2.4-8.

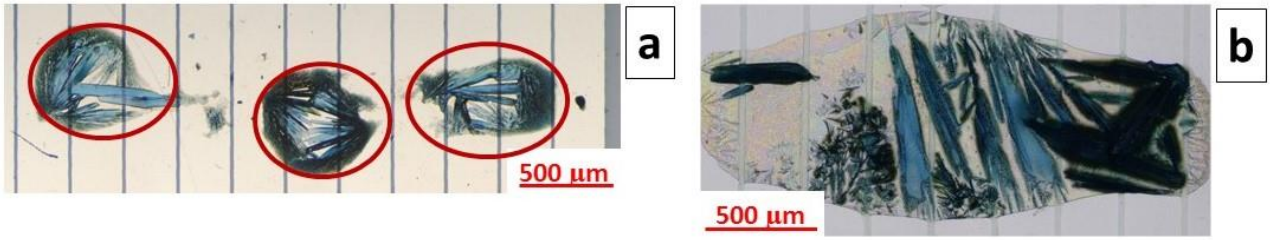

Figure 2.4-8: polycrystalline growth from solution on heterogeneous substrate.

First tests carried out showed that the solution printed within high aspect ratio corrals tends to split into multiple circular drops, signaling surface wettability problems. In *figure* 2.4-8 "a" it is possible to see the outcome of this procedure in a 6.4 L/W-ratio (corral dimensions: 3.2 mm long, 0.5mm wide) within which 0.5 μL of TIPS-based ink were printed. Due to this ink coalescence, the grown crystals weren't affected by the presence of the high aspect ratio corral, and they grew with random directions, presenting a high percentage of poly-crystals. On the other hand, this phenomenon hasn't been observed in samples prepared with corrals with a lower aspect ratio (*figure* 2.4-8 "b": here the corral has an aspect ratio of 4.3), where the solution remained compact and didn't coalesce into smaller drops. However, crystals grown into corrals with such a low aspect ratio didn't grow along the desired direction, and the presence of small polycrystalline areas was still considerable.

In order to solve this problem, the composition of the ink was slightly changed, adding tetrahydrofurane (THF), a low boiling point solvent of TIPS, to the ink. Moreover, printing drop spacing was slightly incremented from five to seven, in order to slightly reduce the amount of deposited TIPS. This setting has been made because crystals obtained from higher amounts of

printed solution were often found to be too thick for effective charge transfer properties. Crystals obtained with these new settings and ink are shown in *figure* 2.4-9. As it can be seen, these changes delivered crystals with a more regular shape and a slightly changed crystal habit with respect to those printed from just tetralin (increased platelet width). Moreover, the presence of polycrystalline areas was also strongly reduced.

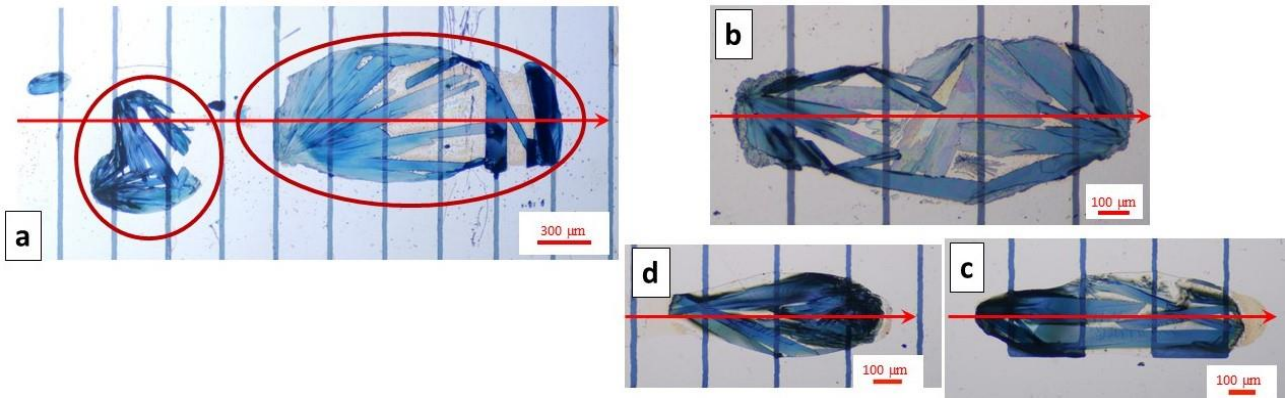

Figure 2.4-9: aligned crystals growth with the geometrical method and the new TIPS ink containing THF. The L/W-ratios are: a)4.9; b)4.4; c)3.9; d)3.9.

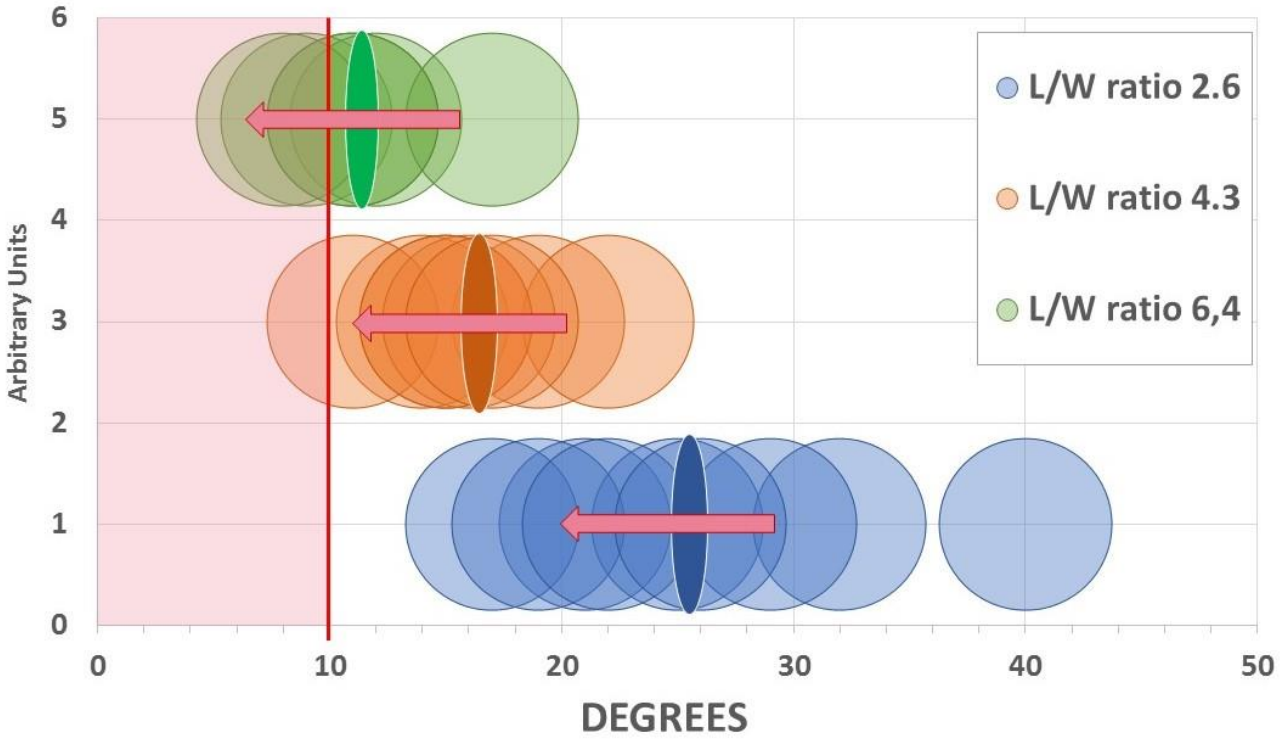

Figure 2.4-10: representation of the crystals average and total average angles due to the different L/W ratio used.

These improvements are because THF evaporates much more quickly than tetralin (BP= 56.5°C, against about 207°C of tetralin), countering the Marangoni effect (part 2.3) and limiting to a minimum the coffee ring.

In addition, this new ink formulation helped in achieving a uniform coverage of the interdigitated electrodes surface, due to the changed crystal habit. Finally, this formulation was more appropriate to be used to control crystal orientation, as until aspect ratios as high as 5 no solution coalescence into smaller drops have been observed (figure 2.4-9 “b”, “c” and “d”), allowing a very effective crystal orientation, as can be seen in the images “c” and “d” of *figure* 2.4-9. In *figure* 2.4-10 the increase in crystals orientation produced by the changing in corral geometry is clearly visible. Every semi-transparent circle represents the average angles inside a single sample, whereas the opaque eye-form shows the total average angle for each L/W ratio. The total average angles for each L/W ratio are shown in table 2.4-1.

Table 2.4-1

L x W corral size [mm]	3.2 x 0.5	1.5 x 0.35	1.2 x 0.45
L/W-ratio	6.4	4.3	2.6
Volume of the printed drop [μL]	0.5	0.3	0.3
Average crystals orientation [degrees]	11.3	16.3	25.6

While the chemical confinement strategy appears to be effective, with proper tuning also on highly heterogeneous structures like interdigitated electrodes on plastic substrates, it is difficult to inkjet print a corral with a width lower than 250 μm, hence higher aspect ratios were not realized. Another point to be considered in this strategy is that due to the relatively high aspect ratios of the corrals, the full coverage of the substrate requires multiple high aspect ratio corrals, hence to obtain multiple, aligned crystals it is necessary to print multiple corrals onto the same device.

2.5 ELECTRICAL CHARACTERIZATIONS

The whole process of printing solutions onto interdigitated electrodes for growing crystals was devised in order to use the grown TIPS as x-ray detectors. Of course, to reach this goal the grown crystals must be electrically contacted with the underlying electrodes. In order to verify this point, preliminary electrical measurements have been carried out by collaborating researchers at the Dept. of Engineering and Architecture of the Univ. of Trieste (UniTs), and more thorough characterizations have been made by the Department of Physics and Astrophysics of the University of Bologna (UniBo), a collaborating group in the frame of the i-FLEXIS project.

2.5.1: PRELIMINARY ELECTRICAL CHARACTERIZATIONS

First electrical characterizations were carried out in UniTs in order to assess if the obtained samples were electrically contacted or not. Simple measurements of the I/V curve in the range between 0-150 V allowed to observe if the crystals were able to sustain currents higher than 10/100nA. Moreover, at the higher voltages, the I/V curve for OSSCs should show a typical Space Charge Limited Current (SCLC) behavior [50, 51, 52]. Examples of a badly and well contacted TIPS crystals are shown in the *figure* 2.5-1 and in *figure* 2.5-2, respectively.

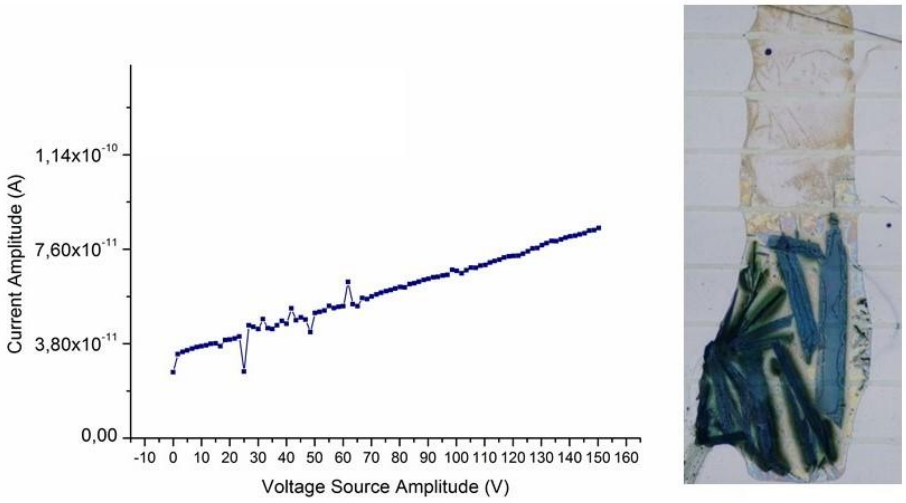

Figure 2.5-1: example of a badly connected TIPS crystals growth on gold interdigitated electrodes.

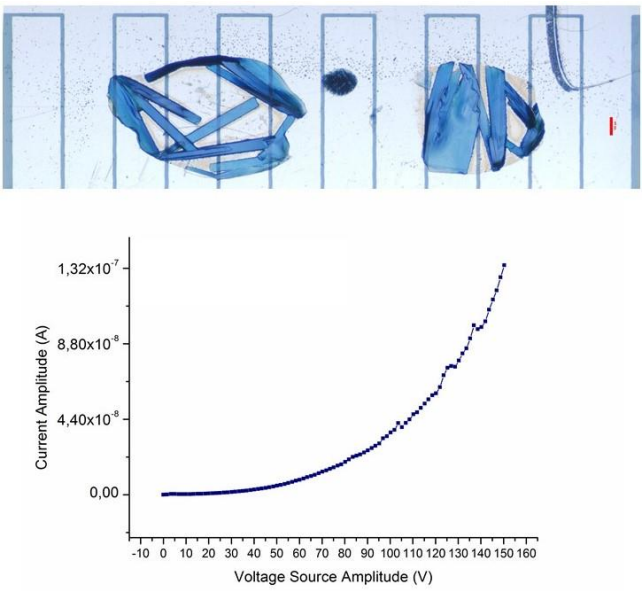

Figure 2.5-2: example of a well connected TIPS crystals growth on gold interdigitated electrodes

2.5.2: TIPS-BASED DEVICES

Crystals printed onto the patterned electrodes showed nice performances in terms of electrical contact. As visible in *figure* 2.5-3, millimeter-sized printed single crystals are grown (*figure* 2.5-3 "a") and the electrical current as function of the applied bias in the range of -10V ÷ +10V is reported (*figure* 2.5-3 "b").

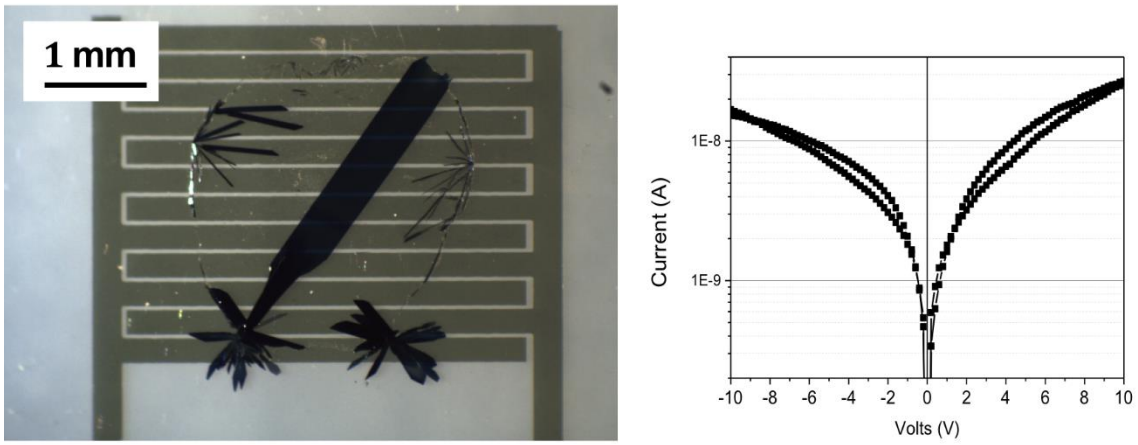

Figure 2.5-3: a) IJ printed TIPS pentacene single crystals, and b) IV characterization of the imaged crystals.

The current-voltage characteristic (I-V) shows current values up to 25nA@10V, the lack of rectification effects leading to nearly ideal ohmic behavior and a negligible hysteresis. The above reported features are indicative of a good mechanical adherence between gold and TIPS, and of a

good charge transfer between them. These conditions enable the onset of Space-Charge-Limited Current behavior in crystals when a high electric field is applied; this can be also saw in other tested samples. From the SCLC theory, [53] the charge carrier mobility is estimated to be 4.0 ±0.7 x 10^{-2} cm^2/Vs.

Some of the crystals printed inside the corral have been tested for UV and X-ray detection effectiveness. In particular, in *figure* 2.5-4 "a" the UV-VIS photoinduced current as function of bias voltages is reported. The photocurrent (I_{light} - I_{dark}) is about 60 nA at low voltage (1V), and reaches values of 17 µA at 50V; the responsivity ranges between 0.2 A/W (at 1 V) and 70 A/W (at 50V), which is a very high value for organic semiconductors, that at best present responsivities in the range of 0.1-0.2 A/W [54, 55]. Also, the signal-to-noise ratio ($\Delta I/I_{dark}$) (SNR) is very high in this device, reaching values between 10^2 and 10^4. The large values of both the responsivity and the SNR are attributed to the high crystallinity of the printed samples, that leads to combine low intrinsic charge carriers density and high transport properties of the charges (due to absence of grain boundaries) to be collected.

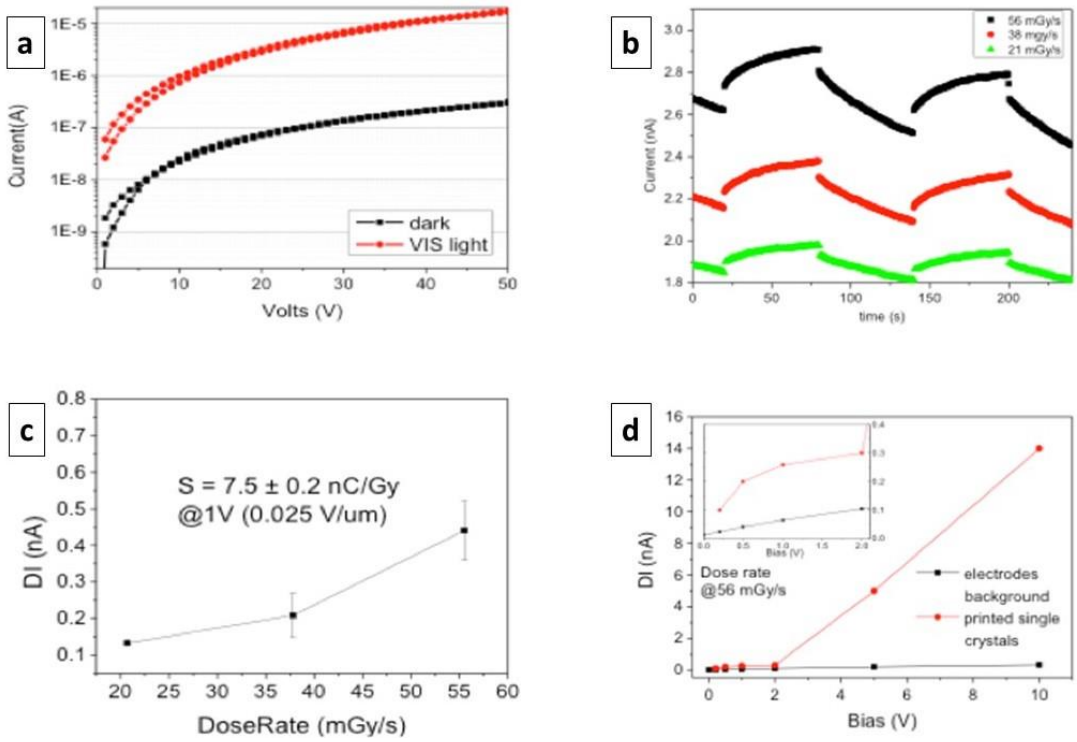

Figure 2.5-4: Photocurrent response of a TIPS printed crystal a) under UV-Vis light (P = 19.8µW) at different biases; b) under X-rays (accelerating voltage of 35kV) as time-dependent current response at different dose rates and applied bias of 1 V; c) under X-rays in function of the dose rate, evidencing the crystal sensitivity at 1 V; d) under X-rays in function of the applied bias (red plot), in comparison with the contribution from bare electrodes (i.e., bare interdigitated electrodes onto PET substrate; black plot).

The printed TIPS-pentacene single crystals are able to collect charge carriers created by the absorption of ionizing radiation, joining together in printable devices the two concepts of organic direct x-ray detectors based on solution-grown single crystals (already reported but on different molecules) [6, 18] and high sensitivity of low-voltage TIPS-pentacene thin film detectors [8]. *Figure* 2.5-4 “b” and “c” report, respectively, the current vs. time and the photocurrent vs. dose rate plots, when the crystals are biased at 1 V. The x-ray induced photocurrent (nA) is smaller than that of the UV-VIS case in (*figure* 2.5-4 “a”), due to the much smaller x-ray photons absorbed fraction compared to the UV-VIS photons one. However, the shape of the response is in line with what it has been observed for TIPS-pentacene thin film X-rays detectors, and the sensitivity is comparable with that of single crystals with the same electrode configuration and electric field value. The x-ray response slightly increases at low bias (inset in f*igure* 2.5-4 “d”); at higher bias voltages, the x-ray response present non-uniform steep increases, with a threshold-like behavior at 2 V (*figure* 2.5-4 “d”), enhancing also the sensitivity. This latter effect could be ascribed to a potential barrier between the metal electrodes and the organic crystals, probably due to a known small mismatch between the gold work function and TIPS-pentacene HOMO [56] rather than to crystal defects, ruled out from the previously reported I/V and photodetection measurements. At higher bias, the baseline dark current increases more than the x-ray signal and presents a pronounced current drift with time, reducing the SNR and the stability of the device. An important complementary test to exclude possible spurious contribution to the x-ray signal is the measurement of x-ray induced photocurrent from the device without the printed organic active layer (only PEN substrate and gold electrodes): the so called background x-ray photocurrent is reported as black dots in f*igure* 2.5-4 “d”, and it is negligible compared to the TIPS-pentacene response.

2.6 CONCLUSIONS

During this PhD research work it was demonstrated the possibility to use the inkjet printing technique to deposit organic semiconductor molecules from solution. In particular, controlling the solvent evaporation rate, OSSCs have been grown on the top of gold interdigitated electrodes. This has been achieved thanks to the precision of the printer, that allowed to deposit fluorinated SAMs, creating solvo-phobic corrals, giving the possibility to divide the surface in separated parts or to confine a single ink drop in a determined position. Appropriate printing shape geometry and printing process optimization can increase effectiveness of the surface properties modification overtaking the limitations of the original surface characteristics.

The presence of the SAMs corral helps also to improve the quality of the crystals, decreasing the evaporation rate of the solvent, blocking the drop spreading over the substrate. Growth of crystals of high quality was possible also thanks to the optimization of the deposited solution composition.

The presence of the corral allowed to achieve these results without changing the surface chemistry. In fact, electrical measurements showed that the printed TIPS single crystals collect effectively charge carriers generated by both UV-Vis and X-ray photons evidencing that it is possible to direct “print” OSSCs directly onto electrodes originating working devices.

The geometry of the corral is another important aspect that was underlined in this work. Increasing the ratio between the length and the width of the corral, it is possible to force the crystals alignment along the corral main axe and to reduce the coffee-ring effects. With this simple approach, it was demonstrated the ability to grow OSSCs along a fixed direction, even onto higly heterogeneous substrates constituted by gold interdigitated electrodes on PEN.

2.7 MATERIALS & METHODS

2.7.1: PRELIMINARY SCREENING OF OSSC OF INTEREST

All the materials were purchased from Sigma-Aldrich. The organic molecules DNN, NTI, 4HCB were purified to eliminate as many impurities as possible. Only TIPS have been used as purchased.

Used compounds and their main properties are listed in the table 2.7-1 below.

Table 2.7-1

NAME	CAS	BOILING PIONT [°C]	MELTING POINT [°C]	MOLECULAR WEIGHT [g/mol]	DENSITY [g/mL]	VISCOSITY [cP]	PURITY
Acetone	67-64-1	56,2	-95.4	58.08	0.79	0.306 (25°C)	>99.5%
Ethanol	64-17-5	78,24	-114.14	46.068	0.789	1.074(25°C)	99%
Chloroform	67-66-3	61	-63	119.38	1.47	0.563 (20°C)	98%
Toluene	108-88-3	111	-95	92.14	0.87	0.59 (20°C)	99%
THF	109-99-9	66	-108.4	72.11	0.889	0.48 (25°C)	99%
ChloroBenzene	108-90-7	131	-45	112.56	1.11	O.753 (25°C)	99.8%
DiChloroBenezene	95-50-1	180,5	-17.3	147.01	1.3	1.32 (25°C)	99%
TriChloroBenzene	120-82-1	214	-15	181.45	1.454	1.68 (25°C)	>99%
Anisole	100-66-3	154	-37	108.14	0.995	1.05 (20°C)	>99%
BenzoNitrile	100-47-0	191	-13	103.12	1.01	1.27 (25°C)	>99%
DMSO	76-68-5	189	18	78.13	1.095	1.99 (°C)	99%
Tetralina	119-64-2	207	-5.8	132.2	0.97	2.02 (20°C)	99%
Nitobenzene	98-95-3	211	6	123.11	1.2	1.863 (25°C)	>99%
Menthol	2216-51-5	212	37	156.27	0.89	solid	99%

All the substrates were purchased by Goodfellow [57]

2.7.1.1: Washing procedure

All the plastic substrates were washed before the utilization, as follows:

- Accurate and gentle washing with soap;
- Acetone or isopropanol sonication bath for 10 minutes;
- Rinsing with distilled water;

- Drying with hot air or nitrogen flux to eliminate water molecules adsorbed on the substrate.

Used glasses were washed with the following procedure to eliminate as more as possible the presence of organic residuals: 24 hours in sulfur-nitric solution (3 part of sulfuric acid and 1 part of nitric acid);

- Immersion for 5 minutes in tap water added with soap to neutralize the acid solution;
- Acetone or isopropanol sonication bath for 10 minutes;
- Washing with distilled water;
- Drying with hot air or nitrogen flux.

2.7.1.2: Solution/Ink Preparation

All prepared solutions were stirred at 400 rpm for 15 minutes. Concentration rates were chosen depending on the selected organic semiconductor-solvent pair. Moreover, for NTI, DNN, TIPS, solubility tests were performed. More accurate test had been led on TIPS because it is the most used molecule for this work. Solubility characteristics of the employed solvents were found on product datasheets. The most interesting solvent was found to be tetralin, as it well suitable for inkjet printing. The maximum weight of TIPS dissolved in Tetralin, without precipitation in the temperature range of 20 to 23 degrees, is 30 mg/mL.

TIPS-tetralin solutions does not last for more than two or three days. This rule was introduced to avoid the degradation of the organic molecules in solution. TIPS based solutions start degradations turning their color from dark blue to dark green (and later to yellow, approximately 37 days after) after ten days in tetralin or toluene and after only one week in benzonitrile [58].

2.7.1.3: Crystals Growing Procedure

First crystal growth tests were led on Teflon; a drop of 20 µL was drop cast and put inside a 100 mm diameter polydimethylsiloxane (PDMS) petri dish; in this way evaporation occurred at a constant volume. A foil of aluminum covered the petri in order to protect the sample from light induced degradation. All the experiments, for the crystals growth, are made under the hood and inside a refrigerator (4°C). After crystal formation, optical microscopy images were taken, and the

sample was removed from the substrate to perform electrical measurements on free-standing crystals. These kinds of measurements were made in collaboration with University of Bologna.

2.7.2: PRINTING OF INKS BASED ON ORGANIC SEMICONDUCTOR MOLECULES

2.7.2.1: Inks

All the printing solutions (inks) were prepared according to the most promising solutions obtained from drop casting on Teflon, and used as inks for printing. Anyway, some corrections of the formulation of the TIPS-based ink were performed during the development of the project. The formulations, that gave the better results, can be summarized in the following table 2.7-2:

Table 2.7-2

ORGANIC MOLECULES	SOLVENT	CONCENTRATION [mg/mL]	CRYSTALs QUALITY
TIPS	Tetralin	5.75	First base ink
TIPS	Tetralin	20	Increase in crystals size, and number of single crystals
TIPS	Tetralin – 90% THF – 10%	20	Decrease the presence of coffee-ring, and better crystals morphology

The maximum amount of printed ink in printing experiments is 1 µL for each sample. In order to guarantee the reproducibility of the printing results, printing has been performed under hood at the temperature of about 28°C (the lower possible temperature setting).

Other inks, used in the first part of this work, and then discarded, are listed in the following table 2.7-3:

Table 2.7-3

ORGANIC MOLECUL	SOLVENT	CONCENTRATION [mg/mL]
4HCB	Benzonitrile	8
DNN	Dichlorobenzene	5
NTI	DMSO	5
TIPS	Nitrobenzene	4

TIPS	Dichlorobenzene	6

2.7.2.2: Substrate

The used substrates are composed by a set of interdigitated electrodes realized via physical vapor deposition onto three different polymeric substrates: kapton, PET and PEN. Substrates have been produced at UniCa (*figure* 2.7-1).

The main used substrate support is PEN do to its good properties.

The roughness of the gold layer is in the range of 20 nm ± 2nm *figure* 2.7-1.

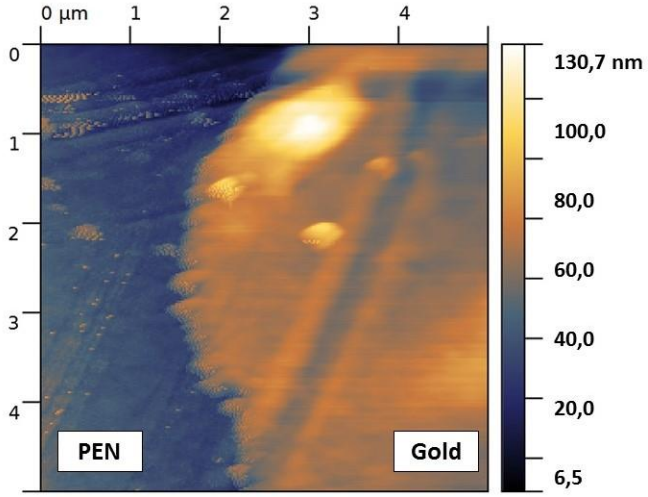

*Figure 2.7-1: AFM figure of the edge gold electrode PVD on PEN substrate. The big PEN roughness is evident***.**

The interdigitated electrodes have a size of 4 x 5 mm, while the electrodes have a width of 300 µm and an average distance of 36 µm, and the average thickness of gold layer is 60 nm. In figure 2.7-2 part "c" it is possible to see presence of the crystalline domains and their size. The gold substrate isn't a single perfect crystal with (1,1,1) orientation.

All the substrates were washed with 5 minutes of sonication in isopropanol alcohol, rinsed with distillated water and dried with nitrogen flux.

The samples photos were made with a CANON EOS 1300D camera. The microscope used to check the samples and take their photos was a Nikon Eclipse 50 I with a intense lighter C-HGFi, the camera was a Nikon Digital Sight DS-2Mv 2 M-pixels. The viscosity measure was made with HAAKE RS 150 Rheo Stress, at the constant temperature of 20°C with the cone at 1% inclination, using three constant speeds of 500, 600 and 700 rpm. The roughness of the gold was detterminated by AFM measurement made by another research group.

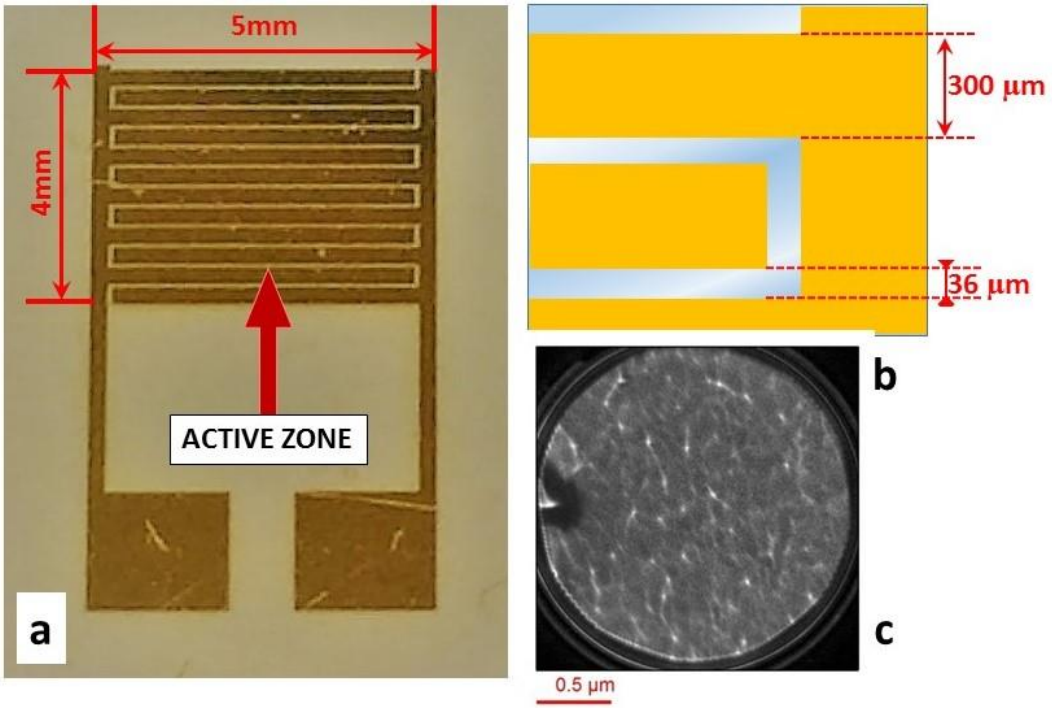

Figure 2.7-2: a) digital photo of a PVD gold electrode on PEN at UniCa; b) Scheme of the electrode size; c) gold crystalline domain.

2.7.3: CHEMICAL MODIFICATION OF THE SURFACE VIA SAMs

2.7.3.1: Materials

The reagents used for the above described experiments have been purchased from Sigma-Aldrich, as for the following tables 2.7-4 and 2.7-5.

Table 2.7-4: Solvents

NAME	CAS	MOLECULAR WEIGHT [g/mol]	DENSITY [g/mL]	VISCOSITY [cP]	PURITY [%]
1-Pentanol	71-41-0	88.15	0.811	3.47 (20°C)	>99%
1-Hexanol	111-27-3	102.18	0.82	4.59 (20°C)	>99%

Table 2.7-5: SAMs

NAME	CAS	MOLECULAR WEIGHT [g/mol]	PURITY	DENSITY [g/mL]
1H,1H,2H,2H-Perfluorodecanethiol	34143-74-3	480.18	97%	1.678
2,3,5,6-Tetrafluorobenzenethiol	769-40-4	182.14	97%	1.53
2,2,2-Trifluoroethanethiol	1544-53-2	116.11	95%	1.305
Mercaptobenzene	108-98-5	110.19	97%	1.0766

2.7.3.2: SAMs Ink Preparation

The inks preparation followed the same procedure of the OSSCs inks. When the SAM molecules did not dissolve completely, a gentle heating for 15 to 20 seconds with hairdryer was applied. The so-prepared ink was fed to the printer cartridge about 20-30 minutes prior printing, for giving the ink sufficient time to fill the print-head nozzles and capillary system.

After printing, samples were covered with a Petri dish and left inside the printer to promote chemical adhesion of the SAM molecules to the substrate, until the evaporation of the solvent was complete (about two hours). The samples were then washed with acetone, isopropyl alcohol, distilled water and in the end dried with a dry nitrogen flow.

2.7.3.3: Zisman diagram tests

The Zisman diagram tests were performed as follow.

Uniform sputtered gold pads have been carefully cleaned using this sequence: soap and distilled water; 5 minutes of sonication in isopropanol alcohol; distillated water rinse; dry nitrogen. The so-prepared gold pads have been then immersed in the selected SAM-precursor solution at room temperature. Each SAM-precursor solution was composed by the SAM to be tested, dissolved in ethanol at 3% w/w. After 24 hours, the substrates have been extracted and cleaned once more, without the sonication step to avoid damaging the organic layer. The organic solvents used to measure the contact angles are listed in the table 2.7-6 below:

Table 2.7-6

SOLVENT	SURFACE FREE ENERGY at 20°C [mN/m]
Benzene	28.8
Benzene Chlorine	33.6
Ethylene Glycol	47.7
Glycerol	64
Water	72.8

All the surface energy values reported in Table 1-2.3 have been taken from the website: http://www.surface-tension.de/, connected at the company "dataphysics - Understanding Interfaces", website: www.dataphysics.de.

Each solvent was dropped three times on the gold pad, and three different photos were taken for each drop, to get a more reliable average value.

2.7.3.4: TIPS-based ink printing

The TIPS-based Ink was prepared as described in the par. 2.2.2, with a concentration of 20 mg/mL dissolved in tetralin as the organic solvent. The printing characteristics were: drop spacing 5 μm; printing shape 1.5 x 1.8 mm (width x length); average total amount of ink was 1 μL. The ink was printed in the middle of the free SAM zone of the IDTs and leaved to enlarge until reaching the internal corral edge. All the samples were left inside the printer until complete crystals formation, protected by a Petri dish covered with an aluminum foil to avoid both the dust contamination and light soaking.

2.7.4: CRYSTALS ALIGNMENT

The ink used in the first part of the work was made with is the TIPS 20 mg/mL in tetralin. The TIPS concentration in the THF-containing ink is still 20 mg/mL, with the solvent composition equal to 90% tetralin: 10% THF, V/V. The general preparation of the ink is the same described in par. 2.1.

The dimensional parameters of the printed corrals and the amounts of ink printed within each corral are reported in Table 2.7-7 and Table 2.7-8.

Table 2.7-7

L x W corral size [mm]	3.2 x 0.5	3.2 x 0.7	3.2 x 0.9	3.2 x 1.2	3.2 x 1.5
L/W-ratio	6.4	4.4	3.5	2.6	2.1
Volume of the printed drop [μL]	0.5	0.5	0.7	0.9	0.9

Table 2.7-8

Type of TIPS ink	TIPS 20 mg/mL, tetralin		TIPS 18 mg/mL, menthol 2mg/mL 90%tetralin + 10% THF		
L x W corral size [mm]	3.2 x 0.5	1.5 x 0.35	3.2 x 0.5	1.5 x 0.35	1.2 x 0.45
L/W-ratio	6.4	4.3	6.4	4.3	2.6
Volume of the printed drop [μL]	0.5	0.3	0.5	0.3	0.3

The SAM-based ink and its printing procedure were the same described in par. 2.3.

The used substrates were PVD gold pads on PEN and gold interdigitated PVD electrodes on PEN made by the University of Cagliari, as described in par. 2.2.

2.7.5: ELECTRICAL CHARACTERIZATIONS

I/V curves recorded at UniTs were measured within the range of 0 – 90V or 0 – 150V, by using a Source Measure Unit Keithley 2400 (*figure* 2.7-3).

I/V measurement were performed by applying a voltage ramp to the sample and then reading the induced current.

The samples were inserted in a metallic box (*figure* 2.7-4). In this way measurements were conducted in dark, dust couldn't access the sample under test and the metallic box, connected to the ground, acted as an electromagnetic shield. Silver paint and thin copper wires were used to connect the interdigitate electrodes.

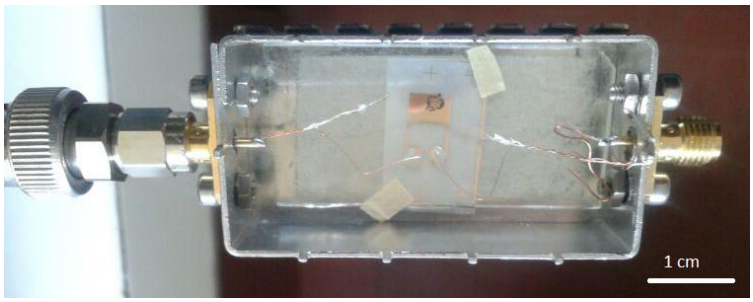

Figure 2.7-3: digital photo of the metallic box where the sample is housed.

Figure 2.7-4: digital photo of the Keithley 6517A Electrometer.

At UniBo electrical measurements were carried out with a Keithley 6517A Electrometer, keeping the sample in dark in a metal Faraday cage to reduce electrical noise. The UV-VIS radiation source was a white LED lamp at P_{VIS} = 19.8 µW. The characterization under X-Rays were performed using an X-ray broad-spectrum tube with Mo target, accelerating voltage of 35 kV and dose rates in the range of 20÷60 $mGys^{-1}$.

BIBILOGRAPHY CHAPTER 2

2.1: PRELIMINARY SCREENING OF OSSCS OF INTEREST

1. Fraboni et al., *Faraday discussion*, **2014**, 174, 219.
2. H. Kallman, *Phys. Rev*., **1950** , 78 , 621.
3. M. G. Schor , F. L. Torney , *Phys. Rev*., **1950** , 80 , 474.
4. K. Yoshino et al. , *Jpn. J. Appl. Phys., Part 2*, **1982** ,21, L569.
5. N. Zaitseva et al*., J. Cryst. Growth*, **2011**, 314, 163.
6. B. Fraboni et al., *Adv. Mater*., **2012**, 24, 2289.
7. Ciavatti A. et al., *Adv. Mater*, **2015** 27, 7213.
8. Basiricò L. et al., *Natt. Comm*., **2016**, DOI: 10.1038/ncomms13063.
9. *Phd Thesis*, M. Sibilia, **2017**, University of Trieste, School of Nanotechnology.
10. B. Fraboni et al., *Org. Electron*., **2009**, 9 ,974.
11. Basiricò L. et al., *15 IEEE Trans. Nucl. Sci*., **2015**, 62, 1791.
12. SakanoueT. Et al., *Nature Materials*, **2010**, 9, 736.
13. Shuang Liu et al., *Sci. Bull*., **2015**, 60(12), 1122.
14. L. Zhou et al., *Appl. Phys. Lett*., **2006**, 88, 083502.
15. F. Eder et al., *Appl. Phys. Lett*., **2004**, 84, 2673.
16. A. L. Briseno et al., *Adv. Mater*., **2006**, 18, 2320.
17. Hui Jiang et al., *MRS BULLETTIN*, **2013**,38.
18. Fraboni B. et al., *Adv. Funct. Mater*., **2016**, 26, 2276.
19. K. P. Weidkamp et al., *J. Am. Chem. Soc*., **2004**, 126, 12740.
20. S. K. Park et al., *Appl. Phys.Lett*., **2007**, 91, 063514.
21. J. Chen et al., *Org. El*., **2009**, 10, 696.

2.2: PRINTING OF INKS BASED ON ORGANIC SEMICONDUCTOR MOLECULES

22. Kang-Jun Baeg et al., *Organic Electronics*, **2013**, 14, 1407.

23. Koji Abe et al., *Anal. Chem*., **2008**, 80, 6928.

24. Shimoda T.et al., *MRS Bulletin*, **2003**, 28 (11), 821.

25. Minemawari et al., *Nature*, **2011**, 474, 364.

26. U. Scherf et al., *Angew. Chem. Int. Ed*. **2008**, 47, 4070.

27. Gonçalves et al., *Int. J. of Thermophysics*, **1989**, 10 (4), 845.

28. Robert D. Deegan et al., *Nature*, **1997**, 389, 827.

29. John E. Anthony et al., *Adv. Mater*. **2012**, 24, 497.

30. Ying Wang et al., *Org. Ele.*, **2014**, 15, 3101.

31. Jung Ah Limet al., *Langmuir*, **2009**, 25(9), 5404.

32. Seungjun Chung et al., *Adv.* Ma*ter*., **2013**, 25, 4773.

2.3: CHEMICAL MODIFICATION OF THE SURFACE VIA SAMs

33. Arunabh Batra et al., *Nature Communications*, DoI: 10.1038/ ncomms2083.

34. David J. Wold et al*., J. Am. Chem. Soc*., **2001**, 123, 5549-5556.

35. Di Benedetto S. et al., *Adv. Mater*. **2009**, 21, 1407-1433.

36. G.P. Rigas et al., *Nature Communications*, 7:13531, DOI: 10.1038/ ncomms 13531.

37. Aizenberg, J. et al., *J. Am. Chem. Soc*. **1999**, 121, 4500.

38. Aizenberg, J. et al., *Nature* (London)**1999**, 398, 495.

39. Han Y.-J., Aizenberg J*., J. Am. Chem. Soc*. **2003**, 125, 4032.

40. Hua Hu et al*., J. Phys. Chem. B*, **2006**, 110(14), 7090.

2.4: CRYSTALS ALIGNMENT

41. W.H. Lee et al., *Appl. Phys. Lett*., **2007**, 90, 132106.

42. B.J. Kang et al., *Jpn. J. Appl. Phys*., **2014**, 53, 05HB09.

43. K. Asare-Yeboah et al., *J. Vac. Sci. Technol*. *B,* **2014**, 32, 052401.
44. B.J. Kang, J.H. Oh, *Thin Solid Films*, **2016**, 598, 219.
45. M.J. Kim et al., *Org. Electron.*, **2011**, 12, 1170.
46. Z. He et al., *Org. Electron.*, **2012**, 13, 1819.
47. Pangiotis et al., *Nature Communications*, **2016**, 7:13531, DOI: 10.1038/ncomms13531.
48. Sheng Bi et al., *API Adv*., **2015**, 5, 077170.
49. W.Ham et al*., J. Mater. Chem*., **2011**, 21, 14248.

2.5 ELECTRICAL CHARACTERIZATIONS

50. R. W. de Boer et al., Phys. Status Solidi A, 2004, 201, 1302.
51. M. Lampert, P. Mark, In Current Injection in Solids, Academic Press, New York, 1970.
52. M. Pope, C. Swenberg, in: Electronic Processes in Organic Crystals and Polymers, Oxford Scient. Publ., Oxford, UK, 1999.
53. Kokil et al., Journal Of Polymer Science Part B: Polymer Physics, 2012, 50, 1130.
54. Xiaofen Wang et al., Adv. Funct. Mater. 2016, 26, 6306
55. Dezhi Yang and Dongge Ma, J. Mater. Chem. C, 2013, 1, 2054.
56. Jung-Pyo Hong et al., App. Phys. Lett., 2008, 92, 143311.

2.7 MATHERIALS AND METHODS

57. Website of Goodfellow company: http://www.goodfellow.com
58. Laila Mohamed Abusen, *Phd thesis*, **2013**, university of Manchester, Faculty of Engineering, and Physical Sciences.

CHAPTER – 3

INK JET PRINTED NANOTHIN DIELECTRIC LAYERS

3.1: PRINTING OF NANOTHIN AlOx DIELECTRIC LAYERS FOR ORGANIC ELECTRONICS APPLICATIONS

Besides organic electronics, also printed conductive tracks and printed inorganic semiconductors are being explored as tools for enabling printed electronics [1, 2, 3].

At this stage, Thin-Film Transistors (TFTs) using metal oxides, as active channel materials or dielectrics, are widely studied to obtain good device performances, high reproducibility, low cost, and a good reliability [4]. However, to achieve good performances in metal oxides-based devices high temperatures (450-600°C) are needed, which makes this type of technology incompatible with organic flexible substrates. In order to allow practical use of metal oxides on plastic substrates, novel ways to process them must be found.

This work has been focused on the use of solution processed amorphous metal oxides (AMOs) for dielectric applications. The solution-based process can be used to deposit large area AMOs with high uniformity, high dielectric constant, without any type of vacuum processing condition [5, 6]. The main wet technologies employed to deposit AMOs are spin-coating, dip-coating, spray-coating, and inkjet printing [7, 8], using both rigid and flexible substrates.

The ideal material to be used in printed devices as dielectric layer should be ultra-thin, to allow flexibility and low voltage operations, and should show high-k dielectric characteristic, thermal stability, high capacitances, smooth surfaces and low leakage current densities [9, 10]. In fact, a dielectric layer with all these characteristics inserted in a TFTs results in high charge density inside the semiconductor at low voltages operations [11]. The main AMOs researched for dielectrics applications are [12]: i) aluminum oxide (Al_2O_3); ii) hafnium oxide (HfO_2); iii) tantalum oxide (Ta_2O_5); iv) zirconium oxide (ZrO_2). All of them can be wet-processed starting from soluble, precursor materials, like for example alcolates. Among all the possible candidates (*figure* 3.1-1)[13] the most attractive AMO is aluminum oxide, due to its interesting characteristics: i) high dielectric constant (~9); ii) low trap density at the semiconductor junction; iii) high breakdown electric field (4 – 5 MV/cm); iv) large band gap (8.9 eV); v) structure stability during thermal treatment[14, 15].

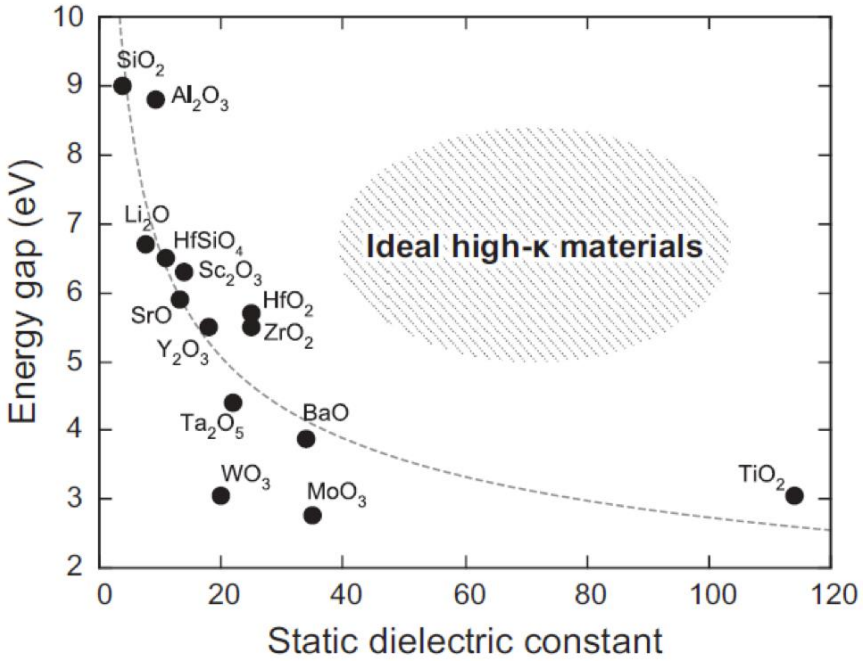

Figure 3.1-1: comparison of the high static k-dielectrics constant between different materials in relation to the energy gap.

The properties of AMOs produced by solution-based techniques, in the last few years, can be compared with those ones produced via PVD. The main differences between the two techniques are the costs and high temperature annealing that must be carried out on solution-processed layers, in the range of 600°C; this must be done to obtain a uniform film. This high temperature treatment restricts the use of flexible substrates, which in most cases are based on organic compounds [16, 17]. To allow a lower processing temperature, a possible approach consist into heating the layer itself during the annealing step, exploiting combustion chemistry [18]. In this chemical reaction, it is always need to heat up the precursor solution up to the ignition temperature of the combustion reaction. The oxide precursor mixed with chemicals considered as "fuel" (for example urea), generating inside most of energy needed for reaction. This fact decreases the total amount of external energy given to the system through high temperature heating, leading to a reliable AMO layer (*figure* 3.1-2) [19]. The difference with the sol-gel synthesis (non-combustion) is that with combustion it is only required to reach $T_{ignition}$ that I lower than the T_{oxide} formation. Using combustion approach, it is possible to deposit metal oxides, intermetallic compounds, carbides, refractory nitrides, and even inorganic semiconductors. All the base precursors are normally dissolved in an organic solvent, and the oxidizer element is usually metal nitrates and the fuels are citric acid, urea or acetylacetone [20, 21].

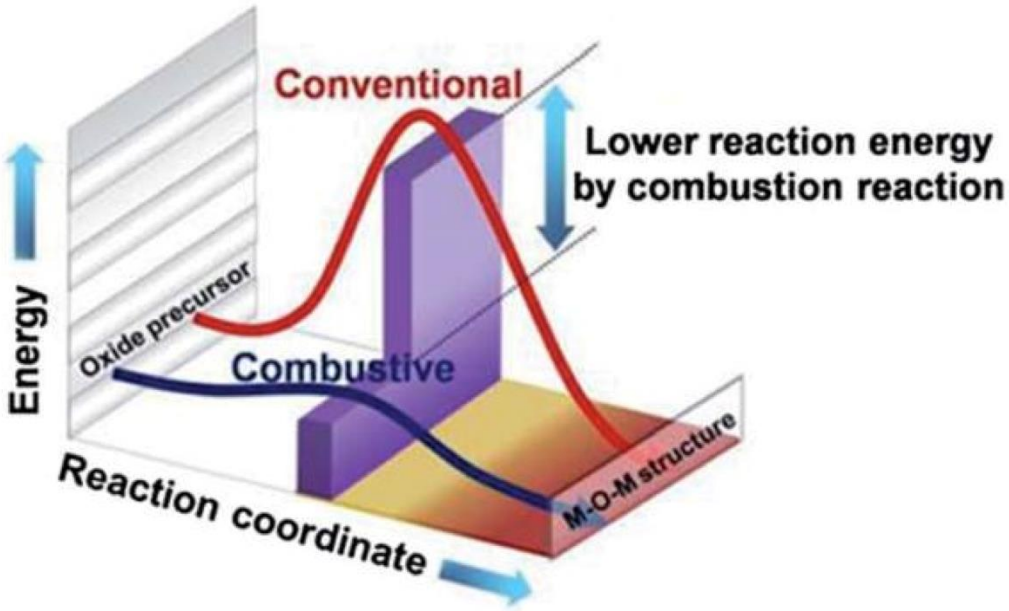

Figure 3.1-2: comparison between the energy of a conventional reaction and the combustion one.

Low temperature combustion reaction generates energy in form of heat, homogeneously distributed into the layer. As the *figure* 3.1-2 shows, the total amount of external energy the combustion process needs is lower when compared with the conventional methods. Nonetheless, a conventional source of energy is still needed to surpass the energetic activation wall of the precursor-to-oxide reaction, but due to the presence of internal heat provided by the combustion process much lower temperatures are needed. In the case of Al_2O_3 the safe temperature for which the complete conversion of the precursors to the oxide occurs is 350°C, which is much lower than the standard 600°C however, it is not compatible yet with the most flexible substrates.

Another way to improve the thin films and produce integrated circuits at low temperature is the combination between thermal annealing and UV treatment, that can be normal UV, DUV (Deep-UV) or FUV (Far-UV). This approach is used in the fabrication of semiconducting AMO layers, since the combination of heat and photon energy promotes at the same time, the use of lower annealing temperatures and the layer densification [22]. UV irradiation breaks all the oxide precursors organic chains on the substrate surface in small parts, allowing a fast organic degradation (10 minutes) and helps to remove oxygen and carbon atoms via gas phase, obtaining a M-O-M film densification [23]. In 2016, Emanuel Carlos and co-workers recently achieved a low thermal annealing temperature (180°C) for 30 minutes using FUV-light with a wavelength of 160 nm, accelerating the densification of a In_2O_3 film structure, and obtaining excellent electrical characteristics of the TFTs device made with it [24].

3.2 INKJET PRINTING OF DIELECTRIC LAYERS IN TFT DEVICE

This work has been focused on the Inkjet printing (IJP) of a solution-based AlOx precursor ink to apply as a dielectric nano-layer growth on silica by low-temperature combustion. This starting solution was developed in the CENIMAT laboratory at the New University of Lisbon, where first studies showed that it can be deposited at low temperature on substrates via spin-coating [24]. In order to allow an effective IJP, the characteristics of the solution suitable for spin coating must be changed to adapt them to a piezoelectric ink jet printer, with particular attention to the viscosity. This change of deposition method is necessary to switch from a laboratory production process to a semi-industrial one. In this specific case, spin-coating is not a good method to achieve working integrated circuits, due to the limitations in substrate size, high amount of wasted material, and patterning capabilities. Moreover, IJP is an additive process which limits materials waste also allows patterning with micrometers precision and larger area deposition.

The starting solution composition was:

CHEMICAL COMPOUND	Urea	Aluminum Nitrate
CONCENTRATION [g/mL]	0.502	0.3752
SOLVENT	2-methoxyethanol	

The work constraints were the following:

- Only the solvent can be changed, while the chemical precursors and their concentrations must be kept fixed;
- Printable solution needs to have also a perfect compatibility with the chemical precursors;
- The so-formulated solution must be compatible with electronic grade silica, with a roughness in the range of 1 nm.

The work was divided in different parallel sections, all looped for a cyclic optimization of the ink and printing process. All these work sections are hereafter separately described, for the benefit of the reader.

3.3 SUBSTRATE PREPARATION

Preliminary wetting tests carried out on the substrate via contact angles measurement showed a strong influence of the substrate washing procedure, as shown in *figure* 3.3-1. The substrate washed with organic solvents only did not promote the spreading of the drop (*figure* 3.3-1 “a”), while the substrate that underwent the complete washing procedure combined with a UV treatment step, showed a complete drop spreading (*figure* 3.3-1 “b”). The surface changing induced by the hydroxyl group that UV treatment generates on the SiOx surface is not permanent, as shown in *figure* 3.3-1 “c”, where it is visible that after 20 hours from the treatment the wettability started to decrease, until reaching later the same observed before the UV pre-treatment.

According to these observations, all the substrates used during the experimentation had a complete washing procedure, including UV treatment, to promote the drop spreading on the silicon surface, and to eliminate possible traces of organic contaminants on the surface, as well as to allow comparisons with the spin-coated samples, that were subject to the same cleaning treatment.

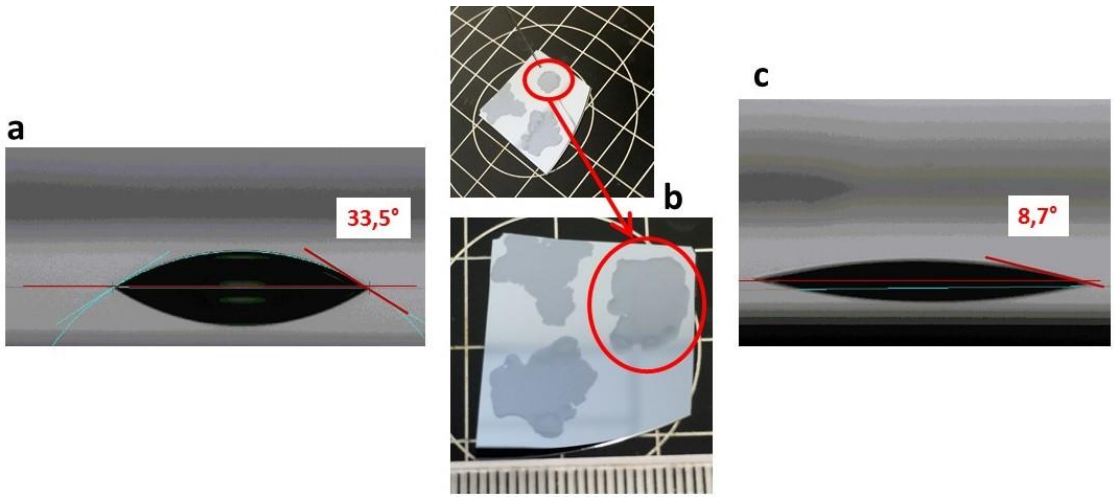

Figure 3.3-1: contact angle measurement of washed silicon substrate: a) substrate washed with organic solvents only; b) substrate washed with organic solvents with UV treatment; c) substrate washed with organic solvents with UV treatment after 20 hours

3.4 SOLUTION PRELIMINARY TESTS AND INK PRODUCTION

Oxide precursors solubility tests are fundamental to identify the best solvents for the ink preparation. The original solvent was 2-methoxyethanol, but it has a low viscosityand it is toxic. To obtain a printable solution the viscosity needed to be increased, either with new solvents or solvent mix.

All the tested solvents have been selected among alcohols. Water has been also considered, since some water-soluble additives have been tested to increase the final solution viscosity. However, it has been discarded after preliminary evaluations showing that its use caused a decrease in the of On/Off current ratio of the final devices, independently from the used conditions [25]. Dimethyl sulfoxide (DMSO) has been tested also, but it resulted to need a little amount of water to properly solve urea (the combustion reaction fuel), hence it was discarded too. After all the tests, 1-butanol and isopropanol were found to be the most suitable solvents for the formulation, since all the alcohols with longer chains promoted the precipitation of urea (*figure* 3.4-1). Therefore, test solutions based on these two solvents, and including propylene glycol as viscosity-enhancer, have been prepared and further tested.

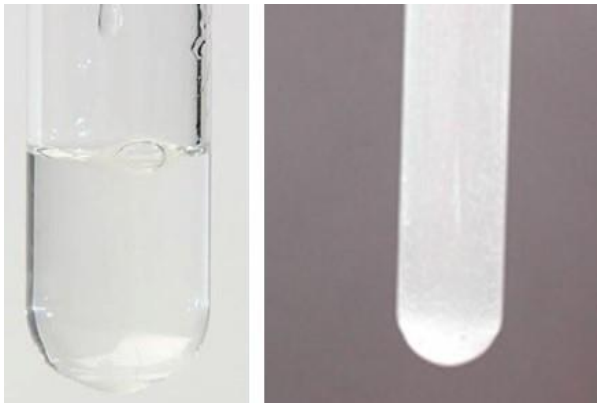

Figure 3.4-1: digital photos of a perfect crystalline solution (left) and a solution with urea precipitation (right).

3.4.1: OPTICAL CHARACTERIZATIONS

To compare the optical characteristics of the new formulated solution (inkjet printable) with those of the original one (spin coating-suitable), optical characterization was performed by means of UV-Visible absorbance measurements. In particular, the behavior of the UV absorption of aluminum precursors upon the addition of the new compounds to the solution was of interest,

due the fact that UV-assisted combustion process is a sought-for improvement of the combustion process. The main absorption peaks for the spin coating-suitable solution (based on 2-methoxyethanol as solvent, urea as fuel, and aluminum nitrate as the oxidizer) are 245 nm and 299 nm. In *figure* 3.4-2, it is possible to see the UV absorption of some modified solutions in comparison with that of the reference solution. In all curves, for both peaks significant changes were not observed. Therefore, both the identified possible solvents (i.e., 1-butanol and isopropanol) are suited for the goals of this work.

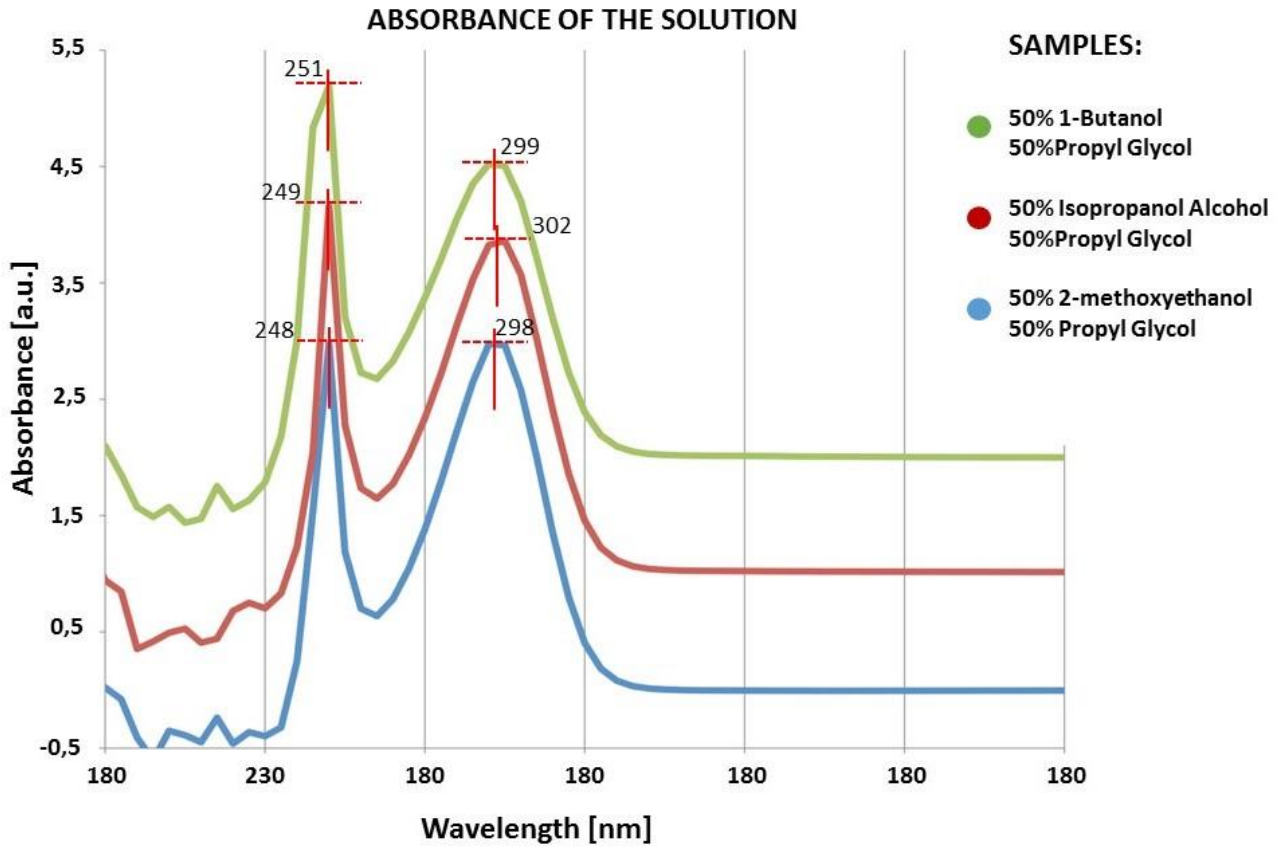

Figure 3.4-2: UV absorption of the new solutions.

3.4.2: THICKNESS OF THE DIELECTRIC SPIN-COATED FILM

All the solutions have been spin-coated on a silicon substrate, and annealed at 350 °C for 30 minutes. The thickness of all samples has been measured by ellipsometry. The results of these tests are summarized in table 3.4-1.

Table 3.4-1

NAME	THICKNESS [nm]	χ^2
50% 1-Butanol 50% Propyl Glycol	26	0.17
50% Isopropanol Alcohol 50%Propyl Glycol	22	0.22
50% 2-methoxyethanol 50% Propyl Glycol	40	0.61

As visible, the general thicknesses obtained using this three test formulations aren't dramatically different from the reference solution which is equal to 30 nm. This indicates that the proposed compositions can meet the final requirements for the dielectric layer dimensional characteristics.

3.4.3: FOURIER TRANSFORM INFRARED SPECTROSCOPY (FTIR)

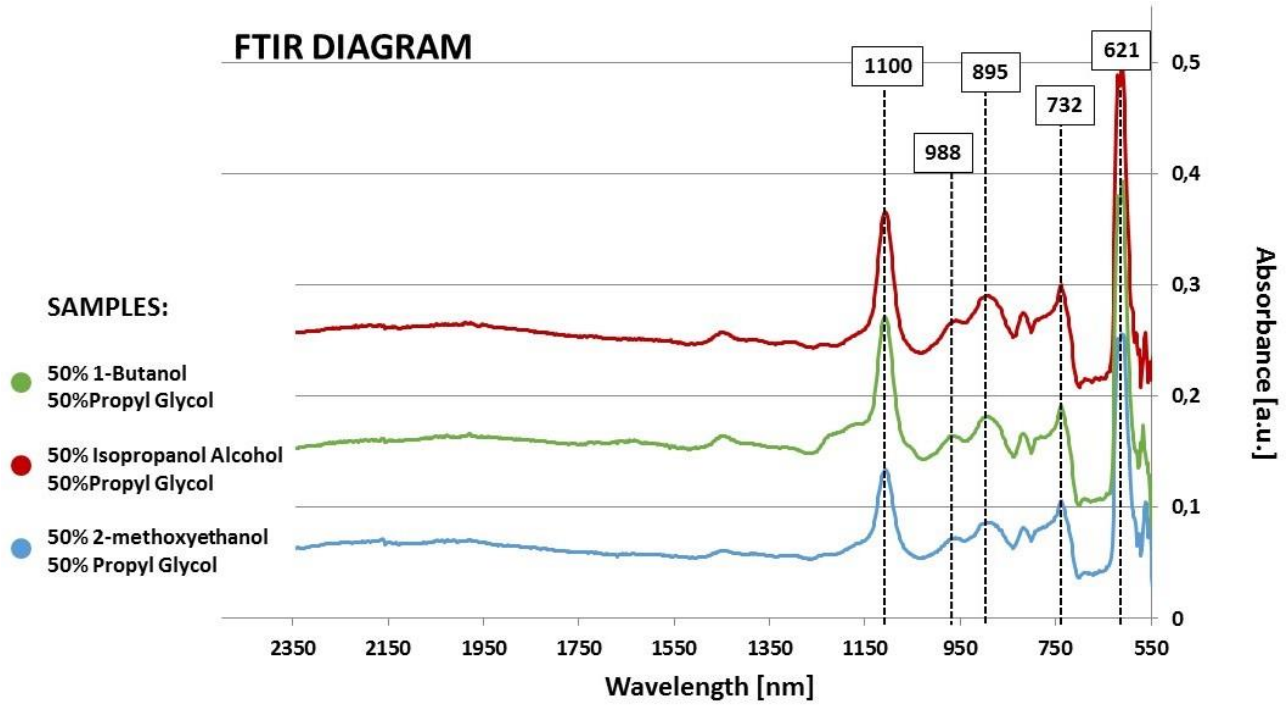

Figure 3.4-3: FTIR-ATR curves of the new solutions

After the annealing step (350 °C for 30 minutes), FTIR measurement were made to identify possible residues of organic materials left in the dielectric layers. The spectra were measured by attenuated total reflectance (ATR) in the range of 4500 – 525 cm^{-1} but only data in 2500 and 540 cm^{-1} range is shown as it is the relevant part of the spectrum for the considered compounds. *Figure* 3.4-3 shows the FTIR-ATR curves, where all the significant absorbance peaks are in the region between 1100-600 cm^{-1}. As shown in table 3.4-2 [26] these peaks correspond to the characteristic vibrational modes of amorphous AlO_x, confirming the presence of an amorphous alumina layer on the silicon substrate.

Table 3.4-2

POSITION [cm^{-1}]	**MODE TYPE**	**CHEMICAL BOUND**
1107	Transversal Optic Stretching	Si-O
968	Longitudinal Optic Stretching	Al-O
889	Condensed Tetrahedral	$Al-O_4$
739	Condensed Tetrahedral Stretching	$Al-O_4$
611	Transversal Optic Bending	$Al-0_2$

3.4.4: ELECTRICAL CHARACTERIZATION OF THE AlOx SPIN-COATED LAYER

Electrical measurements of AlO_x MIS devices prepared using the new formulations were performed in order to compare their electrical behavior with the reference layer. In particular, the following measurements were carried out: i) capacity-voltage (C-V); ii) current-voltage (I-V); iii) capacity-frequency (C-f). A brief overview of the results of these measurements is hereby given.

- **C-V measurements** [27]: capacitance is the property of a material which express its capability to store electrical charges. Two conductors plate constitute the simplest capacitor; in the middle of them a dielectric material (such as a polymers insulator or air) is required. Its electrical capacitance depends only by the conductor plates geometry (area and distance) and by electrical permittivity of the dielectric material. The measurement unit of capacitance is Farad [F], that

represents a 1 coulomb charge with a potential difference between the plate of 1 volt. A C-V measure identifies capacitive behavior of a dielectric layer inside a Metal Insulator Semiconductor, in function of the applied voltage.

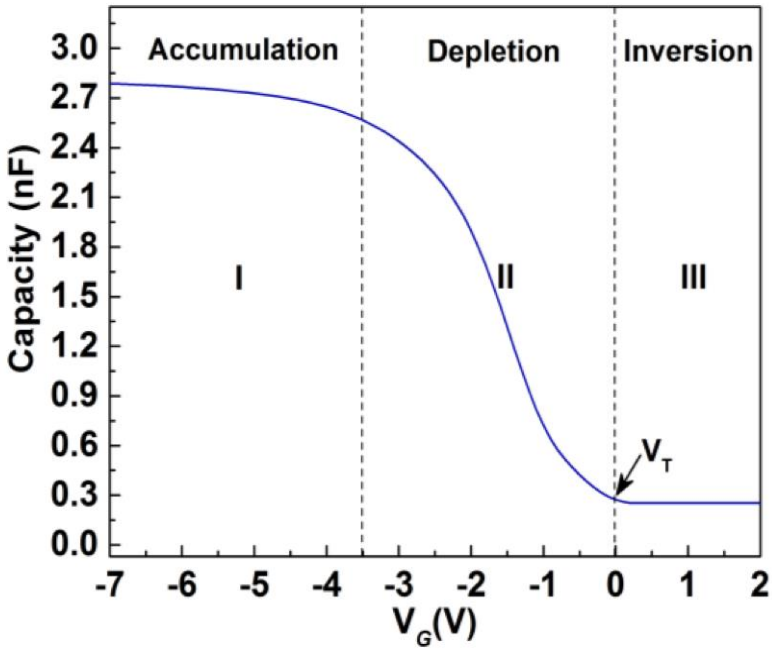

Figure 3.4-4: ideal C-V diagram in a p-type Metal-Insulator-Semiconductor (MIS) device.

The *figure* 3.4-4 represents the C-V diagram in a p-type Metal-Insulator-Semiconductor (MIS) device, and it is divided in three specific regions. In the negative voltage region, an accumulation zone (I) is recognizable, in which hole concentration increases at the insulator-semiconductor interface. The negative charge present inside the metal electrode causes this phenomenon. The total capacity in this region is given by the oxide capacity (the total capacity of the device is split between the oxide and the semiconductor, as in equation: $\frac{1}{C_t} = \frac{1}{C_{ox}} + \frac{1}{C_{se}}$, where C_t is the total capacity, C_{ox} is the capacity of the oxide and C_{se} is the capacity of the semiconductor). When voltage approaches higher values (II), the holes are driven away from the junction, the capacity decreases and the total capacity of the system is the parallel sum of the oxide and the semiconductor capacities. It the voltage is increased (III) over a positive value (threshold voltage, V_T) there is an accumulation of the electrons (negative charge) inside the insulator-semiconductor interface, on the semiconductor-dielectric interface. The polarity in this region is inverted and the total measured capacity is the sum in series between the oxide capacity and the maximum depletion capacity, that is considered the minimum capacity

Thanks to C-V diagrams based on spin-coated samples, the best solutions for the dielectric growth have been identified, which formed the basis for the IJP deposition approach. In *figure* 3.4-5 the C-V diagram of the three best performing solutions are showed. It is evident that in the 2-methoxyethanol (blue line) there is the presence of a second hump due to the organic solvent residue, that in the other two samples is not present. The capacity of the spin-coated reference is 350 nF/cm^2 and the sample with the nearest value is the 2-methoxyethanol one (blue), while the 1-butanol is the worst one. The three samples show hysteresis behavior, likely caused by the presence of ion and residual unreacted precursors, in the case of the 2-methoxyethanol and the isopropanol alcohol base solutions the hysteresis is well visible. These compounds affect the electrical response of the device, creating the hysteretic behavior, and for this reason the 1-butanol (green line) is considered the best sample.

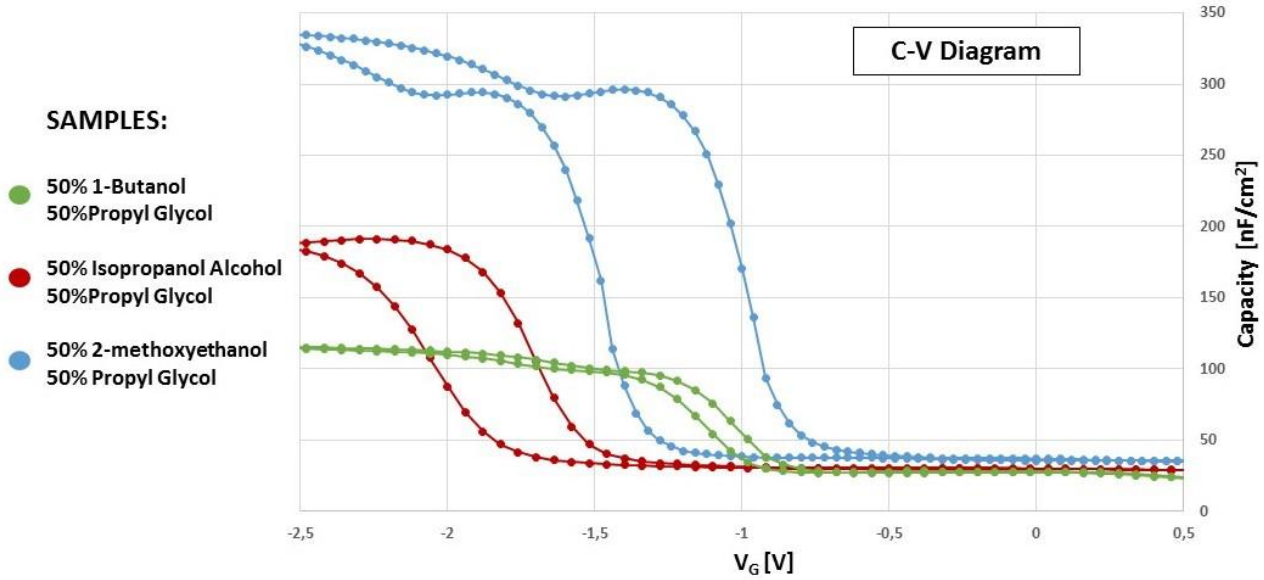

Figure 3.4-5: electrical characterization, C-V diagram of the three best performing solutions. All the measurements were made at a frequency of 50 kHz

- **C-f measurement**: this measurement shows the dielectric capacity at different alternated current (AC) frequencies, and allows to understand in which range of frequencies the dielectric has the best performance. Through this graph, it is possible to predict what will be the capacitance characteristic of the dielectric substrate integrated in a device, by knowing the frequency of work. This permits to select the correct dielectric and production method.

The isopropanol and 2-methoxyethanol-based layers are more stable at lower frequencies *figure* 3.4-6 “b” shows, while the 1-butanol have a higher variation at low frequencies, as visible in *figure* 3.4-6 “a”.

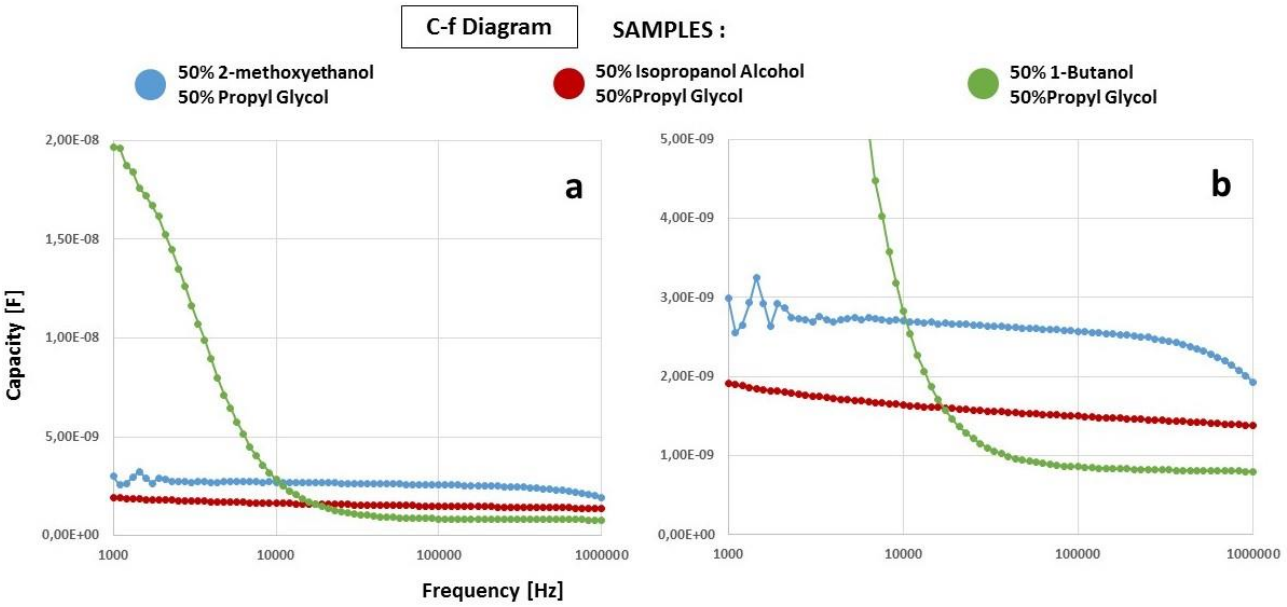

Figure 3.4-6: electrical characterization, C-f diagram of the three best performing solutions.

- **<u>I-V measurement</u>**: this type of measurement allows the possibility to understand the current behavior through the dielectric layers, and to identify the presence leakage current. The leakage current (off-current) represents a continuous energy loss by charge accumulated in the capacitator discharging the capacitor itself.

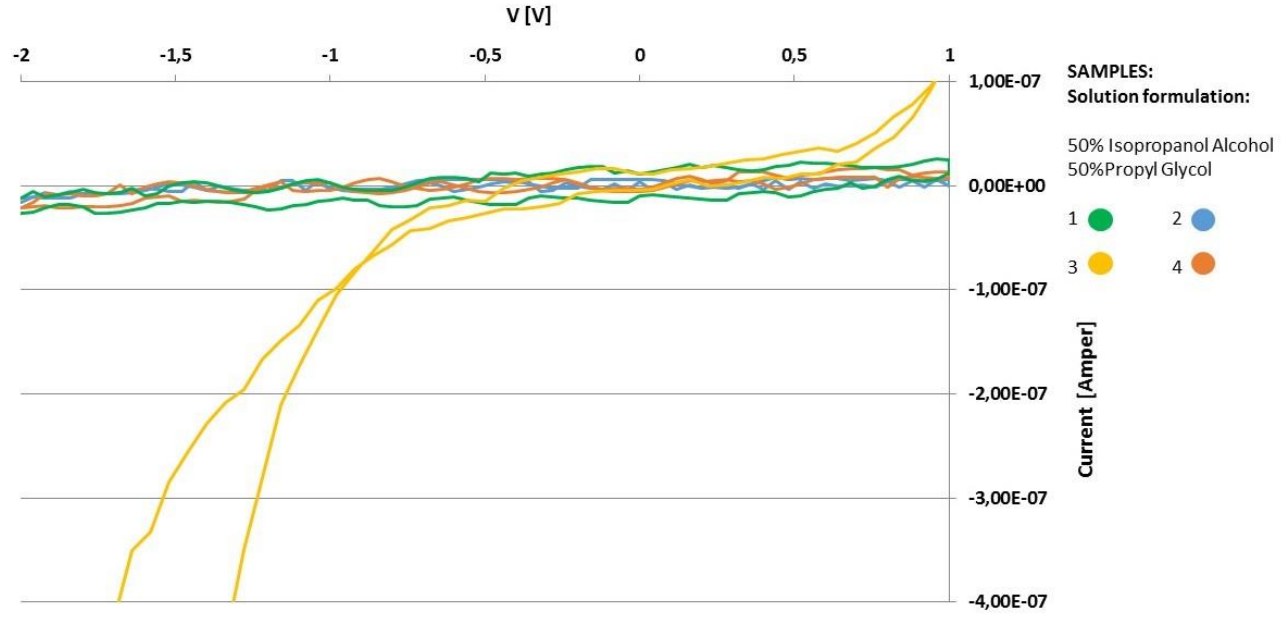

Figure 3.4-7: I-V measurement to compare the homogeneity and the reproducibility of the sample in the same batch.

It depends on the presence of charge defects within the film and/or a non-uniform dielectric layer where pinholes can occur. Performing these measurements over several samples it is possible to evaluate both the overall homogeneity of the layers, and their reproducibility within the same

batch, as in *figure* 3.4-7, where three of four samples, present on the same substrate, fabricated from isopropanol have low leakage current. The average leakage current of these three working samples are -3,5x10^{-8} A for sample 1, -2x10^{-8} A for sample 2 and -2,5x10^{-8} A for sample 4, the sample 3 is out of range (the reference value is in the range of 10^{-9} A).

Further tests have been made comparing different solution batches made with different organic solvent compositions, as in *figure* 3.4-8. From these tests the best solution composition was 1-butanol with polypropylene glycol in a 1:1 ratio.

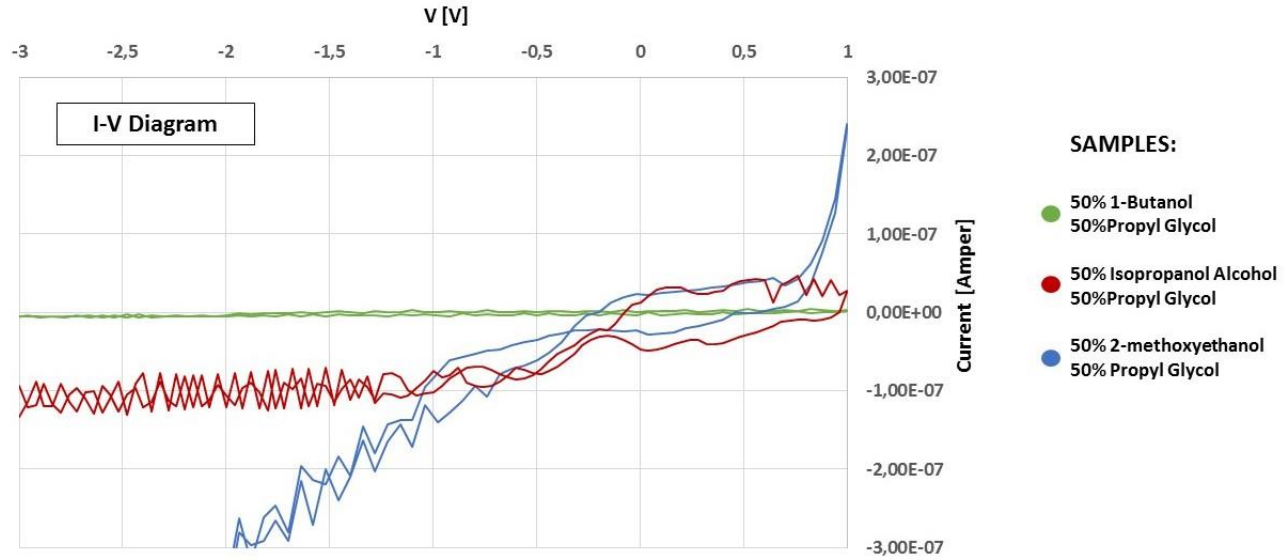

Figure 3.4-8: electrical characterization, I-V diagram of the three best performing solutions

3.5 INK JET PRINTING

3.5.1: VISCOSITY TEST

After the preliminary evaluation of the newly formulated solutions, that were spin-coated to test their effectiveness in forming homogeneous layers, the work moved on to printing the solutions. In a first step, all the solutions that delivered layers with good electrical properties and homogeneity have been tested in a viscometer, and in case slightly modified in composition for achieving a perfect ink viscosity. This was a fundamental step prior to advancing to the printing process and to printer parameter optimization.

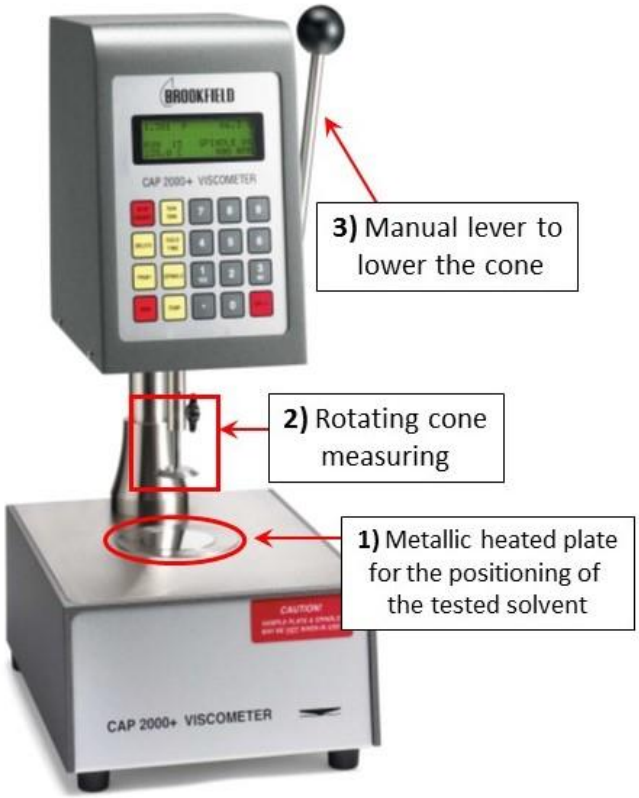

Figure 3.5-1: digital photo of the BROOKFIELD CAP 2000+ viscometer.

All viscosity tests were made at 30 °C (the fixed temperature of the printer cartridge nozzles), the ink was dropped (67 µL) on the metallic plate of the viscometer (1) (BROOKFIELD CAP 2000+ viscometer *figure* 3.5-1). The rotating cone for the test had an inclination of 0.45 degree and a radius of 1.511 cm. A computer controlled the viscometer, to start the measure it was needed to pull down the manual lever thus blocking the sample. Viscosity of the ink solution was measured by maintaining constant the number of the cone rpm and noting the force increasement

necessary to overcome the shear stress given by the liquid. Each ink was tested with three different rotating speeds, 500, 600 and 700 rpm. At each of these speeds, the Ink should have the same viscosity or only a little variation, because it is assumed to be a Newtonian fluid.

The viscosity of each tested ink is listed in table 3.5-1:

Table 3.5-1

INK NUMBER	ORGANIC SOLVENTS COMPOSITION	VISCOSITY [cP at 30 °C]
12	50% 2-Methoxyethanol 50% Propyl Glycol	7,1
15	60% Isopropanol Alcohol 40% Propyl Glycol	9,5
16	75% 1-Butanol 25% Propylen Glycol	7,3
17	75% 1-Butanol 25% Ethylene Glycol	5,9

Since the printing system requires an ink viscosity range between 2 to 12 cP, and all the inks are perfectly in the range, in principle all the above described inks should be printable.

3.5.2: PRINTING PARAMETERS

Initial printing tests were made with ink 12 (see table 3.5-1 for the ink formulations), and all the printing parameters were optimized for this ink. Printer used to carry out the printing tests was a PIXDRO LP 50, equipped with a DIMATIX 2813 cartridge holder and a corresponding 10 pL cartridge. The main characteristics of the PIXDRO LP 50 printer, compare with the DIMATIX 2831 used in the PhD work at University of Trieste, are: i) possibility to print in both direction X (print head movement) and Y (movement of the printing plate); ii) it is possible to rotate the printed with the cartridge using the pc software without openings of the lid ; iii) resolution depend by three factors, the printing direction, the cartridge angle and the quality factor; iv) plate temperature can be increase until 90°C. Printing process optimization in is in part empirical with a huge number of test and printing simulations.

The *figure* 3.5-2 shows the different behavior of 6 stacked ink layers (all in the same direction along X and with an angle of 0°) at different substrate temperatures. At 30 °C *figure* 3.5-2 “a” the drops are highly spread, while at 50 °C *figure* 3.5-2 “b” the drops are pinned to the substrate. A perfect substrate coverage was obtained allowing a little spreading of the drops, to homogenize the printed shape. For this reason, the chosen temperature during printing tests was 45 °C, and printing tests were carried out using the ink with lower viscosity, number 17 (see table 3.5-1 for the ink formulations).

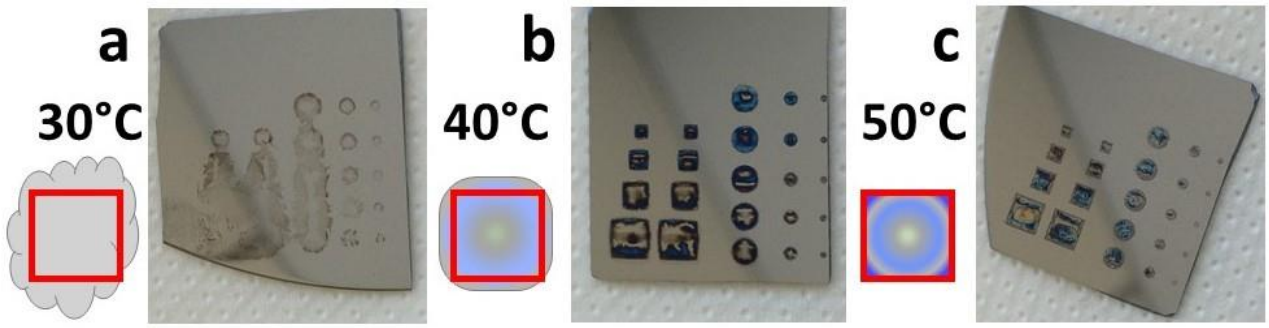

Figure 3.5-2: comparison between the three-different tested temperatures of the platen. It is possible to see the different ink behavior from a complete spreading in sample “a” to a perfect square shape in sample “b”.

For a good resolution, after different simulations and experiments, the most effective printing parameters were:

- Number of nozzles: 6 or 10 printing nozzles
- Printing Direction: to obtain the more homogenous substrate it was necessary to print overlapping layers with different drop textures. In particular, the best results have been obtained printing at first in the X direction with a 45 ° rotation of the printing head, and subsequently in the Y direction with a 0 ° rotation of the printing head.
- Quality factor: quality factor is the number of nozzles used to print one line in in-scan direction (parallel to print direction). The quality factor used is 3.

Sections	Voltage level start	Voltage level end
1	0	V_{mid}
2	V_{mid}	V_{mid}
3	V_{mid}	V_{low}
4	V_{low}	V_{low}
5	V_{low}	V_{high}
6	V_{high}	V_{high}
7	V_{high}	V_{mid}
8	V_{mid}	V_{mid}
9 (=1)	V_{mid}	0

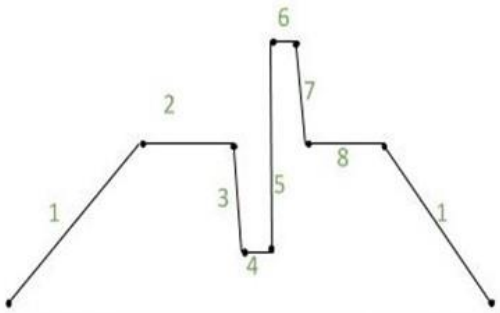

	Amplitudes (µs)								Voltages (V)		
Positions in the waveform	1	2	3	4	5	6	7	8	V_{high}	V_{mid}	V_{low}
Time [µs]	90	40	1	4	2	4	1	40	25	10	2

Figure 3.5-3: printer cartridge-head wave parameters, and the shape of the electrical wave

The last important parameter is the piezoelectric waveform. For the used printer, the waveform is divided in 9 steps, each characterized by a duration (measured in microseconds) and two voltage levels, at which the pulse starts and stops, as indicated in *figure* 3.5-3. For each time step it is possible to choose three different voltages (low, mid and high). In *figure* 3.5-3 the whole set of piezo parameters used during the printing process is shown.

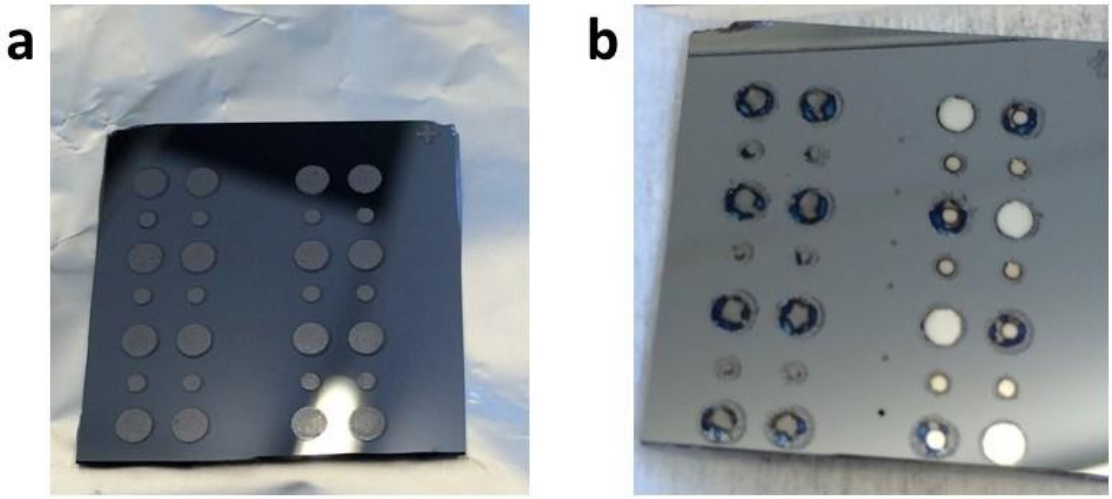

Figure 3.5-4: a) an example of the printed layers after the annealing; b) an example of the final device with the PVD aluminum electrode.

In the *figure* 3.5-4 is possible to see an example of the printed layers (a) and the aluminum electrode coating applied to the printed layer to create a MIS junction. All the spots are single

devices not connected with the others. In *figure* 3.5-5 “a” and “b” schematic exemplification of this structure is given.

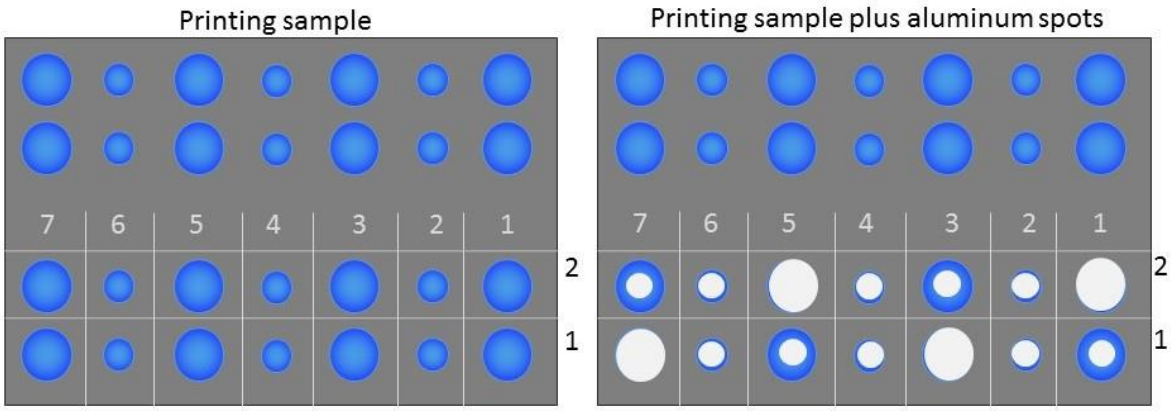

Figure 3.5-5: schematic illustration of the sample only printed and heated, and the one with also aluminum electrode

3.5.3: THICKNESS MEASUREMENT

Printed samples thickness coated by aluminum were measured by cross section with the SEM in FIB milling experiments, where Ga+ ions were accelerated to 30 kV at 5 pA and the etching depth was around 200 nm.

Tested samples were printed with ink 17 (see table 3.5-1 for the ink formulations), and samples were produced with two different thermal annealing: i) 350 °C for 30 minutes; ii) 150 °C + UV light for 120 minutes. In case of the thermal annealing at 150 °C + UV light for 120 min 12 layers of ink 17 (see table 3.5-1 for the ink formulations) were printed; while at 350 °C thermal annealing, two samples were prepared, one with 12 ink layers and the second with only 6 layers, in order to verify if this last approach was sufficient to produce uniform layers. In the sample produced at 150 °C plus UV light for 120 minutes the average layer thickness was around 140 nm (*figure* 3.5-6). As it is possible to see in *figure* 3.5-6 “b”, several bubbles were formed inside the dielectric layer (red circle), due to the reaction itself because all waste products are gaseous (besides the AlOx formations). UV helps for the densification of the films but it has high effective only in thin layers, no more than 30 nm. Low annealing temperature can leave high boiling point solvents inside the dielectric layer, as for example the ethylene glycol (boiling point equal to 197,3°C), which could thus increase the formation of bubbles inside the layer.

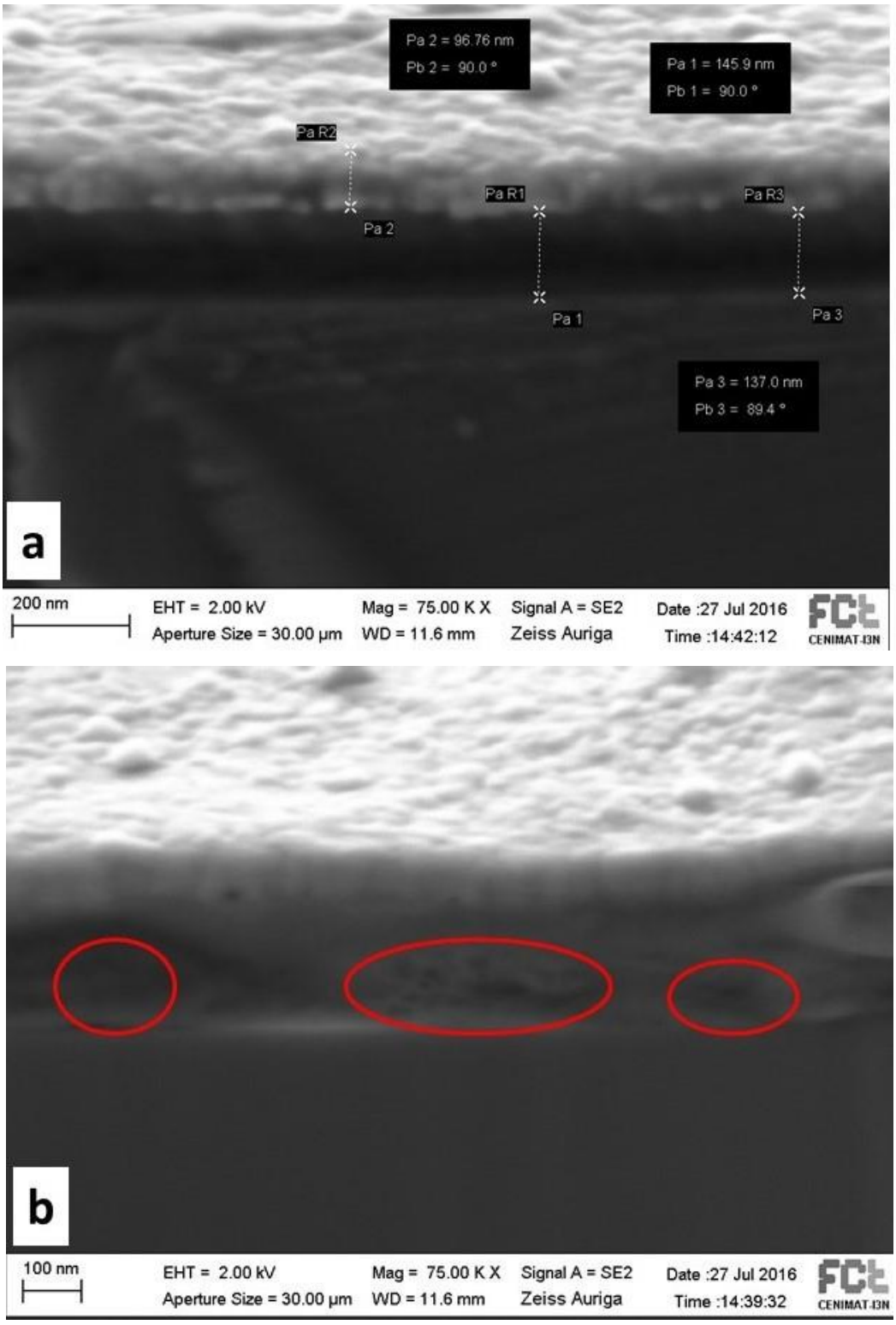

Figure 3.5-6: SEM imagine of a printed sample with ink #17 and annealed at 150°C for 120 minutes. In photo ''b'' the bubbles in the substrate are underlined by red circles.

On the contrary, the sample annealed at high temperature (350 °C) showed a good film densification, with an average thickness of 80 nm (*figure* 3.5-7 "a") in the case of 12 layers, while

the 6 layers showed an average thickness of 32 nm (*figure* 3.5-7 "b"). In the second case the dielectric layer is also well compact and uniform.

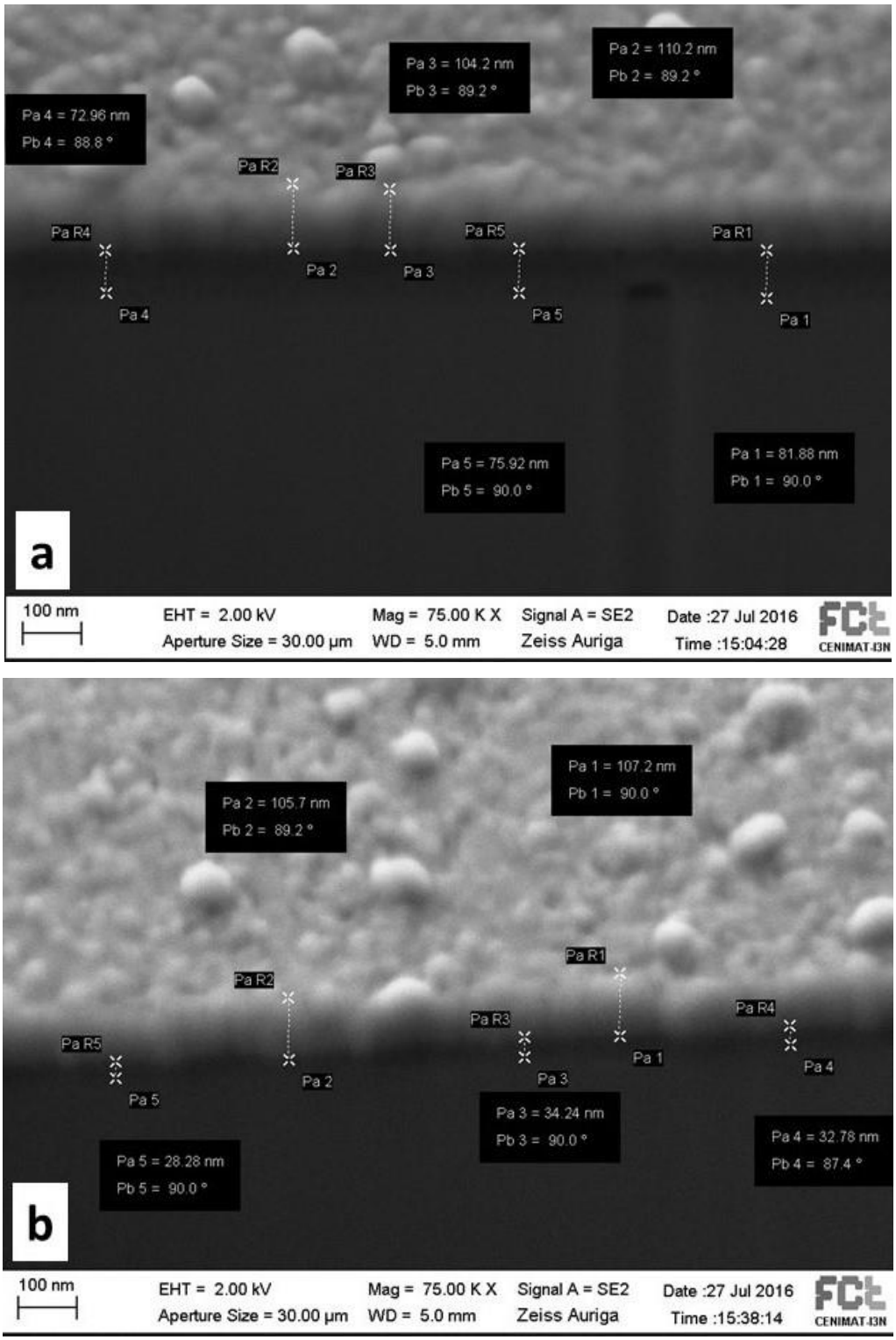

Figure 3.5-7: SEM image of a printed sample with ink #17 and annealed at 350°C for 30 minutes. Photo "a" shows a 12 layers sample and photo "b" shows the 6 layers sample.

3.5.4: ELECTRICAL MEASUREMENTS

In *figure* 3.5-8, it is possible to see examples of printed layers after annealing treatment and before aluminum evaporation. All of them have a non-perfectly uniform surface. Uniformity of the samples is relatively good (considering that the imaged dots have been inkjet printed) in the cases 17A and 17B, although in sample 17 B the printing texture is improved. Sample 17C shows a good uniformity only in its central part.

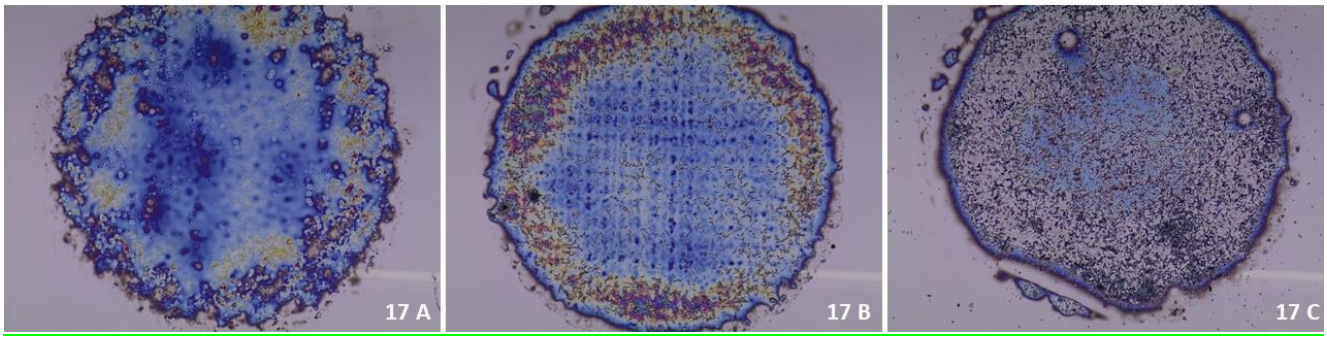

Figure 3.5-8: digital photos of the three electrically characterized samples made by ink #17 at three different annealing temperatures: 17A) 350°C for 30 minutes; 17B) 150°C plus UV-light for 120 minutes (8 cm distant from the UV-lamp); 17C) 200°C plus F-UV light for 90 minutes (9 cm distant from the FUV-lamp). The average diameter of these circles is 2 mm.

All the printed samples were electrically characterized in MIS devices with the C-V, C-f and I-V curve, and the electrical characteristics of the layers obtained using ink 17 (see table 3.5-1 for the ink formulations).

The three curves with three different colors present in the *figure* 3.5-9, 10 and 11, refer to different types of annealing treatment of the printed samples: 17A – 350 °C for 30 minutes (yellow); 17B – 150 °C plus UV-light for 120 minutes (2 cm distant from the UV-lamp) (orange); 17C – 200 °C plus FUV light for 90 minutes (9 cm distance from the FUV-lamp)(violet). The I-V measure *figure* 3.5-9 shows different behavior for the different annealing treatments, samples A and C have a current in the order of $-2x10^{-8}$ A and $-7x10^{-8}$ A respectively, an order of magnitude higher than in the same sample product for spin-coating and using high temperature annealing ($-2,5x10^{-9}$ A). The sample B has higher leakage current in the order of $-1,5x10^{-7}$ A. These three samples showed the best performance at lower frequency, between 1 and 5 kHz (*figure* 3.5-10).

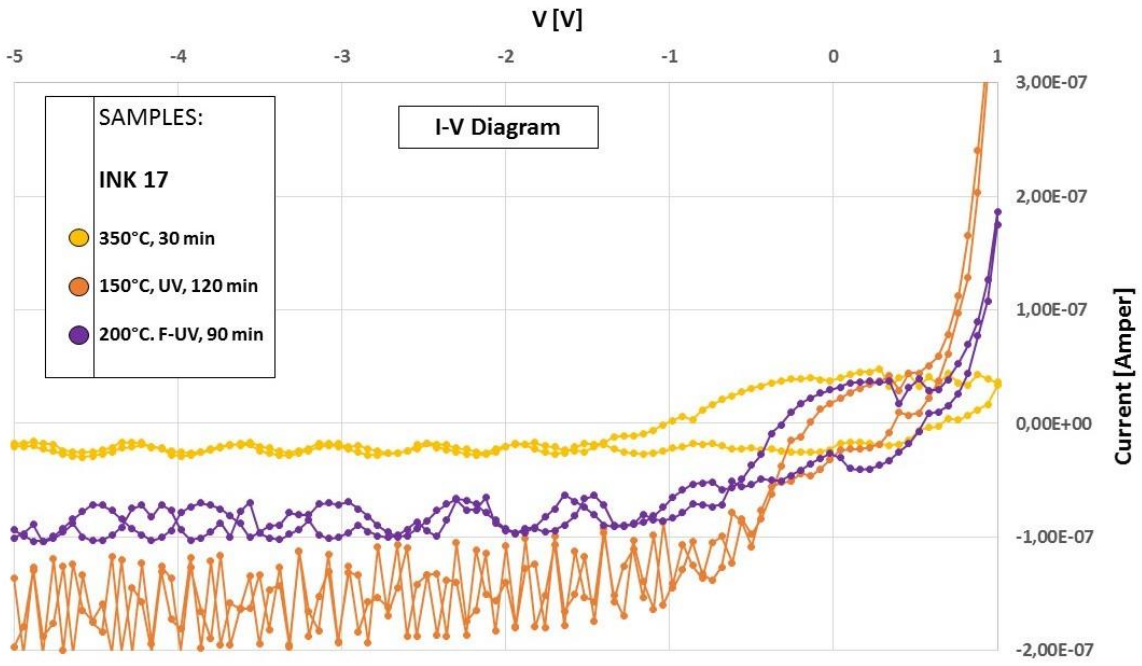

Figure 3.5-9: I-V curve of the ink #17 sample at the three different annealing temperatures.

The hysteresis is present in the C-V curves, being slightly higher for sample 17A *figure* 3.5-11. The capacitance c is smaller, when compared with the reference spin-coated layer, but a second hump, which indicate the presence of organic residues, is not observed (*figure* 3.5-11). Devices annealed at 150 °C showed the lowest capacity variation with frequency, however the most promising devices for TFTs are the ones produced at 350 °C due to complete organics degradation.

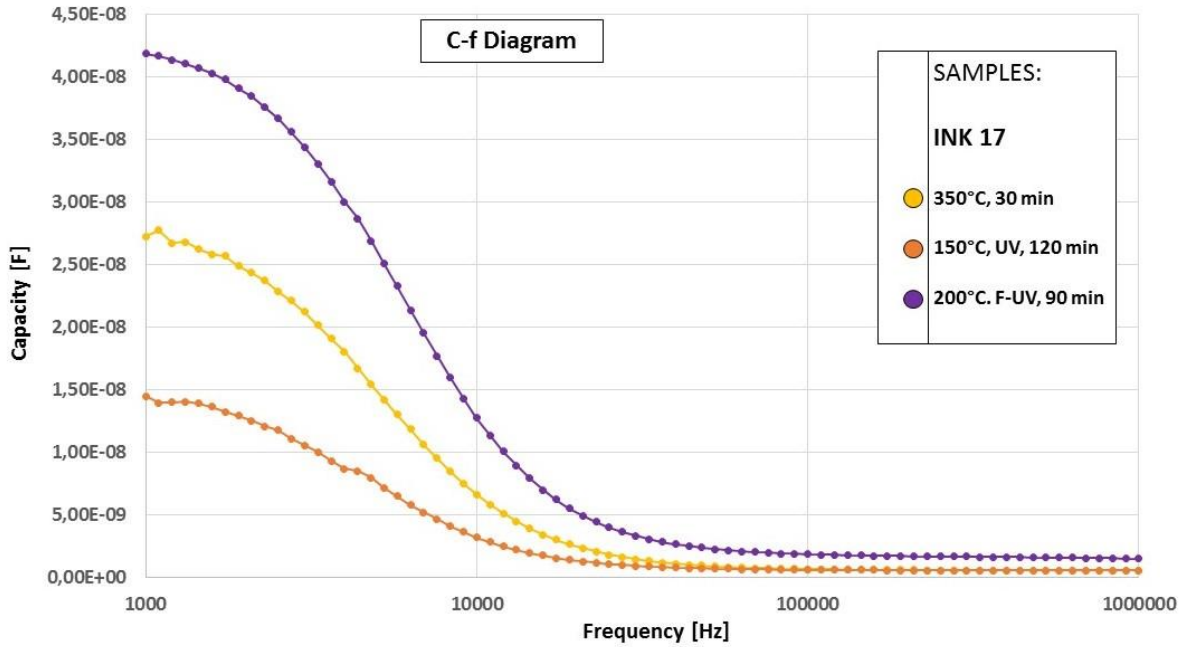

Figure 3.5-10: C-f curve of the ink #17 sample at the three different annealing temperatures.

Upon these evidences, ink 17 (see table 3.5-1 for the ink formulations) was used to fabricate the dielectric layer for TFT devices. The annealing treatments used during this last set of tests were: 350 °C for 30 minutes; 150 °C plus UV-light for 120 minutes.

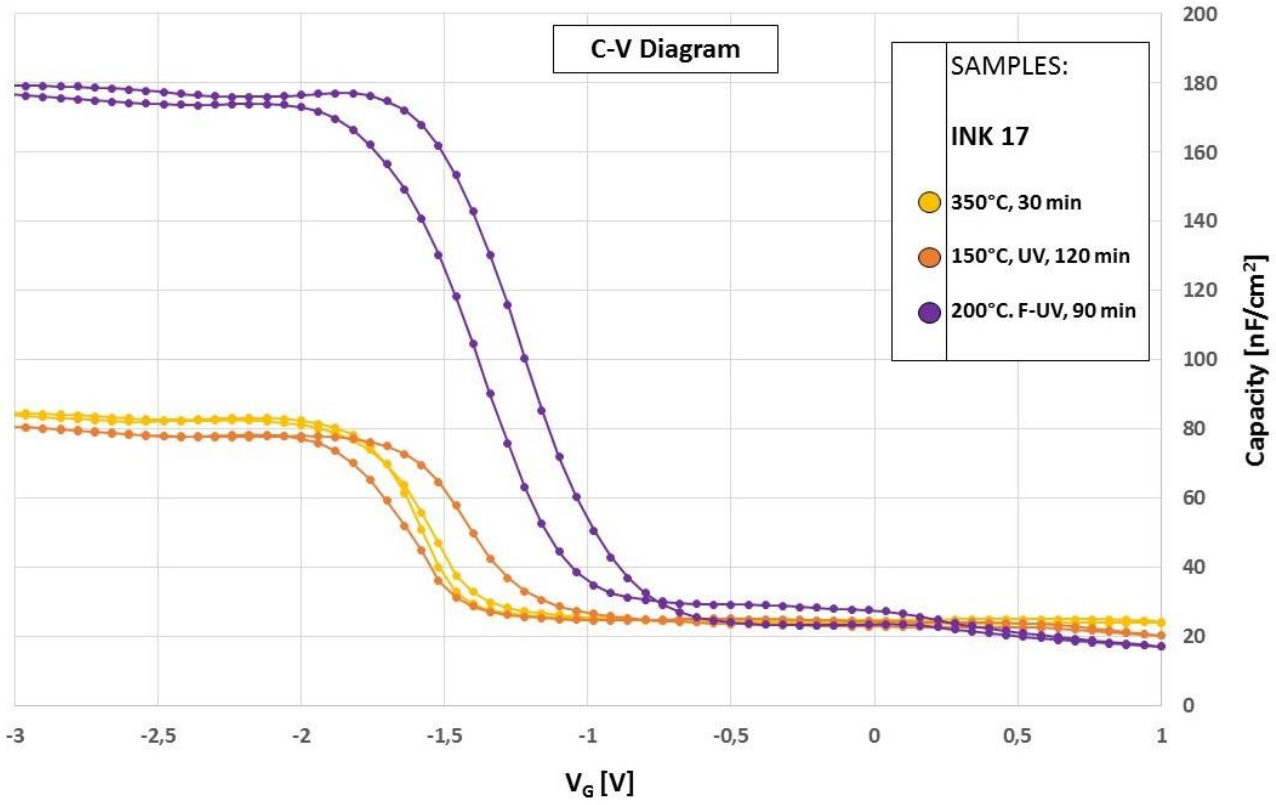

Figure 3.5-11: C-V curve of the ink #17 sample at the three different annealing temperatures. All the tests were made at 50 kHz.

3.6 TFT PRODUCTION

In this section, we report the first fabrication of GIZO/AlO_x TFTs using inkjet printing to deposit AlO_x dielectric at 150 °C. The TFT devices (*figure* 3.6-1) were electrically characterized after fabrication by a different research group at CENIMAT (University of Lisbon).

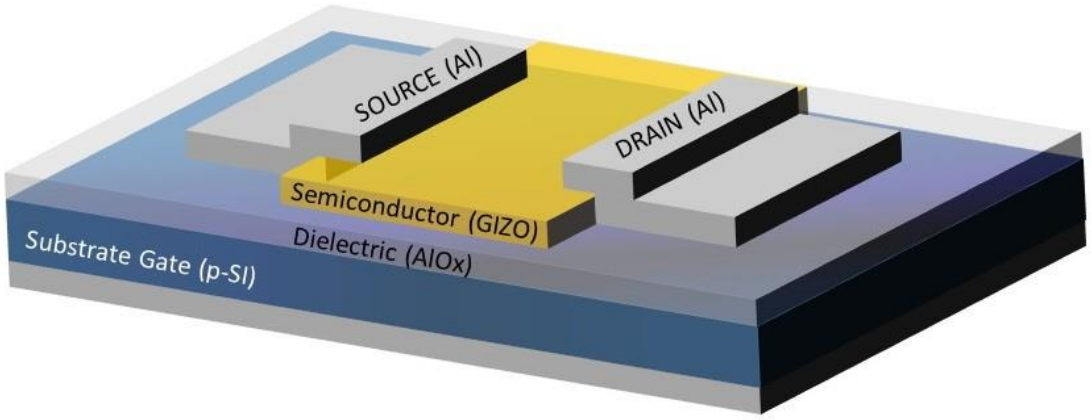

Figure 3.6-1: schematic illustration of the Thin Film Transistor used to test the printed dielectric layer

The results of these characterizations are reported in the *figure* 3.6-2 and in the *figure* 3.6-3, and in the table 3.6-1.

Table 3.6-1: electrical characteristics of TFT with printed dialectic

Semiconductor	Solution based dielectric	T (°C)	W/L	V_{on} (V)	V_T (V)	V_{Hyst} (V)	S (V/dec)	$I_{ON/OFF}$
GIZO	**AlO_x**	150	10	- 0.1	0.12	0.35	0.24	8×10^2
		350	5	- 0.1	0.22	0.22	0.18	3×10^3

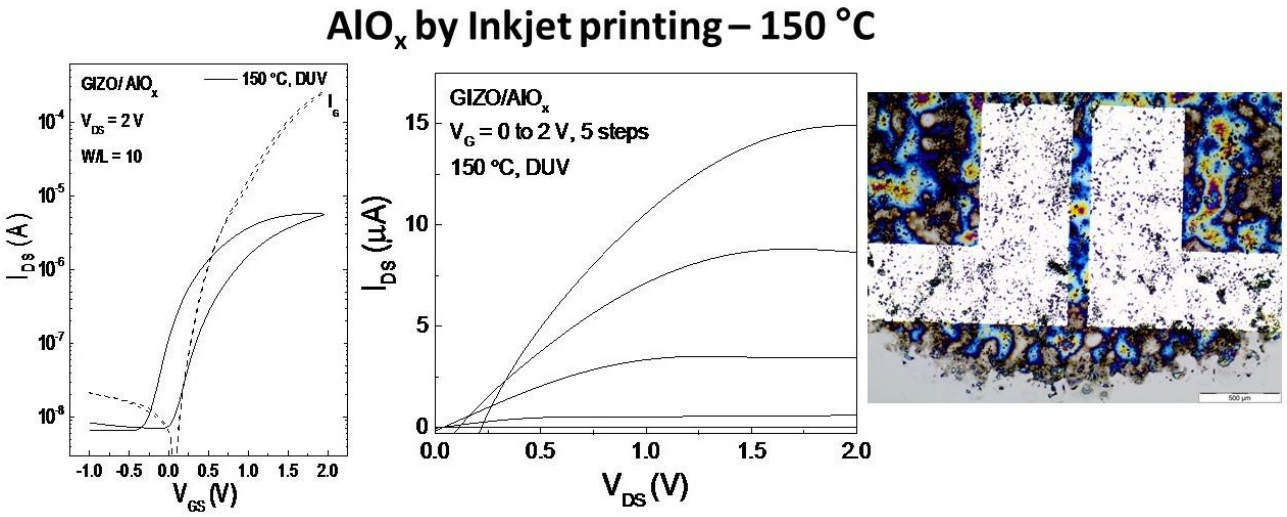

Figure 3.6-2: TFT sample with the printed dielectric layer and annealed at 350°C for 30 minutes. I-V measure and a digital photo of the PVD aluminum source and drain, from the photo it is possible to see the heterogeneity of the dielectric layer.

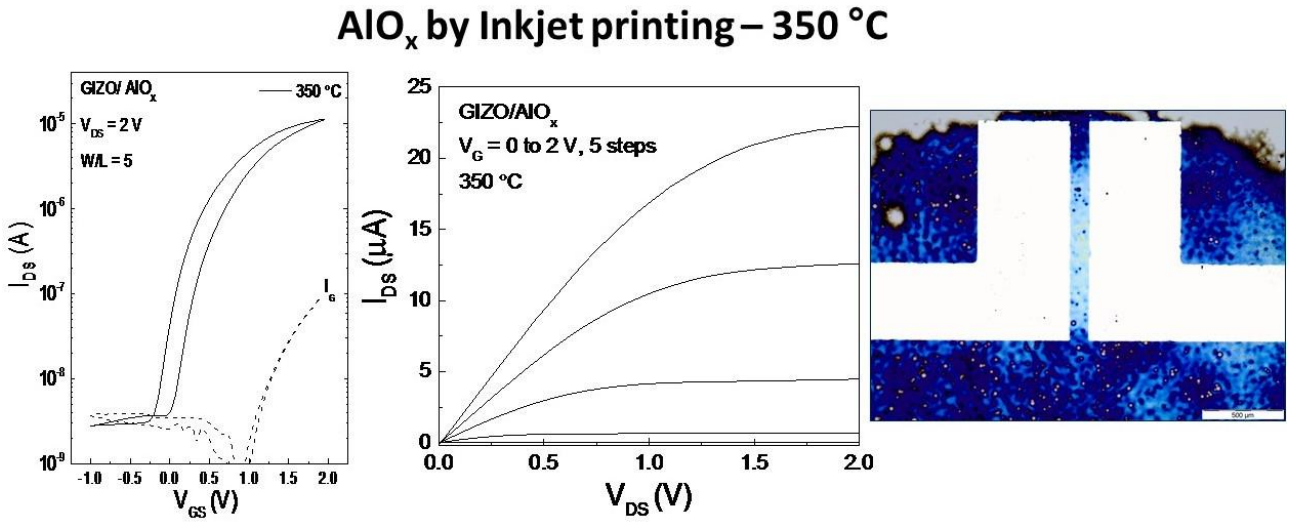

Figure 3.6-3: TFT sample with the printed dielectric layer and annealed at 350°C for 30 minutes. I-V measure and a digital photo of the PVD aluminum source and drain, from the photo it is possible to see the homogeneity of the dielectric layer.

Figures 3.6-2 and 3.6-3 show the electrical behavior of the printed TFTs at different annealing treatments. Devices annealed at 350 °C showed a better performance however; both devices showed a clear saturation at low operation voltage and a turn on voltage close to 0. The devices at low temperature showed a higher leakage current, which is visible too in the beginning of the output curve.

If compared with the reference devices, prepared using the spin-coated films annealed at 350 °C (table 3.6-2), performances of it printed device are are reduced. Nevertheless, the interface between the insulator and the semiconductor is the same for the printed devices and the reference device, which is really promising and will be optimized in further study.

Table 3.6-2: reference sample electrical characteristics

Semiconductor	Solution based dielectric	T (°C)	W/L	V_{on} (V)	V_T (V)	V_{Hyst} (V)	S (V/dec)	**µSAT** (cm^2/Vs)	$I_{ON/OFF}$
GIZO	**AlO_x**	150	4	- 0.57	0.21	0.12	0.18	16,68	$2,89\times10^4$
		350	14	- 0.88	-0.14	0.13	0.14	27,93	$7,24\times10^5$

An important difference between the reference and the printed samples is the concentration of the precursors respectively, 0.1 and 0.2 molar, and the solvents used in order to increase the viscosity to apply in inkjet printing. Recently, E. Carlos [24] showed that the capacitance characteristics decrease with the increasing of the precursors concentration.

Printed samples exhibit good properties in electronic devices. In order to improve the results achieved at low temperature, the dielectric uniformity needs to be optimized with the use of a new solvent with a boiling point below 150 °C, that can achieve the viscosity needed for printing.

3.7 CONCLUSIONS

During the PhD period, abroad at the University of Lisbon, inks for printing dielectric nano-layers of AlOx via a low temperature combustion approach were formulated and optimized. The original solution was optimized for deposition via spin-coating inside the laboratories of the University of Lisbon. It is possible to change only the concentration of the precursors and the organic solvents to gain the optimal physical characteristics for the IJP, whereas the precursors type is fixed. Mixtures of different solvents with different viscosity were tested to obtain the correct solution for inkjet printing; in addition, before the solutions became inks, each solution was evaluated with a series of tests to check the properties of the grown layer and successively compare it with the dielectric layer produced by the original solution. Four inks were moved from the test-stage to the printing procedure, as indicated in table 3.5-1. The ink that can be considered the best one in terms of stamp-ability and electrical properties is number 17. Ink 15 also must be mentioned because it is made by substances that, in small amount, may be considered non-toxic for the worker and the environment. An important optimization during the printing process is the plate temperature (45°C for all the printing device) that promotes a correct substrate coverage without any spreading that reduces the printing shape quality. Ink 17, which generated the high quality dielectric layer in terms of electrical properties and homogeneity, was used successively in TFTs devices, where it worked perfectly.

All the three annealing techniques are good to obtain the final layer, but the high temperature one (350°C for 30 minutes) gives the best results. By changing the solvent or the precursors, it is possible to implement the other two low temperature techniques (150°C plus UV-light for 120 minutes; 200°C plus FUV-light for 90 minutes), moving from the silicon substrate, which is rigid, to polymeric substrates, which are flexible.

This experimentation underlines the possibility to print inks that promote the formation of very good dielectric layers of oxide materials grown by means of the combustion technique and their organic precursors. The innovative aspects are simplicity without expensive equipment, high throughput and the precision of the printing process, which also reduces the amount of waste material and makes the devices cheaper. The use of polymeric substrates in the future will make them flexible, stretchable and thinner increasing their application in industrial electronics.

3.8 MATERIALS AND METHODS

3.8.1 SUBSTRATE PREPARATION

The contact angle measurement device was a DATA PHYSICS Contact Angles System OCA.

The substrates come from the same silicon wafer, and the solvent used for the test is distillated water with a surface energy of 72 dyn/cm = mN/m. Each drop had a volume of 0.5 µL. An image for each test has been taken after no more than 5 seconds from the drop-substrate contact.

The complete washing procedure is described below:

- The substrate is inserted in a sample holder that maintain it vertical and promotes the falling of the dirt particles;
- The sample holder is inserted inside a beaker full of acetone, where is left for 15 minutes in an ultrasonic bath;
- The sample holder is transferred inside a second beaker full of isopropanol alcohol where is left further 15 minutes in an ultrasonic bath;
- At the end of the sonication every sample is washed with distillated water and dried with nitrogen flux;
- The substrate is put under UV light for 15 minutes before the use.

Three different substrate experiments have been carried out: i) the substrate have been washed only in organic solvents and water, and dried with the nitrogen flux; ii) the substrates have been subjected to a complete washing treatment (including UV); iii) the substrates with the full washing treatment have been measured also the day after the treatment.

3.8.2: SOLUTION PRELIMINARY TESTS AND INK PRODUCTION

3.8.2.1: Solution Preparation

The dielectric precursor solutions were prepared dissolving aluminum nitrate nonahydrate and urea in the organic solvents mix. The concentration of the chemical compounds is 0.2 mmol/mL. The tested solutions are listed in the 3.8-1.

Table 3.8-1

SOLVENTS [mL]	Urea [g]	Aluminum Nitrate Nonahydrate [g]
50% - 2-METHOXYETHANOL – 2.5 50% - PROPYLENE GLYCOL – 2.5	O.502	0.3752
50% - 1-BUTANOL – 2.5 50% - PROPYLENE GLYCOL – 2.5		
50% - ISOPROPANO ALCOHOL – 2.5 50% - PROPYLENE GLYCOL – 2,.5		

The solvent placed in a 10 mL beaker with the aluminum nitrate nonahydrate and it is put under stirring (430 rpm speed) until all the solid compound is dissolved (normally it takes from 5 to 10 minutes, depending on the solvent mix). The urea is added only when the solution is completely transparent, and the solution must be magnetically stirred for 1 h at 430 rpm.

The chemical compounds used for the solutions are listed below in the table 3.8-2:

Table 3.8-2

NAME	**MOLECULAR WEIGHT [g/mol]**	**BOILING POINT [°C]**	**VISCOSITY [cP]**	**DENSITY [g/cm^3]**	**PURITY**
ALUMINUM NITRATE NONAHYDRATE (7784-27-2)	375.13	73 (MELTING)	SOLID	1.401	99%
UREA (57-13-6)	60.06	133 (MELTING)	SOLID	1.33	98%
2-METHOXYETHANOL (109-86-4)	76.09	124	1.534 (20°C)	0.965	99%
ISOPROPANO ALCOHOL (67-63-0)	60.1	82	2.04 (25°C)	0.786	>99%
1-BUTANOL	74.12	117.7	2.54 (25°C)	0.81	99%

(71-36-3)					
PROPYLENE GLYCOL (57-55-6)	76.09	188.2	40.4 (25°C)	1.036	98%
ETHYLENE GLYCOL (107-21-1)	62.07	197.6	16.1 (25°C)	1.11	99%

3.8.2.2: Substrate preparation

Before use, the silicon substrates (2.5x2.5 cm size) were cleaned in ultrasonic bath for 15 minutes in acetone and for other 15 minutes in isopropanol alcohol. After the ultrasonic bath, they were washed in distillated water and dried with nitrogen flux, followed by 15 minutes under UV light, 5 cm distance from the lamp (PSD-UV Novascan system).

3.8.2.3: Sample Preparation

On all the substrates, a single layer of AlOx solution was deposited by spin coating (35 seconds at 2000 rpm). Samples have been then immediately annealed by hot plate at 350 °C for 30 minutes.

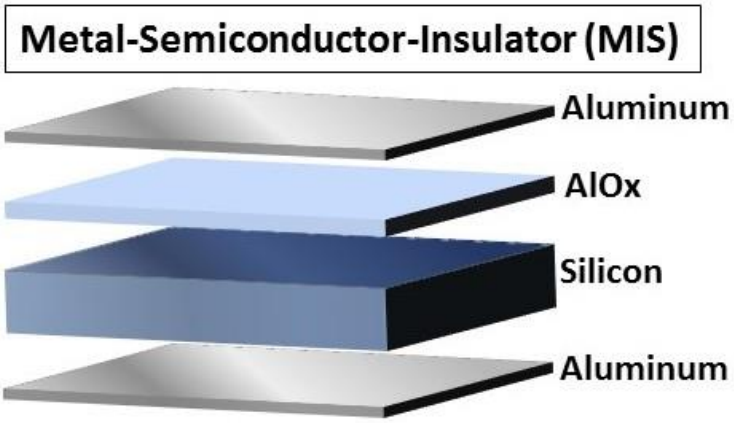

Figure 3.8-1: schematic illustration of a Metal-Insulator-Semiconductor structure cross section

The Metal-Insulator-Semiconductor structure visible in *figure* 3.8-1 was produced to test the electrical characteristics of the dielectric layers, spin coating the AlOx layer precursor solution onto p-type silicon substrates (1−10 Ω cm). Annealed layers have been covered with about 80 nm of

PVD aluminum as the electrode, with variable areas (*figure* 3.8-2 "a"). On the back of the samples, further 80 nm of aluminum were also deposited, to improve the electrical contact with silicon.

In *figure* 3.8-2 it is possible to see a typical sample deriving from this procedure. Each aluminum spot is considered as a single device. In general, smaller devices are preferred due to lower probability to find defects however, often the edge part of the aluminum was oxidized in the smaller devices, hence all the here presented measurements were carried out on the 1 mm diameter devices.

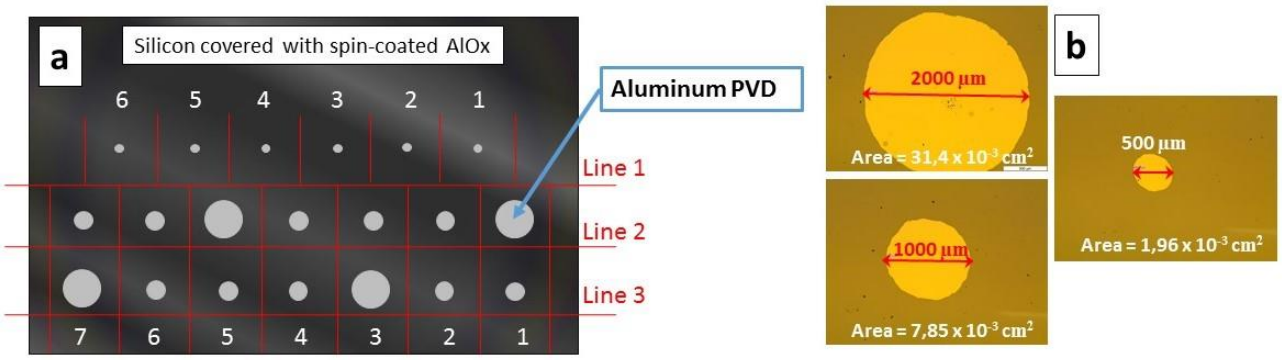

Figure 3.8-2: a) schematic illustration of the PVD aluminum electrodes on the silica substrate covered by AlOx dielectric layer; b) microscope photos of the three-different aluminum electrode size.

3.8.2.4: Optical and electrical analyses

The optical properties of the realized layers were investigated using a Perkin Elmer lambda 950 UV/VIS/NIR spectrophotometers in the range of 190 nm to 800 nm. Spectroscopic ellipsometry measurements to determine the thickness of thin films deposited on silicon substrates were made over an energy range of 1.5−6.0 eV, with an incident angle of 70 °, using a Jobin Yvon Uvisel system. The ATR-FTIR measurements were made using a Nicolet 6700 FT-IR in the range from 525 nm to 4500 nm. The electrical measurements were made using a Cascade Microtech – keySIGHT B1500 A Semiconductor Device Analyzer.

BIBLIOGRAPHY CHAPTER 3

3.1: PRINTING OF NANOTHIN AlOx DIELECTRIC LAYERS FOR ORGANIC ELECTRONICS APPLICATIONS

1. http://lib.tkk.fi/Reports/2009/isbn9789522480781.pdf.
2. Coatanéa, E et al., Printed Electronics, Now and Future. In Neuvo, Y., & Ylönen, S. (eds.), Bit Bang.
3. Rays to the Future. Helsinki University of Technology (TKK), MIDE, Helsinki University Print, Helsinki, Finland, 2009, 63-102.
4. Kuo Y., Thin Film Transistor Technology, Past, Present, and Future, The Electrochemical Society Interface, Spring 2013.
5. M.-G. Kim, et al., Nat. Mater., 2011, 10(5), 382.
6. Y.-H. Kim et al., Nature, 2012, 489, 7414, 128.
7. C. Avis and J. Jang, J. Mater. Chem., 2011, 21(29), 10649.
8. X. Yu et al., Proc. Natl. Acad. Sci., 2015, 112(11),3217.
9. G. D. Wilk et al., Appl. Phys., 2001, 89(10), 5243.
10. P. Barquinha et al., J. Soc. Inf. Disp., 2010, 18(10), 762.
11. S. Y. Lee et al., Thin Solid Films, 2010, 518(11), 3030.
12. J. Robertson et al., Phys. J. Appl. Phys., 2004, 28(3), 265.
13. K. Yim et al., NPG Asia Mater., 2015, 7(6), 190.
14. A. Sharma et al., Adv. Appl. Sci. Res., 2012, 3(4), 2151.
15. H. Tan etal., J. Mater. Chem. C, 2014, 2(28), 5695.
16. K. Nomura et al., Nature, 2004, 432(7016), 488.
17. Y. Sun and J. A. Rogers, Adv. Mater., 2007, 19(15), 1897.
18. M.-G. Kim et al., Nat. Mater., 2011, 10(5), 382.
19. E. J. Bae ey al., J. Mater. Chem. C, 2014, 2(28), 5695.
20. H. C. Yi and J. J. Moore, J. Mater. Sci., 1990, 25(2), 1159.
21. M. Epifani et al., J. Eur. Ceram. Soc., 2007, 27(1), 115.
22. Y.-H. Kim et al., Nature, 2012 489(7414), 128.
23. H. Imai et al., J. Appl. Phys., 1999, 85(1), 203.

24. Emanuel Carlos et al., ACS Appl. Mater. Interfaces, 2016, 8, 31100.

3.4 SOLUTION PRELIMINARY TESTS AND INK PRODUCTION

25. J. S. Park et al., Appl. Phys. Lett., 2008, 92(7), 34.
26. J. M. Reyes et al., J. Electrochem. Soc., 2013, 160(10), B201.
27. Wiley: Physics of Semiconductor Devices, 3rd Edition - Simon M. Sze, Kwok K. Ng, 2006. [Online]. Available: http://eu.wiley.com/WileyCDA/WileyTitle/productCd-0471143235.html.

CHAPTER 4

SUMMARY OF THE CONCLUSIONS AND FUTURE WORKS

SUMMAY OF THE CONCLUSIONS

During this PhD research work it was demonstrated the possibility to use the inkjet printing technique to deposit organic semiconductor molecules from solution. In particular, controlling the solvent evaporation rate, OSSCs have been grown on the top of gold interdigitated electrodes. This has been achieved thanks to the precision of the printer, that allowed to deposit fluorinated SAMs, creating solvo-phobic corrals, giving the possibility to divide the surface in separated parts or to confine a single ink drop in a determined position. Appropriate printing shape geometry and printing process optimization can increase effectiveness of the surface properties modification overtaking the limitations of the original surface characteristics.

The presence of the SAMs corral helps also to improve the quality of the crystals, decreasing the evaporation rate of the solvent, blocking the drop spreading over the substrate. Growth of crystals of high quality was possible also thanks to the optimization of the deposited solution composition.

The presence of the corral allowed to achieve these results without changing the surface chemistry. In fact, electrical measurements showed that the printed TIPS single crystals collect effectively charge carriers generated by both UV-Vis and X-ray photons evidencing that it is possible to direct “print” OSSCs directly onto electrodes originating working devices.

The geometry of the corral is another important aspect that was underlined in this work. Increasing the ratio between the length and the width of the corral, it is possible to force the crystals alignment along the corral main axe and to reduce the coffee-ring effects. With this simple approach, it was demonstrated the ability to grow OSSCs along a fixed direction, even onto higly heterogeneous substrates constituted by gold interdigitated electrodes on PEN.

During the PhD period, abroad at the University of Lisbon, inks for printing dielectric nano-layers of AlOx via a low temperature combustion approach were formulated and optimized. The original solution was optimized for deposition via spin-coating inside the laboratories of the University of Lisbon. It is possible to change only the concentration of the precursors and the organic solvents to gain the optimal physical characteristics for the IJP, whereas the precursors type is fixed. Mixtures of different solvents with different viscosity were tested to obtain the correct solution for inkjet printing; in addition, before the solutions became inks, each solution was evaluated with a series of tests to check the properties of the grown layer and successively

compare it with the dielectric layer produced by the original solution. Four inks were moved from the test-stage to the printing procedure, as indicated in table 3.5-1. The ink that can be considered the best one in terms of stamp-ability and electrical properties is number 17. Ink 15 also must be mentioned because it is made by substances that, in small amount, may be considered non-toxic for the worker and the environment. An important optimization during the printing process is the plate temperature (45°C for all the printing device) that promotes a correct substrate coverage without any spreading that reduces the printing shape quality. Ink 17, which generated the high quality dielectric layer in terms of electrical properties and homogeneity, was used successively in TFTs devices, where it worked perfectly.

All the three annealing techniques are good to obtain the final layer, but the high temperature one (350°C for 30 minutes) gives the best results. By changing the solvent or the precursors, it is possible to implement the other two low temperature techniques (150°C plus UV-light for 120 minutes; 200°C plus FUV-light for 90 minutes), moving from the silicon substrate, which is rigid, to polymeric substrates, which are flexible.

This experimentation underlines the possibility to print inks that promote the formation of very good dielectric layers of oxide materials grown by means of the combustion technique and their organic precursors. The innovative aspects are simplicity without expensive equipment, high throughput and the precision of the printing process, which also reduces the amount of waste material and makes the devices cheaper. The use of polymeric substrates in the future will make them flexible, stretchable and thinner increasing their application in industrial electronics.

FUTURE WORK

Future work to further the described research includes:

1. To increase the corral performance to enhance alignment reproducibility, with particular attention to the small corral widths, which has presented the higher percentages of failure. A possibility is the introduction of masks that would allow a reduction in sample fails. Parallelly new alignment strategies involving the geometrical one, up to now developed, combined with flux of inert gas, temperature gradient or both will be attempted.

2. To increase charge transfer between crystals and electrodes by modifying the surface with SAMs. In this case, it is required a strong research activity to understand how the modification of the electronic properties of the gold substrate affect the charge transfer with the organic semiconductors.

3. To develop and print new inks based on other organic molecules able to generate single crystals optimized as detector for ionizing radiation.

4. To study the X-ray detector characteristics and behaviors of the sample during and after mechanical stress. Because the device is based on flexible substrate and the prospected application is linked to a flexible device, crack and detachment of the crystals must be prevent.

5. For oxide-based TFTs production, future work will be focused essentially on printing on flexible substrate, with electrical measurements under stretching and bending stress; also, the screening of further AlOx precursors to expand the suitable substrate range, will be pursued.

Acknowledgements

I would like to thank all the research group with whom I have worked for three years at the University of Trieste, from my supervisor - Alessandro Fraleoni Morgera - to all my former and present colleagues - Mirta Sibilia, Marco Bogar, John Mohanraj and Luca Cozzarini - who have helped and supported me for all this long time.

A special thank goes to the Department of Engineering and Architecture, which have hosted me during all the research. In a special way, I thank all those who work in the Department of Materials Engineering, where I first became an engineer and now also a researcher.

I am also grateful to all the people I have worked with during these last three years, especially all my project colleagues from the University of Bologna and Cagliari that have helped and supported me.

The best experience of all this time of research is represented by the months which I spent abroad in the fantastic country of Portugal and in the happy city of Lisbon, where I met kind people that gave me the opportunity to grow from both working and personal point of view. For all these reasons, I would like to say a big thank you to all the CENIMAT department – New University of Lisbon - where I stayed for five beautiful months.

Another thank goes to the i-Flexis project for the PhD funding, which gave me the possibility to experience concretely what research is.

Finally, but at the first place in my heart, I would like to thank my parents and my girlfriend, who have supported me a lot during all this time. Thank you so much, without you I would have never become who I am today.